Probabilistic-based methods for extreme traffic loads mapping to assist bridge portfolio management

Mendoza Lugo, M.A.

DOI
10.4233/uuid:09bd9c99-be6b-487d-b835-c0f073ab3c1e

Publication date
2025

Document Version
Final published version

Citation (APA)
Mendoza Lugo, M. A. (2025). *Probabilistic-based methods for extreme traffic loads mapping to assist bridge portfolio management*. [Dissertation (TU Delft), Delft University of Technology]. https://doi.org/10.4233/uuid:09bd9c99-be6b-487d-b835-c0f073ab3c1e

Probabilistic-based methods for extreme traffic loads mapping to assist bridge portfolio management

Probabilistic-based methods for extreme traffic loads mapping to assist bridge portfolio management

Dissertation

for the purpose of obtaining the degree of doctor
at Delft University of Technology
by the authority of the Rector Magnificus prof. dr. ir. T.H.J.J. van der Hagen,
chair of the Board for Doctorates,
to be defended publicly on
06-05-2025 at 10:00 o'clock

by

Miguel Angel MENDOZA LUGO

Master of Science in Civil Engineering,
Autonomous University of the State of Mexico, Mexico,
born in Temoaya, Mexico.

This dissertation has been approved by the promotors.

Composition of the doctoral committee:

Rector Magnificus,	chairperson
Dr. ir. O. Morales Nápoles,	Delft University of Technology, promotor
Dr. ir. M. Nogal,	Delft University of Technology, copromotor
Independent members:	
Prof. dr. P. H. A. J. M. van Gelder,	Delft University of Technology
Prof. dr. J. R. Casas,	Polytechnic University of Catalonia, Spain
Prof. dr. ir. M. A. N. Hendriks,	Delft University of Technology
Dr. ir. D. L. Allaix,	TNO, Netherlands
Prof. Dr. ir. S. N. Jonkman,	Delft University of Technology, reserve member
Other members:	
Dr. D. J. Delgado Hernández,	Autonomous University of Mexico State, Mexico

This work was supported by the Mexican National Council for Science and Technology (CONACYT) under project number 2019-000021-01EXTF-00564 CVU 784544.

Keywords: Bayesian networks, copulas, extreme value, traffic loads, bridges

Printed by:

Cover: Roberto Omar Ignacio Mondragón

Style: TU Delft House Style, with modifications by Moritz Beller
https://github.com/Inventitech/phd-thesis-template

The author set this thesis in LaTeX using the Libertinus and Inconsolata fonts.

ISBN 978-94-6384-780-3

An electronic version of this dissertation is available at
http://repository.tudelft.nl/.

... Small axe fall big tree. So mi no fraid a yuh, no fraid a yuh...

Cebert Bernard

Contents

Summary

From Synthetic Vehicle Load Observations to Bridge Criticality and Beyond.

Vehicle load investigation is crucial for assessing the reliability of existing road infrastructure, given the potential threats posed by extreme traffic loads, including risks to road transport operations and the integrity of pavements and bridges. The most reliable source for gathering massive vehicle load information is Weigh-in-Motion (WIM) technology. WIM systems play a pivotal role in collecting data on vehicular loads, individual axle loads, vehicle types, and axle counts, holding significant relevance in engineering for the design of new bridges and the reliability assessment of existing structures. However, the inherent high costs associated with WIM systems have limited their adoption, leading many regions to rely on the use of less sophisticated traffic counters (LSTC). The drawbacks of such alternatives, including inaccurate axle counting during high truck volumes and the absence of vehicle weighing, must be considered when assessing the reliability of road infrastructure at a network level.

One of the first steps in the reliability assessment of road infrastructure at the network level is the identification of critical locations within the network. This involves, for example, identifying critical road locations due to extreme gross vehicle weights and critical bridge locations due to extreme load effects. The goal is to generate optimal bridge intervention programs taking into account these performance indicators to minimize costs. Therefore, in cases where WIM data is unavailable (or limited), the computation of synthetic WIM observations becomes crucial. Synthetic WIM observations should approximate statistical characteristics (including dependencies). of real traffic data.

After the introduction section of this dissertation, *the second chapter* discusses a methodology for generating probabilistic models describing the weight and length of various heavy vehicle types. By analyzing WIM measurements from the Netherlands and Brazil, the second chapter presents a set of Gaussian Copula-based Bayesian Networks (GCBNs). The primary objective is to construct a WIM data model specifically for heavy vehicles (total weight exceeding 34 kN) using data from the studied WIM stations. The constructed model generates statistically representative synthetic data of the primary variables in a WIM dataset, including vehicle type, gross vehicle weight, individual axle loads, total vehicle length, and inter-axle distances. To enhance usability, a graphical user interface for Dutch highway WIM locations has been developed, and a major update has been made to an existing MATLAB software to quantify GCBNs. The demonstrated methodology proves widely applicable, improving upon prior results by enabling the generation of inter-axial distance observations, incorporating multiple data sources into the modeling process, and providing software for researchers and practitioners interested in generating synthetic observations based on vehicle type distribution.

The third chapter explores the utilization of hazard maps for pinpointing critical locations associated with extreme vehicle load events, a crucial aspect in evaluating the reliability of road infrastructure. Acknowledging the increasing pressure on road systems attributed to outdated highways, and the rising percentage of trucks exceeding legal weight limits. As mentioned, as the deployment of WIM systems is limited, road managers often use LSTCs. However, they lack the capacity to measure vehicular axle loads, prompting the introduction of a methodology that uses LSTC data to estimate axle loads and map extreme gross vehicle weights. A case study focusing on the major highways in Mexico demonstrates the feasibility of this approach, where the absence of WIM stations is compensated by data from a network of 1,777 counting stations and origin-destination surveys. The study utilizes GCBNs to generate synthetic site-specific axle loads, enabling the calculation of gross vehicle weights for selected return periods using extreme value analysis (EVA) and facilitating the identification of hazardous locations. Over 180 million heavy vehicles were simulated, and due to the numerous simulations needed, a fully open-source software tool, based on Python, was developed to quantify GCBNs. This development derived from a major update from an earlier implemented closed-source version of the software. These findings, complemented by an interactive web map and graphical user interface, lay the groundwork for maintenance strategies for existing roads and bridges.

The fourth chapter emphasizes the major role of bridge structures in a country's transportation system, managed through Bridge Management Systems (BMS). Despite the conventional four-module structure of BMS, many countries operate single-module BMSs primarily focused on inventory management. This limitation impedes their ability to make decisions regarding the risk and reliability of the bridge stock. The lack of structural assessments for numerous bridges underscores the need for a holistic network reassessment.

Traffic load effects on bridges, especially extreme load effects (ELEs), are crucial for infrastructure safety and reliability. However, challenges arise when studying traffic load effects at a network scale due to the absence of WIM systems in many locations and insufficient detailed bridge inventory information. In response, we introduce a methodology to map and estimate extreme load effects due to heavy vehicle traffic. By employing GCBNs, the methodology allows for the simulation of site-specific traffic conditions, providing an understanding of heavy vehicle interactions. The incorporation of extreme value theory enhances the accuracy of estimating extreme load effects, ensuring a comprehensive assessment of bridge criticality at the network level. Furthermore, the case study involving Mexico's national bridge network of 576 structures demonstrates the practical application of the methodology, showcasing its effectiveness in identifying bridges in need of inspection based on limited available information. The methodology's adaptability and simplicity make it a valuable tool for countries operating with single-module BMSs, offering a pathway for more informed and prioritized maintenance strategies for their bridge infrastructure.

Bridge networks face degradation from aging, heavy traffic loads, and natural disasters, posing risks to service quality and safety. Effective bridge management with constrained funding requires objective assessments for the optimal utilization of aging bridges. Maintenance, repair interventions, and strategic planning can enhance infrastructure availability while minimizing costs. Previous studies emphasize the need to consider both direct and indirect costs associated with transport disruptions in optimal planning, as traveler delays during bridge closures can incur costs higher than those of the bridge repair itself. Integrating performance indicators from individual bridges at the network level enhances overall bridge system performance, surpassing traditional structural rating-based planning.

The fifth chapter introduces a methodology for optimizing maintenance and repair activities in bridge networks, taking into account central and non-central interventions. This integrative multi-system and multi-stakeholder optimization approach considers bridges as components of a transportation system, addressing the additional costs due to the interconnected effects of interventions on individual bridges within the network. The formulation accounts for deterioration, budget constraints, and time between interventions, extending existing frameworks by incorporating repair interventions. Furthermore, the methodology allows the inclusion of various performance indicators for bridge prioritization. The affordable computational time of the mathematical program allows practical applicability to portfolios containing a large number of bridges. The methodology provides practical guidance for estimating both direct and indirect costs, making it a valuable tool for efficiently planning interventions within extensive bridge networks.

This thesis focuses on enhancing the reliability estimates of bridges at a network level by addressing four key subjects that effectively model dependence between traffic load variables. The aim is to assist decision-making in bridge management strategies, particularly in regions where WIM data is limited, and a single-module BMS may fall short in detecting critical locations beyond visual inspections. The proposed approach advocates for advanced tools utilizing probabilistic-based reliability methodologies, enabling the formulation of strategic action plans aimed at preserving the structural integrity of road bridges, thereby minimizing disruptions and safety risks for society.

Samenvatting

Van Synthetische Voertuigbelastingobservaties tot Brugkritikaliteit en Verder.

Voertuigladingonderzoek is cruciaal voor het beoordelen van de betrouwbaarheid van bestaande weg infrastructuur, gezien de potentiële bedreigingen die extreme verkeersladingen met zich meebrengen, waaronder risico's voor wegtransportoperaties en de integriteit van verhardingen en bruggen. De meest betrouwbare bron voor het verzamelen van uitgebreide voertuigladingsinformatie is Weigh-in-Motion (WIM) technologie. WIM-systemen spelen een belangrijke rol bij het verzamelen van gegevens over voertuigladingen, individuele asladingen, voertuigtypen en asaantallen, en zijn van groot belang in de techniek voor het ontwerp van nieuwe bruggen en de betrouwbaarheidsevaluatie van bestaande structuren. De inherente hoge kosten die gepaard gaan met WIM-systemen hebben echter hun adoptie beperkt, waardoor veel regio's afhankelijk zijn van minder geavanceerde verkeersmeters (LSTC). De nadelen van dergelijke alternatieven, waaronder onnauwkeurige astelling tijdens hoge vrachtwagenvolumes en de afwezigheid van voertuigweging, moeten in overweging worden genomen bij het beoordelen van de betrouwbaarheid van weg infrastructuur op netwerkniveau.

Een van de eerste stappen in de betrouwbaarheidsevaluatie van weg infrastructuur op netwerkniveau is de identificatie van kritieke locaties binnen het netwerk. Dit houdt bijvoorbeeld in dat kritieke weglocaties worden geïdentificeerd vanwege extreme bruto voertuiggewichten en kritieke bruglocaties vanwege extreme laadeffecten. Het doel is om optimale bruginterventieprogramma's te genereren rekening houdend met deze prestatieindicatoren om kosten te minimaliseren. Daarom wordt, in gevallen waarin WIM-gegevens niet beschikbaar zijn (of beperkt), de berekening van synthetische WIM-waarnemingen cruciaal. Synthetische WIM-waarnemingen moeten de statistische kenmerken (inclusief afhankelijkheden) van echte verkeersgegevens benaderen.

Na de inleidende sectie van deze dissertatie bespreekt *het tweede hoofdstuk* een methodologie voor het genereren van probabilistische modellen die het gewicht en de lengte van verschillende zware voertuigtypen beschrijven. Door WIM-metingen uit Nederland en Brazilië te analyseren, presenteert het tweede hoofdstuk een set van op Gaussian Copula gebaseerde Bayesian Networks (GCBN's). Het primaire doel is om een WIM-gegevensmodel te construeren dat specifiek gericht is op zware voertuigen (totaal gewicht van meer dan 34 kN) met behulp van gegevens van de bestudeerde WIM-stations. Het geconstrueerde model genereert statistisch representatieve synthetische gegevens van de primaire variabelen in een WIM-dataset, waaronder voertuigtype, bruto voertuiggewicht, individuele asladingen, totale voertuiglengte en inter-asafstanden. Om de bruikbaarheid te verbeteren, is er een grafische gebruikersinterface ontwikkeld voor WIM-locaties op Nederlandse snelwegen, en is er een grote update uitgevoerd op bestaande MATLAB-software om GCBN's te kwantificeren. De gedemonstreerde methodologie blijkt breed toepasbaar en verbetert eerdere resultaten door de generatie van inter-asafstandswaarnemingen mogelijk te maken, meer-

dere gegevensbronnen in het modelleringsproces te integreren en software te bieden voor onderzoekers en praktijkmensen die geïnteresseerd zijn in het genereren van synthetische waarnemingen op basis van voertuigtypeverdeling.

Het derde hoofdstuk verkent het gebruik van gevarenkaarten voor het pinpointen van kritieke locaties die verband houden met extreme voertuiglaadevenementen, een cruciaal aspect bij het evalueren van de betrouwbaarheid van weg infrastructuur. Dit hoofdstuk erkent de toenemende druk op wegsystemen als gevolg van verouderde snelwegen en het stijgende percentage vrachtwagens dat de wettelijke gewichtslimieten overschrijdt. Zoals eerder vermeld, is de inzet van WIM-systemen beperkt, waardoor wegbeheerders vaak gebruikmaken van LSTC's. Deze systemen hebben echter niet de capaciteit om de asladingen van voertuigen te meten, wat de introductie van een methodologie noodzakelijk maakt die LSTC-gegevens gebruikt om asladingen te schatten en extreme bruto voertuiggewichten in kaart te brengen. Een casestudy die zich richt op de belangrijkste snelwegen in Mexico toont de haalbaarheid van deze aanpak aan, waarbij de afwezigheid van WIM-stations wordt gecompenseerd door gegevens van een netwerk van 1.777 telstations en oorsprong-bestemmingsonderzoeken. De studie maakt gebruik van GCBN's om synthetische locatie-specifieke asladingen te genereren, waardoor de berekening van bruto voertuiggewichten voor geselecteerde terugkeertijdsperioden mogelijk wordt gemaakt met behulp van extreme waarde-analyse (EVA) en de identificatie van gevaarlijke locaties vergemakkelijkt. Meer dan 180 miljoen zware voertuigen werden gesimuleerd, en vanwege het aantal benodigde simulaties werd er een volledig open-source softwaretool ontwikkeld, gebaseerd op Python, om GCBN's te kwantificeren. Deze ontwikkeling is voortgekomen uit een grote update van een eerder geïmplementeerde gesloten-source versie van de software. Deze bevindingen, aangevuld met een interactieve webkaart en grafische gebruikersinterface, leggen de basis voor onderhoudsstrategieën voor bestaande wegen en bruggen.

Het vierde hoofdstuk benadrukt de belangrijke rol van brugstructuren in het transportsysteem van een land, beheerd via Bridge Management Systems (BMS). Ondanks de conventionele vier-module structuur van BMS, opereren veel landen met enkelvoudige-module BMS'en die zich voornamelijk richten op voorraadbeheer. Deze beperking belemmert hun vermogen om beslissingen te nemen over het risico en de betrouwbaarheid van de brugvoorraad. Het gebrek aan structurele beoordelingen voor talrijke bruggen onderstreept de noodzaak voor een holistische herbeoordeling van het netwerk.

De effecten van verkeerslading op bruggen, vooral extreme laadeffecten (ELE's), zijn cruciaal voor de veiligheid en betrouwbaarheid van infrastructuur. Echter, er ontstaan uitdagingen bij het bestuderen van verkeersladingseffecten op netwerkschaal door de afwezigheid van WIM-systemen op veel locaties en onvoldoende gedetailleerde bruginventarisinformatie. In reactie hierop introduceren we een methodologie om extreme laadeffecten als gevolg van zwaar verkeer in kaart te brengen en te schatten. Door gebruik te maken van GCBN's maakt de methodologie de simulatie van locatie-specifieke verkeersomstandigheden mogelijk, wat inzicht biedt in de interacties van zware voertuigen. De integratie van extreme waarde-theorie verbetert de nauwkeurigheid van het schatten van extreme laadeffecten, wat zorgt voor een uitgebreide beoordeling van de kritikaliteit van bruggen op netwerkniveau. Bovendien toont de casestudy met het nationale brugnetwerk van Mexico, bestaande uit 576 structuren, de praktische toepassing van de methodologie aan, waarbij de effectiviteit in het identificeren van bruggen die inspectie nodig hebben op basis van beperkte beschikbare informatie wordt belicht. De aanpasbaarheid en eenvoud van de methodologie maken het een waardevol hulpmiddel voor landen die werken met enkelvoudige-module BMS'en, en bieden een pad voor meer geïnformeerde en prioritaire onderhoudsstrategieën voor hun bruginfrastructuur.

Brugnetwerken ondervinden degradatie door veroudering, zware verkeersladingen en natuurrampen, wat risico's met zich meebrengt voor de servicekwaliteit en veiligheid. Effectief brugbeheer met beperkte financiering vereist objectieve beoordelingen voor de optimale benutting van verouderende bruggen. Onderhoud, reparatie-interventies en strategische planning kunnen de beschikbaarheid van infrastructuur verbeteren terwijl de kosten worden geminimaliseerd. Eerdere studies benadrukken de noodzaak om zowel directe als indirecte kosten die verband houden met transportonderbrekingen in optimale planning in overweging te nemen, aangezien vertragingen voor reizigers tijdens brugsluitingen kosten kunnen veroorzaken die hoger zijn dan die van de brugreparatie zelf. Het integreren van prestatie-indicatoren van individuele bruggen op netwerkniveau verbetert de algehele prestaties van het brugensysteem, wat de traditionele planning op basis van structurele beoordelingen overstijgt.

Het vijfde hoofdstuk introduceert een methodologie voor het optimaliseren van onderhouds en reparatieactiviteiten in brugnetwerken, waarbij zowel centrale als niet centrale interventies in overweging worden genomen. Deze integratieve optimalisatiebenadering voor meerdere systemen en belanghebbenden beschouwt bruggen als componenten van een transportsysteem en pakt de extra kosten aan die voortvloeien uit de onderlinge effecten van interventies op individuele bruggen binnen het netwerk. De formulering houdt rekening met veroudering, budgetbeperkingen en de tijd tussen interventies, en breidt bestaande kaders uit door reparatie-interventies op te nemen. Bovendien maakt de methodologie de opname van verschillende prestatie-indicatoren voor brugprioritering mogelijk. De betaalbare rekentijd van het wiskundige programma maakt praktische toepasbaarheid mogelijk voor portefeuilles met een groot aantal bruggen. De methodologie biedt praktische richtlijnen voor het schatten van zowel directe als indirecte kosten, waardoor het een waardevol hulpmiddel is voor het efficiënt plannen van interventies binnen uitgebreide brugnetwerken.

Deze thesis richt zich op het verbeteren van de betrouwbaarheidsschattingen van bruggen op netwerkniveau door vier belangrijke onderwerpen aan te pakken die effectief de afhankelijkheid tussen verkeersladingvariabelen modelleren. Het doel is om de besluitvorming in brugbeheerstrategieën te ondersteunen, met name in regio's waar WIM-gegevens beperkt zijn en een enkelvoudige-module BMS mogelijk tekortschiet in het detecteren van kritieke locaties buiten visuele inspecties. De voorgestelde aanpak pleit voor geavanceerde tools die gebruikmaken van probabilistisch gebaseerde betrouwbaarheidmethodologieën, waardoor de formulering van strategische actieplannen mogelijk wordt die gericht zijn op het behoud van de structurele integriteit van wegbruggen, en daarmee verstoringen en veiligheidsrisico's voor de samenleving minimaliseren.

1

Introduction

This thesis explores the properties of Gaussian copula-based Bayesian networks (GCBNs), extreme value analysis (EVA), and optimization techniques. By focusing on their application in traffic load analysis to estimate bridge reliability at the network level, particularly in bridge networks where traffic data is limited. GCBNs are graphical models that represent multivariate probability distributions. This thesis utilizes GCBNs to model crucial variables for bridge reliability analysis, such as axle loads and inter-axle distances of heavy vehicles. To enhance the reliability analysis of bridges, the EVA approach is used for accurately predicting extreme load effects induced by axle loads of heavy vehicles. The reliability of a bridge is a key indicator of its structural integrity and safety. Consequently, integrating this key indicator into optimal budget allocation at a bridge network level will enhance the development of more effective scheduling for bridge maintenance and repair activities. As a case study, this thesis focuses on the Mexican bridge network comprising 576 bridges situated along the toll-free fifteen major highway corridors. These corridors extend over approximately 20 000 *kilometres and accommodate more than 55% of the country's highway traffic flow.*

1.1 Motivation

The backbone of any country's transportation system is its national highway networks. These networks are essential to ensure the mobility of people and goods, supporting international trade links [1, 2]. Nevertheless, road infrastructure is under increasing pressure. On one hand, a large part of the highway infrastructure is outdated, which means that many of the roads and their assets need to be repaired or replaced. On the other hand, the percentage of trucks that exceed the maximum legal weight is increasing.

One of the most critical components within highway networks is their inventory of bridge structures. When bridges are not used or maintained properly, disruptions occur in the traffic network. These disruptions create stress within the network, leading to increased travel costs and potential economic losses [3]. Globally, bridge infrastructure is ageing. In the American continent, bridge inventories indicate that the majority were constructed between 1960 and 1980 [4, 5]. Similarly, in Europe, most bridges were built between 1970 and 2001 [6]. Past structural design deficiencies, structural deterioration, and increasing traffic volume reveal the need for a structural reassessment of the entire bridge network infrastructure to address ageing concerns. The need becomes evident when considering the impact of non-operational bridges on the entire network. Therefore, a system-level analysis is crucial, taking into account both the direct costs and the indirect costs associated with unavailability.

Effectively monitoring vehicle loads within the road network is necessary to maintain the condition of its critical assets. Truck overloading has become a common phenomenon worldwide, especially in developing countries [7–10]. Overloaded vehicles introduce uncertainty and raise safety concerns for road infrastructure [11–13]. According to [14], the 1,000-year gross vehicle weight (GVW) can be used to determine the so-called “aggressiveness” of traffic for bridges. By examining extreme GVWs of numerous sites and applying Bayesian updating techniques, the posterior distribution of extreme GVWs for lightly trafficked sites can be obtained [15]. With this information, extreme vehicles can be modelled addressing the challenge of their typically having very few records [16]. Therefore, it is important to identify hazardous road locations, which are sites where there is potential for infrastructure damage due to extremely overloaded vehicles. These are locations where the extreme values of GVWs are higher than the GWs of standard trucks. Additionally, identifying bridge locations where the extreme values of load effects surpass those obtained with the design live loads is essential. This identification process serves as an aid for ensuring the safety and reliability of the entire network.

Identification and mapping of hazardous locations is the initial phase for the development and implementation of maintenance strategies. The utilization of hazard location maps allows for the visual identification of changes and patterns within the overall infrastructure system. These types of maps have been used widely and recently in the field of reliability engineering as a tool for emergency management and mitigation planning purposes (see [17–19] for example). In transport engineering, hazard maps have been employed to present various aspects, such as optimal evacuation paths on the road network during toxic gas leak incidents [20], welfare loss as a measure of road network performance [21], rainfall-induced flooding to plan road closures ahead of heavy precipitation events [22] and management and prevention of landslides disaster risk for regional roads [23]. Regarding overload vehicles, maps have been used as a tool for investigating fatigue resulting from truck overloading [24], heavy vehicle traffic volume prediction [25], and analysis of oversize-overweight truck routes[26] to name a few.

With the previous ideas in mind, it becomes clear that one of the most important elements of transport network reliability analysis is the traffic loads. The most reliable source of information for describing traffic characteristics is the data collected by Weigh-In-Motion (WIM) systems. WIM is a technology that allows measuring vehicle attributes while the vehicle is travelling at full highway speed. Hence, significant amounts of data such as axle loads, vehicle type, and inter-axle distance are collected. Consequently, WIM systems are widely used around the world. For instance, countries such as Slovenia, Ireland, and England, operate 216 WIM sites installed in their national road networks [27]. However, when information regarding individual traffic loads is scarce or not available, computer simulations have become the most prominent approach to estimating them.

Implementing probabilistic-based assessment methods for traffic loads at the network level, considering the dependence structure of the traffic data is important. This holds the potential to enhance the reliability analysis of road infrastructure by estimating performance indicators and developing optimal bridge management strategies. This perspective is particularly relevant for regions or bridge networks where WIM systems are not the primary source of traffic data. The highways of Mexico, particularly the major highway corridors, provide an example of the challenges faced due to the lack of WIM systems. The primary issue in this context is the overloading of vehicles, which significantly increases the deterioration of road and bridge infrastructure. Without WIM systems to monitor the current gross vehicle weights and axle loads, it becomes difficult to assess the effects of these loads on the bridges within the network. This lack of information reduces the ability to manage the maintenance and repair interventions effectively, as the effects caused by heavy loads are not accurately taken into account. Bridge managers now acknowledge that effective planning should consider performance indicators and user costs associated with transport disruptions of other bridges due to spatial proximity, and not solely rely on budget availability [28]. Such improvements have the potential to reduce societal impact and lead to more efficient investments in road infrastructure.

1.2 Knowledge gaps

The following paragraphs discuss the knowledge gaps associated with the development and application of more accurate assessment methods for hazard identification due to traffic loads in road infrastructure where WIM data is limited. The thesis focuses on four main aspects, i.e., (a) synthetic WIM data generation, (b) mapping extreme gross vehicle weights, (c) extreme bridge loading caused by traffic loads, and (d) optimal bridge portfolio intervention scheduling.

Regarding the computation of *synthetic WIM data*, to achieve accurate simulations of WIM observations, it is important to model the statistical correlations between variables. While previous studies have utilized methods such as empirical factors, linear correlations, and copulas for this purpose (see[29], [30], [31], [32] for example), they have primarily focused on axle loads or fixed inter-axle distances, overlooking the broader context by grouping vehicles with similar characteristics and not taking into account all the different types of vehicles in the database. This suggests a knowledge gap in adequately addressing the statistical correlations among variables in WIM data, especially when considering the diverse range of vehicle types.

Accurately estimating and mapping traffic loads, particularly *extreme gross vehicle weights* (EGVW), requires measuring individual axle loads, often achieved through WIM systems. However, permanent WIM stations incur substantial costs, making it economically unfeasible to deploy the required number of stations to cover the entire road network. To address this challenge, many countries employ origin-destination surveys and less-sophisticated traffic counters (LSTC), such as manual counting or pneumatic road tubes, for cost-effective insights into road usage and traffic patterns [33, 34].

Generally, LSTCs do not provide data regarding individual axle loads [35, 36] unless static weighing is used, in which trucks usually have to make a time-consuming stop on a scale at a weigh station, and inspections are carried out [37]. Due to the logistical difficulties of static weighing, only a small amount of data is usually collected. While numerous studies and techniques have focused on data generation and collection, the mapping of extreme traffic loads using information obtained from LSTCs remains limited. Hence, there is a need for a framework for estimating and mapping site-specific traffic

1

loads in locations where WIM data is scarce or not available.

Extensive research has been conducted on modeling *extreme bridge loading caused by traffic loads*, with studies such as those by [38–41]. However, the majority of prior work is based on the assumption of having complete traffic data from WIM systems and comprehensive information on bridge geometry and material properties. Additionally, these studies often focus on individual bridges or small sets of bridges with different span lengths. While such studies serve as a foundation for calibrating bridge design codes, estimating characteristic values for the load effects of an entire bridge network is often impractical [38].

This gives rise to two main challenges when investigating the extreme load effects (ELE) of traffic loads on bridges at a network scale. First, in many locations, the use of WIM systems is not viable due to their high costs. Second, bridge inventories commonly lack detailed information on the geometric and material properties of bridges. These challenges underscore the necessity of addressing the knowledge gap in comprehensive methodologies for assessing the impact of traffic loads on bridges at the network level, whose outcomes are capable of presenting condensed information such as maps. To the best of the authors' knowledge, there is a lack of scientific literature concerning interactive, publicly available maps that depict EGVWs, ELEs, or performance indicators related to load effects in bridge networks. Such maps could significantly aid in the decision-making process regarding the development of maintenance and repair interventions for bridge networks.

Research has demonstrated that incorporating performance measures from each individual bridge into optimal budget allocation algorithms for *bridge portfolio intervention scheduling* can significantly enhance the overall performance of bridge systems [42]. For effective intervention programs, it is clear that optimal planning should consider both the direct and user costs associated with transport disruptions, rather than solely budget availability [28]. Furthermore, at a network level, a significant number of bridge structures need to be analyzed, making it infeasible to re-analyze each bridge on an annual basis. Consequently, systems that continuously monitor bridge conditions are established to plan interventions based on structural ratings and prioritization indexes, which justify the funding of conservation actions [43].

Numerous studies have shown how to allocate maintenance resources for a group of bridges or individual bridges in a transportation network (see for example, [44], [45] and [46]). However, existing studies often overlook the interconnected effects of bridge interventions on individual bridges within a network, particularly in terms of their spatial proximity. This highlights the need to develop comprehensive and computationally efficient methodologies for optimizing bridge intervention scheduling. Such methodologies should take into account bridge performance indicators, direct costs associated with bridges, user costs, and the additional costs incurred by interventions on neighbouring bridges within the network system.

1.3 Research Aim and Questions

This thesis aims to improve the reliability estimates of bridges at a network level by quantifying site-specific extreme values of traffic loads. It examines the extreme effects of these loads, such as bending moments and shear forces, on the bridges. The goal is to enhance the development of optimal bridge intervention strategies, particularly in locations where traffic load information is limited. This aim is reflected in the main research question:

How can enhance bridge reliability estimates by integrating probabilistic quantification of traffic data to provide site-specific traffic load extremes to aid the development of effective intervention strategies?

The main question is analyzed with four key research questions, which are addressed in various chapters.

1. How to generate synthetic traffic data taking into account the appropriate statistical dependence of axle loads and inter-axle distances of real observations? (Chapter 2)
2. How to identify the road locations with the highest extreme values of gross vehicle weights using data from origin-destination surveys and less-sophisticated traffic counters? (Chapter 3)
3. How to identify bridges where the extreme values of the load effects associated with the actual loads exceed those obtained with the design live loads when traffic data and bridge information are limited? (Chapter 4)
4. How to develop an optimal maintenance and repair program for bridge networks based on critical interventions and performance indicators? (Chapter 5)

1.4 Scope and outline

This section briefly describes the methods used for the different chapters of the research. Figure 1.1 outlines the general structure of the thesis, encompassing four research topics, aligned with the four research questions:

(i) Generate synthetic data statistically representative of the real heavy vehicles observations.

(ii) Identify road hazardous locations due to extreme gross vehicle weights.

(iii) Estimate bridge criticality as a performance indicator of the impact of traffic loads.

(iv) Optimal intervention program for bridge networks based on performance indicators considering direct and indirect costs.

After this introduction, Chapter 2, research topic (i), introduces the main definitions and concepts of GCBNs used in this thesis, together with a methodology for simulating site-specific synthetic axle loads of heavy vehicles using GCBNs to address Research Question 1. Chapter 3, research topic (ii), introduces the case study and addresses Research Question 2 by proposing a five-step methodology to identify hazardous locations due to gross vehicle weights (GVW) using GCBNs and EVA to estimate extreme GVWs. While Chapter 2 uses Weigh-In-Motion (WIM) observations for model development and validation, Chapter 3 applies this methodology to the case study where WIM systems are not the primary source of traffic data.

1

In Chapter 4, research topic (iii), a methodology is presented to evaluate bridge criticality as a load effect performance indicator, assessing how a structure responds to in-service traffic loads compared to its response under the design live load model provided by the bridge owner, addressing Research Question 3.

The final research question is answered in Chapter 5, research topic (iv), where a methodology for optimizing maintenance and repair intervention scheduling is proposed, considering bridges as integral components of a transportation system. This takes into account factors such as deterioration, budget constraints, the time between two consecutive interventions, and the load effect performance indicator.

Finally, in Chapter 6, the main conclusions are presented, and recommendations for future research are provided.

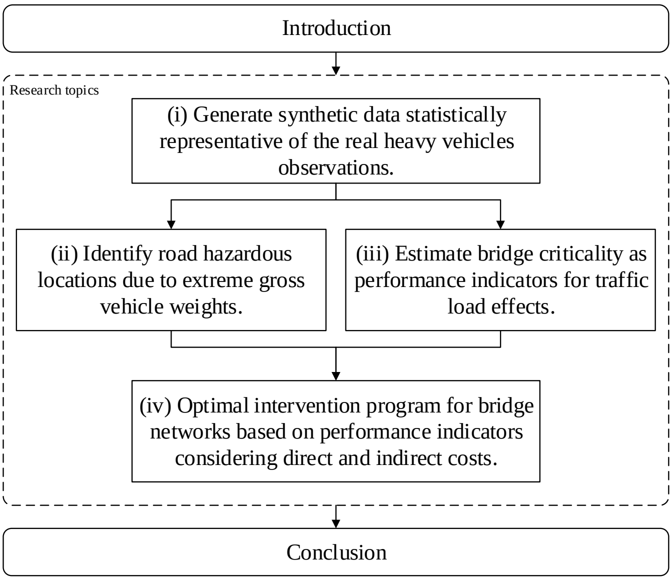

Figure 1.1: General outline of this thesis. Each research topic is related to one of the research questions and chapters.

1.5 Contribution

The main contribution of this thesis is that it provides an integral study of the in-service traffic loads and their effects on bridges, along with a bridge budget allocation program for maintenance and repair interventions in a network-level context. All the methodologies provided herein are adaptable and can be implemented in any bridge network. They utilize probabilistic quantification of traffic data obtained through less sophisticated traffic information techniques than WIM systems. This is particularly valuable in locations where data is limited. By employing these methods, bridge reliability estimates are improved, contributing to the development of a more robust bridge management system. Furthermore, this research compiled, analysed and produced the largest dataset of extreme gross vehicle weights, extreme traffic load effects (bending moments and shear forces) on bridges, and bridge performance indicators resulting from traffic loads for Mexico's fifteen major highway corridors.

Chapter 2 presents an improved methodology for computing synthetic WIM observations of heavy vehicles through GCBNs. The model accurately simulates the dependence structure of empirical data and can be applied at any WIM location, providing site-specific synthetic WIM records and site-specific vehicle types.

Chapter 3 offers an accurate estimation of site-specific characteristic loads that can assist in identifying hazardous locations. This is especially useful when WIM data is unavailable but common traffic counters data is available. The methodology presented in Chapter 4 presents various advantageous attributes, including the capability to identify bridges that require more detailed inspections based on their condition as assessed by the methodology. It offers a simple conceptualization that is easy to apply and only requires basic information regarding traffic and bridge characteristics. This research provides the first comprehensive spatial analysis and the largest dataset of extreme gross vehicle weights and extreme traffic load effects in bridges of the studied road network.

Chapter 5 provides a novel methodology for optimizing intervention scheduling that considers bridges as components of a transportation system, addressing a significant gap by considering the interconnected effects of interventions on individual bridges within the network system. Furthermore, it provides practical guidance for estimating both direct and indirect costs through the analysis of an actual bridge network. This can be applied in conjunction with various bridge ranking systems that rely on performance indicators, including condition state and traffic load effects criticality. This makes it a valuable tool for efficiently planning interventions within extensive bridge networks.

Lastly, an open-source implementation based on Python programming language of a closed-source programming and numeric computing platform (MATLAB) toolbox to quantify, visualize, and validate GCBNs has been developed including new features [47]. Simultaneously, the MATLAB toolbox [48] has received significant updates to enhance its functionality.

2

2

Gaussian Copula-based Bayesian Networks for modelling Weigh-in-Motion System Data

Weigh-in-motion (WIM) systems help to collect data such as vehicular loads, individual axle loads, vehicle type, and the number of axles. This is relevant in engineering because traffic load performs an essential function in the design of new bridges and in the reliability assessment of existing ones. Therefore, when WIM data is not available, computing synthetic WIM observations that adequately approximate the statistical dependence between variables is important. This chapter presents a methodology to generate statistical models to describe the weight and length of different vehicle types. WIM measurements from the Netherlands and Brazil were analyzed, and a set of Gaussian Copula-based Bayesian Networks is presented. Significant improvements have been made by allowing the generation of observations of inter-axial distance, permitting the use of several sources of data in modelling, and making software available to researchers and practitioners interested in generating synthetic observations based on the distribution of vehicle types. This chapter shows that the methodology here presented is widely applicable and depends only on the assessment of vehicle type configuration.

Parts of this chapter have been published verbatim in **Mendoza-Lugo, M. A.**, Morales-Nápoles, O., & Delgado-Hernández, D. J. (2022). A Non-parametric Bayesian Network for multivariate probabilistic modelling of Weigh-in-Motion System Data. Transportation Research Interdisciplinary Perspectives, 13, 100552. doi: https://doi.org/10.1016/j.trip.2022.100552 and **Mendoza-Lugo, M. A.**, & Morales-Nápoles, O. (2023). Version 1.3-BANSHEE; A MATLAB toolbox for Non-Parametric Bayesian Networks. SoftwareX, 23. doi: https://doi.org/10.1016/j.softx.2023.101479

2.1 Introduction

Vehicle load investigation is essential for the reliability assessment of existing road infrastructure because the exceedance of legal weight limits may cause serious threats to road transport operations and road infrastructure. For example, by increasing the risk of deterioration of pavements and bridges. One approach for describing the traffic flow characteristics is data gathered through WIM systems.

Applications of the data gathered by the Weigh-in-Motion system include reliability assessment of bridges, pavements and, monitoring of overloaded traffic. Consequently, WIM systems are widely used around the world. However, WIM systems are expensive in terms of initial capital costs and life cycle maintenance costs. As a result, a large number of countries or regions around the world do not operate any WIM system at present. They are mostly using common techniques such as pneumatic road tubes, some disadvantages of this technique include inaccurate axle counting when truck volumes are high and the absence of vehicle weighing [29]. Therefore, computing good artificial WIM data modelling statistical correlations between the variables is relevant in road infrastructure safety assessment because an accurate model enhances the reliability estimation.

The aim of the research in this chapter is to construct a WIM data model of heavy vehicles (total weight above 34 kN) from data obtained in the available WIM stations. In order to generate synthetic data statistically representative of the real observations. The model is constructed using a Bayesian network (BN) type previously identified in literature as the Non-parametric Bayesian network (NPBN). For clarity, it is now denoted it as *Gaussian copula-based Bayesian network* (GCBN) in reference to its underlying theory. Unlike previous studies, the model provides data that describes all the main variables of a WIM data set i.e. vehicle type, gross vehicle weight, individual axle loads, total vehicle length, and inter-axle distances. Furthermore, to make use of the model more convenient, a graphical user interface (GUI) of the Dutch available highway WIM locations is developed.

In Section 2.2, the main definitions and concepts of GCBNs used in the work are presented. In Section 2.3, the framework for generating synthetic WIM data is presented. Observations of six Dutch WIM locations by clustering the vehicle types by vehicle configuration are used. Section 2.5 present the main results and the validation of the GCBN models. Next, in Section 2.6, two case studies of the framework are presented: an GCBN quantified with WIM observations collected in Rotterdam city in the Netherlands by classifying vehicle types according to the number of axles, and an GCBN quantified with data collected in Araranguá city in Brazil by clustering vehicle types by classification WIM codes. As will be seen later, the validation of the methodology is performed with the Dutch case (Section 2.3.1) while the cases in Section 2.6 are presented as examples of the use of the methodology. Section 2.7 presents the developed GUI together with one possible application of the model when WIM data is not available. Finally, the conclusions are drawn in Section 2.8.

2.2 Gaussian Copula-based Bayesian Networks

When modelling multivariate probability distributions, Bayesian Networks (BNs) are considered effective tools [49]. BNs are directed acyclic graphs (DAG), consisting of nodes and arcs. The nodes of BNs represent random variables and the arcs represent the probabilistic relations between these variables [50]. A BN encodes the probability density or mass function on a set of variables $\boldsymbol{X} = \{X_1, ..., X_n\}$ by specifying a set of conditional independence statements in the DAG associated with a set of conditional probability functions [51]. A major overview of applications of BNs may be found in [52], [53] and [54].

One type of BN which has the advantage of managing hundreds of variables in a rapid manner is the Gaussian copula-based Bayesian Network (GCBN)[1]. The GCBN methodology proposes a technique for dealing with any one-dimensional marginal distribution (as long as it is invertible) while inducing the dependence structure given by the DAG of the BN using one parameter copulas for which zero correlation entails independence [55]. The theory of GCBNs introduced in [56] is based around bivariate copulas. Distributions are assigned to the nodes and one (conditional) parameter copulas to the arcs of the DAG [57]. Copulas are a class of bivariate distributions whose marginals are uniform [58]. The copula of two continuous random variables X_i and X_j with $i \neq j$ is the function C such that their joint distribution can be written according to equation (2.1) [51]. For one parameter copula families, the vector of parameters $\boldsymbol{\theta}$ in equation (2.1) provides a relationship between the copula and measures of association namely rank correlation (r) which assess the strength of the monotonic relationship between variables.

$$F_{X_i,X_j}(X_i, X_j) = C_\theta \left[F_{X_i}(X_i), F_{X_j}(X_j)\right] \tag{2.1}$$

In an GCBN, different bivariate copulas parameterized by rank correlation so that zero correlation implies independence, can in principle be used for different arcs. For large models, the usage of the Gaussian copula grants computational advantages. In fact, this is the main advantage of the choice of Gaussian copulas in our framework. In [59] the authors have provided evidence for accepting the Gaussian copula as a valid underlying model for WIM data when compared with the Gumbel and Clayton copulas. As will be seen later in Section 2.5, the choice of the Gaussian copula still renders valid results for applications of the proposed model. Hence, to simplify and reduce the joint distribution sampling, the Gaussian copula is assumed. The Gaussian copula, with ρ as a parameter, is given by equation (2.2). Where Φ_ρ is the bivariate standard normal cumulative distribution function with product-moment correlation ρ and Φ^{-1} the inverse of the one dimensional (1D) standard normal distribution function. A correlation equal to 0 implies independence for the Gaussian copula.

$$C_\rho(u, v) = \Phi_\rho[\Phi^{-1}(u), \Phi^{-1}(v)]; (u, v) \in [0, 1]^2 \tag{2.2}$$

The dependence measure of interest is the conditional rank correlation due to its relationship with conditional copulas. The conditional rank correlations of X_i and X_j given $X_k = x_k, ..., X_z = x_z$ are [51]:

$$r(X_i, X_j \mid X_k = x_k, ..., X_z = x_z) = r(\widetilde{X_i}, \widetilde{X_j}) \tag{2.3}$$

where $\widetilde{X_i}$ and $\widetilde{X_j}$ have the conditional distribution of $X_i, X_j \mid X_k = x_k, ..., X_z = x_z$. Mathematical details can be found in [60].

[1] In previous literature, Gaussian copula-based Bayesian Networks are sometimes referred to as “non-parametric" Bayesian networks (NPBN). This study uses however sometimes parametric one-dimensional margins and hence the name “Gaussian copula-based Bayesian Network" is used.

The relationship between the parameter ρ and the Gaussian copula correlation r is given by equation (2.4) [61]. Partial correlations can be computed from correlations with the recursive equation (2.5) [62]. Partial correlations are equal to conditional correlations for the joint normal distribution. To compute the correlation matrix of the standard normal transformation of $\mathbf{X}$ by using equation (2.5) and the conditional independence statements of the BN. Rank correlation could be converted to partial correlations with equation (2.4).

$$\rho(X,Y) = 2sin\left(\frac{\pi}{6}r(X,Y)\right) \tag{2.4}$$

$$\rho_{1,2;3,...,m} = \frac{\rho_{1,2;4,...,m} - (\rho_{1,3;4,...,m})(\rho_{2,3;4,...,m})}{\sqrt{(1-\rho^2_{1,3;4,...,m})(1-\rho^2_{2,3;4,...,m})}} \tag{2.5}$$

In an GCBN, the immediate precursor of a node X_i are called parents denoted by $pa(X_i)$. For each variable X_i with m-parents, $X_1 = pa_1(X_i), ..., X_k = pa_m(X_i)$, associate the arc $pa_j(X_i) \rightarrow X_i$ with the rank correlation. The assignment is empty if $pa(X_i) = \emptyset$.

$$\begin{aligned} &r[X_i, pa_j(X_i)], j = 1 \\ &r[X_i, pa_j(X_i) | pa_1(X_i), ..., pa_{j-1}(X_i)], j = 2, ..., m \end{aligned} \tag{2.6}$$

In general, [55] show that given: i) a DAG with m nodes specifying conditional independence relationships in an GCBN; ii) m random variables $X_1, ..., X_m$, assigned to the nodes, with invertible distribution functions $F_1, ..., F_m$; iii) the (non-unique) specification Equation (2.6) of conditional rank correlations on the arcs of the GCBN; iv) a copula realizing all correlations $\in (-1,1)$ for which correlation 0 entails independence; the joint distribution of the m variables is uniquely determined. The joint distribution satisfies the characteristic factorization Equation (2.7) and the conditional rank correlations in Equation (2.6) are algebraically independent.

$$f(X_i, ..., X_m) = \prod_{i=1}^{n} f_{X_i | pa(X_i)} \tag{2.7}$$

The following criteria are established in order to read conditional independence statements of the graph: i) X_1 is not marginally independent of X_3 ($X_1 \not\perp X_3$) i.e. $X_1 \rightarrow X_2 \rightarrow X_3$, ii) X_1 and X_3 are conditionally independent given X_2 ($X_1 \perp X_3 \mid X_2$) i.e. $X_1 \leftarrow X_2 \rightarrow X_3$ and iii) X_1 and X_3 are not conditionally independent given X_2 ($X_1 \not\perp X_3 \mid X_2$) i.e $X_1 \rightarrow X_2 \leftarrow X_3$. In [49, 60] more details and a complete discussion of the semantics of a BN is presented.

In order to find a given conditional distribution, the conditional distribution on the standard normal transformation of $\mathbf{X}$ is calculated. Then, by using the inverse distribution function of each one-dimensional margin, the margins are transformed back to their original units. For a complete treatment of the GCBN framework, the reader is referred to [55] and references therein. Now that the concepts of the GCBN used in this work have been introduced, the steps for building the network of interest will be presented.

2.3 Framework for generating synthetic WIM data

In this section, the methodology to generate synthetic WIM data through Gaussian Copula-based Bayesian Networks is presented. Figure 3.1 shows the whole framework divided into four categories: WIM data, One-dimensional marginal distributions, dependence structure and GCBN output and validation.

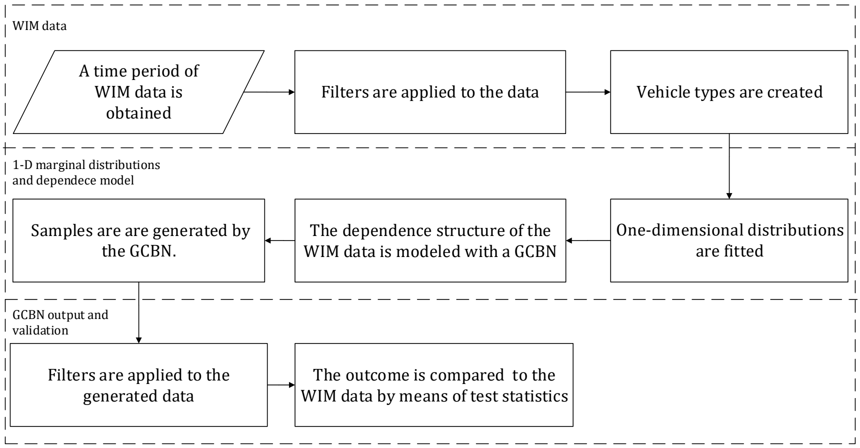

Figure 2.1: Framework for building the GCBN and generating WIM samples.

First, a period of WIM observations is obtained. The data collected through WIM system includes the type of vehicle, road and direction, vehicle length [cm], gross vehicle weight [kN], one observation per axle load [kN], distance from vehicle front to first axle [cm], and one observation per inter-axle distance [cm]. Filters are applied to the data in order to detect and exclude unreasonable measurements or possible errors of the WIM system's vehicle classification algorithm. Then, vehicle types are created either by clustering vehicles based on the number of axles, body configuration (trailer, semi-trailer, bus, single unit, etc.) or vehicle classification according to the classification code of the WIM system (this will be further discussed in section 2.3.1). A one-dimensional probability distribution is fitted for each axle load and inter-axle distance of the created vehicle types (section 2.3.2). Next, the dependence structure of the WIM data is modelled through a GCBN in which the nodes represent the individual axle loads and individual inter-axle distances and the arcs represent probabilistic dependence between connected nodes (section 2.3.3). Once the model has been adequately quantified, a sample of a size similar to the WIM observations in the analysed period is generated by the model. Then, filters are applied to the samples to leave out non-heavy vehicles and unreasonable values. Finally, the outcome is compared statistically with respect to the WIM data (section 2.5). Each step within the framework is detailed next.

2.3.1 Weigh In Motion data

According to [63], a measurement period of about one month outside public holidays in the Netherlands is representative of the traffic load distribution in highways. Thus, WIM data corresponding to April 2013 for three Dutch locations in both the right (-R) and the left (-L) driving directions, were used. The measurements were taken in highways A12 (km

42) Woerden, A15 (km 92) Gorinchem and A16 (km 41) Gravendeel. Thus, in this chapter, when referring for example to data from the A15 in the right direction is written as A15-R and similarly for all other data sources.

The number of observations available ranged from 124 347 in the A15-L to 220 840 in the A16-L. Moreover, previous research shows that WIM observations have a number of incorrect measurements [64],[65], [66]. In this chapter, twenty seven filter criteria were applied as presented in Table A.1.1, described in [27] and [67]. Furthermore, Table 2.1 shows an overview of the number of WIM registrations that were removed based on the filtering criteria.

Table 2.1: Percentage of filtered vehicles.

	A12-L	A12-R	A15-L	A15-R	A16-L	A16-R
Vehicles in the database	165373	161589	124449	124789	220920	203598
Vehicles after filter criteria	161519	152537	120216	121179	215530	199751
% of filtered vehicles	2,3%	5,6%	3,4%	2,9%	2,4%	1,9%

Once the filtering procedure is completed, a total of 264 different vehicle codes were observed in the April 2013 WIM data with five main body configurations: Buses (B), Tractor—Semitrailer—Trailer (R), Tractor—Semitrailer (T), Single-unit multi-axle vehicle and/or Single unit multi-axle vehicle—Semitrailer (V) and Others vehicles (O). Figure A.1.1 shows an overview of the vehicle codes observed in the WIM measurements. The codes used in the WIM system consist of letters and digits that define the sequence of axle groups. For example, a seven axle vehicle with the configuration Tractor—Semitrailer with one axle at the front of the cabin and two at the rear and the rear semitrailer with a quad is coded as T12O4. Notice that the letter O in the T12O4 code represents the semitrailer unit (*oplegger* in Dutch). Because of the database size, it is not feasible to investigate the complete configuration of axle loads for each vehicle. Therefore, 26 vehicle types were created. These are presented in Table 2.2, grouped per vehicle configuration and number of axles. Letters represent the vehicle configuration and digits correspond to the number of axles. The complete table with all vehicle categories in the WIM system is presented in Table A.1.2. It may be observed that in the data corresponding to the A12-L highway all vehicle types are present. However, for the other data sets, two categories were excluded. This is the case of category O6 (according to the notation in the second column of Table 2.2), for data sets A12-R, A16-L, and A16-L and category O11 for data sets A15-L, A15-R, and A16-R. Also, the resulting filtered data does not include vehicles with more than eleven axles.

2.3.2 One-dimensional marginal distributions for individual axle load

Once the data are filtered and the vehicle types are created, for each axle load, a one-dimensional marginal distribution is approximated with a Gaussian Mixture (GM) [68]. Gaussian Mixture distribution has been used in previous studies [32, 69, 70] because of its ability to approximate multi-modal distributions. These are typical for individual axle loads in WIM data. A GM is a weighted sum of G Gaussian densities (each one referred to

Table 2.2: Created vehicle types from most observed WIM observations.

Vehicle (i)	Type	No. Axles (n_i)	Code					
1	B2	2	B11					
2	B3	3	B111	B12				
3	O3	3	O3					
4	O4	4	O4					
5	O5	5	O5					
6	O6	6	O6					
7	O8	8	O8					
8	O9	9	O9					
9	O10	10	O:					
10	O11	11	O>					
11	R5	5	R11111					
12	R6	6	R111111	R11112	R11211	R1122		
13	R7	7	R111121	R11113	R11221	R1123	R1222	
14	R8	8	R112121	R12221	R1223			
15	R9	9	R121221					
16	T3	3	T11O1					
17	T4	4	T11O4	T11O11	T12O1			
18	T5	5	T11O3	T11O21	T11O111	T12O2	T12O11	T21O11
19	T6	6	T11O4	T11O1111	T12O3	T12O21	T12O111	
20	T7	7	T12O4	T12O1111				
21	V2	2	V11					
22	V3	3	V11A1	V12	V21	V111		
23	V4	4	V11A2	V11A11	V13	V22	V211	V1111
24	V5	5	V11A12	V12A2	V12A11			
25	V6	6	V12A12	V22A2	V22V11			
26	V7	7	V22A12					

as a component) expressed as follows:

$$f(x) = \sum_{g=1}^{G} \pi_g \phi\left(x \mid \mu_g, \sigma_g\right) \tag{2.8}$$

where $g = 1, ...G$, $\sum_g \pi_g = 1$ are the mixture weights and $\phi\left(x \mid \mu_g, \sigma_g\right)$ are components of Gaussian densities with parameters μ_g and σ_g .

The expectation maximization (EM) algorithm [71] is used to fit the Gaussian Mixtures to the individual axle load data per vehicle type. The relative goodness-of-fit Akaike information criterion (AIC) [72] is used to choose the best-fitting Gaussian mixture distribution that describes individual axle loads per vehicle type. The AIC score rewards models with high log-likelihood while accounting for the number of parameters to prevent over-fitting. The model with the lower AIC score is expected to have a balance between its ability to fit the data and avoid over-fitting. As a result, the number of components of the fitted distributions ranged from four to seven. As observed in [67], by adding more components, the tail of the fitted distribution function is increasingly dominated by individual observations in the tail of the distribution which would result in an overestimation of individual axle loads. A total of 837 distributions were fitted for all locations. As an example, Figure 2.2 shows the fitted GM distribution function for the vehicle type B3 in highway A15-L, and its parameters are presented in Table 2.3.

Although fitting a GM distribution to axle loads is an appropriate approach, this is not the case for the inter-axle distances because, differently to axle loads, there are a finite number of or vehicle lengths according to vehicle category. Therefore, for each inter-axle

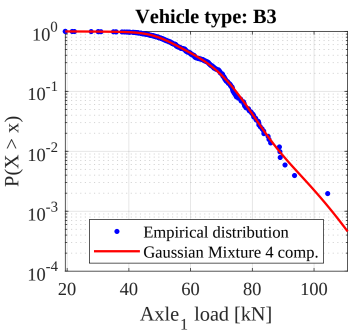

(a)

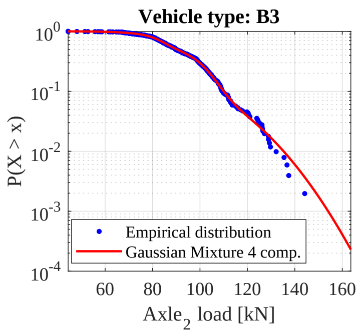

(b)

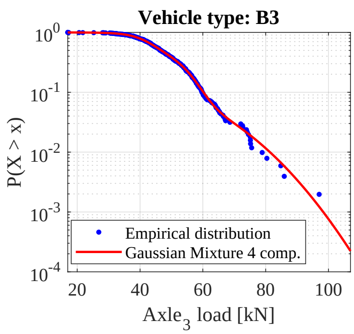

(c)

Figure 2.2: Gaussian mixture of 4 components fitted distribution function for vehicle type B3 in highway A15-L: (a) Axle 1 load [kN]; (b) Axle 2 load [kN]; (c) Axle 3 load [kN].

Table 2.3: Gaussian mixture components for vehicle type B3 in highway A15-L.

Axle 1 load [kN]			
Component	μ	σ	π
1	52.40	5.89	0.506
2	66.13	16.76	0.115
3	68.37	7.01	0.347
4	39.79	12.26	0.032

Axle 2 load [kN]			
Component	μ	σ	π
1	98.67	8.52	0.400
2	70.51	2.92	0.074
3	82.98	3.92	0.260
4	95.89	21.78	0.266

Axle 3 load [kN]			
Component	μ	σ	π
1	51.25	15.47	0.197
2	42.08	5.90	0.358
3	50.66	7.67	0.441
4	99.61	2.45	0.003

distance and vehicle length, the empirical cumulative distribution function (ECDF) is used, defined as:

$$\hat{F}_n(x) = \frac{1}{N+1}\sum_{i=1}^{N} \mathbf{I}\{X_i \leq x\} \tag{2.9}$$

where $\mathbf{I}$ is the indicator function, namely $\mathbf{I}\{X_i \leq x\}$ is one if $X_i \leq x$ and zero otherwise. Now that the data to be used in our framework and the one-dimensional marginal distributions have been described, the characterization of probabilistic dependence is presented.

2.3.3 Dependence

After the one-dimensional marginal distributions for the random variables were selected, the dependence structure of the WIM observations was modelled with a Gaussian copula-based Bayesian Network. A total of 26 submodels, that correspond to each vehicle type are built from each of the six WIM databases. Let $i = \{1, 2, 3, ..., 26\}$ be a set of indices corresponding to the 26 vehicle types, previously presented in Table 2.2, and n a set whose elements represent the number of axles of each vehicle type (see Table 2.2). $X_{i,j}$ denotes the random variable representing the j^{th} axle load. Notice that $j = \{1, ..., n_i\}$ according to the i^{th} vehicle type. X_{i,n_i+1} denotes total vehicle length. Inter-axle distance per vehicle type i is denoted as X_{i,n_i+1+j}. The first inter-axle distance per vehicle type X_{i,n_i+2} corresponds to the distance between the front of the vehicle and the first axle. Our data does not report the distance between the last axle and the end of the vehicle and hence it is not modelled.

Notice that the model assumes that within axle load and inter-axle distance nodes $X_{i,j} \perp X_{i,j-2} | X_{i,j-1}$ for $\forall j$, where $A \perp B|C$ means that A and B are conditionally independent given C. This assumption indicates, for example, that for a particular intermediate axle (or intermediate inter-axle distance), if the values of the loads (or distances) of two axles adjacent to it were known, knowing the value of any other axle load (or inter-axle distance) not adjacent to it would not update the distribution of the particular intermediate axle load (or inter-axle distance).

The gross vehicle weight per vehicle type (GVW_i) is given by Equation (2.10). The total vehicle length of the vehicle type i is $L_i = X_{i,n_i+1}$. Notice that GVW_i and L_i are deterministic functions of vehicle type i. For example, if $i = 2$ (vehicle type B3 according to Table 2.2), then the gross vehicle weight of B3 is the sum of its individual axle loads, i.e. $W_2 = X_{2,1} + X_{2,2} + X_{2,3}$ and its total length is $L_2 = X_{2,4}$. Therefore, GVW is the random variable representing vehicle weight regardless of vehicle type. The distribution of gross vehicle weight is often used when investigating bridge reliability for certain elements of the bridge. Similarly, as for GVW, L is a random variable representing vehicle length regardless of the vehicle type. If the distance between the last axle and the end of the vehicle were to be required, this could be computed per vehicle type as: $X_{i,n_{i+1}} - \sum_i X_{i,n_{i+1+j}}$.

$$GVW_i = \sum_{j=1}^{n_i} X_{i,j} \tag{2.10}$$

As an example, a representation of the GCBN for highway A15-L is shown in Figure 2.3. In this case, $i = \{1, 2, 3, ..., 25\}$. The model consists of 301 nodes and 436 arcs. The arcs represent correlations between axle loads, between axle loads and total vehicle length, and between inter axle distance per vehicle type.

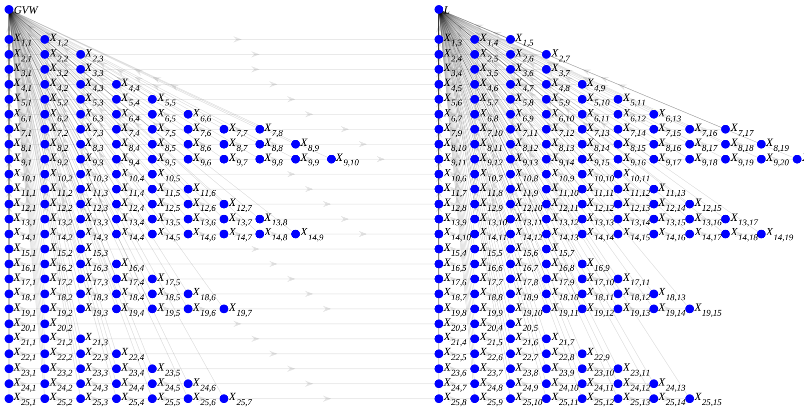

Figure 2.3: BN model for A15-L highway of the WIM system in the Netherlands. The left side of the network represents the $X_{i,j}$ axle loads. The right side represents the vehicle length $X_{i,n_{i+1}}$ and the inter-axle distances $X_{i,n_{i+1+j}}$.

The unconditional rank correlations $r(X_{i,j}, X_{i,j-1})$, for all i and for $j > 1$, between individual axle loads and inter-axle distances per vehicle type for the GCBN A15-L model can be found in Tables A.2.1 and A.2.2. Notice that the correlation of the last axle load (X_{i,n_i}) to total vehicle length $(X_{i,n_{i+1}})$ is also presented. No clear pattern regarding its size or direction is observed across vehicle types. For example, as can be seen in Table A.2.1, the correlation ranges between (roughly) -0.3 and 0.79. A possible reason for this dependence is the design length of the vehicle according to its purpose. For example, longer vehicles might be able to carry heavier loads in the last axle which could explain a correlation as high as 0.79. As mentioned earlier this pattern is not clear across vehicle types. Further investigation of this dependence could be a way to improve the model here presented. The corresponding conditional rank correlations matrices between the random variables, as colour maps, for the six WIM locations can be found in Figures A.2.1 to A.2.3.

In order to implement the GCBN model, a significant update to the MATLAB toolbox BANSHEE [73] has been developed and is presented in the following section.

2.4 Version 1.3 - BANSHEE

This update (v1.3) to BANSHEE introduces a major new functionality and additional features [48]. The original software BANSHEE [73] was released in 2020 and comprised five functions:

(I) `bn_rankcorr`

(II) `bn_visualize`

(III) `cv_statistics`

(IV) `gaussian_distance`

(V) `inference`

These functions allow for quantifying the BN, validating the underlying assumptions of the model, visualizing the network and its corresponding rank correlation matrix, and finally making inferences with a BN based on existing or new evidence. In Version 1.3 of BANSHEE, function (III) has been modfied to make the t copula available. Function (IV) allows for choosing different sample sizes for the validation. Function (V) has been modified to allow users to freely define a one-dimensional parametric distribution function for each node in the BN. Notice that by default non-parametric (empirical) marginal distributions are assigned to the nodes. Additionally, three new functions are available: (VI) `generate_samples`, (VII) `sample_based_conditioning` and (VIII) `conditional_margins_plot`. Function (VI) allows to explicitly increase the number of unconditional samples of the BN. Function (VII) allows conditionalizing nodes on intervals. Function (VIII) allows visualizing the comparison between unconditional and conditional histograms of the BN samples when a non-parametric BN model is used. On the other hand, when a parametric model is used, function (VIII) shows the cumulative distribution functions plots comparison between unconditional and conditional nodes. Figure 2.4 depicts BANSHEE's new structure. For more detailed information on previous functions, the reader is referred to the original paper [73] and to the BANSHEE v1.3 documentation.

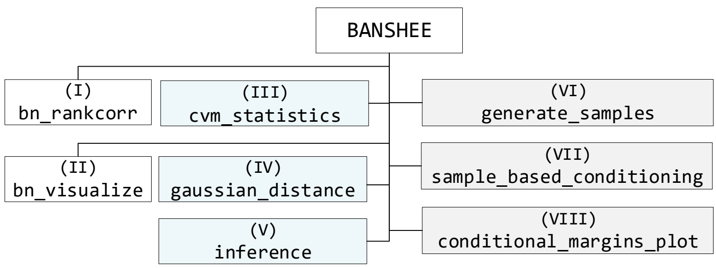

Figure 2.4: Functions (I) to (V) correspond to the main functions of the previous release v1.X. Changes were made in functions (III) to (V) (boxes filled in light-blue). Functions (VI), (VII), and (VIII) (boxes filled in light-grey) correspond to the newly added functions.

The BANSHEE documentation (quick start guide) has been updated, which is now available at https://github.com/mike-mendoza/matlab_banshee. The documentation includes a user guide with examples and how to use the functions available. BANSHEE v1.3 comprises two major changes compared to BANSHEE 1.X: (1) It is possible to quantify fully parametric BNs. The user can employ one-dimensional parametric distribution function for each node in the BN and user-defined (un)conditional rank correlations for the edges and (2) Three new functionalities have been added. These major changes, while retaining the original software functionality, make BANSHEE more robust and versatile overall.

After the detailing of three categories of the framework and the software developed, in the successive section, the results and validation of the GCBN will be presented.

2

2.5 Results

2.5.1 Model output

The output of the model is a data set, similar to the WIM measurements, with 26 columns. The first column corresponds to vehicle type according to the notation in the second column of Table 2.2. The second corresponds to gross vehicle weight (GVW) in kN. Columns 3 to 13 to individual axle loads (A) in kN. The 14th column to total vehicle length (L) in m, the 15th to the distance from vehicle front to the first axle ($D1$) in m, and columns 16 to 25 to individual inter-axle distance in m, i.e. distance from axle 1 to axle 2 ($D2$), distance from axle 2 to axle 3 ($D3$) and so on. Not a number (NaN) strings are placed in fields where no data is computed. An example of the output table is presented in Tables 2.4 and 2.5. Note that the gross vehicle weight is the sum of the individual axle load observations.

Table 2.4: BN model data set output (1st to 13th column).

Type	GVW	A1	A2	A3	A4	A5	A6	A7	A8	A9	A10	A11
V5	303.97	64.74	93.89	48.20	43.53	53.60	NaN	NaN	NaN	NaN	NaN	NaN
T4	222.66	58.27	59.71	51.35	53.33	NaN	NaN	NaN	NaN	NaN	NaN	NaN
...	...	...	...	...	...	...	...	...	...	...	...	...
T3	176.42	59.62	51.29	65.51	NaN	NaN	NaN	NaN	NaN	NaN	NaN	NaN
T6	283.02	58.14	57.4	50.20	35.99	43.29	38.01	NaN	NaN	NaN	NaN	NaN

Table 2.5: Table 2.4 (continued,14th to last column).

L	D1	D2	D3	D4	D5	D6	D7	D8	D9	D10	D11
18.95	1.73	5.21	1.37	6.51	1.42	NaN	NaN	NaN	NaN	NaN	NaN
13.19	12.80	30.40	52.20	1.44	NaN	NaN	NaN	NaN	NaN	NaN	NaN
...	...	...	...	...	...	...	...	...	...	...	...
16.77	20.40	43.50	68.30	NaN	NaN	NaN	NaN	NaN	NaN	NaN	NaN
17.16	16.80	32.10	14.10	5.96	1.36	1.39	NaN	NaN	NaN	NaN	NaN

2.5.2 Validation

To validate the model, one month period of random samples per WIM location were generated from the corresponding GCBN model. As an example, the observed and simulated W and L for the A15-L highway (165 000 random samples) are presented in Figure 2.5. Selected test statistics, the Nash–Sutcliffe model Efficiency Coefficient (NSE) [74] and the Mean Absolute Error (MAE) [75] are summarised in Table 2.6. The NSE takes values in $(-\infty, 1]$, where 1 indicates a perfect fit while the MAE takes values within $[0, \infty)$, where zero indicates a perfect fit.

To graphically assess if the generated synthetic data represent the real WIM observations the scatter plot presented in Figure 2.5 is used. The scatter plot was created by plotting the sorted WIM observations against the sorted synthetic observations for a single simulation. If both datasets are the same, one would expect to see the points lying in a straight line. As can be seen, Figure 2.5a shows that the model slightly underestimates GVW (for this particular realization) in the interval between 900 kN and 1100 kN and Figure 2.5b shows a slight overestimation of L in the interval between 12 m to 17 m. In general, as expected, for axle loads, more deviations with respect to the original data are observed in the tail of the distribution of *GVW*. Nevertheless, the model provides an overall good fit for the data. This can also be observed in the results of Table 2.6, where the values of NSE and MAE for *GVW* and *L* are close to 1 and 0 respectively. For example, for the A15-L highway, the NSE and MAE values for *GVW* are 0.99 and 0.46 respectively, while for *L* the corresponding values are 0.96 and 0.35.

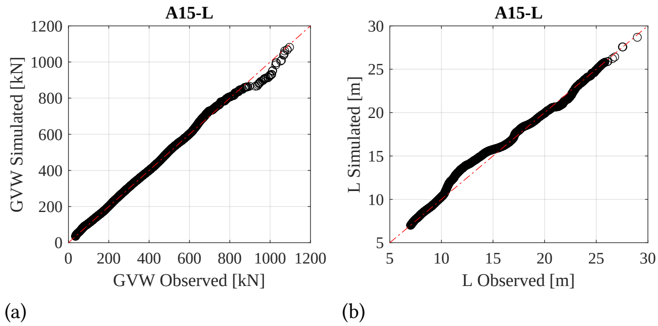

Figure 2.5: Comparison of Gross Vehicle Weight (a) and Total Vehicle Length (b) through a one-month period of observed and simulated data

Table 2.6: Test statistics of the model for different WIM locations in The Netherlands.

Highway	Gross vehicle weight		Total Vehicle Length	
	NSE	MAE	NSE	MAE
A12-L	0.99	0.30	0.98	0.24
A12-R	0.99	0.37	0.98	0.25
A15-L	0.99	0.46	0.96	0.35
A15-R	0.99	0.48	0.97	0.30
A16-L	0.99	0.25	0.97	0.26
A16-R	0.99	0.32	0.97	0.25

Additionally, Figure 2.6 and Figure 2.7 shows the correlation matrix plot of axle loads and inter-axle distances for both, the observed and simulated data. The figures show the results of the most observed vehicle type (T5) at the A15-L highway. Notice that, the correlations of the simulated data between each axle load and the correlation between each inter-axle distance differ slightly compared to the WIM data. This means that the GCBN model, under the assumption of the normal copula, correctly approximates the dependence structure of the empirical data. Furthermore, Figure 2.8 shows the exceedance probability plots comparison of the observed and simulated variables, gross vehicle weight, and total vehicle length at the A15-L. As can be seen in Figure 2.8, the synthetic data shows similar behaviour as the observed data at the tail of the distributions. Figures A.2.4 to A.2.6 show the same comparison plots for the other locations under study. Notice that this corresponds to a single realization of our GCBN. Perfect agreement between the observed data and every simulation is neither expected nor desired. Rather, approximating the general traffic configuration is the aim of the model especially for later use in the investigation of infrastructure reliability.

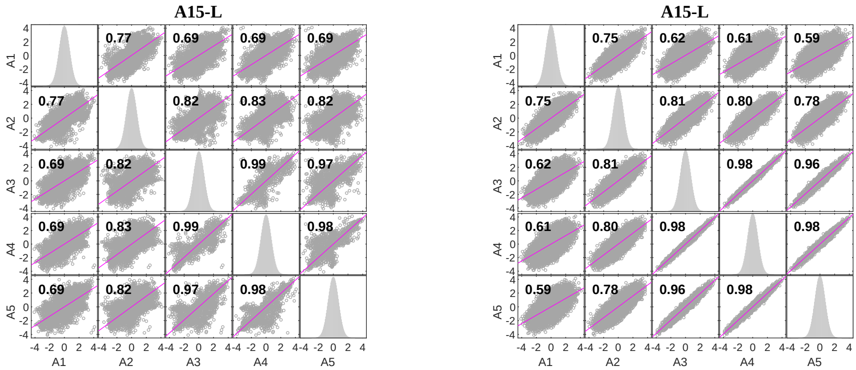

(a) (b)

Figure 2.6: Comparison between axle loads generated by the GCBN model and the WIM data of the T5 vehicle type in highway A15-L: (a) Correlation matrix for the empirical data standard transformed; (b) Correlation matrix for the synthetic data standard transformed

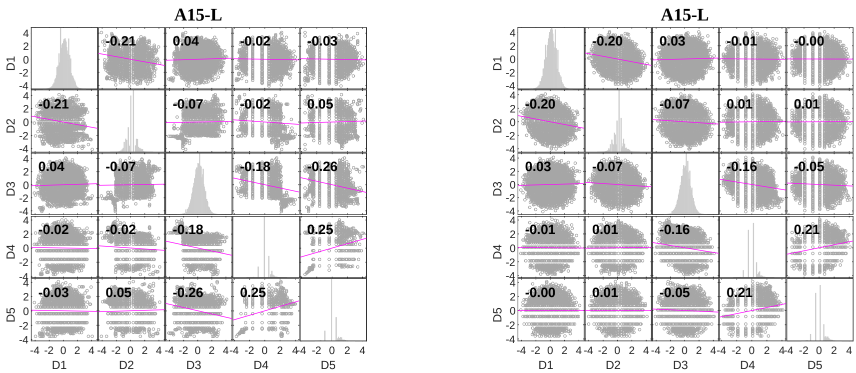

(a) (b)

Figure 2.7: Comparison between inter axle distances generated by the GCBN model and the WIM data of the T5 vehicle type in highway A15-L: (a) Correlation matrix for the empirical data standard transformed; (b) Correlation matrix for the synthetic data standard transformed

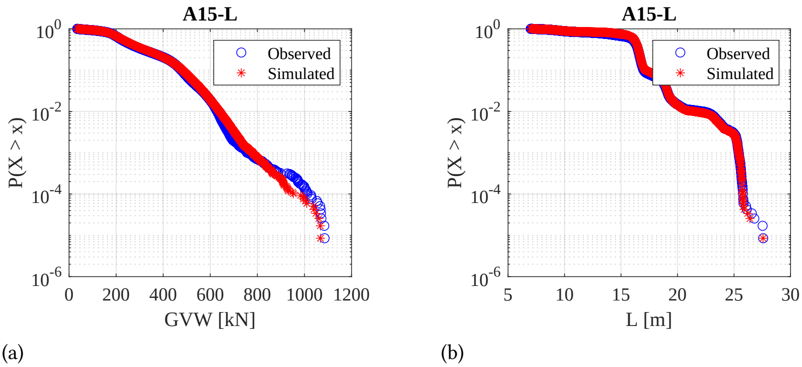

Figure 2.8: Exceedance probability plots comparison between variables of interest (W and L) generated by the GCBN model and the WIM data in highway A15-L: (a) Gross vehicle weight distribution [kN] for original data and data generated with GCBN model. (b) Total vehicle length distribution [m] for original data and data generated with GCBN model.

Diverse engineering applications are often interested in determining the extreme observations of the phenomena. Thus, accurate synthetic data should be able to approximate them. Table 2.7 shows the load corresponding to the heaviest (Max GVW) and longest vehicles (Max L) in the original data. It shows their corresponding exceedance probability and the value observed in one simulation of the GCBN for the same probability of exceedance $P(X > x) = 1 - P(X \leq x)$. This is shown for the six locations under investigation. For example, the heaviest vehicle observed at A15-L has a total weight of 1085.89 kN with a probability of exceedance of $P(X > x) \approx 8.52E-06$ (as can be seen in Figure 2.8a). The gross vehicle weight in the simulation with a probability of exceedance of $8.52E-06$ has a GVW of 1067.94 kN. This means that the difference between observed and simulated Max GVW at A15-L is around 1.62%. Similarly, the longest vehicle observed at A15-L has a $L = 27.58$ m with $P(X > x) \approx 8.52E-06$ (see Figure 2.8b). The total vehicle length in the simulation with a probability of exceedance of $8.52E-06$ has a $L = 27.57$ m. The resulting difference between observed and simulated Max L at A15-L is around 0.4%. According to Table 2.7, highway A12-R has the biggest difference for Max W and Max L with 2.59% and 3.58%, respectively. The smallest difference can be found in highway A16-R with 0.06% for Max GVW and 0.88% for Max L. Overall, the differences between the estimations from the observed and simulated data are minor for all study locations. This shows that the performance of the method and GCBN models can be considered effective. In order to further investigate model validity a split-sample analysis is performed. Appendix A.2 presents a comparison between synthetic data generated by the model quantified with the training data set (80%) and the observations of the test data set (20%). This is a commonly used split fraction in traffic analysis (see [76–78], for example). The observations correspond to the A16-R highway. From these results, it is clear that the performance of the model is in agreement with the results of the GCBN model quantified with the unsplit data set. In order to profit from all data available, further, all our analysis is performed with models quantified with the full data set.

Next, to show the adaptability of the framework, two case studies are presented in Section 2.6: (i) a GCBN quantified using data of a Dutch city road by classifying vehicle types according to the number of axles, and (ii) a GCBN using data of a Brazilian highway, classifying vehicle types according to the automatically generated WIM vehicle codes.

Table 2.7: Comparison of the simulated heaviest and largest vehicles.

highway	$P(X > x)$	Observed Max GVW [kN]	Simulated Max GVW [kN]	Difference %	Observed Max L [m]	Simulated Max L [m]	Difference %
A12-L	6.19E-06	1080.50	1090.01	0.88	29.62	29.05	1.92
A12-R	6.54E-06	1096.87	1068.43	2.59	29.36	28.31	3.58
A15-L	8.52E-06	1085.50	1067.94	1.62	27.58	27.57	0.04
A15-R	8.34E-06	1085.89	1075.20	0.98	29.11	28.93	0.62
A16-L	4.67E-06	1016.26	1007.44	0.87	28.36	28.26	0.35
A16-R	5.03E-06	1044.21	1044.80	0.06	27.23	27.47	0.88

2.6 Case studies

2.6.1 GCBN from Rotterdam city WIM data

One WIM station in the municipality of Rotterdam (South Holland, The Netherlands) is considered for this case study. The WIM system was located in the bridge *Beukelsbrug* in the S115 city route. The observations correspond to May 2013. In total, 14 different heavy vehicle codes were observed in the S115 WIM data set. The WIM recorded vehicle codes are only numbers that define the sequence of axle groups. These codes differ from the ones found in the WIM system of the Dutch highways described in Section 2.3.1. Hence, a similar classification as the one presented in Table 2.2 is not possible.

Moreover, Figure 2.9 shows a comparison of the exceedance probability plots of GVW and L between the Dutch WIM locations (A16-L with the lowest heavier GVW observation and A12-R with the highest heavier GVW measurement) and the S115 location. As can be seen in Figure 2.9, as expected, heavier and longer vehicles circulate on the Dutch highways compared to those circulating on regional roads. Consequently, the GCBN purposed in Section 2.3.2 does not meet the requirements to compute similar S115 city route WIM observations. Hence as a consequence, a new model has to be quantified with data from Rotterdam. By modifying the vehicle classification and then applying the framework described in Section 2.3, the synthetic WIM data can be generated. For this case study, vehicle types were created grouping them by the number of axles. Therefore, four vehicle types were generated as presented in Table 2.8.

Table 2.8: Created vehicle types WIM vehicle codes grouped by number of axles.

Vehicle (i)	Type	No. Axles (n_i)	Codes				
1	2 axles vehicle	2	2	11			
2	3 axles vehicle	3	12	21	111		
3	4 axles vehicle	4	22	31	211	1111	
4	5 axles vehicle	5	212	221	311	1211	2111

A total of 14 Gaussian Mixtures (9 Gaussian mixtures of 4 components, 3 GM of 5 components and 2 GM of 6 components) were fitted to the axle loads choosing the best

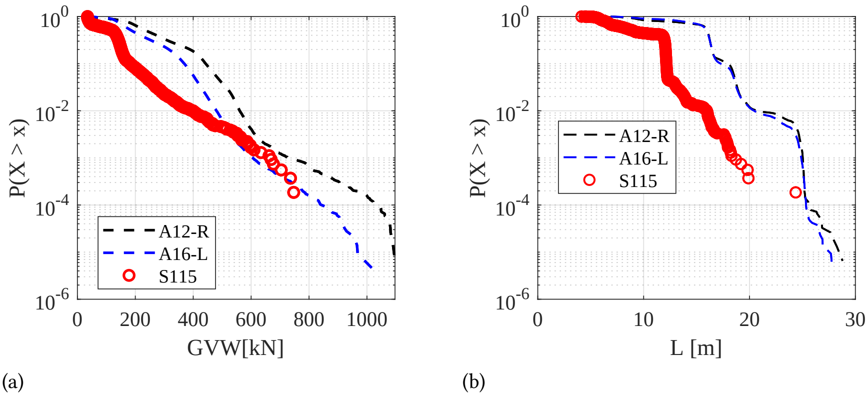

Figure 2.9: Exceedance probability plots of: (a) Gross vehicle weight [kN] and (b) Total vehicle length [m] for the locations: A12-R, A16-R, and S115.

fit according to the AIC criterion. Figure 2.10 shows the GCBN model for the S115 WIM location with $i = \{1, 2, \ldots 4\}$. The DAG consists of 34 nodes and 46 arcs. A random sample with a size similar to the WIM observations was generated from the GCBN model. The comparison between the S115 location WIM data and that generated by the model is presented in Figure 2.11. The figure was generated with 6000 samples. As can be seen, the Figure 2.11a shows that the model slightly underestimates *GVW* in the interval between 400 kN to 600 kN. In Figure 2.11b no important deviations are presented. Overall, the model approximates well the measured gross vehicle weight and total vehicle length.

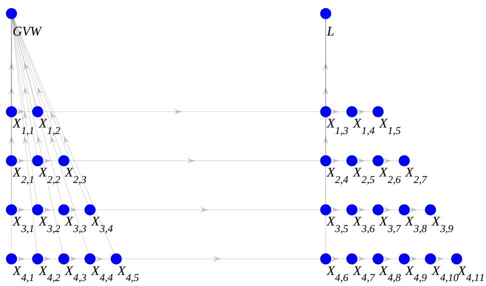

Figure 2.10: GCBN model for S115 road WIM location. The left side of the network represents the $X_{i,j}$ axle loads. The right side represents the vehicle length $X_{i,n_{i+1}}$ and the inter axle distances $X_{i,n_{i+1+j}}$.

2.6.2 GCBN from Araranguá, Brazil WIM data

For this case study, WIM data provided by the Transport and Logistics Laboratory (LabTrans) of the Santa Catarina Federal University (UFSC for its acronym in Portuguese) is analysed using the automatically determined WIM codes to assign vehicle types. The data was gathered at the Federal Highway route BR-101 km 418, located in the city of Araranguá

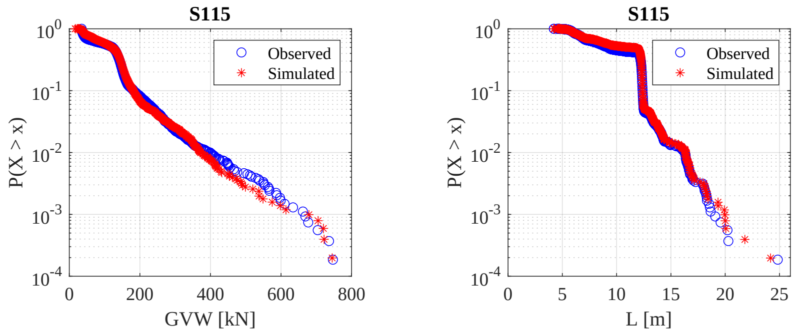

(a) (b)

Figure 2.11: Comparison between variables of interest generated by the GCBN model and the WIM data in S115 location: (a) Gross vehicle weight distribution [kN] for original data and data generated with the GCBN model, (b) Total vehicle length distribution [m] for original data and data generated with the GCBN model.

in the South of Brazil. The measurements were taken in April 2014. The data set has a total of 66 820 vehicles with gross vehicle weight above 34 kN.

Following the framework for generating WIM synthetic data, described in Section 2.3, the WIM database is analyzed. About 6.2% of the observations were excluded and 45 different classification codes were found with vehicles from 2 up to 8 axles. The codes were automatically determined by the WIM system according to the Brazilian National Department of Transport Infrastructure (DNIT for its acronym in Portuguese) [79]. As stated in [79], the numbers in the code correspond to the number of axles and the letters to vehicle classification. To name a few: C is a Tractor—Trailer, S a Tractor—Semitrailer, and I is a Trailer—Semitrailer with an inter-axle distance of more than 2.4 m. Letter D corresponds to a tandem (group of 2 axles), T to a tridem (group of 3 axles), and Q to a quad (group of 4 axles). For example, a 2C2 vehicle represents a Tractor with 2 axles plus a 2 axles Trailer. The 45 classification codes (or vehicle types) are presented in Table 2.9.

Table 2.9: Registered vehicle classification codes in the WIM data set of BR-101 highway. April 2014.

Vehicle(i)	Type	No. Axles(n_i)	Vehicle(i)	Type	No. Axles(n_i)	Vehicle(i)	Type	No. Axles(n_i)
1	2C	2	16	3C	3	31	3S2	5
2	2C2	4	17	3C2	5	32	3S3	6
3	2CB	2	18	3C3	6	33	3T4	7
4	2D4	6	19	3D4	7	34	3V5	8
5	2DL	4	20	3DB	3	35	4C	4
6	2I1	5	21	3DL	5	36	4CD	4
7	2I2	4	22	3I1	6	37	4DB	4
8	2I3	5	23	3I2	5	38	4DT	7
9	2LD	5	24	3I3	6	39	4R2	6
10	2N3	5	25	3JD	6	40	Unknown 3 axles	3
11	2N4	6	26	3LD	6	41	Unknown 4 axles	4
12	2S1	3	27	3N3	6	42	Unknown 5 axles	5
13	2S2	4	28	3P5	8	43	Unknown 6 axles	6
14	2S3	5	29	3QD	7	44	Unknown 7 axles	7
15	3BC	3	30	3S1	4	45	Unknown 8 axles	8

A total of 230 Gaussian Mixtures were fitted to one-dimensional axle loads choosing the best fit according to the AIC criterion. Next, the dependence structure can be constructed. Figure 2.12 shows the GCBN model for the BR-101 highway with $i = \{1, 2, \ldots 45\}$. The network consists of 507 nodes and 735 arcs. Finally, a random sample with a size similar to the WIM observations was generated from the GCBN model. The comparison between the BR-101 WIM data and that generated by the BN model is presented in Figure 2.13. The figure was generated with 71 000 samples as described in Section 2.3.3.

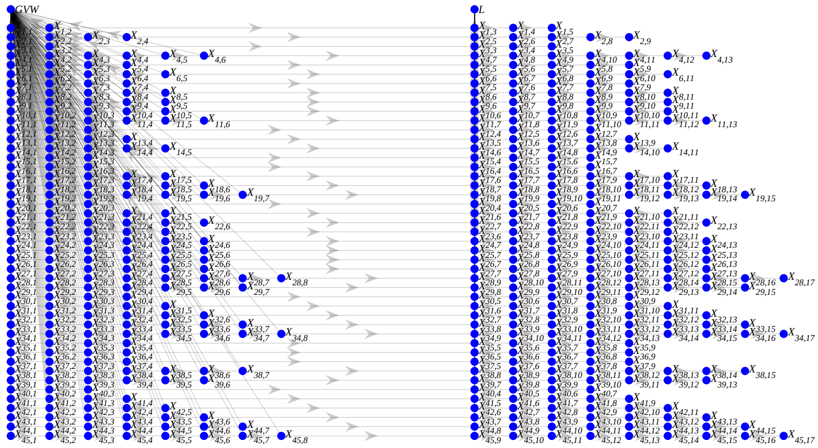

Figure 2.12: GCBN model for the 45 vehicle types of the WIM system in BR-101 highway located in Araranguá, Brazil. The left side of the network represents the $X_{i,j}$ axle loads. The right side represents the vehicle length $X_{i,n_{i+1}}$ and the inter-axle distances $X_{i,n_{i+1+j}}$.

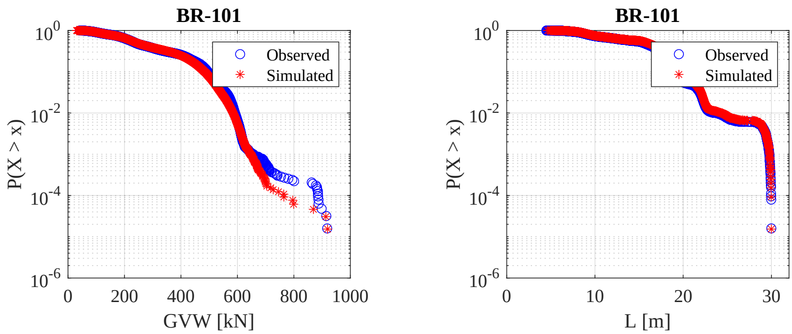

(a) (b)

Figure 2.13: Comparison between variables of interest generated by the GCBN model and the WIM data in BR-101 highway: (a) Gross vehicle weight distribution [kN] for original data and data generated with the GCBN model; (b) Total vehicle length distribution [m] for original data and data generated with the GCBN model.

As can be seen in Figure 2.13a, the exceedance probability computed with synthetic observations shows a deviation in the interval of 750 kN to 850 kN with respect to the one computed with WIM measurements. Nevertheless, the model still approximates the maximum values of the empirical distribution. The computed values for *L* are quite similar to the observed ones (see Figure 2.13b). As has been noted, in this case, the methodology for computing synthetic WIM observations also approximates the data. The results are consistent for all studied WIM locations. In the following section, a Graphical User Interface (GUI) for the six Dutch WIM highway locations will be presented. The GUI illustrates a possible use of the model when WIM data is not available. The GUI is used to compute synthetic WIM observations using data collected through (for example) traffic counters as input.

2.7 Graphical User Interface application

When WIM data is not available due to the scarcity or absence of proper equipment, the most utilized devices to collect traffic data are the pneumatic road tubes. The change in air pressure within the tube is measured as the vehicle's wheels pass over the tube [35]. Pneumatic road tubes are mainly used for vehicle classifications, estimation of average daily traffic and estimation of direction of travel. Consequently, information regarding axle loads and inter-axle distances can not be collected. Therefore, to have an insight into possible axle loads and axle inter-distances the GCBN described in Section 2.3 with data obtained from pneumatic road tubes as input, i.e. vehicle classification and proportion of vehicle types, can be used.

A simple stand-alone Graphical User Interface (GUI) of the six Dutch highways WIM locations model described in Sections 2.3.1 to 2.3.3 has been developed. Notice that no fitting or goodness of fit procedures are implemented in the GUI. Rather, the results from the fitting and goodness-of-fit procedures, BANSHEE v1.3, and the created vehicle types introduced in Section 2.3.2 are the core of the GUI engine. To exemplify the use of the GUI, a speculative example is presented. Using data from pneumatic road tubes gathered in the low-speed lane of the Paseo Tollocan Avenue (Mexican federal highway 15) located in the city of Toluca Mexico. The data was obtained in the last week of August 2014. The information was provided by the Autonomous University of the State of Mexico (UAEMex). Table 2.10 shows the number of observed vehicles per vehicle type according to the vehicle classification of the Ministry of Communications and Transport (SCT for its acronym in Spanish) of Mexico [80]. Table 2.10 shows also the GCBN equivalent vehicle types (matched with the Mexican types according to their body configuration) and the proportions of the registered vehicles by the pneumatic road tubes.

Now, it is possible to enter the information in Table 2.10 into the GUI (see Figure 2.14) to compute the axle loads and inter-axle distances together with gross vehicle weight and total vehicle length. Thus, the information obtained by the pneumatic road tubes is extended. It is noted that the matched SCT and WIM GCBN vehicle types shown in Table 2.10 may not precisely mirror reality, given the substantial variations in truck populations across different nations. However, we employ this approach purely for illustrative purposes, using the matched types as examples to show the GUI's functionality.

The output of the GUI are histograms (Figure 2.15a) and exceedance cumulative plots (Figure 2.15b) of *GVW* and *L*. Additionally, the computed observations can be stored in a comma-separated value (CSV) file. For this example, to compute the observations, the so-called "Hypothetical highway" which is the mixture of the six available highways in

Table 2.10: Selected corresponding vehicle types.

SCT	WIM GCBN	No. Vehicles	Proportion
B2	B2	11041	0.68000
C2	V2	3576	0.22020
C3	V3	887	0.05462
C4	V4	2	0.00012
T2S2	T4	7	0.00043
T3S2	T5	523	0.03220
T3S3	T6	184	0.01133
T2S1R2	R5	2	0.00012
T2S2R2	R6	10	0.00062
T3S2R2	R7	3	0.00018
O9	O9	5	0.00031
Total		16240	1

the GUI is used. This means that each computed observation comes from one randomly selected GCBN Dutch highway model. A quick user guide for the GCBN WIM graphical user interface can be found in A.3.

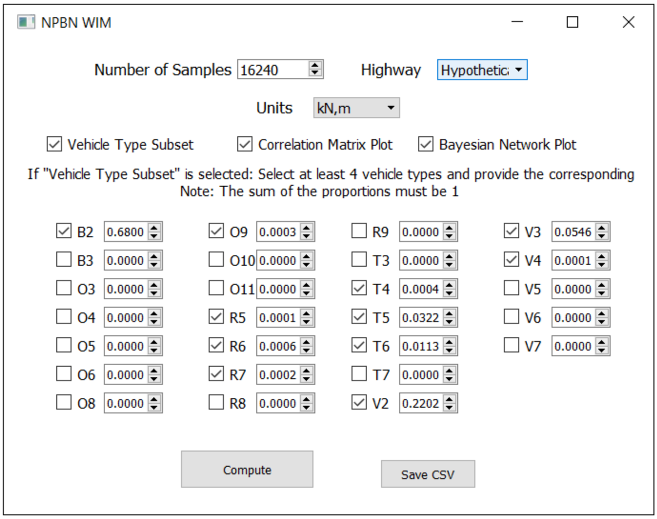

Figure 2.14: GUI Main window

As can be seen in Figure 2.15, the maximum GVW is around 600 kN and the maximum L is approximately 25 m. The most frequent vehicles are the ones with 100 kN to 150 kN and those with a total length of 11 m to 12.5 m. Which correspond to Buses (B2) and single-unit two-axle vehicles (V2) representing around 90% of the total observed vehicles.

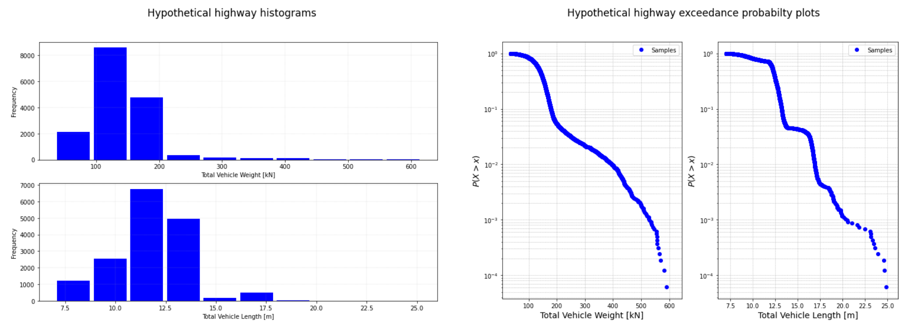

(a) (b)

Figure 2.15: GCBN WIM GUI output: (a) *GVW* and *L* histograms. (b) *GVW* and *L* exceedance probability plots.

2.8 Conclusions

An improved methodology to compute synthetic WIM observations of heavy vehicles through GCBNs has been presented. The model provides data that describes: vehicle type, gross vehicle weight, individual axle loads, total vehicle length, and inter-axle distances. In total eight high dimensional GCBNs with up to 507 nodes and 735 arcs were quantified. The first six GCBNs were quantified with data corresponding to six WIM locations of the highway network of the Netherlands. 26 vehicle types were created grouping the registered vehicles in the WIM data set per vehicle configuration and per number of axles. The seventh GCBN was quantified using WIM observations collected in a city route in Rotterdam City, The Netherlands. 4 vehicle types were created classifying vehicle types by the number of axles. Data collected in Araranguá city in Brazil were used to quantify the last GCBN. For this model, 45 vehicle types were created according to the vehicle classification WIM codes.

The GCBN models properly simulate the dependence structure of the empirical data. The correlations of the simulated data between axle loads and inter-axle distances slightly deviate from the ones computed with the WIM observations. Small differences in the exceedance probabilities of the empirical and simulated data can be observed for *GVW* in the range of 800 kN to 1000 kN. For *L*, the models show a minor overestimation of the exceedance probabilities of lengths in the interval between 12 m and 17 m. Nevertheless, the models provide a good fit for the data. Values of NSE for *GVW* and *L* are in the interval of 0.97 to 0.99 and, while for MAE are in the range of 0.24 to 0.48. The difference between the estimation of the tail of the distributions, i.e., the heaviest vehicle and longest vehicle for the same probability of exceedance are around 0.04% and 3.6%. In general, it can be noted that all presented GCBN models correctly approximate the WIM observations. Additionally, to make use of the GCBN model more convenient, a Graphical User Interface (GUI) for the models of the six Dutch WIM highways has been developed. A potential application of the model when WIM data is not available was presented by using the GUI to compute synthetic WIM observations. Using data collected through traffic counters, gathered in Toluca City in central Mexico, as input.

The framework for computing synthetic WIM observations here presented can be applied in any WIM location, using site-specific WIM records and site-specific vehicle types. The key aspect of the methodology is a good assessment of the vehicle types when constructing the model. Usually, previous studies have constructed vehicle types by grouping per number of axles. This vehicle classification works. However, often more insight into the different vehicle types is required. In these cases, a better classification can be performed, for example, by using the WIM automatically generated codes or grouping vehicles by body configuration. Our methodology allows the use of these classifications. Thus, more accurate data can be simulated. The next steps in our research correspond to the application of the models here presented in risk and reliability of individual infrastructure (bridges for example) and road networks including multiple infrastructures.

3

Mapping hazardous locations on a road network due to extreme gross vehicle weight.

This chapter investigates the application of hazard maps in identifying critical locations associated with extreme vehicle load events. Examining extreme vehicle loads can offer valuable insights into the reliability of road infrastructure. Weigh-In-Motion (WIM) systems are commonly employed for this purpose; however, their limited availability often necessitates the use of less-sophisticated traffic counters (LSTCs). Unfortunately, LSTCs are unable to measure vehicular axle loads, posing a significant drawback. To overcome this limitation, this chapter proposes a methodology that utilizes data from LSTCs to estimate axle loads and map extreme gross vehicle weights. To demonstrate the feasibility of this approach, a case study concentrating on the major highway corridors in Mexico is presented. While WIM stations are absent, data from a network of 1,777 counting stations and origin-destination surveys are available. By quantifying Gaussian copula-based Bayesian networks using the existing information, synthetic site-specific axle loads are generated. Subsequently, gross vehicle weights for selected return periods are computed. The study findings facilitate the identification of hazardous locations for road infrastructure due to extreme gross vehicle weights. Additionally, an interactive web map and a graphical user interface to generate synthetic axle loads are provided. These tools, along with the proposed methodology, can serve as the foundation for maintenance strategies for existing roads and bridges.

Parts of this chapter have been published verbatim in **Mendoza-Lugo, M. A.**, Morales-Nápoles, O. (2023). Mapping hazardous locations on a road network due to extreme gross vehicle weights. Reliability Engineering and System Safety. doi: https://doi.org/10.1016/j.ress.2023.109698 and Koot, P., **Mendoza-Lugo, M.A.**, Paprotny, D., Morales-Nápoles, O., Worm, D.T.H., Ragno, E. (2023). PyBanshee version (1.0): A Python implementation of the MATLAB toolbox BANSHEE for Non-Parametric Bayesian Networks with updated features. SoftwareX. doi: https://doi.org/10.1016/j.softx.2022.101279

3.1 Introduction

Healthy infrastructure and road systems are fundamental requirements for economic success since they facilitate the mobility of people and goods and provide links that support international trade [1, 2]. However, road infrastructure is under increasing pressure. On one hand, a large part of the highway infrastructure is outdated, which means that many of the roads and their assets need to be repaired or replaced. On the other hand, the percentage of trucks that exceed the maximum legal weight is increasing. Nowadays, truck overloading is a common phenomenon throughout the world, especially in developing countries [7–10].

In terms of traffic loads, hazardous road locations are sites where infrastructure damage may occur due to extremely overloaded vehicles. These are locations where the extreme values of gross vehicle weights (EGVW) exceed those of non-overloaded trucks. Consequently, areas with heavier truck traffic may be more likely to exceed design load limits. By using hazard road location maps and analyzing trends, it becomes possible to identify areas of potential risk, thereby facilitating the development and implementation of maintenance strategies.

To map extreme gross vehicle weights (EGVW), it is essential to measure individual axle loads, typically obtained through WIM systems. In cases where information on individual axle loads is limited or unavailable, computer simulations have become the most prominent approach to estimating them. Due to the intricate nature of vehicle configurations, the dependence structure of the data becomes complex. Among the available tools, Bayesian Networks (BNs) have been used for modelling WIM data [51, 59, 81] as they provide a means to represent the intricate dependency structures inherent in WIM data. Furthermore, BNs enable inference in the presence of evidence.

While numerous studies and techniques have focused on data generation and collection, the mapping of extreme traffic loads using information obtained from LSTCs remains limited. To address this gap, this chapter introduces a framework for estimating and mapping site-specific traffic loads in locations where WIM systems do not serve as the primary source of traffic data. The development of the methodology in this study is guided by three primary objectives: (a) conducting a large-scale simulation of site-specific traffic loads, (b) accurately estimating EGVWs across an entire road network, and (c) performing spatial analysis through the utilization of geographic information system (GIS) software.

The proposed methodology consists of five essential tasks: (i) analysis of available traffic data, (ii) simulation of site-specific traffic loads, (iii) extreme value analysis to assess gross vehicle weights, (iv) generation of return period maps, and (v) identification of hazardous locations due to EGVWs. To accomplish these objectives, this chapter introduces a straightforward method that employs GCBNs to simulate site-specific synthetic axle loads of heavy vehicles. Moreover, it utilizes extreme value theory to estimate EGVWs. The methodology offers various advantages. Firstly, it demonstrates the capability to identify locations requiring attention based on the model's assessment of their condition. Secondly, the methodology requires basic information concerning traffic characteristics. Lastly, the methodology proposed exhibits the flexibility to be applied to any road network, enhancing its adaptability and applicability. To implement the proposed methodology, the fifteen major highway corridors in Mexico are selected as a case study. This selection was motivated by the limited utilization of WIM systems in the country and the unavailability of WIM public databases. In total, a comprehensive set of 1777 site-specific BNs were quantified to simulate over 180 million heavy vehicles for assessing the studied road network.

The value of the proposed methodology is to provide an accurate estimation of the characteristic loads that can assist in the identification of hazardous locations, taking into account site-specific information on traffic configuration and a non-site-specific distribution of axle loads per vehicle type when WIM data is not available at the network level but LSTCs data is. To do so, the appropriate statistical dependence of axle loads per vehicle type is described through site-specific BNs. Simpler models that ignore such dependence or the site-specific character of the traffic configuration would lead to a severe overestimation of the characteristic loads.

In subsequent sections, the proposed framework to identify hazardous locations and the case study will be presented (Section 3.2). Next, the available datasets will be explained in Section 3.3. Then, in Section 3.4 the model with the variables considered in the research along with its use in the road network is presented. Later, in Section 3.6 extreme value analysis is employed to estimate gross vehicle weights for 50 and 1000-year return periods. Section 3.7 present the results of the practical application of the methods proposed in Section 3.4 and Section 3.6. Finally, in Section 3.8 the conclusions of the research will be drawn.

3.2 Mapping hazardous locations framework

In this section, the methodology to identify and map hazardous locations on a road network due to extreme gross vehicle weights is presented. GCBN is used to simulate site-specific gross vehicle weight distributions and extreme value analysis of gross vehicle weights to find the gross vehicle event with selected return periods at a specific site. Figure 3.1 shows the proposed framework. First, the available traffic data sources of the road network of interest are gathered, cleaned, and analysed to obtain the variables of interest. The variables of interest are the type of vehicle, gross vehicle weight and individual axle loads (Section 3.3). It is important to note that special vehicles, such as large cranes or other oversized trucks that require a special permit to circulate, are excluded from the calculation of gross vehicular weight presented in this chapter. It is assumed that the authorities are aware of these vehicles and that special measures are taken for the movement of these vehicles to ensure that they do not pose a hazard to the public and the infrastructure. Then, site-specific synthetic observations are generated using an GCBN quantified with origin-destination information (Section 3.4). Next, a gross vehicle weight extreme value analysis is performed to obtain characteristic values with selected return periods (Section 3.6). Then, the computed extreme gross vehicle weights are mapped and spatial analysis is performed (Section 3.7.1). Finally, the generated maps allow for identifying clusters of vehicular weights whose 50- or 1000- years return periods are high, hence, hazardous locations can be spotted (Section 3.7.2.).

In this research, the fifteen Mexican major highway corridors have been chosen to test how the methodology works. Mexico has around 377 659 km of highway network divided into four main sub-networks: i) federally administered network, ii) feeder network, iii) rural network and iv) improved road network. The federally administered network is the main component of the national road transportation system. It serves around 98% of the passengers that move between cities and around 74% of the land cargo [82]. The

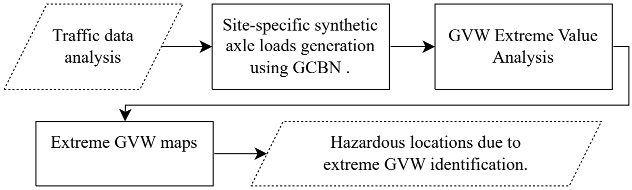

Figure 3.1: Framework for identifying and mapping hazardous locations.

increase in demand in Mexico due to economic and population growth will be translated into growth in the number of vehicles transiting the road network and increased vehicle loads. An important part of the federally administered highway network are the 15 major highway corridors (MHC), presented in Figure 3.2. The Network is shown in Figure 3.2 is managed by the Ministry of Communications and Transportation (SCT, for its acronym in Spanish). It is the pillar of the national transportation system, linking different regions of the country and connecting important cargo and passenger hubs. In the following sections, each step within the framework is detailed.

Figure 3.2: Major highway corridors.

3.3 Traffic data

This section describes the two sources of data used: the statistical field study of the domestic road transportation database and the road data database. In addition, the information provided by each of these two sources is outlined and the variables of interest are presented.

3.3.1 EECAN database

The Statistical Field Study of Domestic Road Transportation (EECAN, for its acronym in Spanish) database is a compilation of data of vehicles travelling through origin-destination survey stations (SS) installed in the federally administered highway network [83]. The surveys have been conducted for four consecutive days per year by the Mexican Ministry of Communications and Transports, in a varying number of stations surveyed every year from 1991 until 2017. For example, three survey stations were installed in 1992 and twenty-seven stations were installed in 1994, representing the lowest and highest number of stations installed respectively in the years where surveys were conducted. The EECAN database presents information regarding vehicle attributes (such as plate, occupants, vehicle type, vehicle weight and axle weights), transported load and origin-destination data. In particular, the information concerning vehicle attributes is of interest, i.e., vehicle type, gross vehicle weight (gvw) and individual axle weights.

In total, 366 survey stations have been installed of which 223 (from 2002 until 2017) are publicly available on the website of the Mexican Transport Institute (IMT, for its acronym in Spanish) [84]. The 223 stations include data from about 1.3 million surveyed vehicles. The recorded EECAN measurements were filtered according to previous literature regarding the filtering rules for identifying erroneous axle load data [27, 67, 85]. The following criteria are applied: (i) Gross vehicle weight under 34 kN (3.5 t). Only heavy vehicles are considered. (ii) Sum of axle loads not within 0.49 kN of the gross vehicle weight. (iii) Any axle load exceeding 147 kN (15 t) where this axle represents more than 85% of the gross vehicle weight. (iv) Any axle weight larger than 392 kN (40 t). The reliability of an individual truck's record is questioned if any axle load exceeds 40 t. (v) Mismatch between vehicle type and the number of axle loads, and (vi) duplicate records. Note that (ii) and (iii) are employed as established in the basic data cleaning criteria of WIM data in Slovakia. [85].

After all the filters were applied, the most common heavy vehicles (V) types are: $\mathtt{C2}$, $\mathtt{C3}$ (single unit vehicles with two or three axles), $\mathtt{T3S2}$ (three-axle tractor plus two-axle semitrailer), $\mathtt{T3S3}$ (three-axle tractor plus three-axle semitrailer) and $\mathtt{T3S2R4}$ (three-axle tractor plus two-axle semitrailer plus four-axle trailer). The codes of the Mexican vehicle types are given by the Ministry of Communications and Transport [80]. These five vehicle types account for around 95 percent of the total surveyed heavy vehicles which is in line with what is reported in [83]. The vehicle type or code (i^{th} vehicle type), its corresponding number of axles (n_i), and its visual representation (silhouette) are presented in Table 3.1.

Table 3.1: Main heavy vehicle types with $GVW \geq 34$ kN found in ECCAN database.

Silhouette	Vehicle (i)	Type (code)	No. axles (n_i)
	1	C2	2
	2	C3	3
	3	T3S2	5
	4	T3S3	6
	5	T3S2R4	9

As an example, Table 3.2 presents an overview of the gross vehicle weights found in 2017 per vehicle type for the 223 studied survey stations. The first column corresponds to vehicle type, the second to their corresponding proportion of the traffic flow, followed by the median of the gross vehicle weight distribution (GVW). The fourth and fifth columns show the maximum gvw[1] permitted according to the Mexican standards [80] and the percentage of overloaded vehicles correspondingly. Additionally, the sixth and seventh columns show the recorded maximum gvw and the corresponding year. As expected, the nine-axle vehicle T3S2R4 is the heaviest vehicle in the database with a maximum gross vehicle weight of 975.76 kN in 2004. Figure 3.3 shows basic statics (5th, 50th, 95th percentiles and maximum) of the GVW distribution of the vehicle type T3S2R4. Notice that the maximum gross vehicle weight reported each year is under 980 kN, this could suggest that this is the maximum capacity of the scales used in the survey stations. In addition, it can be observed that before 2005, the 95th percentile of GVW exceeds the maximum permitted gwv. Speculatively, this could be an indication of a change in the devices used to measure axle weights.

Table 3.2: 2017 summary per vehicle type and maximum gross vehicle weight (gvw) reported from the year 2002 to 2017 for the 223 studied survey stations.

Vehicle type	2017				Max gvw [kN]	Year
	Proportion of the traffic flow (%)	GVW median [kN]	*gvw max permit [kN]*	Overloaded vehicles (%)		
C2	24.4	70.6	*186.34*	0.6	300	2008
C3	15.9	131.4	*269.69*	9.6	414.8	2009
T3S2	17.6	226.5	*456.01*	14.4	873.7	2014
T3S3	8.4	404.0	*529.56*	23.0	892.4	2011
T3S2R4	28.7	423.6	*740.41*	26.4	975.7	2004
Oth	5.00	–	–	–	–	–

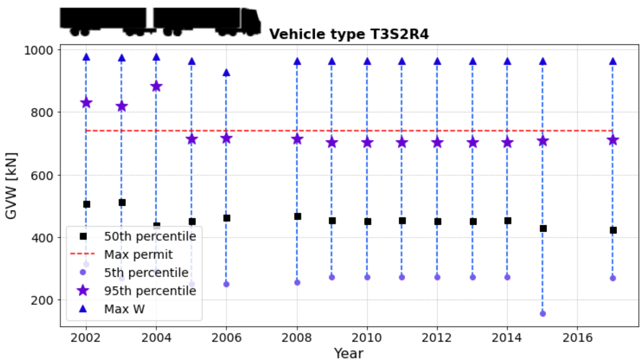

Figure 3.3: Basic statistics for vehicle type T3S2R4 from the year 2002 to 2017 (223 studied survey stations). Notice that the 2007 and 2016 data are missing. This is because unreasonable measurements (such as excessive gvw and total number of axles - individual axle weights mismatch) were found.

[1] GVW (uppercase) is used to denote the random variable representing gross vehicle weight, whereas gvw (lowercase) denotes a specific value of GVW.

3.3.2 *Datos viales* (road data, in English) database

The second source of traffic data is the *Datos viales* (road data, in English) database. With the purpose of knowing the yearly traffic trends, the SCT installed a set of automatic vehicle counters in key locations of the highway network. The observations gathered are published by the Department of Infrastructure [86]. This database constitutes one of the most comprehensive sources of traffic information in Mexico, as the records have details for more than 11 000 counting stations. It includes information such as (i) name of the road; (ii) name of the counting station (CS); (iii) travel lane direction (TLD) [2]; (iv) annual average daily traffic (AADT); and (v) the proportion of vehicle types (including nine vehicle types: the 5 vehicle types described in Section 3.3.1 plus vehicle types `M`, `A`, `B` and `Otros` that correspond to motorcycles, automobiles, buses and "others") that conform the traffic flow. However, information regarding gross vehicle weight and individual axle loads is not available. Table 3.3 and Table 3.4 presents an example of the *Datos Viales* database.

Table 3.3: *Datos Viales* 2018 example for two counting stations.

Road name	Rute	CS	TLD	Latitude	Longitude
Toluca - Morelia	MEX-015	Tuxpan	2	19.55236	-100.4710
Chalco - Tláhuac	EM-CDMX	Tláhuac	1	19.26436	-98.9926
⋮	⋮	⋮	⋮	⋮	⋮

Table 3.4: Table 3.3 (Continued).

AADT	M	A	B	C2	C3	T3S2	T3S3	T3S2R4	Otros
5610	3	82.2	0.8	10.3	1.3	1.3	0.9	0.1	0.1
10860	4.4	85.3	0.3	7.4	1.0	0.8	0.7	0.0	0.1
⋮	⋮	⋮	⋮	⋮	⋮	⋮	⋮	⋮	⋮

The database was filtered to take into account only the CSs that are located at the fifteen major highway corridors, as a result, 1777 counting stations were obtained. Given that the interest of this work is vehicles with a total vehicle weight of 35 kN or more (heavy trucks). Motorcycles, automobiles, buses and "others" were left out of the records. Then, by subtracting their corresponding proportion of the traffic volume from the AADT, the average daily truck traffic (AADTT) is obtained.

For illustration purposes, Figure B.2.1 shows the locations of the 233 EECAN survey stations and the 1777 *Datos Viales* counting stations that are taken into account in this study. Despite a large number of counting stations, as mentioned before, the *Datos Viales* database does not include measurements of axle loads or gross vehicle weight. Consequently, in order to estimate the missing data, statistical models that correctly simulate the dependence structure between the vehicle variables are used. With this intention, the next section will present a Gaussian copula-based Bayesian Network to simulate synthetic EECAN axle loads.

[2] In *Datos Viales* database, the number 1 in TLD column indicates the direction of traffic corresponding to the increasing road numbering, number 2 indicates the direction of traffic flow of the decreasing road numbering and number 0 indicates both directions.

3.4 Site-specific synthetic axle loads generation

Chapter 2 provides a methodology that employs GCBNs to simulate axle loads of heavy vehicles. The use of GCBNs provides computational advantages for large models. Therefore, this chapter proposes the use of GCBNs to investigate extreme values of heavy vehicle load events for situations when a limited amount of data (or no data) is available. Along these lines, for the case study, a GCBN model is proposed to create realistic synthetic axle load observations, similar to those presented in the EECAN database. This approach serves as a basis for the study of extreme gross vehicle weights at the counting stations where information on individual axle loads is not available. To quantify the GCBN the methodology presented in previous studies such as [51, 59, 81, 87] is used. For details of the methodology, the reader is referred to [81]. Variables included in the model (variables of interest) are vehicle type, gross vehicle weight, and individual axle loads.

3

3.4.1 EECAN Gaussian copula-based Bayesian Network

The approach to quantifying the ECCAN GCBN ($GCBN_{EECAN}$) consists of several steps. First, the measurements obtained from all EECAN locations (introduced in Section 3.3.1) were combined to build a national network level representative sample of the five main types of heavy trucks as shown in Table 3.1. Moreover, the measurements from 2016 were left out because of the excessive maximum gross vehicle weight reported per vehicle type. For example, vehicles C2 with up to 85.2 tonnes (835 kN) and vehicles T3S2 with *gvw* of 265 tonnes (2598 kN). This was also observed in the IMT 2017 report [88] in which the authors recommend the supervision of the field and data processing work of the company in charge of information gathering.

Then, once the EECAN database was filtered and unreasonable measurements were left out, a total of 755 173 heavy vehicles remained (214 465 C2, 134 298 C3, 276 994 T3S2, 68 020 T3S3, and 61 396 T3S2R4). The dependence structure of the data was modelled with 26 nodes (variables of interest) and 45 arcs illustrated in Figure 3.4. The model was built in the python-based open source software PyBanshee [47, 48] which allows for quantifying the GCBN, analysing the underlying assumptions of the model, visualizing its corresponding rank correlation matrix and its DAG.

Each "row" of nodes in Figure 3.4 represents one of the vehicle types illustrated in Table 3.1. Individual nodes represent individual axle loads. Let $i = \{1, 2, ..., 5\}$ be a set of indices corresponding to the 5 vehicle types. It is noted that $A_{i,j}$ is used to denote the random variable representing the j^{th} axle load. Additionally, $j = \{1, ..., n_i\}$ according to the i^{th} vehicle type, where n_i is the largest index (axle number) corresponding to vehicle type i (see the 3rd column of Table 3.1). The model assumes that for a particular intermediate axle if the load values of two axles adjacent to it were known, knowing the value of any other axle load not adjacent to it would not update the distribution of the particular intermediate axle.

The gross vehicle weight per vehicle type (GVW_i) is given by $GVW_i = \sum_{j=1}^{n_i} A_{i,j}$. GVW_i is a deterministic function of vehicle type i. For example, if $i = 3$ (5 axles vehicle, type T3S2, according to Table 3.1), then the gross vehicle weight of T3S2 is the sum of its individual axle loads, i.e. $GVW_3 = A_{3,1} + A_{3,2} + A_{3,3} + A_{3,4} + A_{3,5}$. Therefore, GVW (the node at the top of the Figure 3.4) is the random variable representing vehicle weight regardless of vehicle type.

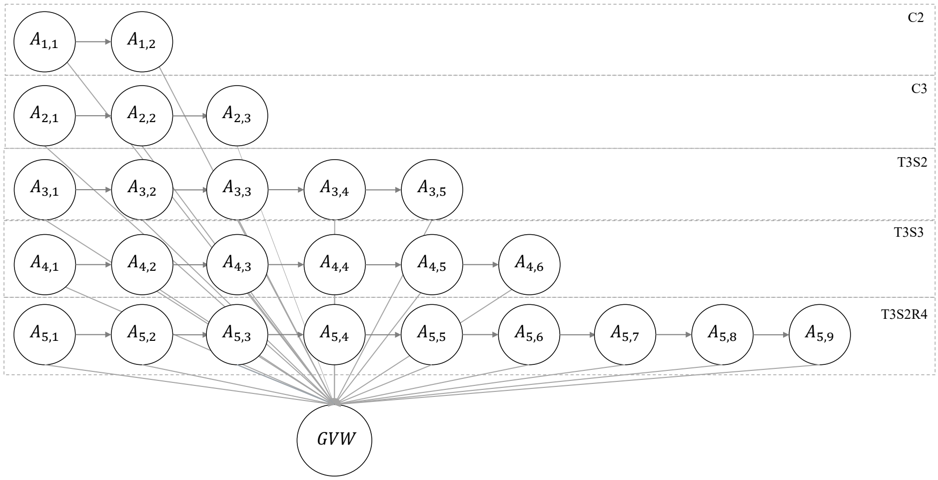

Figure 3.4: EECAN Gaussian copula-based Bayesian Network ($\mathrm{GCBN}_{\mathrm{EECAN}}$)

The arcs in Figure 3.4 between individual axle loads nodes per vehicle type correspond to the (un)conditional rank correlations, $r(A_{i,j}, A_{i,j-1})$. These are presented in Table 3.5. The first two columns indicate the vehicle type i and its corresponding code, and the third column, the corresponding number of axles (n_i). Every entry in the next eight columns indicates the rank correlations between the first and second axle ($A_{i,1}, A_{i,2}$), second and third ($A_{i,2}, A_{i,3}$), and so on until the 8th and 9th axle ($A_{i,8}, A_{i,9}$) per vehicle type. Notice that, as the number of axles increases, the correlations are stronger in the axles close to the end of the vehicle.

Table 3.5: Rank correlation per vehicle type between axles.

Vehicle (i)	Type	No Axles (n_i)	$A_{i,1}, A_{i,2}$	$A_{i,2}, A_{i,3}$	$A_{i,3}, A_{i,4}$	$A_{i,4}, A_{i,5}$	$A_{i,5}, A_{i,6}$	$A_{i,6}, A_{i,7}$	$A_{i,7}, A_{i,8}$	$A_{i,8}, A_{i,9}$
1	C2	2	0.63							
2	C3	3	0.56	0.79						
3	T3S2	5	0.52	0.90	0.82	0.90				
4	T3S3	6	0.41	0.91	0.79	0.85	0.85			
5	T3S2R4	9	0.40	0.93	0.86	0.92	0.83	0.90	0.86	0.92

Each axle load of each vehicle type was fitted to a Gaussian Mixture distribution (GM). Which is a weighted sum of G Gaussian densities [68] (see Equation (2.8)).

For each fitted distribution, visual inspection on the right tail of the distribution (to best represent heaviest axle loads) and the relative goodness-of-fit Akaike information criterion (AIC) [72] were used to select a distribution. A two-sample Kolmogorov-Smirnov (KS) test [89] was used on the selected distribution to test the hypothesis that the sample and the selected distribution come from the same population. If the KS test was not rejected then the selected distribution was regarded as a valid representation of the sample and used further in the analysis. As a result, a total of 25 GMs were estimated (one GM per axle load of each vehicle type) ranging from 4 to 6 components. As an example, Table 3.6 shows the best-fitted Gaussian mixture distributions corresponding to the axle loads of vehicle C2. For this vehicle, its axle loads were approximated with GMs of $G = 6$ components. Figure B.1.1 shows a comparison between the EECAN axle loads observations of the vehicle type C2 and synthetic random observations generated with the corresponding six-components GM model. In Tables B.1.1 to B.1.4 the GMs for the other vehicle types used in this work can be found.

Table 3.6: Gaussian mixture components representing both axles of vehicle type C2

Axle 1 ($A_{1,1}$)				Axle 2 ($A_{1,2}$)			
g	π_g	μ_g [kN]	σ_g [kN]	g	π_g	μ_g [kN]	σ_g [kN]
1	0.29	23.32	4.24	1	0.23	22.87	4.59
2	0.15	43.2	6.17	2	0.14	89.47	14.90
3	0.31	16.69	3.49	3	0.17	48.66	7.83
4	0.05	52.86	10.82	4	0.06	91.55	32.62
5	0.17	32.38	5.03	5	0.14	66.66	10.42
6	0.02	71.84	23.79	6	0.26	35.28	6.82

In order to investigate model validity, the EECAN data set was split into 80:20, i.e., 80% of the data set becomes the training set and 20% of the data set becomes the testing set. This split ratio has been used frequently in several traffic analysis studies (see [76–78], for example). Later, N' un-conditional samples (synthetic observations) using the $\text{GCBN}_{\text{EECAN}}$ model are generated, where N' is the number of observations in the testing set. Figure 3.5 shows a comparison between the observed GVW of the testing set and the synthetic GVW computed with the $\text{GCBN}_{\text{EECAN}}$ model per vehicle type. This allows us to graphically assess if the synthetic observations can represent the GVW reported in the EECAN database.

The scatter plots in Figure 3.5 were created by plotting the sorted gross vehicle weights of the testing set against the sorted synthetic GVWs for a single simulation with $N' = 151\,035$ samples. The dataset was grouped by vehicle type because the output of the model is a simultaneous sample (different every time the model is run) for all five vehicle types. If the test datasets and the synthetic dataset are the same, one would expect to see the points lying in a straight line. Additionally, the selected test statistics, Nash–Sutcliffe model Efficiency Coefficient (NSE) [74] and the Mean Absolute Percentage Error (MAPE) [90] are presented in each scatter plot. The NSE takes values in $(-\infty, 1]$, where 1 indicates a perfect fit while the MAPE takes values within $[0, \infty)$, where zero indicates a perfect fit.

As can be seen, Figure 3.5 shows that (for this particular realization) for vehicle type C2 the model slightly underestimates GVW in the interval between 260 kN and 300 kN. In the scatter plot that corresponds to vehicle type C3 there is an overestimation for GVW from 350 kN to 400 kN approximately. For vehicle type T3S2, the underestimation occurs for GVW from 650 kN to 700 kN. Synthetic observations of the six-axle vehicle T3S3 show that the model underestimates GVW in the interval between 370 kN and 500 kN, and overestimates in the interval between 650 kN and 800 kN. Finally, for vehicle type T3S2R4 there is an overestimation for GVW from 180 kN to 250 kN and from 930 kN to 980 kN approximately. In general, as expected, more deviations with respect to the original data are observed in the tails of the distribution of gross vehicle weight, particularly for the six-axle and nine-axle vehicles. Regardless, the synthetic observations provide an overall very good representation of the original data. This can also be observed in the results of test statistics, where the values of NSE and MAPE are close to 1 and 0 respectively for each vehicle type.

All things considered, the $\mathrm{GCBN}_{\mathrm{EECAN}}$ quantified with the train data set captures the main complexities of the axle loads reported in the EECAN data set to a good degree and can be considered effective. However, in order to profit from all data available, further, all our analysis is performed with the $\mathrm{GCBN}_{\mathrm{EECAN}}$ quantified with the full data set. In the next section, the combination of the *Datos viales* database and the proposed Gaussian copula-based Bayesian Network model for predicting axle loads for counting stations where no axle information is provided.

3.4.2 Site-specific Gaussian copula-based Bayesian Network

This section briefly describeS the site-specific synthetic *Datos Viales* axle loads generation approach based on the $\mathrm{GCBN}_{\mathrm{EECAN}}$. The results will be further used to compute extreme vehicle weights with selected return periods. First, the input data is defined. Let $c = \{1, 2, ..., 1777\}$ be a set of indices corresponding to the 1777 counting stations of the Mexican major highway corridors presented in Section 3.2 and $k_c = \{1, 2, ..., 5\}$ a set whose elements represent the number of vehicle types registered in counting station c. Then, the necessary input data are: (i) c and k_c, (ii) the heavy vehicle types that conform to the traffic flow ($V_{i,c}$), (iii) the proportion of the traffic flow per vehicle type i ($p_{i,c}$) and, (iv) the annual average daily truck traffic (AADTT_c). In fact, (ii) and (iii) are the vehicle distribution at any given location c of interest. Next, a site-specific GCBN_c model is quantified using only the k_c vehicle types registered in the counting station c, i.e, $\mathrm{GCBN}_c = \mathrm{GCBN}_{\mathrm{EECAN}}\left(k_c; V_{i,c}; p_{i,c}, \mathrm{AADTT}_c\right)$. Finally, $N_c = \sum_{i=1}^{k_c}(\mathrm{AADTT}_c \cdot p_{i,c})$ unconditional samples using the site-specific GCBN_c is computed. Therefore, the output of the model is site-specific synthetic EECAN axle load observations (from synthetic vehicles equal to the daily average) for the CS of interest. The output database contains the variables: vehicle type, gross vehicle weight and individual axle loads. The Figure 3.6 presents an overview of our approach for generating representative EECAN synthetic axle loads. In total 1777 site-specific GCBNs were quantified (one site-specific GCBN per counting station).

To clarify the axle loads generation approach, an example of generating one day of synthetic observations for one of the 1777 counting stations is presented. For this example, the CS *Veracruz* is selected ($c = 1567$). First, the input data of the counting station is extracted from the *Datos viales* database. As can be seen in Table 3.7, the vehicle types that conform to the traffic flow are: $V_{1,1567} = \mathrm{C2}$, $V_{2,1567} = \mathrm{C3}$, $V_{3,1567} = \mathrm{T3S2}$, $V_{4,1567} = \mathrm{T3S3}$ and $V_{5,1567} = \mathrm{T3S2R4}$. Their corresponding proportions $p_{i,1567}$ of the total vehicles are: $p_{1,1567} = 48.4\%$, $p_{2,1567} = 9.1\%$, $p_{3,1567} = 18.3\%$, $p_{4,1567} = 12.5\%$ and $p_{5,1567} = 11.7\%$. Next, since the five vehicle types presented in Table 3.1 were registered, i.e. $k_{1567} = 5$, the corresponding site-specific GCBN_{1567} is similar to the one presented in Figure 3.4. Finally, $N_{1567} = \mathrm{AADTT}_{1567} = 2746$ un-conditional samples using the GCBN_{1567} model are computed.

The output is a database presented in a 12-column table with synthetic axle load observations (different every time the model is run), of the vehicles with up to nine axles registered in the CS. For example, Table C.3.1 corresponds to the output database of one day simulation of axle loads for the *Veracruz* CS. The first column in table Table C.3.1

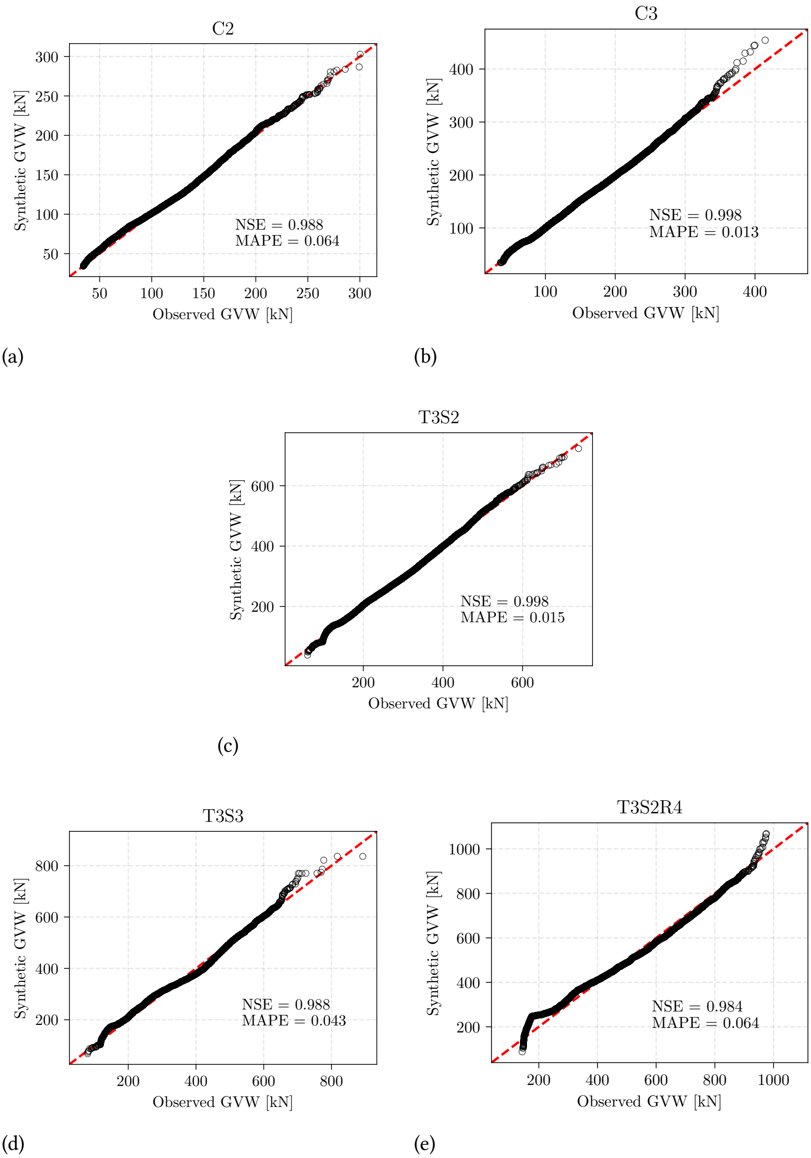

Figure 3.5: Scatter plots comparison synthetic *GVW* versus test *GVW* observations: (a) Vehicle type C2; (b) Vehicle type C3; (c) Vehicle type T3S2; (d) Vehicle type T3S3 and (e) Vehicle type T3S2R4

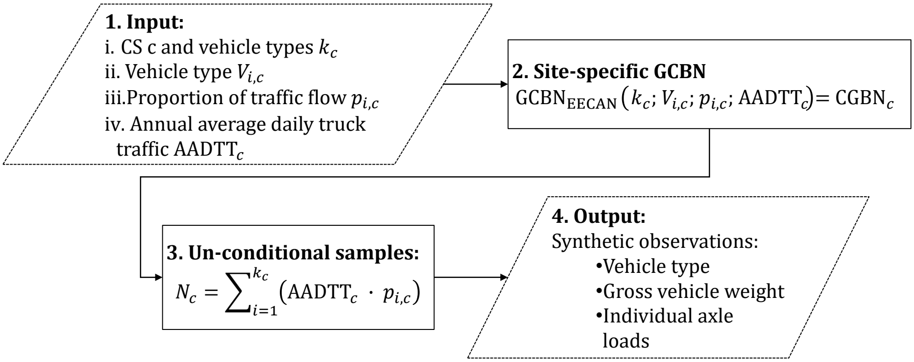

Figure 3.6: Generation of site-specific synthetic observations based on the GCBN quantified with EECAN database.

Table 3.7: Input data for the site-specific EECAN GCBN model CS *Veracruz*

Location (19.2153512, -96.211168)	Traffic information

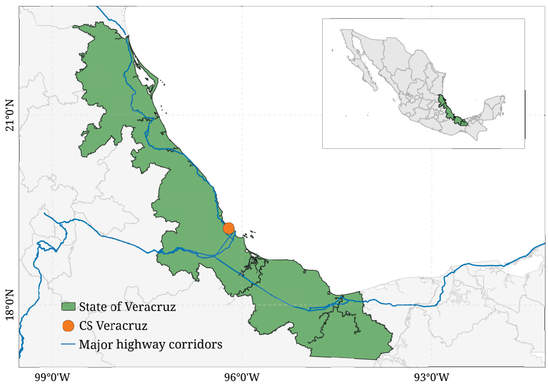

AADTT: 2746

V_i	p_i
C2	0.484
C3	0.091
T3S2	0.183
T3S3	0.125
T3S2R4	0.117

represents the id of the synthetic observation, the second the vehicle type, the third the total vehicle weight (gvw) in kN, and columns 4 to 12 the individual axle load (A) in kN. "Not a Number" (NaN) entry is placed in the fields where no data is computed. For example, the 6-axle vehicle T3S3 will have three NaN cells corresponding to the weight of the seventh, eighth and ninth individual axles. Notice that the *gvw* is the sum of the individual axle loads. Furthermore, a graphical user interface (GUI) called EECAN BN GUI is developed to provide a user-friendly graphical interface to compute site-specific synthetic observations based on the $\mathrm{GCBN_{EECAN}}$ model. This graphical user interface can be found at the corresponding repository of this work[3].

To further compute the return periods of gross vehicle weights 450 days of traffic loads in each one of the 1777 counting stations that are located at the fifteen major highway corridors are simulated. This means that 1777 site-specific GCBNs were quantified. In total, axle loads of around 180 million heavy vehicles were computed.

Table 3.8: Example of a random realization (output) of the $\mathrm{GCBN_{1567}}$ for *Veracruz* CS.

	Type	gvw	A1	A2	A3	A4	A5	A6	A7	A8	A9
1	C2	66.35	11.89	54.45	NaN	NaN	NaN	NaN	NaN	NaN	NaN
2	C2	44.90	24.69	20.21	NaN	NaN	NaN	NaN	NaN	NaN	NaN
⋮	⋮	⋮	⋮	⋮	⋮	⋮	⋮	⋮	⋮	⋮	⋮
2743	T3S3	563.82	45.72	99.69	107.75	114.14	96.64	99.88	NaN	NaN	NaN
2744	T3S2	314.48	35.71	69.74	77.06	64.63	67.33	NaN	NaN	NaN	NaN

3.5 PyBanshee

In order to quantify the 1777 site-specific GCBNs to simulate the axle loads of around 180 million heavy vehicles, a big implementation has been made. PyBanshee [47], the Python-based version of MATLAB BANSHEE [48, 73] is introduced. Python offers distinct advantages over MATLAB when it comes to numerous computations. One notable strength lies in the open-source nature of Python. This facilitates the integration of a wide array of external tools and libraries. The scalability of Python across diverse computational tasks, coupled with its robust support for parallel and distributed computing makes a preferred choice for introducing our software fully open-source so that it can be more accessible to non-MATLAB licensed users.

In addition to the functionalities available in our first release (MATLAB BANSHEE), PyBanshee allows for the use of (i) fully parametric one-dimensional margins, (ii) user-defined sample sizes for model-validation tests based on the Hellinger distance, (iii) getting user-defined sample sizes of the GCBN, (iv) sample based conditioning and (v) advanced graphics for the underlying graph of the Bayesian Network and the visualization of the comparison between the histograms of the unconditional and conditional marginal distributions.

Feature (i) is useful when the interest is in values that have not been observed in a particular sample. For example in civil engineering percentiles with a low probability of exceedance are often required for design purposes. These are obtained by extrapolation using a parametric one-dimensional margin. Regarding (ii), since model validation is

[3]Instructions for download and install EECAN BN GUI can be found at https://github.com/mike-mendoza/extreme_gvw_mexico/tree/main/EECAN_NPBN

still in its infancy when it comes to GCBNs, it is often desired to estimate the minimum sample size at which the null hypothesis would not be rejected to give some guidance about statistical power. Feature (iii) is useful when statistically robust results are needed. This can be done by increasing the number of samples drawn from the GCBN. Sample-based conditioning (feature (iv)) is implemented to allow for conditionalizing on intervals. Advanced graphics (feature (v)) are implemented to facilitate further analysis for users. In this manner, PyBanshee and MATLAB BANSHEE v1.3 exhibit the same available features (see Section 2.4).

3.5.1 Software description

Similarly to its MATLAB predecessor, the code of PyBanshee consists of a set of functions. These functions allow for quantifying the CGBN, analyzing the underlying assumptions of the model, visualizing the network and its corresponding rank correlation matrix, and making inferences with an GCBN based on existing observations or new evidence. In addition, new functions were added to: generate random samples of the GCBN, perform sample-based conditioning, and visualize unconditional and conditional distributions. To show and better explain the features of PyBanshee, examples are provided as standalone scripts.

3.5.2 Software architecture

The PyBanshee package contains six Python files (`.py` extension files) in which eight main functions are located as can be seen in Figure 3.7. The main functions are:

(1) `bn_rankcorr`, to compute the BN rank correlation matrix. It requires a defined directed acyclic graph (DAG, as a `list`) and a matrix of data (as a `DataFrame`). Additionally, it includes an option to compute the BN rank correlation without such data;

(2) `bn_visualize`, to visualize the structure of the defined GCBN. In this release, an GCBN with marginal histograms inside of the nodes can be displayed (feature (v));

(3) `cvm_statistics`, to measure the degree of agreement of the Gaussian copula with the data based on the Cramer–von Mises statistic;

(4) `gaussian_distance`, to perform model validation based on the distance between the empirical (ERC) and Bayesian Network's rank correlation (BNRC) matrices and the empirical normal rank correlation matrix (NRC) using data. The distance is computed based on the d-calibration score ([91]). PyBanshee allows users to define different sample sizes (feature (ii));

(5) `inference`, to compute the uncertainty distribution of nodes other than those that the user conditionalized on. In this release, parametric distributions can be an input for the `inference` function (feature (i));

(6) `conditional_margins_hist`, to visualize the comparison between unconditional and conditional histograms (feature (v)) of the `inference` function output;

(7) `generate_samples`, to explicitly increase the number of unconditional samples of the GCBN (feature (iii));

(8) `sample_based_conditioning`, to conditionalize nodes on intervals (feature (iv)).

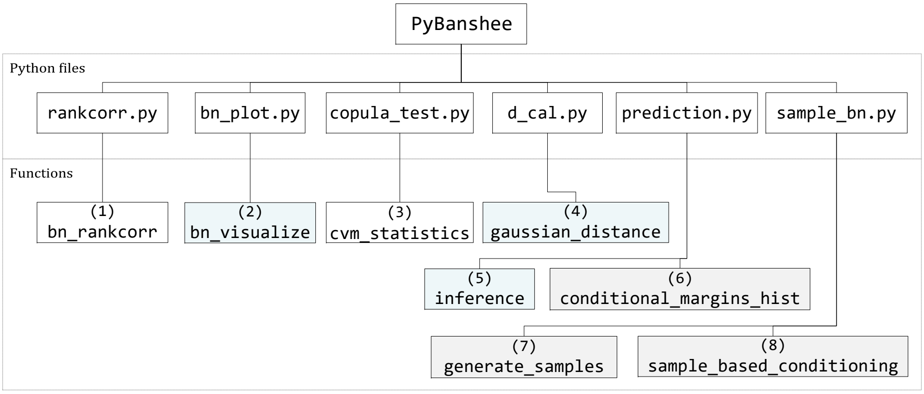

Figure 3.7: PyBanshee structure. Functions (1) to (5) correspond to the main functions of the previous MATLAB release. Changes were made in functions (2), (4), and (5) (boxes filled in light-blue) to add feature (v), feature (ii), and feature (i) correspondingly. Functions (6), (7), and (8) (boxes filled in light-grey) correspond to the newly added functions (features (v), (iii) and (iv) respectively).

For more detailed information on the functions, illustrative examples, and their corresponding scripts, the reader is referred to the original sources [47, 48, 73].

3.6 Return periods of gross vehicle weights

The Mexican Ministry of Communications and Transports and the Mexican Institute of Transport (IMT) suggest a return period for the road bridge design loads of 50 years [92]. Likewise, in the traffic road models for road bridges, load model one (LM1), and load model two (LM2) [93] a characteristic value of a 1000-year return period for traffic loads on the main roads in Europe is specified. Therefore, as the Mexican bodies suggest, estimations of extreme events of gross vehicle weight with a 50-year return period (GVW_{50}). Additionally, for comparative purposes, the GVW with a 1000-year return period (GVW_{100}) is also presented. Assumptions are made for the calculation of extreme loads based on 254 working days per year, excluding weekends and holidays. Data for 450 days are computed and extrapolated to determine the return periods of interest as per CS. Extreme value theory has been widely used to assess extreme events in many areas of application, including recently, machine learning, environmental incidents and risk assessment [94–96]. Regarding traffic loads, extreme value projections have been extensively used (see [97–99] for example). For this work, the conventional generalized extreme value approach [100, 101] is used. The 450 days per CS were filtered and only the block maximum is retained. A block length of one day is used, i.e., the maximum gross vehicle weight per day and per CS was retained. The daily maxima selection responds to a limitation on the data available. Follow-up research could use monthly or yearly maxima (if available) or a peak over-threshold approach to construct the distribution of extremes.

The tail of the distribution for the determination of extreme vehicle events is of particular interest. Furthermore, to avoid unrealistic estimates, the subset extrapolation averaging (SEA) approach [102] was used. A representative subset of 120 gross vehicle weight daily maxima observations per counting station c ($GVW_{d,c}$) was randomly sampled from the computed synthetic data. In principle, with 120 observations, $GVW_{d,c}$ would be representative of the computed 450 days of synthetic observations. Later, the subset is fitted and extrapolation is performed to estimate the characteristic values $GVW_{50,c}$ and $GVW_{1000,c}$. Regardless, to reduce the potentially poor performance of extrapolation, subsetting was performed by fitting and extrapolation steps 30 times (each time with different random sampled $GVW_{d,c}$). Therefore, the characteristic values reported in this work are the ones corresponding to the 50th percentile of $GVW_{50,c}$ and $GVW_{1000,c}$ distributions.

To find the statistical distribution that “best" fits the empirical distributions the Akaike Information Criterion (AIC) measure is used. AIC values for different parametric distributions varied significantly between counting stations. On average, the AIC value was the lowest for the generalized extreme value (GEV) distribution. However, extrapolations performed using this distribution gave unrealistically large gross vehicle weights for several stations. Considering that the outcome of an extrapolation is highly dependent on the distribution type, to improve the fitting procedure the truncation of the likelihood [103] is chosen to find the parameters and distributions to better describe the data. This is done by selecting a truncated gross vehicle weight $gvw_{0,c}$. The choice of $gvw_{0,c}$ value is guided by two considerations: (i) the larger the truncated value, the better the found distribution will accurately describe the tail of the frequency distribution and (ii) the smaller the truncated load, the more data is involved in the tail analysis and the smaller the uncertainty in the found distribution parameters. First, the data in $GVW_{d,c} = gvw_{1,c}, gvw_{2,c}, ..., gvw_{m,c}$ is rearranged so that: $gvw_{1,c}, ..., gvw_{l,c} \leq gvw_{0,c}$ and $gvw_{l+1,c}, ..., gvw_{m,c} > gvw_{0,c}$. Now, the likelihood function of the sample gvw_c can be written as follows:

$$L_{gvw_c}(gvw_c; \mathbf{a}_c) = \left\{ F_{gvw_c}(gvw_{0,c}; \mathbf{a}_c) \right\}^l \prod_{h=l+1}^{m} f_{gvw_c}(gvw_{c,h}; \mathbf{a}_c) \tag{3.1}$$

where $\mathbf{a}_c$ is the parameter vector of the distribution per counting station c, m the is the number of total gross vehicle weights in the sample. The first factor in the right-hand term of the Equation (4.3) ($\left\{ F_{gvw_c}(gvw_{0,c}; \mathbf{a}_c) \right\}^l$) means that for values smaller than $gvw_{0,c}$ we only include the probability that they are smaller than $gvw_{0,c}$. In the other hand, the second factor ($\prod_{h=l+1}^{m} f_{gvw_c}(gvw_{c,h}; \mathbf{a}_c)$) means that for values greater or equal than $gvw_{0,c}$ only their probability density is included. For mathematical convenience, the logarithm is used instead of the likelihood itself, which is calculated according to Equation (3.2). The logarithm of the likelihood is monotonically increasing with the likelihood itself, so the maximum likelihood estimator for $\mathbf{a}_c$ can also be determined by maximizing the logarithm of the likelihood. This method is used in [59] and in [104] to advise the Dutch authorities regarding overloaded vehicles.

$$\log L_{gvw_c}(gvw_c;\mathbf{a}_c) = l \log F_{gvw_c}(gvw_{0,c};\mathbf{a}_c) + \sum_{h=k+1}^{m} \log f_{gvw_c}(gvw_{c,h};\mathbf{a}_c) \tag{3.2}$$

Two types of extreme value distributions are considered, the Gumbel and the Weibull distribution. A truncated value $gvw_{0,c}$ that corresponds to the 95th percentile of $GVW_{d,c}$ is used. For each distribution type, the maximum likelihood estimator of the parameters is determined. In general, for the counting stations included in this study, the “truncated" Gumbel performs better compared to the “truncated" Weibull and GEV distributions. As an example, Figure 3.8 show the fitted Gumbel, Weibull, GEV, and “truncated" Gumbel distributions comparison for one randomly sampled subset of the synthetic observations of CS *Veracruz* ($c = 1567$, presented in Section 3.4.2). Notice that for this particular case, the GEV and Weibull distributions provide larger characteristic gross vehicle weights. In contrast, the “regular" Gumbel fit produces significantly lower characteristic vehicle weights. The “best" fit is provided by the “truncated" Gumbel distribution as a function of the truncated value $gvw_{0,1567} = 1064.63$ kN.

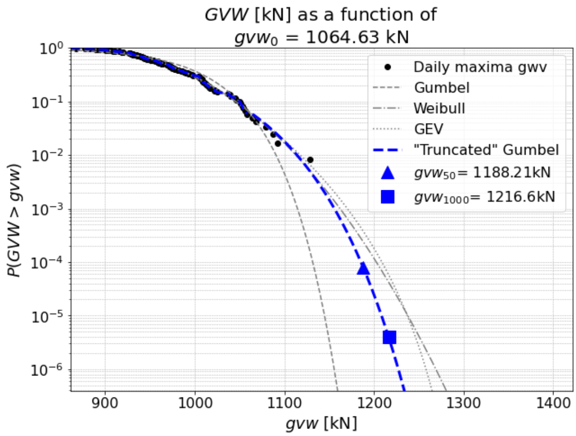

Figure 3.8: Exceedance probability plot comparison. In blue, the gross vehicle weight fitted distribution as a function of a $gvw_{0,c} = 1064.63$ kN. The triangle marker represents the extrapolated value that corresponds to a *gvw* with a 50-year return period. The square marker represents the extrapolated value that corresponds to a *gvw* with a 1000-year return period.

Additionally, Figure 3.9 shows the characteristic value distribution resulting from the SEA approach and their respective reported characteristic values, $gvw_{50,1567} = 1190.0$ kN and $gvw_{1000,1567} = 1215.0$ kN. Figure B.3.1 presents a simple sensitivity analysis on SEA in terms of the number of extrapolations performed. In this case, for $GVW_{50,1567}$, the difference between the reported value estimated with a 30 times extrapolation averaging and 500 times is around 0.42% while compared to the 1500 times is 0.33%. Based on these results, performing 30 times the extrapolation step does not affect drastically the results and reduces the computational cost. As has been noted, the subset and extrapolation averaging approach is performed on each of the counting stations. Hence, the characteristic values reported in the next section are the result of 30x1777 fitted distributions.

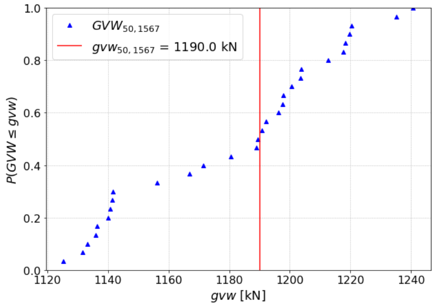

(a)

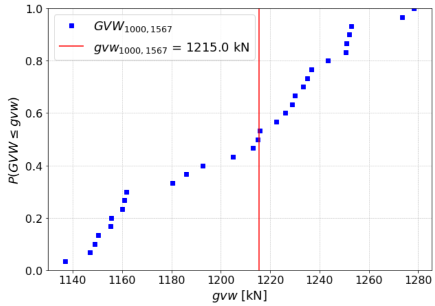

(b)

Figure 3.9: Empirical cumulative distribution of computed $GVW_{50,1567}$ and $GVW_{1000,1567}$ values for *Veracruz* CS. The red line represents the 50th percentile (reported value). (a) Distribution of $GVW_{50,1567}$ values (b) Distribution of $GVW_{1000,1567}$ values.

3.7 Results

3.7.1 Mapping extreme gross vehicle weights in Mexico

Following the procedures described in Sections 3.4.2 and 3.6, synthetic observations and extreme gross vehicle weights have been estimated for 1777 studied counting stations. As a result, the distributions GVW_{50} and GVW_{1000} represent the characteristic values of interests for *gvw*s with 50 and 1000-year return periods. A summary of the estimated gross vehicle weights can be found in Table 3.9. The data is grouped into seven *gvw* classes according to the 5th, 15th, 25th, 50th, 75th, and 95th percentiles of the empirical distribution of characteristic gross vehicle weight with a 1000-year return period. The first column of Table 3.9 represents the *gvw* interval of each one of the classes, and the second and third columns represent the lower bound (LB) and the upper bound (UB) of the corresponding class in kN. The fourth column shows the number of counting stations (No of CSs) with a 120-day return period estimated extreme gross vehicle weight within the LB-UB interval. Similarly, in columns five and six the number of CSs for GVW_{50} and GVW_{1000} is presented. In general, around 80% of the CS has gvw_{50} above 980 kN (100 tons). This is to be expected because, according to the EECAN database, the median value of the maximum gross vehicle weight observed in all studied survey stations corresponds to 964 kN. Additionally, as reported in [105, 106] trucks with GVW over 1000 kN were recorded in central Mexico (Irapuato – La Piedad highway). Notice that 29 stations will have values that will surpass 1258 kN (column 5 in Table 3.9) for return periods of 50 years, while for return periods of 1000 years, 86 stations will surpass the P95 percentile (column 6 in Table 3.9). This represents 1.63% and 4.83% of the stations respectively.

Figure 3.10 shows the map of the computed gvw_{50} per counting station. The histogram of frequencies for 50-year return period vehicular weight across the whole country is included in the upper right corner of the map. A similar map for GVW_{1000} is presented in Figure B.4.2. Additionally, the corresponding interactive web map can be found at https://mike-mendoza.github.io/extreme_gvw_mexico. The open-source Geographic Information System (GIS) software QGIS 3.10.14 was used to produce the maps and to perform the

Table 3.9: Number of counting stations per *gvw* class and per characteristic value

Class	LU [kN]	UB [kN]	GVW_{50}	GVW_{1000}
			No. of CSs	No. of CSs
$gvw_{\min} < gvw \leq P5$	342	772	106	90
$P5 < gvw \leq P15$	772	960	222	177
$P15 < gvw \leq P25$	960	1022	197	178
$P25 < gvw \leq P50$	1022	1131	546	443
$P50 < gvw \leq P75$	1131	1190	433	446
$P75 < gvw \leq P95$	1190	1258	244	357
$P95 < gvw \leq gvw_{\max}$	1258	1333	29	86

spatial analysis of extreme gross vehicle weights. Regarding the map in Figure 3.10, simple geometric markers (circles) were chosen for representing individual counting stations to increase legibility. The colours of the geometric markers used to symbolize the seven *gvw* classes of Table 3.9 are in accordance with the colour code provided by the inverted spectral cpt-city colour ramp. As can be seen in Figure 3.10, two groups are clearly distinctive the lightest and the heaviest heavy vehicles. The lightest heavy vehicles (up to *gvw* 772 kN, blue circles) are found on the major highway corridors *Del Pacífico* located on the Pacific coast and *Transpeninsular Baja California* in the Baja California peninsula in northwestern Mexico. On the other hand, the heaviest heavy vehicles (*gvw* above 1258 kN, red dots) are mostly concentrated in the major highways corridors *México —Nuevo Laredo, Piedras Negras, México —Puebla, Progreso* and *Manzanillo —Tampico, Lazaro Cardenas.* These pass through the states of Veracruz, Puebla, México, Querétaro, Guanajuato, San Luis Potosí, Colima and Jalisco.

A kernel density map is produced to represent the global trend of the heaviest gross vehicle weights with a 50-year return period ($HGVW_{50}$, those above 1190 kN). The map was created at 1 km^2 grid cells, with a bandwidth of 100 km, determined by kernel density interpolation using a quartic kernel shape and weighted by the number of observed T3S2R4 vehicles per CS. As a result, Figure 3.11 shows a heat map of the concentration of statistically heaviest vehicle type (T3S2R4) compared with the estimated $HGVW_{50}$. As can be seen, the majority of the counting stations with a $gvw > 1190$ kN follow the paths of the hotspots. Important clusters of T3S2R4s were formed in the central region, while some less intense clusters were emerging on the Pacific coast and Baja California regions.

Locations with a higher proportion of heavy vehicles in their traffic volume are expected to suffer more significant damage to their road infrastructure. These observations are important because they show that the method is able to detect trends in extreme gross vehicle weights for the counting points considered in this study.

3.7.2 Discussion

The analysis of the extreme gross vehicle weights by major highway corridor needs at first an overview of corridor-specific extreme *GVW* distributions. Thus, additional analyses were performed after dividing the study counting stations into fifteen groups (each group corresponds to one major highway corridor). Let $h = \{1, 2, 3, ...15\}$ be a set of indices corresponding to the fifteen major highway corridors in accordance with the enumeration

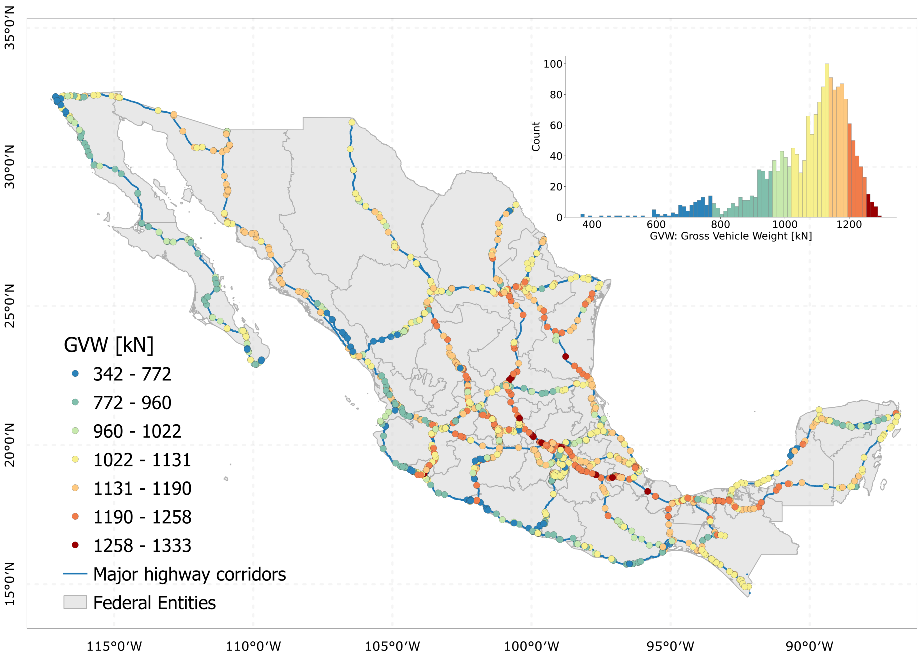

Figure 3.10: Gross vehicle weight [kN] for a 50-year return period.

3

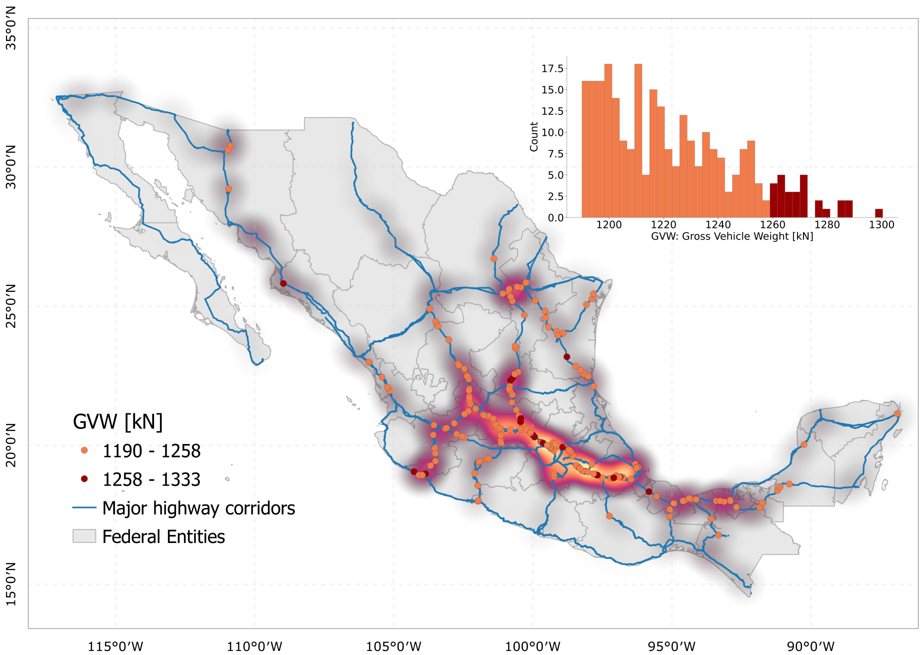

Figure 3.11: T3S2R4 heat map compared to the heaviest GVW_{50}.

presented Figure 3.2. To identify hazardous locations, corridor-specific percentiles (5th, 25th, 50th, 75th and 95th) of the extreme gross vehicle weights empirical distributions GVW^h_{50} and GVW^h_{100} are computed. Then, *gvw* values that lie at the upper extremes of each corridor-specific distribution (the 95th percentiles) are analysed. This is because the distribution of extreme gross vehicle weights for a given MHC tends to be negatively skewed. Hence, using mean values for analysis will provide a deceitful insight compared to an analysis carried out with extreme values. In particular, the 95th percentile of the gross vehicle weight with a 50-year return period ($GVW^h_{50,\mathrm{P95}}$) distributions ranges from 1064.46 kN to 1266.87 kN. It is highest in MHCs *México —Nuevo Laredo, Piedras Negras* ($gvw^2_{50,\mathrm{P95}}$ = 1266.87 kN) and *México —Puebla, Progreso* ($gvw^{11}_{50,\mathrm{P95}}$ = 1263.35 kN). As the map presented in Figure 3.10 suggests, the lowest values of $GVW^h_{50,\mathrm{P95}}$ can be found in the major highway corridors *Del Pacífico* with $gvw^{15}_{50,\mathrm{P95}}$ = 1122.70 kN and *Transpeninsular Baja California* with $gvw^6_{50,\mathrm{P95}}$ = 1064.46 kN. The latter represents a difference of 16% compared with the $gvw^2_{50,\mathrm{P95}}$ of the *México —Nuevo Laredo, Piedras Negras* corridor. Similar behaviour can be observed when comparing the computed 95th percentiles of the corridor-specific *gvw* distributions with a return period of 1000 years. The reader can find the corridor-specific percentiles for 50-, and 1000-year sorted by the corresponding 95th percentile in Tables B.4.1 and B.4.2.

For 1000-year events, $gvw_{1000,\mathrm{P95}}$ range from 1086.75 kN to 1293.36 kN. Overall an average increase of 2.24% is expected when comparing $gvw_{50,\mathrm{P95}}$ with $gvw_{1000,\mathrm{P95}}$. The biggest increase (+2.91%) could be found in the major highway corridor *Del Pacífico* which has a $gvw^{15}_{50,\mathrm{P95}}$ = 1122.7 kN, this value increases to $gvw^{15}_{1000,\mathrm{P95}}$ = 1155.43 kN. As an illustration, Figure 3.12 shows the computed corridor-specific percentiles of GVW^h_{50}. The red markers in Figure 3.12 represents the $gvw^h_{1000,\mathrm{P95}}$ values. From the discussion in this section, it is shown that *México —Nuevo Laredo, Piedras Negras* and *México —Puebla, Progreso* major highway corridors present the heaviest heavy vehicles events than the other corridors.

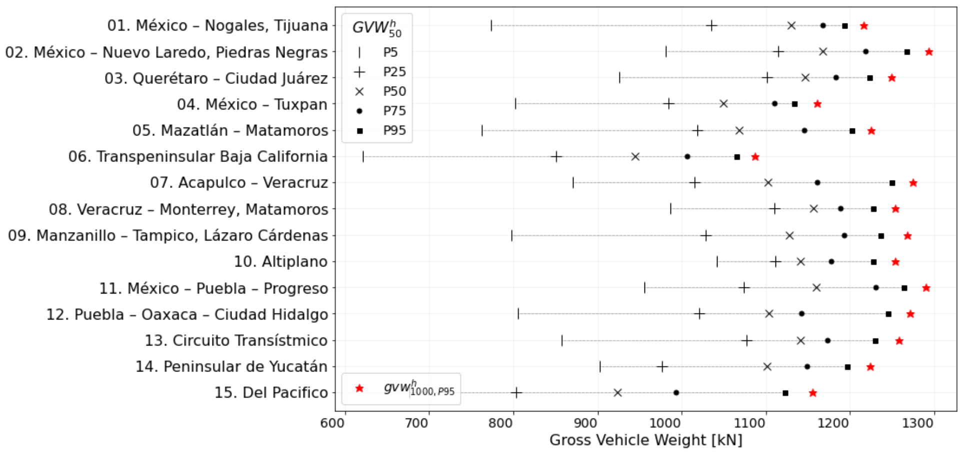

Figure 3.12: *GVW* comparison between the fifteen major highway corridors of Mexico

3.8 Conclusions

This chapter developed a methodology to identify potentially hazardous locations of a road network by computing and mapping extreme gross vehicle weights when axle load information is scarce using data obtained from less-sophisticated traffic counters. The extreme traffic events were computed using extreme value theory and Gaussian copula-based Bayesian Network (GCBN) approach. Later, the open-source Geographic Information System software QGIS was used to produce maps of extreme traffic events. The methodology was applied to the 15 major highway corridors network of Mexico.

Although the information regarding gross vehicle weight or axle loads is nonexistent for all the studied counting stations, this chapter deals with this scarcity by presenting the first GCBN dependence model to generate synthetic axle loads of Mexican heavy vehicles ($GCBN_{EECAN}$). The GCBN was quantified using manual axle load measurement of 223 origin destinations surveys conducted from 2002 until 2017. Therefore, the axle loads derived from $GCBN_{EECAN}$ should provide a good approximation to the true distribution of the heavy vehicles found in the studied counting stations.

More than 180 million synthetic heavy vehicles were computed using 1777 site-specific GCBNs that correspond to the studied counting stations. Later, extreme value analysis was performed to estimate the characteristic values of gross vehicle weight with a 50-year return period (GVW_{50}) and a 1000-year return period (GVW_{1000}) in each counting station. The analysis was further refined to improve the fitting procedure with a truncated likelihood by selecting a truncation gross vehicle weight $gvw_{0,c}$ that corresponds to the 95th percentile of daily maxima gross vehicle weight distribution per counting station c.

In terms of heaviest vehicles, the results indicate that the hazardous locations with $GVW_{50} > 1190$ kN are located primarily on major highway corridors number 2, 3, 7, 9, and 11 (see Figures 3.2 and 3.11), particularly segments that cross the federal entities: Aguascalientes, Colima, Guanajuato, Jalisco, México, Nuevo Leon, Puebla, Querétaro, Tabasco, Tamaulipas and Zacatecas. The same is true when analysing 1000-year events. It is suggested that future EECAN (Statistic Field Study of Domestic Road Transportation) studies focus on these regions.

This chapter delivered the first comprehensive spatial analysis and the largest dataset of Mexico's extreme gross vehicle weights (or elsewhere in the scientific literature as far as the authors are aware) with a 50-year and 1000-year return period. This demonstrates the capability and applicability of the methodology requiring basic information concerning traffic characteristics. Additionally, a user interface is provided to facilitate the generation of synthetic axle load observations. It acknowledges the limitations of the data used and advocates for utilizing WIM systems to obtain additional traffic data. This will lead to more accurate and reliable results in traffic load analysis.

The methodology presented in this chapter is limited to the investigation of extreme loads, specifically extreme gross vehicle weights. However, this methodology can be extended to assist in the investigation of failure mechanisms in bridges. The heaviest vehicles cannot be interpreted as the most hazardous for bridges without a comprehensive understanding of specific characteristics. This consideration is particularly relevant in the context of short-span bridges, where the load effects generated by a group of axles may present a greater risk than the gross vehicle weight of the truck. In such cases, the presented methodology can easily be implemented to study other extreme loads, such as extreme individual axle loads or extreme truck tandems. Decision-makers can benefit from the tools and methodologies presented in this chapter, which outline the steps for identifying locations with the highest extreme load values. This information can significantly aid in bridge health monitoring. Furthermore, since decision-makers often seek information about extreme load locations, road network analysis can help identify clusters of areas with extreme gross vehicle weights. Overall, this methodology for computing and mapping extreme gross vehicle weights can be applied virtually in any country or road network where traditional traffic counts are the primary source of traffic data.

4

Estimating bridge criticality due to extreme traffic loads in highway networks

Around the world, an increasing amount of bridge infrastructure is ageing. The resources involved in the reassessment of existing assets often exceed available resources and many bridges lack a minimum structural assessment. Therefore, there is a need for comprehensive and quantitative approaches to assess all the assets in the bridge network to reduce the risk of collapse, damage to infrastructure, and economic losses. This chapter proposes a methodology to quantify the structural criticality of bridges at a network level. To accomplish this, long-run site-specific simulations are conducted using Bayesian Networks and bivariate copulas, utilizing recorded traffic data obtained from permanent counting stations. To enhance the dataset, information from Weigh-in-Motion systems from different regions was integrated through a matching process. Subsequently, the structural response resulting from the simulated traffic is assessed, and the extreme values of the traffic load effects are obtained for selected return periods. Site-specific bridge criticality as a performance indicator for traffic load effects is derived by comparing the extreme load effects with the design load effects. The outcomes are mapped to facilitate visualization employing an open-source geographic information system application. To illustrate the application of the methodology, a total of 576 bridges within a national highway network are investigated, and a comparison with a popular simplified method is shown. The methodology herein presented can be used to assist in assessing the condition of a bridge network and prioritizing maintenance and repair activities by identifying potential bridges subjected to major load stress.

Parts of this chapter have been published verbatim in **Mendoza-Lugo, M. A.**, Nogal, M., Morales-Nápoles, O. (2023). Estimating bridge criticality due to extreme traffic loads in highway networks. Engineering Structures. doi: https://doi.org/10.1016/j.engstruct.2023.117172

4.1 Introduction

The backbone of any country's transportation system is its national highway networks and its bridge structures stock. Bridge management systems (BMS) are employed to control the bridge stock and provide data on the structural performance of bridges. A typical BMS consists of four modules, the Inventory Module, the Inspection Module, the Maintenance, Repair and Rehabilitation Module and the Optimisation Module [107]. In many countries, their Bridge Management Systems (BMSs) are limited to the inventory module (single-module BMS). As a result, these BMSs are rarely used to make decisions regarding the risk and reliability of the bridge stock. However, single-module BMSs have revealed that bridge infrastructure is becoming old and outdated worldwide. Consequently, monitoring bridge loads, especially vehicular loads, is essential for maintaining bridge safety conditions. The data obtained from WIM is essential for many applications such as the calculation of bridge performance indicators [108, 109]. To compute these performance indicators based on traffic load monitoring, the primary step involves determining the load effects caused by the current traffic conditions.

Numerous bridges lack a minimum structural assessment, which should include processes such as visual inspection, site-specific traffic assessment, basic numerical models, examination of structural materials, and documentation review. This assessment serves to identify early concerns and maintenance needs, allowing bridge owners to prioritize further interventions based on the findings. Therefore, for bridge management the reassessment of the entire network is necessary. Information regarding the deterioration state of bridges and their structural behaviour over time are critical elements for bridge management on a network scale [110, 111]. For example, recent studies in bridge maintenance strategies, use deep reinforcement learning (DRL)-based methods [112–114]. The DRL approach facilitates the selection of improved bridge maintenance strategies through interactive processes. It can be adjusted to obtain various performance metrics [115]. The inclusion of traffic loads can serve as one of the input parameters for DRL approaches.

Analyzing traffic load effects on bridges, particularly the extreme values of the load effects (ELEs) is essential to assess the influence of heavy traffic on bridges. ELEs represent the maximum forces, usually bending moments and shear forces, experienced by a bridge during its lifetime. This analysis is crucial for ensuring the safety and reliability of infrastructure design and maintenance. Various probabilistic methods have been developed for this purpose, for example in [116] a methodology of extrapolating maximum load effects based on the level-crossing theory was introduced, [117] presents a Bayesian framework for predicting non-stationary bridge maximum traffic load effects and [97] proposes a clustering algorithm based on the generalized extreme value mixture model for data classification and extreme value extrapolation. However, the most common methods to estimate traffic ELEs include (i) fitting the Rice formula to the level-crossing rate of traffic load effects and extrapolating the load effects under the assumption of a stationary Gaussian process [118, 119]; (ii) the peak-over-threshold method. In which the data above the threshold is fitted to the Generalised Pareto distribution [29, 120], and (iii) the block maxima method in which the load effect due to each vehicle is computed and the maximum values of the selected block of time (usually one day) are selected and fitted to one of the three extreme value (EV) distributions, i.e., Gumbel, Weibull, and Frechet. The reader is referred to [121] for a complete overview of the techniques to estimate extreme load effects on bridges.

On the other hand, one of the most popular simple methods of computing ELEs on two-lane bridges is the (extended) Turkstra's Rule [122, 123]. According to this rule, the N-year loading event, where N could be any return period in years, is generated when the N-year truck encounters a more frequent truck, such as the one-month or one-week truck. Another variation of Turkstra's rule, as reported by [124], suggests that for bridges with high lateral distribution, the critical loading event for bending moment involves a very heavy vehicle, 60% to 80% of 1000-year Gross Vehicle Weight (GVW), in the slow lane and a moderately heavy vehicle (50 to 60 tons) in the fast lane. In the case of shear at the supports, the dominant event type is usually a single extremely heavy truck in the slow lane, 75% to 95% of the 1000-year GVW. Despite its accuracy in specific scenarios, Turkstra's Rule has shown significant inaccuracies in other cases [125, 126].

Two main problems exist when studying the effects of traffic loads on bridges at a network scale. (i) In many locations, WIM systems are not a viable option due to their elevated costs. Traditional traffic counters are the option when a large volume of traffic data is needed. The disadvantage of these devices is that axle loads are typically not measured. (ii) Bridge inventories usually lack detailed information regarding the geometric and material properties of the bridges. Typically, the information contained in the inventories is the number of spans, the length of the bridge, and its width. Specific information on cross-section, material strengths, and steel reinforcement is rarely recorded. These two problems highlight the need for approaches and methodologies that can overcome the limitations imposed by cost constraints and insufficient inventory information. Furthermore, when large-scale studies are needed, maps are needed because of their ability to present summarised information that can be required in the decision-making process. Different engineering fields such as hydraulic, wind, seismic, and transport engineering [127–130] have used maps as a useful tool for hazard modelling. However, to the best of the authors' knowledge, maps of ELEs or load effects performance indicators of a bridge network do not exist in the scientific literature.

In this chapter, a valuable methodology that allows mapping and estimating the extreme load effects due to heavy vehicle (HV) traffic is introduced. Our main objective is to evaluate the structural effect of actual traffic loads in comparison to its effect under the design live load model provided by the bridge owner. This comparison serves as a means to assess the criticality of bridges as performance indicators for traffic load effects at the network level. The specific traffic configuration at each site and the limited information available on single-module BMSs have been considered. This is of relevance for bridge maintenance strategies since it can help the development of strategies to prioritise maintenance, especially in locations or bridge networks in which WIM systems are not the main source of traffic data. The development of the methodology had a dual purpose: (a) to perform a large-scale simulation of site-specific truck traffic and compute its effects on corresponding bridges and (b) to estimate the ELEs of an entire bridge network and perform spatial analysis using geographic information system (GIS) software. The methodology consists of four tasks: site-specific traffic simulation, numerical modelling and analysis of bridge structures, extreme value analysis for ELEs, and bridge criticality computation. To achieve these objectives, this chapter proposes a simple method that uses Gaussian copula-based Bayesian Networks to simulate site-specific synthetic observations of HVs, copulas to characterize inter-vehicle gaps that will simulate traffic flow and extreme value theory to estimate ELEs. The methodology presents various favourable attributes, such as the capability to identify bridges that require more detailed inspections due to their condition as assessed by the model, a simple conceptualization that is easy to apply and requires only basic information regarding traffic and bridge characteristics, the flexibility to be applied to any bridge network, and the ability to help create a more robust single-module BMS.

To illustrate the use of the methodology, the national bridge network of Mexico is selected. Mexico's national bridge network is a clear example in which there is no WIM information available and is bound to a single-module BMS. Therefore, the results of the applied methodology will allow for easily identifying bridges in need of inspection given the limited information available. The remaining document is organized as follows. In Section 4.2 the methodology together with the bridge network case study is presented. The application of the method for one particular bridge is shown in Section 4.3. The results regarding all bridges on the example network, and the comparison with the simplified Turkstra's Rule method are given in Section 4.4. Finally, in Section 4.5, the conclusions are drawn.

4.2 Methodology to estimate extreme load effects and bridge criticality

The aim of this research is to determine and map the extreme load effects and the bridge criticality arising from traffic loads across a bridge network, where data obtained from WIM systems is not the principal source. In order to carry out this extensive task, a simple methodology is presented, shown in Figure 4.1, that can be summarized into four main tasks. (i) Site-specific traffic simulation; statistically representative synthetic traffic is simulated based on real traffic data from the study sites by modelling correlations between the variables of interest (axle loads, inter-axle distances, and inter-vehicle gaps). This step leverages previous research (see [81, 87, 131]). (ii) Numerical modelling and analysis of the bridge structures; selected load effects time histories of the bridges under study are computed by applying the synthetic traffic to a numerical model of the structures. (iii) Extreme value analysis for extreme load effects; statistical analysis of load effects time histories by extreme value theory is carried out to characterize extreme events with selected return periods. (iv) Calculation of the bridge criticality; load effect performance indicators are derived by comparing the extreme load effects with the design load effects. In addition, the computed extreme events and bridge criticality are mapped to visually identified changes, trends, and hot spots that may require attention and support in the design and implementation of maintenance strategies.

This study is conducted using open-source tools. The analysis is done through Python programming language, extensively used nowadays. The Python libraries used in this work (in addition to the main libraries such as NumPy, pandas and SciPy) are `PyBanshee` [47] and `pyvinecopulib` [132] for traffic simulation, `PyNite` [133] for the computation of the load effects on bridges and `Geopandas` [134] to work with the geospatial data. The outcome maps are implemented using QGIS v3.10 [135], a free and open-source cross-platform desktop geographic information system (GIS) application. To enhance clarity and ease the introduction of the methodology, the four tasks will be described in the following

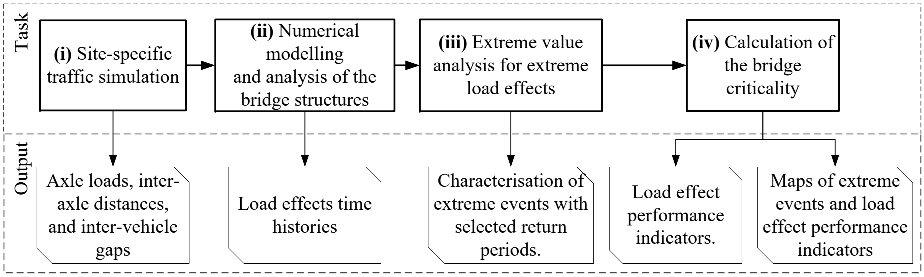

Figure 4.1: Framework estimating extreme load effects and bridge criticality.

sections, using the case study as a context.

4.2.1 Case study: Major highway corridors bridge network of Mexico

The most important elements of the national road network of Mexico are the toll-free fifteen major highway corridors (MHC) which extend over 20 000 km approximately and account for over 55% of the country's highway traffic flow. The toll-free MHC network is managed by the Ministry of Communications and Transportation (SCT, for its acronym in Spanish). The fifteen MHC are shown in Figure 3.2.

Mexican bridge system

Mexico has a system for bridge management, conservation, and maintenance called the Mexican Bridges System (SIPUMEX, for its acronym in Spanish). This system logs the structural state of individual assets in order to program maintenance work. The SIPUMEX database [136], provides general information, such as the name of the bridge, construction date, total bridge length, number of spans, material, and type of structure. Concerning traffic data, the database provides design load, annual average daily traffic (AADT), the vehicle types and the vehicle type distribution that constitutes the traffic flow per bridge. However, the only reported vehicle types are trucks, buses and normal passenger cars and no further specification is presented.

For the purpose of this investigation, the filter criteria shown in Table 4.1 is applied. These criteria have been selected to align with the objectives of the presented study. Firstly, bridges situated on the fifteen MHCs under examination (filter 1) are included. Secondly, according to SCT standards [137], a bridge is defined as having a minimum span length of 6 meters (filter 2). Furthermore, the study focuses on heavy traffic loads, hence only road bridges are considered (filter 3). This criterion aligns with SCT standards, which stipulate a minimum carriage width of 4 meters for road bridges (filter 4) [137]. It is important to note that SCT manages only Overpass bridges (filter 5). To simplify the structural analysis, only non-horizontal curved, non-skewed, and concrete bridges (filters 6, 7, 8) are considered. Additionally, the methodology used to estimate bridge criticality requires bridges with reported design live loads (filter 9). Finally, the inclusion of the span length criterion was intended to eliminate any erroneous measurements or inconsistencies within the dataset (filter 10). As a result, 576 bridges remained, hereafter referred to as the major highway corridors bridge database (MHCB).

Table 4.1: Filter criteria to select the bridges under study.

Filter no.	Criteria	Number of bridges remained after the filter	Number of filtered bridges
1	Bridges located at the 15 MHC	1776	5828
2	Minimum span length of 6 m	1552	224
3	Road bridges	1416	136
4	Minimum carriageway width of 4 m	1390	26
5	Overpass bridges (PSV for its acronym in Spanish)	1317	73
6	Non-horizontally curved bridges	1222	95
7	Non-skew bridges	801	421
8	Concrete bridges	695	106
9	Bridges with reported design live load	675	20
10	The sum of span lengths should be equal to the total bridge length	576	99

4

Figure 4.2 shows a general statistical characterization of the MHCB database. Regarding the age of the structures, around 65% of the bridges (376 bridges) are 50 years old or more, most of them constructed in 1960 (older than 60 years, see Figure 4.2a). The most frequent max span length is 6.6 m (Figure 4.2b). Similarly, most of the bridges have a carriage width of 7 m (two lanes, Figure 4.2c). Approximately, 50% of the bridge structures are single-span systems, while the other structures consist of multi-span bridges with up to seventeen spans, out of which 28 are continuous bridges (Figure 4.2d). As can be seen in Figure 4.2e around 67% of the bridges (387 bridges) were originally designed for load model HS15-44 (three-axle AASHTO standard HS truck with a gross vehicle weight (*GVW*) of 24.5 t approximately [138]) or HS20-44 (three-axle AASHTO standard HS truck with GVW ≈ 32.6 t [138]). The remaining were designed for the Mexican vehicles T3S3 (three-axle truck plus three-axle semitrailer) and T3S2R4 (three-axle truck plus two-axle semitrailer plus four-axle trailer). Regarding the condition of the bridges, 234 structures (41%) have a 2 or 1 rating which corresponds to bridges with minor problems and bridges in good condition (see Figure 4.2f).

Traffic data

As mentioned in Section 4.2.1, information regarding traffic in the SIPUMEX database is limited. Additionally, the use of WIM systems in Mexico is very scarce [139, 140]. Nevertheless, in an effort to know the yearly traffic trends on the Mexican highway network, the SCT installed a set of automatic vehicle counters and survey stations in key locations. As a result, the Mexican authorities publish the two most important traffic data sources in Mexico: the road data (*Datos viales* in Spanish) database [141] and the statistic field study of domestic road transportation (EECAN, for its acronym in Spanish) database [84], previously described in Sections 3.3.1 and 3.3.2.

4.2.2 Site-specific traffic simulation

In order to generate accurate synthetic traffic data statistically representative of the real observations, statistical correlations between the variables of interest need to be modelled. Previous studies such as [29–31], have simulated traffic data using empirical factors, linear

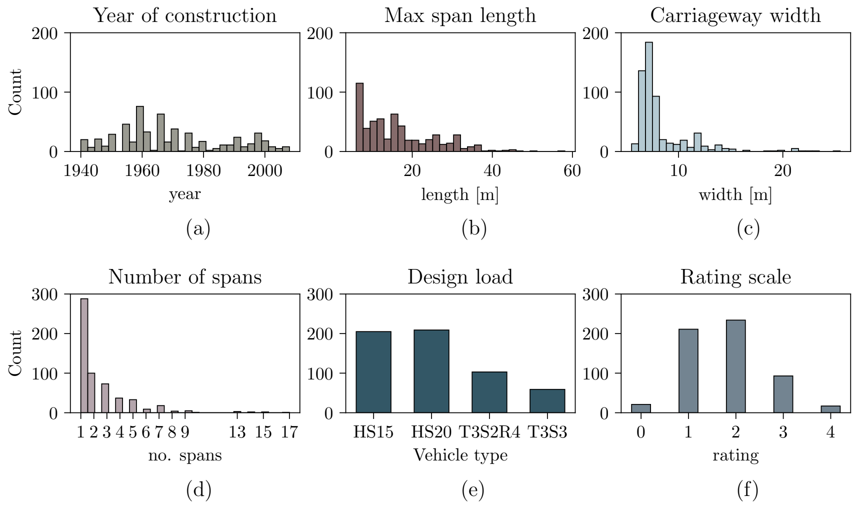

Figure 4.2: General statistical characterization of the bridges under study.(a) Year: Max = 2008, Min = 1940, Mode = 1960. (b) Length[m]: Max = 58.1, Min = 6.0, Mode = 6.6. (c) Width[m]: Max = 25.5, Min = 5.5, Mode = 7.0. (d) No. spans: Max = 17, Min = 1, Mode = 1. (e) Vehicle type: Mode = HS20. (f) Rating: Max = 4, Min = 0, Mode = 2.

4

correlations, and copulas. These studies focus only on axle loads, some provide fixed inter-axle distances and in most of them, the correlation between axle loads is not taken into account. However, it is of interest to modelling GVW, individual axle loads, inter-axle distances and inter-vehicle gaps. With this aim, the Bayesian Network approach presented in [131] which is based on previous studies such as [51, 67, 142] and recently used in [143] is used. This approach is explained in the following sections.

Synthetic heavy vehicles

The GCBN model $\mathrm{GCBN_{EECAN}}$ developed by [131] (see Section 3.4.1) is used. As the name of the model suggests, $\mathrm{GCBN_{EECAN}}$ allows the generation of synthetic axle load observations similar to those reported in the EECAN database. The model, originally quantified with over 750 000 HVs, consists of 26 nodes representing individual axle loads of the five HVs presented in Table 3.1 and 45 arcs corresponding to the (un)conditional rank correlations between axle loads (see Figure 3.4). The output of the GCBN model is a database (different every time that the model runs) that contains the variables: vehicle type, gross vehicle weight and individual axle loads.

One of the limitations of the $\mathrm{GBBN_{EECAN}}$ model is that inter-axle distances and inter-vehicle gaps are not modelled, as information on these variables is not recorded in the EECAN database or in other available Mexican traffic sources. The most reliable technology that delivers loads and wheelbases (inter-axle distances) is WIM, unfortunately, as mentioned in Section 4.2.1, the use of WIM systems in Mexico is very scarce, and publicly available WIM data is non-existent. To complement the missing data information from a Dutch WIM database is used. WIM traffic observations taken on highways A12 (kilometre point, KP, 42) Woerden, A15 (KP 92) Gorinchem and A16 (KP 41) Gravendeel in April

2013 constitute the database. It includes information on more than 150 000 HVs grouped into more than 200 vehicle classes according to their WIM codes. This database has been employed in several studies such as [67, 81, 144, 145].

For a complete overview and details regarding the accuracy of the GCBN model $GCBN_{EECAN}$, the reader is referred to the original source [131]. In this source, EECAN measurements are discussed, including the application of filtering criteria to ensure data quality and the utilization of Gaussian Mixture distributions to model individual axle loads to deal with the uncertainty of the measurements. Similarly, for detailed information regarding specific details and the modelling of dependence and uncertainty in the Dutch WIM database, the reader is referred to [81].

As the SCT report [146] provides the only reliable source of inter-axle distances for the five main Mexican heavy vehicles, the Dutch and Mexican vehicles based on the number of axles, number of consecutive axles, and body configuration have been matched. The consecutive axles are defined as those with centre distances ranging from 100 cm to 243 cm apart, as specified in previous literature [147, 148]. For example, the Mexican vehicle T3S2 will correspond to the Dutch WIM code T1202. For each matched vehicle, inter-axle distance samples from the WIM data have been selected, which exhibited similar mean and coefficient of variation as reported in [146]. Then, the Pearson correlation between inter-axle distances of the matched vehicles is calculated and the resulting values are stored. Five empirical GCBNs, one for each vehicle type, to generate synthetic samples of inter-axle distances have been created. As an example, Figure 4.3 shows the GCBN for vehicle type T3S2, which consists of five nodes representing individual inter-axle distances and four arcs corresponding to the (un)conditional rank correlations between inter-axle distances. For each group of axle loads of a particular vehicle type generated with the $GCBN_{EECAN}$ model, the inter-axle distances are generated using the corresponding inter-axle distance GCBN. Table C.1.1 presents a comparison between the general statistics mean and coefficient of variation between the synthetic inter-axle distances and the reported in the SCT study. A similar approach used for axle space modeling is described in [81].

$$D_{3,1} \rightarrow D_{3,2} \rightarrow D_{3,3} \rightarrow D_{3,4} \rightarrow D_{3,5}$$

Figure 4.3: T3S2 Inter-axle distances GCBN. $D_{i,j}$ denotes a random variable representing the j^{th} inter-axle distance of the vehicle type i ($i = 3$ correspond to vehicle type T3S2). $D_{i,1}$ is the distance between the front of the vehicle and the first axle, $D_{i,2}$ is the distance of the first axle to the second, and so on. The arcs correspond to the (un)conditional rank correlations between individual inter-axle distances.

Inter-vehicle gaps using copulas

The distance between vehicles (gaps) has been studied by many researchers. Some used standard free-flow models by modelling the distance between stationary vehicles with a beta distribution (for example see [38, 149]). Others have used advanced techniques, such as traffic microsimulation based on Intelligent Driver Model [150], which is capable to model car following or lane changing [151, 152]. These advanced techniques are needed when conducting detailed and local-scale bridge analyses, such as the performance of hinged joints [153]. On the other hand, when a global bridge assessment is conducted, standard free-flow models can serve to simulate the distance between vehicles and to indicate the transverse position with the lane where the vehicle is located [152].

For this work, a free-flow traffic pattern is assumed for all lanes of all bridges under study. This is because the traffic loading congestion effect is usually more characteristic of long-span bridges [154] and urban studies due to the complexity of the traffic network and abundant local detours [155]. In order to capture the dependence between gaps [124], a copula-based approach is used. The copula-based approach can characterize the random variable inter-vehicle gap by estimating its auto-correlation. This approach has been used in [51, 142, 143]. Copulas are joint distributions with uniform marginals in [0,1]. Any multivariate joint distribution can be written in terms of a copula that describes the dependence between the random variables and their corresponding uni-variate marginal distribution functions [156]. For specific details regarding copula modelling the reader is referred to [157] and references therein.

Let Y denote a random variable representing the inter-vehicle gap with distribution F_Y. Since the time series $\{Y_t\}, t \in \mathbb{N}$ are the interest, the conditional distribution function of a bivariate copula $C_{\theta_Y}\{F(y_t), F(y_{t-1})\}$ is given by

$$H(y|y_{t-1}) = P(Y_t \leq y_t | Y_{t-1} = y_{t-1}) = C_{\theta_Y}(F(y_t)|F(y_{t-1})) \tag{4.1}$$

where $C_{\theta_Y}(F(y_t)|F(y_{t-1}))$ is the conditional copula and it would model the order 1 auto-correlation for the time series of interest. θ_Y are the parameters that summarize the dependence between $F(y_t)$ and $F(y_{t-1})$. To model the inter-vehicle gaps the following assumptions are made: (1) Only HVs are considered, (2) the distance from the HV's rear to the front of the subsequent HV is considered, (3) correlations between lanes are not taken into account, (4) due to the absence of reliable inter-vehicle gap data for Mexico, the Dutch WIM database from highway A12 (see Section 4.2.2) is used to model the inter-vehicle gaps and (5) only weekdays are considered. Hence, the vehicle gaps simulation algorithm can be summarized as follows:

i Select only the weekdays of the month and group each day dataset by hours.

ii Select the first weekday and the vehicle gaps observations of the first hour $F(y_t)$.

iii Fit the suitable copula $C_{\theta_Y}\{F(y_t), F(y_{t-1})\}$.

iv Repeat steps ii and iii for the remaining hours of the day and weekdays. Let $hr = \{1, 2, \ldots 24\}$ be a set representing hours of a day and $d = \{1, 2, \ldots 20\}$ the set that represent weekdays. Hence, for the study WIM dataset, 480 copulas $C_{\theta_Y}^{d,hr}\{F(y_t), F(y_{t-1})\}$ for one lane are quantified.

v Simulate the desired vehicle gaps for the first hour using the conditional copula according to the best-fitted copula. Use as seed for the first value of the next hour and the last value of the previous hour.

In total, 960 (2 lanes x 20 weekdays x 24 hrs/day) copulas are quantified Bayesian information criterion [158] is used to select the best-fit copula. As an example, Table C.2.1 shows the copula fits of weekday $d = 7$ (9 of April 2013). The first column corresponds to the hour of the day. The 2nd column corresponds to the copula notation. Columns 3 and 4 to the name of and parameter of the copula correspondingly. The 5th column to Spearman's ρ rank correlation [159]. The last column corresponds to the percentage of the total HVs in one day per hour. Notice that for this particular case, stronger correlations can be found at the latest hours of the day and the traffic volume is mostly concentrated between 4:00 hrs and 18:00 hrs. Additionally, Figure 4.4 shows 5 days of HV inter-vehicle gaps observations. Peaks occur at the end (or beginning) of each day since fewer HVs circulate in the early hours of the day. It is important to note that traffic densities, and consequently inter-vehicle gaps, are site-sensitive and can vary significantly based on the specific characteristics and conditions of each country's transportation network. However, for the purpose of demonstrating the methodology presented here and acknowledging the unique characteristics of the study network, it is pointed out that the traffic volume of HVs in the study network is lower compared to the Dutch highway A12 WIM location. Consequently, the results obtained from the analysis may be conservative.

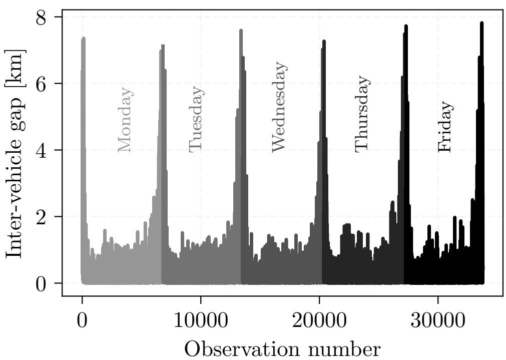

Figure 4.4: Inter-vehicle gaps time series of observations measured in the WIM station A12 left lane corresponding to the days 8 to 12 of April 2013.

Traffic simulation

In order to simulate site-specific HV traffic flow for each one of the 576 bridges in the MHCB, SIPUMEX, EECAN and *Datos Viales* are merged. First, by using QGIS neighbor analysis is conducted to find the nearest counting station to each bridge. The resulting output provides a map of the spatial distribution of the nearest counting stations (298 in total) to each of the bridges under study. The traffic information provided by the resulting counting stations is used to simulate the traffic passing by a particular bridge. It should be noted that the information regarding HV types in the three databases corresponds to the HV types presented in Table 3.1.

Let $\{b\} = \{1, 2, ..., 576\}$ be a set of indices that correspond to the 576 bridges under study and $\{c\} = \{1, 2, ..., 298\}$ a set of indices corresponding to the 298 counting stations. $K_c = \{1, 2, ..., 5\}$ a set whose elements represent the number of total HV types registered in counting station c. H is a set whose elements represent the individual HV types presented in Table 3.1. The necessary input data to compute site-specific traffic for a bridge b are: (i) the number of HV types at the closest counting station of the study bridge b (K_c^b), (ii) the subset $I \subseteq H$, with K_c elements, registered in c (I_c^b), (iii) the proportion of the traffic flow per HV type $i \in I$ ($p_{c,i}^b$) and, (iv) the annual average daily truck traffic (AADTT_c^b). Therefore, a site-specific GCBN_c^b model is quantified using only the K_c^b vehicle types registered in the counting station c travelling over bridge b, i.e, $\mathrm{GCBN}_c^b = \mathrm{GCBN}_{\mathrm{EECAN}}\left(K_c^b; I_c^b; p_{c,i}^b; \mathrm{AADTT}_c^b\right)$. $N_c^b = \sum_1^{K_c^b}(\mathrm{AADTT}_c^b \cdot p_{c,i}^b)$ un-conditional samples using the site-specific GCBN_c^b have been computed. The output of the model is the site-specific synthetic axle load observations for the bridge of interest. Finally, for each vehicle generated, inter-axle distances and inter-vehicle gaps are assigned as described in Section 4.2.2. The output database contains $k = 1, ..., N_c^b$ HVs with the attributes: vehicle type, gross vehicle weight, individual axle loads, individual inter axle distances and the gaps between vehicle k and vehicle $k-1$.

4

4.2.3 Numerical modelling and analysis of the bridge structures

In this work, two load effects are considered, i.e., the absolute bending moment (M in kNm) and the absolute shear force (V in kN). For computational efficiency purposes, the methodology to analyse the bridge structures and determine the load effects is based on the method of influence lines. This approach is a conventional engineering technique that employs influence lines to illustrate how a load effect, such as moment, shear force, reaction, or deflection, changes at a specific point or component of a structure as a concentrated loading action moves across the structure. In essence, an influence line visually depicts the variation of the load effect as the concentrated loading action traverses the structure [160, 161].

To perform the structural analysis of the 576 bridges, the following assumptions are made: (1) the bridges are modelled as a series of interconnected beams,(2) the analysis is based on the principles of the Euler-Bernoulli beam theory, (3) to address the lateral distribution of loads, the weights of trucks travelling in the fast lane are adjusted using lane factors. Regarding bending moments, an equal contribution is considered from each lane, which is represented by a factor of 1. As for shear force, a factor of 0.45 is applied based on the references [124, 162], (4) second-order effects are neglected, (5) dynamic effects due to moving loads are neglected and (6) independent streams of synthetic traffic are generated for each lane [162]. It is important to note that the numerical modelling to perform the structural analysis is based on the linear assumption. However, the design of a bridge is based on the non-linear assumption in order to capture more complex behaviour such as fatigue and buckling.

The procedure for computing the load effects is as follows. First, a grid is specified in each bridge with a grid size of 0.2 m, resulting in a total of $\lceil L^b/0.2 \rfloor + 1$ individual positions along the structures, where L^b is the total length in m of the bridge b. The number of individual positions varies since each bridge has different lengths. A discrete unit load is applied on each position along the bridge to compute the resulting bending moments and shear forces cases. These results are gathered in two matrices $\mathbf{U}_M^b$ and $\mathbf{U}_V^b$ that represent the bending moments and the shear forces caused by the point load in each point on the grid along bridge b. By using the superposition principle, each resulting matrix is multiplied by the axle loads vector $\mathbf{A}$ of each convoy of vehicles (or single vehicle). Hence, the axle loads can be acting in any of the grid points. For each situation, the unit matrices are multiplied by the value of the moving axle loads. Finally, the sum of the multiplication leads to the load effect for the particular convoy or single vehicle driving through bridge b ($\mathbf{M} = \mathbf{U}_M^b \cdot \mathbf{A}$ for example). The envelope of all load effects caused by each vehicle provides the maximum load effects.

4.2.4 Extreme value analysis for extreme load effects

Previous studies have provided an assessment of statistical approaches for evaluating load effects using different quantities of data (see for example [163–165]). One of the most comprehensive studies in this regard was conducted by [121]. In this study, seven statistical inference methods, including Peaks-Over-Threshold, Generalized Extreme Value (GEV), Box–Cox, Normal, Rice formula, Bayesian Inference, and Predictive Likelihood, were critically reviewed. The results of this study revealed that, among these seven methods, the approach of fitting block-maximum data to a GEV distribution is the most widely employed and accepted technique for analyzing bridge traffic loading, typically using a one-day block size.

The block maxima approach has a drawback because it considers only one extreme event in each time block, potentially leading to the omission of significant data. On the other hand, this method offers numerous advantages for load effects analysis. It stands out as the default choice, appreciated for its practicality in capturing daily variations and versatility in handling various scenarios. The main advantage is the time referencing of the data, a crucial requirement when computing lifetime probabilities of exceedance, leading to effectiveness in estimating characteristic values in simple and complex scenarios. Consequently, extreme value analysis based on the block maxima method is used in this work to estimate the ELEs on the bridges under investigation.

Assuming that the block maxima load effects are independent, the block maxima is fitted to one of the extreme value distributions described in Equation (4.2), which corresponds to the GEV distribution, where μ is the location parameter, σ is the scale parameter and ξ is the shape parameter. There are three types of extreme value distributions characterized by the parameter ξ. When the parameter ξ equals 0, the distribution is a Gumbel distribution, when ξ is greater than 0, it is a Fréchet, and when ξ is less than 0, it is a Weibull distribution [166]. As noted by [167], finite or bounded variables cannot have a maximal domain of attraction of Fréchet type. Given that the load effects cannot take infinite values, only Gumbel or Weibull distributions are possible [121]. Therefore, these two types of extreme value distributions are considered.

$$F(x;\mu,\sigma,\xi) = \begin{cases} \exp\left(-\left(1+\xi\left(\frac{x-\mu}{\sigma}\right)^{-\frac{1}{\xi}}\right)\right), & \text{if } \xi \neq 0 \\ \exp\left(-\exp\left(-\frac{x-\mu}{\sigma}\right)\right), & \text{if } \xi = 0 \end{cases} \tag{4.2}$$

For this work, the load effect data for each bridge are grouped into blocks of one day and the maximum value in each block is recorded (daily maxima). Maximum likelihood estimation is the preferred method for estimating the parameters that better describe the daily maxima data. In addition, to find the parameters and distributions, the likelihood function has been truncated [103, 168]. This is done by selecting a truncated load effect value x_0. The choice of x_0 is guided by two considerations: (i) the larger the truncated value, the better the found distribution will accurately describe the tail of the frequency distribution and (ii) the smaller the truncated load, the more data will be used in the part of the likelihood function that accounts for the tail. The data in $\mathbf{x} = \{x_1, x_2, ..., x_n\}$ is rearranged so that: $\{x_1, ..., x_l\} \leq x_0$ and $\{x_{l+1}, ..., x_n\} > x_0$. The truncated-likelihood function of the sample $\mathbf{x}$ can be written according to Equation (4.3).

$$L_x(x; \mathbf{a}) = \{F_x(x_0; \mathbf{a})\}^l \prod_{h=l+1}^{n} f_x(x_h; \mathbf{a}) \tag{4.3}$$

where $\mathbf{a}$ is the parameter vector of the distribution. The vector of parameters can be determined as usually by maximizing the logarithm of the likelihood. The first factor in the right-hand term of the Equation (4.3) ($\{F_x(x_0; \mathbf{a})\}^l$) means that for values smaller than x_0, the probability that they are smaller or equal than x_0 are only considered. On the other hand, the second factor ($\prod_{h=l+1}^{n} f_x(x, h; \mathbf{a})$) means that for values greater or equal to x_0, the usual approach to likelihood estimation using the probability density is taken. This method is also used in Section 3.6. It is noted that a truncation value is set that corresponds to the upper nearest integer $\lceil 2\sqrt{n} \rceil$ observation, i.e., $x_0 = x_{\lceil 2\sqrt{n} \rceil}$ where n is the total number of observations. A similar approach is used in [169, 170].

It is noted that, for the estimation of ELEs, it is assumed that traffic follows a stationary process. This assumption is based on previous studies, for example, [117, 171, 172], which show that the increase in traffic volume and the proportion of heavy trucks have an insignificant impact on the predicted ELEs. Specifically, at a 20-year return period, the increase in predicted ELEs is insignificant. Whereas, at a 75-year return period, the increase is generally moderate. Additionally, when using the GEV distribution to model the maximum LE values, the shape and scale parameters do not vary significantly over time despite traffic growth. Sampling-based extreme value analysis is the most straightforward approach for accurate time-variant reliability assessment [173].

To sum up, extreme value analysis is performed to estimate the ELEs. Six parametric distribution fits are applied to the daily maxima load effects per bridge. These distributions are Gumbel (Gumbel), two-parameters Weibull (Weibull$_2$), three-parameters Weibull (Weibull$_3$); and the corresponding fitted distributions with truncated likelihood function of x_0, Gumbel$_{x_0}$, Weibull$_{2;x_0}$ and Weibull$_{3;x_0}$

4.2.5 Bridge criticality

The criticality of the bridge, as defined in this chapter in Equation (4.4), refers to the ratio (r) between the extreme traffic load effect observed (LE$_O$) and the characteristic load effect induced by the design live load model (LE$_D$). Consequently, r can serve as a meaningful load effect bridge performance indicator. For example, in the case study mentioned earlier in Section 4.2.1, it was found that the design of 414 bridges took into account the AASHTO standards for live loads [138], specifically the HS15-44 and HS20-44 vehicles. These vehicles consist of a semitrailer truck with a gross vehicle weight of 240.2 kN and 320.2 kN, respectively, or an equivalent lane load (see Figure C.3.4a). To compute the characteristic values, the type of loading to be used (truckload or lane load) will be the one that generates the maximum load effect. The remaining 162 bridge structures were designed using the Mexican six-axle HVs T3-S3 and nine-axle HV T3-S2-R4 with their corresponding maximum allowable loads established in [147]. It is worth mentioning that these live loads are based neither on probabilistic analysis of traffic loads nor on bridge structural capacity but on road capacity.

In order to identify the critical bridges in the network due to traffic loads, an analytical comparison is conducted between the actual ELEs and the characteristic values resulting from the design live loads. Locations where a value of r exceeds one indicate that the estimated ELE surpasses the characteristic value specified by the corresponding live load model. In such cases, the bridges are considered critical due to the potential for load exceedance. It is important to note that, in the context of this research, "critical" bridges do not refer to the overall safety of the structure. The bridge performance indicator r (bridge criticality) is not necessarily linked to the risk of failure of the structure. While this indicator and failure risk might be correlated in reinforced concrete bridges, this may not be true for prestressed concrete bridges, as they typically have a large capacity to sustain additional bending load effects after reaching the ultimate design bending moment. Hence, r is not intended to be interpreted as a safety factor; rather, it provides valuable information for comparing the extreme traffic load effects caused by site-specific traffic with those caused by the reported design live load model.

$$r = \frac{\mathrm{LE}_O}{\mathrm{LE}_D} \tag{4.4}$$

4.3 Illustrative example application to a specific bridge

The proposed framework is applied to the entire MHCB network. For the sake of illustration, specific results for a selected bridge are presented in this section. Results at a network level are discussed in Section 4.4. The bridge *El Rosario I* is studied in the following illustrative example application. The characteristics of the traffic data for the site are first described. Site-specific traffic simulation is next performed. Later the load effects are computed and finally, the load effects are analysed and ELEs are estimated.

According to the SIPUMEX database, *El Rosario I* is a two-lane nine spans continuous bridge with a total length of 264.4 m. It has a minimum span length of 25.8 m and a maximum span length of 30.8 m. Built in 1982, the bridge is located in the state of Baja California Sur on the MHC number 6 *Transpeninsular Baja California*. The nearest counting station is *Rosario de Arriba* located around 4 km west over the same MHC. The annual average daily truck traffic that circulates by this station is 444 HVs with the following configuration: 45% C2, 9.7% C3, 43% T3S2, 1.4% T3S3 and 0.9% T3S3R4. This information serves as input for the GCBN model. According to the notation introduced in Section 4.2.2, in *El Rosario I* bridge ($b = 9$), with information of the counting station *Rosario de Arriba* ($c = 60$), the five vehicle types presented in Table 3.1 are registered, i.e., $K_{60}^{9} = 5$. Hence the vehicle types that conform to the traffic flow are $I_{60}^{9} = \{\mathrm{C2}, \mathrm{C3}, \mathrm{T3S2}, \mathrm{T3S3}, \mathrm{T3S2R4}\}$. Their corresponding proportions $p_{60,i}^{9}$ of the total vehicles are: $p_{60,1}^{9} = 0.45$, $p_{60,2}^{9} = 0.097$, $p_{60,3}^{9} = 0.43$, $p_{60,4}^{9} = 0.014$ and $p_{60,5}^{9} = 0.009$. The corresponding site-specific direct acyclic graph that represents the GCBN_{60}^{9} model is shown in Figure 3.4.

A total of $N_{60}^{9} = \mathrm{AADTT}_{60}^{9} = 444$ un-conditional samples using the GCBN_{60}^{9} model have been coputed. The inter-vehicle gaps are simulated using the approach described in Section 4.2.2. The output is a database of the synthetic site-specific traffic load observations (different every time the model is run). Table C.3.1 presents the generated synthetic traffic of one day and Figure C.3.1 shows the corresponding bar plot of the number of HVs simulated per hour for lane 1 of the bridge *El Rosario I*.

Once the synthetic traffic is computed, the load effects of interest for each vehicle are calculated according to the procedure described in Section 4.2.3 and the envelope of the results is found. The absolute maximum values of the bending moments and shear forces envelopes per day obtained are stored. In total 200 days are simulated. Therefore 200 daily maxima load effects are obtained. The resulting envelopes of one day of the bending moments are presented in Figure 4.5.

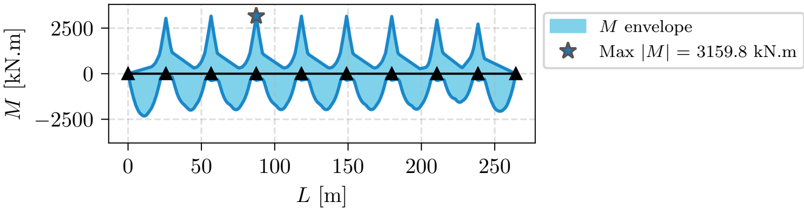

Figure 4.5: Load effects envelopes for the continuous bridge *El Rosario I* corresponding to one day of traffic simulation. Envelope of bending moments.

As described in Section 4.2.4, the ELEs are computed with a return period of 50 years and 1000 years according to the specifications [174, 175] correspondingly. As stated in [176], it is considered that there are 254 working days excluding weekends and holidays in Mexico. The daily absolute maxima load effects are fitted to the selected parametric distributions. Figure 4.6 shows the comparison of the fitted distributions presented in Section 4.2.4 for the absolute bending moment for bridge *El Rosario I*. The parametric distributions Weibull$_2$ and Gumbel produce significantly lower characteristic values for this particular case. A visual inspection suggests that the best fit is provided either by Gumbel$_{x_0}$ or Weibull$_{3;x_0}$ with $x_0 = 2838.4$ kNm. However, using the Akaike Information Criterion (AIC) [177] to measure the quality of the fitting, Weibul$_3$ (black dashed line in Figure 4.6) is the selected distribution that better describes the data. The estimated extreme bending moments are 3614 kNm and 3766 kNm with 50-year (M_{50}) and 1000-year (M_{1000}) return periods, respectively. When analysing the absolute shear force for the same bridge, the best fit is provided by Wibull$_{2;x_0}$ with $x_0 = 681.7$ kN. The estimated extreme shear forces are 928 kN and 1011 kN with 50-year (V_{50}) and 1000-year (V_{1000}) return periods accordingly.

Finally, the load effect bridge performance indicator (Section 4.2.5), denoted as r is computed to evaluate the performance of the bridge under consideration. According to the SIPUMEX database, for the design of the bridge, the AASHTO standard truck HS20–44 model is used as the representative design live load model. The maximum bending moment induced by the design live load model (M_D) amounts to 4501.4 kNm. Additionally, the maximum shear force caused by the same design live load model (V_D) corresponds to 928.1 kN. Subsequently, the load effect performance indicator for the bending moment, considering a 50-year return period is $M_{50,r} = M_{50}/M_D = 3614/4501 = 0.80$. Similarly, the load effect performance indicator for the shear force is $V_{50,r} = V_{50}/V_D = 928/982 = 0.95$. When the obtained performance indicators are contrasted with the load effects

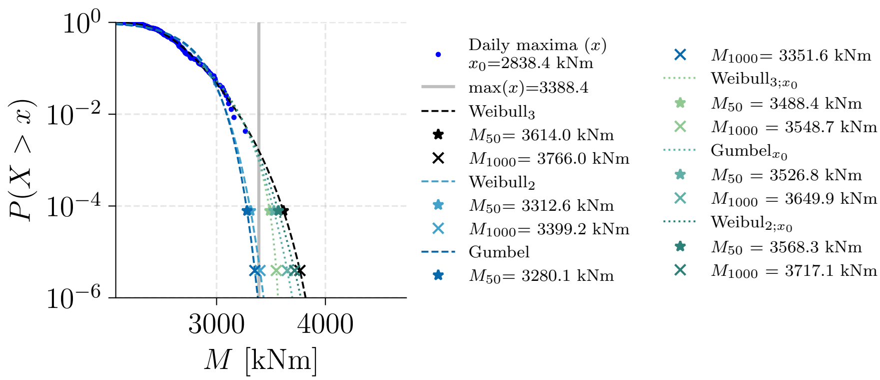

Figure 4.6: Exceedance probability plot comparison bridge *El Rosario I*. In blue circles, the absolute bending moment daily maxima values. The vertical grey solid line represents the value of the maximum daily maxima recorded observation. The star markers represent the extrapolated value that corresponds to an ELE with a 50-year (M_{50}). The triangle markers represent an ELE with a 1000-year (M_{1000}) return period.

corresponding to a 1000-year return period, the resulting ratios for the bending moment and shear force are 0.84 and 1.03, respectively. These ratios are denoted as $V_{1000,r}$ and $M_{1000,r}$.

4.4 Extreme Load Effects at a network level

The methodology explained in section 4.2 and illustrated in section 4.3 is applied to the 576 bridges of the MHCB. Over 159 million HVs are simulated using 278 site-specific GCBNs. The loading effect on the respective bridge of each HVs has been calculated. This long-run traffic load simulation involves a high computational cost of around 13 000 core hours, performed on the DelftBlue supercomputer at TU Delft [178]. Out of the 576 maximum 254-day load effects computed, 529 are caused by individual HVs and 47 by a convoy of vehicles. For illustration purposes, Figure C.3.2 shows the vehicle types that caused the maximum 254-day absolute bending moment and the corresponding *GVW* distribution of the first two lanes of all bridges. Notice that around 96% of the studied bridges have two lanes. A bi-modal-like distribution can be observed for the *GVW* with two peaks at around 580 kN and 950 kN. These values are likely to be due to the vehicles meeting the maximum allowable *GVW* and overweight vehicles, correspondingly. The max *GVW* according to Mexican standards [147] is 740.41 kN. The vehicle types C2 and C3 caused the maximum bending moment in only five bridges.

Extreme value analysis is performed on each one of the bridges under study to find the characteristic values of the load effects. In order to select a particular distribution for the maximum at each bridge AIC together with visual inspection was used. AIC values for different parametric distributions vary significantly between bridge structures mainly due to the large variation in moments and shear forces calculations across bridges (notice that for all bridges 254 daily maxima are used). In general, mostly the Weibull$_3$ distribution and the Weibull$_{2;x_0}$ distribution are the ones that better describe the individual daily maxima load effects.

Once all the distributions that better describe the data are selected, the ELEs M_{50}, M_{1000}, V_{50} and V_{1000} are estimated for the 576 bridges. Let E denote a random variable representing any of the four estimated ELEs. The resulting ELEs are categorised into 6 classes according to: $[E_{\min}, E_5)$, $[E_5, E_{25})$, $[E_{25}, E_{50})$, $[E_{50}, E_{75})$, $[E_{75}, E_{95})$ and $[E_{95}, E_{\max}]$. Where E_q denotes the qth percentile of the distribution of E. As an example, the ELE M_{50} map is presented in Figure 4.7, to increase legibility, simple geometric square markers are used to represent individual bridges. The colour code of the geometric markers represents each of the 6 M_{50} percentile classes. For this example the 6 classes are (in kNm):$[592, 800)$, $[800, 1327)$, $[1327, 2507)$, $[2507, 4918)$, $[4918, 9320)$ and $[9320, 16\,124]$. The corresponding histogram of frequencies of the computed M_{50} distribution is presented at the bottom of the figure. The highest extreme bending moment with a return period of 50 years (1623.8 kNm) corresponds to the 7-span bridge *Rio Fuerte* located in the northwest region of Sinaloa state (star shape maker in Figure 4.7). This result is expected since *Rio Fuerte* bridge has one of the largest spans of the database (44.7 m). A similar map for V_{50} can be found in Figure C.4.3 in the appendix. Mapping the site-specific extreme traffic load effects allows the identification of the most critical bridges for which more detailed information or immediate traffic-related actions may be required.

4

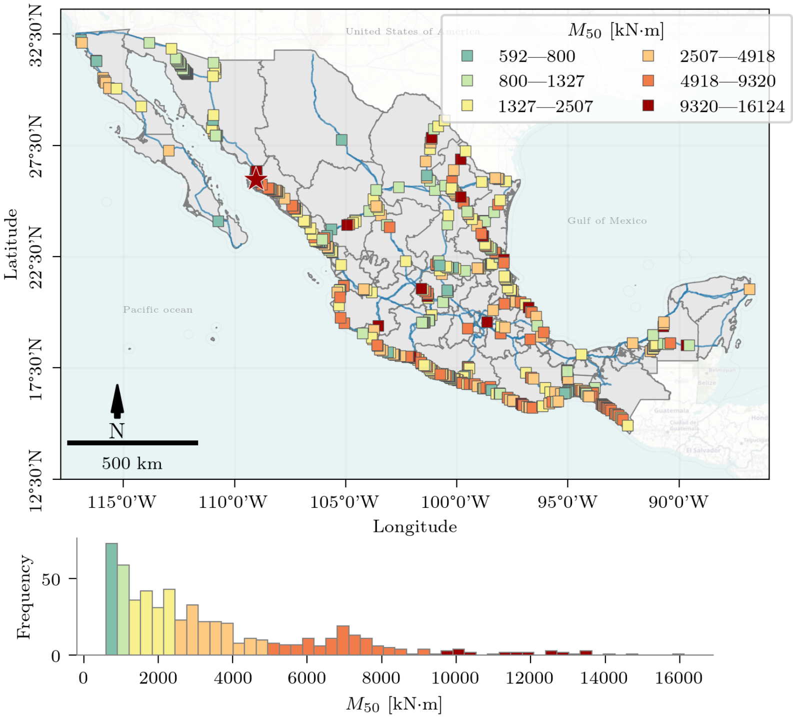

Figure 4.7: Extreme load effects map for the maximum absolute bending moment with a 50-year return period.

4.4.1 Comparison with a simple popular method

When applying Turkstra's Rule it is assumed that the trucks meet at the critical point of the influence line, which represents an extreme loading event. However, the extreme loading events consist of very heavy trucks meeting near, but not exactly at, this critical point. Therefore, as pointed out by [179] a more intuitive model would consider placing one of the trucks at a distance αL from the other, where α represents a scaling factor (see Figure C.3.3). It is important to note that the situation differs for the two load effects, resulting in α_M not being equal to α_V.

Through the analysis of simulations that generate the maximum daily maximum load effects for simply supported two-lane bridges (total of 445 bridges), the application of Turkstra's Rule reveals that the 50-year loading event consists of the 50-year truck in the slow lane, combined with the one-day return period truck for 280 bridges and the one-week return period truck for the remaining bridges. The values of $\alpha_{M_{50}}$ range from 0.02 to 0.70, while $\alpha_{V_{50}}$ varies between 0.06 and 0.89. The selection of α_M and α_v values was based on achieving the closest approximation to the target values, specifically M_{50} and V_{50} obtained from the simulations. Based on this investigation, it can be concluded that in 362 out of the 445 two-lane bridges, the (extended) Turkstra's Rule yields accurate results with discrepancies ranging from -0.3% to +3.0% for M_{50}. Conversely, for V_{50}, the variations range from -0.3% to +3.9% for the same set of bridges. On the other hand, discrepancies of up to 15.8% and 23.0% are obtained when comparing the values of M_{50} and V_{50}, respectively, in cases where Turkstra's Rule fails to produce precise outcomes for bridge analysis.

As can be seen, Turkstra's Rule simplified model provides accurate estimations of the ELEs in the majority of the studied bridges. Nevertheless, a trial-and-error approach is needed to derive the value of alpha. Moreover, the computation of site-specific 50-year trucks requires extensive simulations. While it is conceivable to construct a moderately precise model through this method, it is essential to note that the process is both highly dependent on site-specific factors and time-intensive. Extending Turkstra's Rule model to include continuous bridges and three or more lanes is beyond the scope of this chapter. However, future works will explore the differences between Turkstra's Rule model and our approach, specifically incorporating continuous bridges and three or more lanes.

4.4.2 Mapping bridge criticality

In this section, as mentioned in Section 4.2.5 to identify the most critical bridges on the network, a load effect bridge performance indicator based on the ratio r between the computed extreme load effects and the design load effects is computed. The obtained ELEs are compared with the characteristic values calculated using the reported design live load (HS15-44, HS20-44, T3-S3 or T3-S2-R4) at each bridge site. According to [138], it is assumed that the standard trucks occupy a width of 3.00 m. In load factor design, a live load factor of 1.67 is adopted. Additionally, a reduction of the live load of 90% and 75% may be used in view of improbable coincident loadings for three lanes and for four lanes or more, respectively. Because of the absence of a Mexican bridge design code, the live load factor and live load reductions due to the improbable coincident loadings in lanes established in the AASTHO standards are assumed.

Figure 4.8, shows the computed 50-year absolute bending moment ratios, $M_{50,r}$, for all bridges under study. These ratios indicate that, in most cases, the $M_{50,r}$ values are significantly higher when compared to those generated by the AASHTO standard HS truck live loads. Specifically, they can be up to 1.71 times larger for bending moments (similarly, up to 1.67 times larger for shear forces). On the other hand, when considering the ratios computed with the maximum allowable Mexican HVs, a different trend emerges. In this case, the load effects computed using the maximum allowable values specified in the Mexican standard exceed those computed using our approach, which is based on observed data. Therefore, Figure 4.8 reveals that the computation of ELEs ratios on bridges subjected to AASHTO loads results, usually, in lower load effects than when considering Mexican allowable HVs. Notice that the ratio decreases as the year of construction progresses. The results of the ratios presented above are in line with the fact that the AASHTO standard HS trucks, which were commonly used until the early 2000s for the structural design of bridges in Mexico, underestimate the values of the load effects (shear forces and bending moments) for design [180, 181]. As a result, in 2001 the Mexican Institute of Transportation proposed a live load model named IMT-66.5 [174] better aligned with the actual traffic load demands.

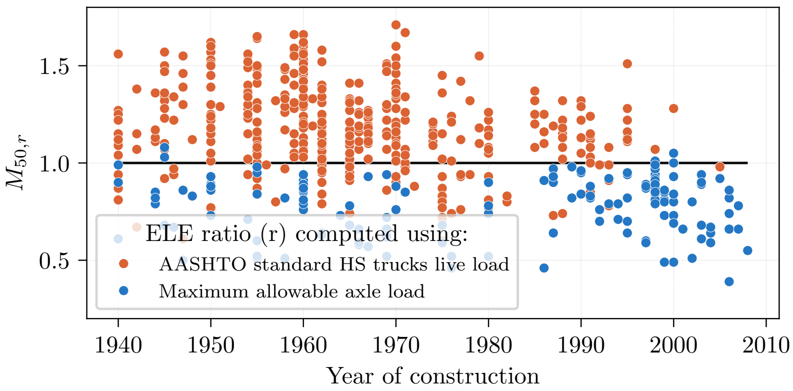

Figure 4.8: Computed extreme load effects ratios per bridge per year. Maximum absolute bending moment with 50-year return period ratios ($M_{50,r}$)

The computed ratios are categorised into 6 classes according to the 5th, 25th, 50th, 75th, and 95th percentiles of the corresponding distribution, i.e., $[r_{\min}, r_5)$, $[r_5, r_{25})$, $[r_{25}, r_{50})$, $[r_{50}, r_{75})$, $[r_{75}, r_{95})$ and $[r_{95}, r_{\max}]$. For illustration, Figure 4.9 present the ratios $M_{50,r}$ map. A similar map of $V_{50,r}$ can be found in Figure C.4.6. As can be seen, the lowest ratio values for both extreme traffic load effects (between 0.41 and 0.67) are mostly concentrated on the bridges located on corridors that cross the states of Sinaola, Guanajuato, and Guerrero accordingly. The ratio is approximately 1-1.3 in most parts of the major corridors highway network. The highest ratios (above 1.42) are primarily concentrated on the highway that connects the cities of Caborca and Sonoyta in northern Mexico. To exemplify a simple use of maps as a tool, a characterization of the computed load effect indicators is presented in the following section.

4

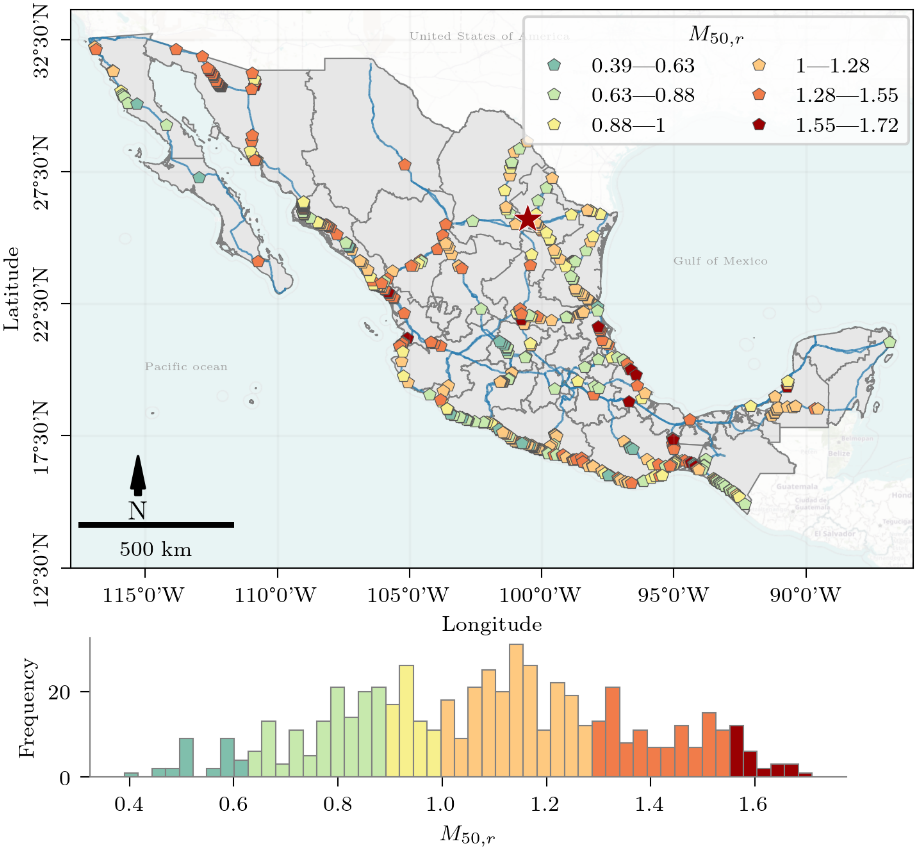

Figure 4.9: Extreme bending moment with 50-year return period ratios ($M_{50,r}$). Each pentagon shape marker represents a computed ratio per bridge. The star marker represents the bridge with the highest $M_{50,r}$ corresponding to *Arboledas* bridge $M_{50,r} = 1.71$.

4.4.3 Comparison of bridge criticality at major highway corridors

In order to perform a load effect bridge criticality characterization, the fifteen MHCs, shown in Figure C.4.1, were considered. The percentage of bridges with r considering load effects with a 50-year return period greater than one, i.e. $\%M_{50,r} > 1$ and $\%V_{50,r} > 1$ are presented in Figure 4.10 for all corridors. It can be observed that both indicators have similar behaviour with the exception of corridor number 14 in which the $\%M_{50,r} > 1$ is more than double the $\%V_{50,r} > 1$ (89% - 39%). The highest $\%M_{50,r} > 1$ values are presented in the MHC *Peninsula de Yucatán* (corridor number 14, 89%), *Circuito Transístmico* (corridor number 13, 76%) and *México-Nogales, Tijuana* (corridor number 1, 71%) Whereas the highest $\%V_{50,r} > 1$ can be found in corridors number 1, 7 (*Acapulco -Veracruz*) and 13. In addition, corridors *México-Tuxpan* and *Altiplano* presented a value of 0% due to the fact that these corridors have few bridges, 2 and 3 bridges respectively. Among the MHCs, it is clear that MHC number 14 is the corridor where attention is needed since the estimated characteristic loading in 16 out of its 18 bridges is greater than the design values specified by the corresponding live load model reported in SIPUMEX database. With 145 bridges in total, *México-Nogales, Tijuana* (MHC number 1) is the corridor with more bridges in the Mexican Federal highway network. This corridor is another point of attention since 103 of its bridges have a $\%M_{50,r} > 1$ and 93 bridges (64%) a $\%V_{50,r} > 1$. It is likely that perturbations on the bridges of these corridors will generate certain stress levels in their road network generating at least an increase in user travel costs. Notice that by omitting corridors number 4 and number 10 the average percentage of bridges with $\%M_{50,r} > 1$ is 62% and the average $\%V_{50,r} > 1$ is 46.5%. It is clear that more than half of the existing bridges in the network need attention.

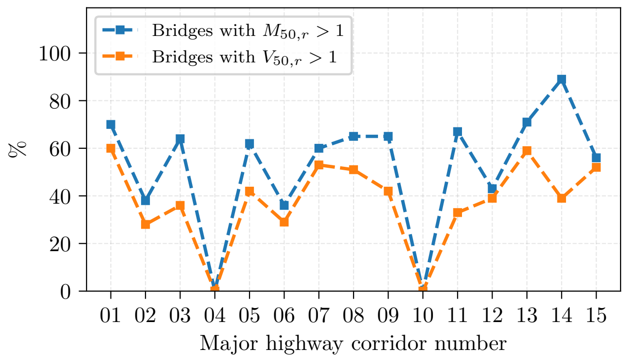

Figure 4.10: Percentage of bridges with a $M_{50,r}$ and $V_{50,r}$ above 1 per major highway corridor.

The previous description was focused on 50-year LEs, but the trends are also representative of other return periods. In contrast to the Mexican standards, in the Eurocode EN 1991-Part 2: Traffic load on bridges [175] the characteristic values are defined with a return period of 1000 years instead of 50 years due to the requirement of serviceability and sustainability of the structures. For example, when considering bending moments with a 1000-year return period, the number of bridges in the most critical group (ratios between 1.55 and 1.72) increases from 31 to 68. As can be seen, the return period is a crucial factor in risk analysis and design. Events with low probabilities may result in greater casualties, direct losses, and indirect effects. The corresponding maps of ELEs with a return period of 1000 years can be found in the appendix (Figures C.4.2, C.4.4, C.4.5 and C.4.7). Additionally, the supplementary material presents individual maps for $M_{50}, V_{50}, M_{50,r}$, and $V_{50,r}$ for each MHC. An interactive map has also been produced using QGIS. The map can be accessed at https://mike-mendoza.github.io/eles_mexico/.

As illustrated, the methodology and maps presented help to visually identify changes, trends, and hot spots that may require attention on a large bridge network. For the Mexican authorities, the maps delivered herein give the first clear picture of the distribution of extreme load effects on concrete bridges due to traffic loads at the Mexican highway network. They provide relevant information that can support the development of a comprehensive approach to bridge management to prioritize structural inspection or maintenance interventions.

4.5 Conclusions

This chapter has presented a 4-step method to estimate and map the extreme bending moments, extreme shear forces, and load effect performance indicators due to traffic in a bridge network at a national scale as realistically and accurately as possible when information is scarce. This approach permits the visualization and measurement of the criticality of elements in the network. Hence, to some extent, the degree to which individual bridges require attention. The criticality of the bridge, as described in this research, relates to the relationship between the chosen extreme traffic load effect and the load effect caused by the design live load model.

The method is low information-intensive per bridge. The necessary information in most cases is usually available in countries with at least one-module bridge management system. Regarding the bridge data, it requires the number of spans and the corresponding length, the number of lanes and the corresponding width, and the design live load. Regarding traffic information, the method requires the Annual Average Daily Traffic and the proportion per vehicle type that conforms to the traffic flow.

The method uses Gaussian copula-based Bayesian Networks to generate site-specific synthetic observations of heavy vehicles. To simulate traffic flow a copula-based approach is used to characterize the inter-vehicle gap by estimating its auto-correlation. A long-run traffic load simulation is used to obtain the traffic load effects on the bridges. Then, the extreme load effects are estimated using the block maxima extreme value analysis approach. The comparison of the obtained values with the design loads reveals interesting information about the criticality of the existing infrastructure. To illustrate the method, it has been applied to a case study involving the bridge network located along the fifteen major toll-free highway corridors in Mexico, which comprises a total of 576 bridges. The results of this study were then used to create four main maps that provide a comprehensive understanding of the load effects on the bridges within a national highway network, enabling the identification of spatial patterns and relationships. It is recommended to draw attention to bridges with values of bridge criticality greater than one. This recommendation does not imply that these bridges experience greater degradation, require more frequent inspections, or incur higher maintenance costs. Rather, it suggests that these bridges should be highlighted for more thorough and reliable inspections.

The main advantages of this methodology include its simplicity and ease of application due to its straightforward conceptualization. Additionally, the required data can be obtained from basic information about the bridges and traffic, as well as publicly available databases, making it highly flexible and applicable to nearly any bridge network. This study encounters certain limitations. Firstly, it relies on a restricted amount and variety of data from a specific bridge network. Therefore, it does not take into account factors such as the impact of ageing on individual bridge structures and bridge component ratings. Secondly, the computational cost of the method increases proportionally with the number of bridges under consideration, making complex structural analyses resource-intensive and demanding extensive material and geometrical data. Lastly, the approach used to estimate characteristic values of load effects primarily relies on the block maxima extreme value analysis method. The sensitivity of the results to a different choice (Peaks-Over-Threshold method for example) has not been tested. However, the goal was to develop a universal, simple method to aid local authorities in regions where WIM systems are not the primary source of traffic data. It is important to note that this chapter acknowledges the limitations of existing traffic data sources and emphasizes the crucial role of collecting additional data through WIM systems. Therefore, it does not suggest that WIM traffic data is unnecessary but rather advocates for its use to obtain reliable results in traffic loading analysis by collecting accurate and substantial amounts of traffic data.

Future work based on the methodology can investigate its applicability in other networks to test its ability as a general approach. Regions in the United States and Europe in which data from robust BMS and WIM systems are available can be used to apply the methodology in its corresponding networks. It is possible, for instance, to quantify a BN model with WIM datasets and analyse its performance relative to the Mexican quantification presented in this chapter, as well as to combine those data. In this manner, several scenarios can be made with an increase in traffic volume and different vehicle configurations passing through specific bridges. Further research can explore the use of different approaches for estimating ELEs. In particular, the Peaks-Over-Threshold method seems like a natural starting point. Additionally, consider the integration of WIM data from diverse regions to assess its influence on the bridge criticality results. Finally, researchers could explore ways to integrate the methodology into decision-making processes by combining bridge performance measurements such as condition rating and bridge criticality presented here to optimize preventive maintenance schedules of all the bridges of the network.

5

Network-level optimization approach for bridge interventions scheduling

This chapter presents a novel extension of the multi-system optimization method known as the 3C concept tailored for optimizing budget allocation for bridge interventions at the network level. The extended methodology takes into account the interdependencies among the bridges in the portfolio caused by the spatial proximity of objects within the network. It incorporates direct and user costs, bridge performance indicators, as well as a bridge deterioration model. A real case involving a bridge portfolio of 555 bridges is presented to demonstrate the practicality of the methodology which efficiently determines the optimal intervention sequence. For an analysis period of 18 years, the proposed methodology achieved a 23% reduction in total costs by combining repairs for bridges with high to severe damage and maintenance for the rest. This improvement is in comparison to the bridge management agency approach, which relies on maintenance. As the results are derived from an optimized procedure, they outperform human intuition in managing complex bridge networks, especially during extended analysis periods. The methodology presented could help transportation agencies to implement and explore various scenarios by adjusting the time between consecutive interventions and budget constraints supporting a comprehensive analysis and informed decision-making process.

Parts of this chapter have been published verbatim in **Mendoza-Lugo, M. A.**, Nogal, M., Morales-Nápoles, O. (2024). Network-level optimization approach for bridge interventions scheduling. Structure and Infrastructure Engineering. doi: https://www.tandfonline.com/doi/full/10.1080/15732479.2024.2403568

5

5.1 Introduction

Bridge networks are susceptible to degradation caused by factors such as ageing, heavy traffic loads, and natural disasters. Such degradation may result in failures that compromise service quality and create safety hazards [182]. Together with constrained funding for bridge management, this underscores the need for objective assessments to achieve better utilization of existing aging bridges [183]. To maintain the functionality of the transport infrastructure and related service parameters, bridge managers have come to recognize that effective planning of interventions can significantly enhance the availability of their infrastructures while minimizing costs.

For effective intervention programs, it is clear that optimal planning should consider both the direct and user costs associated with transport disruptions, rather than solely budget availability [28]. Previous research indicates that when bridges are full or partially closed, the resulting traveler delays can incur indirect costs several times the actual cost of the bridge [184–186]. These higher costs require bridge owners to allocate resources toward optimal strategies for bridge interventions.

Furthermore, at a network-level, a significant number of bridge structures need to be analyzed, making it infeasible to re-analyze each bridge on an annual basis. Consequently, systems that continuously monitor bridge conditions are established to plan interventions based on structural ratings and prioritization indexes to justify the funding of conservation actions [43]. At the network level, it has been shown that integrating performance measures from all individual bridges into optimal budget allocation algorithms can enhance the overall performance of bridge systems [42].

There is an increasing literature on optimal bridge management planning. This literature can be divided into three main categories: (i) Deterioration modeling, (ii) Ranking of management alternatives and (iii) Maintenance planning using optimization techniques [187–189]. The first (i) focuses on developing models to predict the deterioration of bridges over time, and the second (ii) compares different options based on their effectiveness and other factors for bridge prioritization. However, these approaches do not take into consideration constraints such as environmental impact, traffic demand, and budget constraints, which are crucial for a bridge intervention program at the network level. To overcome this, the third category (iii) uses optimization techniques to take into account constraints and find the optimal management scheduling for bridges.

In a bridge-level, generally, six intervention approaches[1] are taken: do-nothing; maintenance, repair, rehabilitation, and improvement; and total replacement. Do-nothing involves minimal intervention but risks long-term deterioration. Maintenance implies routine activities to preserve the bridge in good condition. Repair fixes defects that affect functionality, safety, or performance. While rehabilitation restores the bridge to a better state to increase the service life. Improvement enhances the bridge beyond its original condition to meet new requirements, and total replacement means replacing the entire asset with a new one, often incorporating modern technology [46, 190, 191].

[192] developed a bi-objective optimization model that minimizes the total rehabilitation action cost and maximizes the performance as a result of the latest rehabilitation action

[1]It is noted that previous literature often categorizes and refers to these actions in two main groups: preventive maintenance (which includes maintenance and minor repairs) and corrective maintenance (including major repairs, rehabilitation, improvements, and replacements).

applied to bridge decks. In [44], an optimal budget allocation framework is proposed for maintenance, repair, and total replacement actions for bridge portfolios that minimize the agency costs to have bridges in the portfolio in their like-new state.

A multi-objective optimization model using an exponential chaotic differential evolution algorithm is introduced in [45]. The model includes maximization of performance condition of bridge elements, minimization of agency and user costs, minimization of duration of traffic disruption, and minimization of environmental impact. In [193], optimization is performed to obtain optimal maintenance strategies associated with objectives related to connectivity and maintenance cost, taking into account the conditional failure of network connectivity given the failure of a specific bridge.

[194] presented a methodology to establish the optimal timing conditions for each standard maintenance and rehabilitation intervention used by the Indiana Department of Transportation for each highway bridge, thereby developing long-term, condition-based schedules. Furthermore, the effects on the bridge performance trend resulting from the differences between post-treatment and pre-treatment interventions were explored. However, no budget constraints were taken into account in the optimal scheduling process.

At the bridge network level, [195] developed a specific bridge stock model to optimize the allocation of funds for selecting maintenance or rehabilitation policies for the Bridge Management System of Chiapas State in Mexico. This involved utilizing joint optimization of maintenance and rehabilitation policies that employ a genetic algorithm to find the optimal costs for different policies, taking into consideration the deterioration process with Markovian transition matrices.

[46] developed a bridge management system to determine the overall optimality of investment decisions based on a desired combination of selected performance measures. This approach enables making investment choices based on optimal forecasted performance. The methodology involves conducting a multi-criteria utility function for the selection of bridge interventions, which includes optimizing the identification and evaluating network-level solution approaches.

These previous examples show how to allocate maintenance resources for a group of bridges or individual bridges in a transportation network. However, there are a few studies that consider the impact resulting from executing interventions, such as the interconnected effects of interventions on individual bridges within the network caused by spatial proximity. [196] presented a framework for optimizing preventive maintenance scheduling in bridge networks, considering the correlation between bridge states and utilizing a probabilistic model. This model accounts for the expected damage levels of two bridges subjected to the same extreme event scenario and their spatial proximity. However, an important aspect of this methodology is its computational efficiency and the absence of real-data-based cost evaluations for the interventions. [197] presented an integrative multi-system method, known as the 3C concept, to account for infrastructure connectivity by considering the spatial proximity of objects within infrastructure networks. This involves formalizing a mathematical method for intervention scheduling at a network level, capable of obtaining the most efficient intervention program. These examples underscore the importance of developing intervention programs for spatially close and functionally connected structures simultaneously.

In this study, a novel extension of the integrative multi-system optimization 3C concept is introduced. This extension, named B-3C, focuses on optimizing budget allocation for bridge interventions at the network level, specifically for maintenance and repair activities. B-3C builds upon the core principles of the 3C framework but introduces additional elements and modifications tailored to address optimal budget allocation for bridge intervention programs. The existing framework has been extended by incorporating two types of interventions while maintaining the mathematical linearity of the problem. This mathematical property ensures its applicability to portfolios containing a large number of bridges. Furthermore, it considers factors such as deterioration, budget constraints, and the time between two consecutive interventions. The B-3C methodology for optimizing bridge intervention scheduling addresses a significant gap by considering the interconnected effects (additional costs) of interventions on individual bridges within the network system caused by the spatial proximity of the bridges. Additionally, the methodology herein presented provides practical guidance for estimating both direct and user costs through the analysis of a real-data-based bridge network. It can be applied in conjunction with various bridge ranking systems that rely on performance indicators, including condition state and traffic load effects criticality, making it a valuable tool for efficiently planning interventions within extensive bridge networks.

The remainder of the chapter is organized as follows. In Section 5.2, the theoretical introduction of the concepts used in this study are presented. This section also includes the framework for optimizing intervention activities on bridge networks and the mathematical formulation of the optimization problem. Section 5.3 presents a numerical example to illustrate the applicability of the proposed optimization model. Section 5.4 presents the proposed optimization model applied to a bridge portfolio of 555 bridges. Finally, conclusions are drawn in Section 5.5 together with the proposed future work.

5.2 Methodology

In the context of this study, the goal of optimal intervention planning for a bridge network is to schedule interventions for each bridge in a manner that minimizes the overall intervention cost. While bridge managers often face other explicit goals, such as minimizing vulnerability to damage or maximizing the average condition of the bridge network ([46]), our primary interest is solely to minimize the total cost of interventions. Figure 5.1 illustrates a simplified version of the proposed framework for optimal intervention planning used in this research. First, relevant information about the bridges within the network is gathered, cleaned, and analyzed to obtain key variables for the analysis. These variables include bridge type, number of spans, construction costs, bridge rating, and average annual daily traffic. If construction costs are not available, they can be estimated using parametric cost models. Additionally, the direct and user costs associated with bridge interventions at the initial time step of the analysis are calculated. Next, the rate of bridge deterioration is estimated using a bridge deterioration model. Then, the associated direct and user costs are determined as well. The 3C concept extended to bridge portfolios (B-3C concept) is applied. Finally, the methodology yields an optimal intervention program aimed at minimizing the overall intervention costs. It should be noted that the framework depicted in Figure 1 does not cover all aspects of bridge intervention planning. A practical application of this framework is illustrated in Section 5.3. The following section will introduce the B-3C concept and its mathematical formulation.

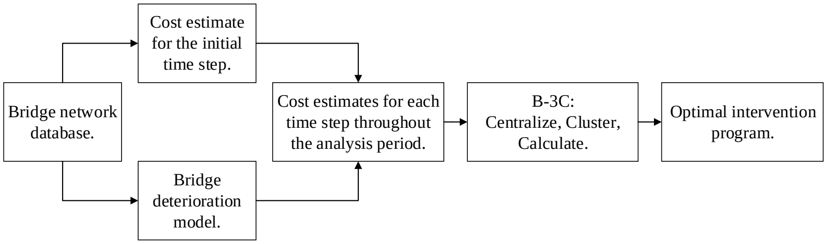

Figure 5.1: Optimal intervention planning of a bridge network framework.

5.2.1 INTEGRATIVE MULTI-SYSTEM OPTIMIZATION APPROACH: 3C CONCEPT.

The integrative 3C concept is an approach, firstly introduced by [197], for optimal intervention planning accounting for the interdependencies between assets that may belong to several infrastructure systems. It includes three stages: (i) *centralize*, (ii) *cluster*, and (iii) *calculate*. In stage (i), intervention types are classified into central and non-central. Central intervention types are those that must occur at a pre-established time moment, where neither delay nor advance is permitted.

During stage (ii), the non-central interventions are clustered with the planned central interventions while respecting some predefined individual constraints, such as the time interval between two successive interventions of the same type. Every k intervention is assigned two values, $G_{min,k}$ and $G_{max,k}$, which are two externally imposed constraints that represent the minimum and maximum time intervals, respectively, between two interventions of the same type. This is the case for maintenance interventions. Since central intervention types are carried out with a fixed time interval, $G_{min,k}$ and $G_{max,k}$ are set equal.

In the final stage (stage iii), the optimization of the intervention program that meets the conditions initially set is calculated. The primary objective of the 3C optimization process is to minimize the overall cost of implementing interventions. This total cost is divided into two components: the direct cost of the interventions themselves and the user costs associated with the interruption of the service of any affected assets. This optimization approach is straightforward and easily scalable. The ability to differentiate between central and non-central intervention types is highly advantageous as it enables effective planning of interventions in systems with numerous interconnected objects, taking into account their interdependencies. For a complete overview of the 3C concept, the reader is referred to [197].

5.2.2 EXTENSION OF 3C CONCEPT TO BRIDGE PORTFOLIO: B-3C CONCEPT

As mentioned in Section 5.1, in this study to optimize budget allocation for intervention planning within bridge networks, two distinct types of interventions will be considered; maintenance and repair. This represents a methodological extension, as the 3C concept only considers one possible intervention per asset. *Maintenance* refers to actions taken proactively to ensure that a bridge gradually wears and tears as expected, while *repair* refers to actions that emend defects that affect functionality or safety. Maintenance activities are classified as non-central interventions whereas repair activities are classified as central interventions.

Given the methodology's consideration of interactions among various assets, it is important to account for the interdependencies that exist between bridges within the network. Interdependencies can be classified into physical and geographical. Physical interdependency refers to the existence of a physical connection between two objects, such as two bridges in a series. Geographical interdependency arises when in the case of an event, such as an intervention, can affect the functionality of multiple bridges due to spatial proximity.

Bridge total costs

Developing a comprehensive and universally applicable methodology for estimating bridge maintenance and repair costs within the context of bridge service life management is challenging. This is due to the substantial variability in costs arising from diverse circumstances. For the purpose of this research, a global intervention cost function, based on [198] and [197], is utilized and described according to Equation (5.1):

5

$$C = C_M + C_{U|M} + C_R + C_{U|R} \tag{5.1}$$

where C represents the total cost of the bridge, C_M stands for bridge maintenance cost, $C_{U|M}$ refers to the bridge user costs due to maintenance interventions, C_R, represents the bridge repair cost, and $C_{U|R}$ indicates the bridge user costs resulting from repair interventions.

Bridge maintenance and repair costs

Estimating maintenance work costs often requires adjustments once the work is in progress [199]. The Organization for Economic Co-operation and Development proposes that maintenance costs should ideally constitute approximately 3% of the asset value [200]. In contrast, the investment in bridge maintenance in Mexico is around 1% of the bridge value [201]. Historical data from UK local authority indicates that their maintenance budgets have traditionally ranged between 0.3% to 0.5% of the bridge construction cost [202]. Similarly, a study on bridge maintenance of the Tamar bridge located in southwest England has observed that the mean annual cost of maintenance is around 0.35% of the total bridge value, according to [203]. Nevertheless, such generalized numbers may lack the necessary specificity for accurately evaluating the maintenance expenses of individual bridge interventions.

Regarding bridge repair costs, the expenses are on average 5% of the initial bridge cost [204]. However, for a more practical application, [198] has developed a more pragmatic approach, building upon the methods introduced by [205] and [206]. This approach offers a straightforward way to estimate repair costs, C_R, by taking into account the bridge reliability levels obtained. It introduces two crucial factors: f_R (see Equation (5.4)), which represents repair costs as a percentage of the total bridge value, C_{BV}. The total bridge value is a function of f_B, which indicates the bridge importance in the transport network and impacts the construction cost, C_0. Consequently, the following relationships have been established:

$$C_R = f_R C_{BV} \tag{5.2}$$

$$C_{BV} = f_B C_0 \tag{5.3}$$

$$f_R = 0.3613\beta^2 - 2.8572\beta + 5.622; \quad \max(f_R) = 2.0 \tag{5.4}$$

Notice that the maximum value for f_R is 2 (200%), applicable to bridges in critical condition. The reliability indices for various damage levels are presented in [198], [205], and [206], as shown in Table 5.1. The bridge importance factor according to [198] can be estimated using Equation (5.5):

$$f_B = 1 + \frac{1}{5}\left[0.25(S_{RC} + S_{AADT} + S_{DD}) + 0.125(S_{LS} + S_{TL})\right] \tag{5.5}$$

where S_{RC} denotes the road category grade; S_{AADT} represents the average annual daily traffic grade; S_{DD} indicates the detour distance; S_{LS} stands for the largest span grade; and S_{TL} represents the total length of the bridge grade. Each of these parameters is assigned a grade from 1 to 5 [207]. As has been noted, the direct cost of each bridge intervention depends on two factors: the geometric characteristics of the bridge, represented by C_{BV}, and the condition of the bridge at the time of intervention, denoted by f_R. It is important to note that in the context of the work done by [198], this approach is under the assumption of full-bridge repair. However, this method is adopted for its practicality in estimating repair costs.

Grades for assessment of bridge importance factor f_B in the network level according to five criteria [207]. Adjusted to the size of the MHC network under study.

5

Table 5.1: Values of reliability index given damage level

Damage level	Description	Reliability index β
1	Minor damage. No influence on the stability, durability, or traffic safety.	3.8
2	Slight damage. Safety in tolerable range, no impact on traffic.	3.3
3	Medium damage. Safety in tolerable range, medium impact on traffic, traffic obstruction.	3.0
4	High damage. Safety under minimum requirements, durability and traffic are severely affected.	2.3
5	Demolition imminent. Component failure.	β <2.3

Bridge user costs

In the context of global cost-benefit analyses of bridge interventions, an increase in bridge user travel time due to congestion relative to the partial or complete closure of the bridge will result in indirect costs [208]. To estimate these costs in terms of daily money loss due to prolonged commuting time the approach of [206] based on the fundamental concepts of [209] is used. Hence, the bridge user costs, C_U, are calculated as follows:

$$C_U = AADT\ C_{ve}\ T_U \tag{5.6}$$

where $AADT$ is the average annual daily traffic on the bridge, C_{ve} are the user costs per vehicle based on the estimated prolonged travel time and T_U is the unavailability period caused by the bridge intervention. Hence, as mentioned in Section 5.2.2, two user costs are considered: the bridge user costs due to maintenance intervention $C_{U|M}$, and the bridge user costs due to repair activities $C_{U|R}$.

The estimation of C_{ve} requires numerous parameters, such as intervention urgency, bridge size and type, to be taken into consideration. Due to the variability involved, the approach presented in [198] to calculate C_{ve} for the unavailability period of one month is employed, as described by the following equation:

$$C_{ve} = (W\,P_{ve}\,w_a + \alpha\,W\,P_{ve}\,w_b)\,t_p \tag{5.7}$$

where W is the average daily wage earned by a passenger, P_{ve} represents the average number of passengers per vehicle, w_a and w_b represents the number of weekdays and weekend days considered correspondingly, α is a factor that accounts for the fraction of costs associated with weekend days and t_p the estimated prolonged travel time.

5

Definition of the relationship matrices

Let's assume a bridge portfolio that represents a bridge network $B = \{1, ..., N\}$. To model the interdependencies among the bridges in the network, an interaction matrix $\mathbf{I}$ is employed. This square matrix, defined in Equation (5.8), utilizes interaction coefficients $I_{i,j}$ to determine whether one bridge affects another. Intervention on one bridge may partially affect other bridges in the network, thus the interdependency between bridges in the network is not necessarily binary [197]. This is mainly due to the existence of alternative routes. In such situations $0 < I_{i,j} < 1$. In this study, to quantify this partial influence, the travel time reliability between bridges i and bridge j according to Equation (5.9) is employed. Where $\min\{tr_{i,j}\}$ is the minimum route travel time of all the routes available between bridge i and bridge j under normal conditions and $\min\{tr_{\text{int},i,j}\}$ is the minimum travel time of all the routes available between bridge i and bridge j under the intervention at bridge i [210]. It is noted that $tr_{\text{int},i,j}$ is dependent on the estimated prolonged time, t_p, caused by the intervention on bridge i, i.e., $tr_{\text{int},i,j} = tr_{i,j} + t_{p,i}$.

$I_{i,j} = 0$, means that bridge i does not influence bridge j, whereas $I_{i,j} = 1$ signifies the opposite, i.e., bridge i has a full influence on bridge j mainly due to the absence of alternative routes between the bridges for example. The interaction matrix can be asymmetric due to non-reciprocal interactions, but its diagonal terms are fixed at $I_{i,i} = 1$ to indicate that a bridge always interacts with itself. Equation (5.9) implies that as t_p becomes long, the value of $I_{i,j}$ approaches 1. Conversely, for short durations of t_p, $I_{i,j}$ tends to 0.

$$\mathbf{I} = [I_{i,j}] = \begin{bmatrix} I_{1,1} & \cdots & I_{1,N} \\ \vdots & \ddots & \vdots \\ I_{N,1} & \cdots & I_{N,N} \end{bmatrix} \tag{5.8}$$

$$I_{i,j} = 1 - \frac{\min\{tr_{i,j}\}}{\min\{tr_{\text{int},i,j}\}} = 1 - \frac{\min\{tr_{i,j}\}}{\min\{tr_{i,j} + t_{p,i}\}} \tag{5.9}$$

To indicate which intervention type k affects each bridge i, a relation matrix $\mathbf{R}$ is established. The components $r_{i,k}$ take binary values, $r_{i,k} = \{0, 1\}$, determining whether bridge

i is affected by intervention k, with $k = \{1, 2, ..., 2N\}$. In the context of bridge interventions, where each bridge can have either maintenance or repair, the range for k is as follows: $k = \{1, ..., N\}$ corresponds to maintenance interventions, while $k = \{N+1, ..., 2N\}$ represents repair interventions. For instance, intervention $k = 1$ is maintenance for bridge 1, and intervention $k = N+1$ corresponds to the repair of bridge 1. When $r_{i,k} = 0$, it means that bridge i is not affected by intervention k, while $r_{i,k} = 1$ implies the opposite. The relation matrix is:

$$\mathbf{R} = [r_{i,k}] = \begin{bmatrix} r_{1,1} & \dots & r_{1,N} & r_{1,N+1} & \dots & r_{1,2N} \\ \vdots & \ddots & \vdots & \vdots & \ddots & \vdots \\ r_{N,1} & \dots & r_{N,N} & r_{N,N+1} & \dots & r_{N,2N} \end{bmatrix} \tag{5.10}$$

Objective function

In this study, the optimum intervention plan can be achieved by minimizing the total intervention cost for the total time of analysis. This cost includes the direct intervention costs as well as the user costs caused by the unavailability of the bridge, i.e., partial closure of the bridge due to the intervention as mentioned in Section 5.2.2. The minimization process should consider both the condition of the bridges and the budget limitations. Within the context of bridge networks, the optimization problem can be expressed as:

5

$$\min_{\mathbf{D}} \left[\left(C_M + C_{U|M} \right) + \left(C_R + C_{U|R} \right) \right] \tag{5.11}$$

where $\mathbf{D} = \{d_{i,t}\}$, with dimensions of $N \times 2T$, is a decision matrix. This matrix indicates when each intervention occurs during the total time of analysis, which is discretized in T time step components representing a $\Delta\tau$ time interval. Thus, the total time of analysis is $T\Delta\tau$. To clarify, two distinct ranges have been defined, $t = \{1, ..., T\}$ corresponds to maintenance interventions, and $t = \{T+1, ..., 2T\}$ represents repair interventions. For example, $t = 1$ indicates maintenance interventions occurring during the first time step, and $t = T+1$ indicates repair interventions occurring during the first time step of the analysis period.

The total direct cost of bridge maintenance is given by:

$$C_M = \sum_{i=1}^{N} \sum_{t=1}^{T} C_{M\,i} \, d_{i,t} \tag{5.12}$$

where $C_{M\,i} \in \mathbb{R}^+$ is the direct cost of performing maintenance of bridge i. $d_{i,t} \in \{0, 1\}$ are the components of the decision matrix indicating at which time step t each maintenance type is conducted.

The total bridge user costs caused by the maintenance given by:

$$C_{U|M} = \sum_{i=1}^{N} \sum_{t=1}^{T} C_{U|M_i} \, \delta \left([I_{i,j}]^\top \, r_{i,k} \, d_{i,t} \right), \quad \text{for } k = 1, ..., N \tag{5.13}$$

where $C_{U|M_i} \in \mathbb{R}^+$ is the user costs of bridge i caused by performing maintenance. The function $\delta(.)$ represents the Kronecker delta defined as follows:

$$\delta(x) = \begin{cases} 0 & \text{if } x = 0 \\ 1 & \text{if } x \neq 0 \end{cases} \tag{5.14}$$

The Kronecker delta is applied to every element of the resulting matrix, which has dimensions of $N \times T$. This use of the Kronecker delta in Equation (5.14) enables the assessment of clustering interventions by incorporating the user costs for an affected bridge only once, even if multiple interventions impacting its performance are happening simultaneously.

The total direct cost of bridge reparation is given by:

$$C_R = \sum_{i=1}^{N} \sum_{t=T+1}^{2T} C_{R_i}\, d_{i,t} \tag{5.15}$$

where $C_{R_i} \in \mathbb{R}^+$ represents the direct cost of performing reparation per bridge i.

The total bridge user costs caused by the reparation is given by:

$$C_{U|R} = \sum_{i=1}^{N} \sum_{t=T+1}^{2T} C_{R|U_i}\, \delta\left([I_{i,j}]^\top r_{i,k}\, d_{i,t}\right), \quad \text{for } k = N+1,...,2N \tag{5.16}$$

where $C_{U|R_i} \in \mathbb{R}^+$ is the user costs of bridge i caused by performing repair. It is noted that each maintenance or reparation intervention is assumed to be entirely performed within a time interval.

5

Constraints

The first constraint set imposes a minimum time interval between any two successive maintenance interventions of type k per bridge i, denoted by $G_{min,k,i}$. As repair interventions are assumed to be central, these interventions do not have any minimum time requirements just the fixed repair time. This first constraint is defined by:

$$0 \leq \sum_{s=t}^{t+G_{min,k,i}-1} d_{i,s} \leq 1 \quad t = 1 \rightarrow T - G_{min,k,i} + 1,\; k = 1 \ldots N,\; i = 1 \ldots N \tag{5.17}$$

The constraints defined by restrict any two successive interventions of type k per bridge i to have a time interval not larger than $G_{max,k,i}$, as shown by Equation (5.18) for maintenance interventions and by Equation (5.19) for repair interventions. Equation (5.19) indicates that the reparation intervention should not be carried out after $G_{max,k,i}$. It is assumed that $G_{max,k,i}$ for $k = \{N+1,...,2N\}$ is equal to $G_{max,k,i}$ for $k = \{1,...,N\}$:

$$\sum_{s=t}^{t+G_{max,k,i}-1} d_{i,s} \geq 1 \quad t = 1 \rightarrow T - G_{max,k,i} + 1,\; k = 1 \ldots N,\; i = 1 \ldots N \tag{5.18}$$

$$\sum_{s=t}^{t+G_{max,k,i}-1} d_{i,s} \geq 1 \quad t = T+1 \rightarrow 2T - G_{max,k,i} + 1,\; k = N+1 \ldots 2N,\; i = 1 \ldots N \tag{5.19}$$

In the context of the analysis, it is important to consider the scenario where repair interventions are required, and maintenance interventions are not needed for the remainder of the time under examination. Let B_m represent a subset of the bridges under study B, containing m elements, which represent the bridges requiring repair, i.e., $B_m = \left\{b_j\right\} \subset B$.

Consequently, the bridges in B_m do not require any maintenance interventions. This constraint set can be defined as follows:

$$\sum_{t=1}^{T} d_{j,t} = 0 \quad \text{for } j = 1, ..., m \tag{5.20}$$

$$\sum_{t=T+1}^{2T} d_{j,t} = 1 \quad \text{for } j = 1, ..., m \tag{5.21}$$

The maintenance and repair costs for each bridge vary significantly from one time step to another, and there is a limited budget, denoted as E_t, for the bridge owner [211]. This budget limitation constraint only impacts the direct costs related to maintenance and repair interventions. The budget limitation constraint is defined as:

$$\sum_{i=1}^{N} (C_{Mi} d_{i,t} + C_{Ri} d_{i,t+T}) \leq E_t \quad \text{for } t = 1, ..., T \tag{5.22}$$

Notice that the mathematical problem defined in Section 5.2.2 is a mixed-integer linear optimization problem where the variables ($d_{i,t}$) are binary.

5.3 Illustrative application

5.3.1 Case study description: Mexican Bridge System

The backbone of Mexico's national road network comprises fifteen major highway corridors (MHC), which extend over 20 000 km approximately. These corridors account for more than 55% of the country's highway traffic flow [212]. To effectively manage, preserve, and maintain the numerous bridges within this network, Mexico employs the Mexican Bridge System, known as SIPUMEX (for its acronym in Spanish) [136]. Managed by the Mexican agency Ministry of Communications and Trasport (SCT, for its acronym in Spanish), SIPUMEX plays a pivotal role by documenting the structural condition of individual assets and allowing the scheduling of necessary maintenance activities. As of 2009, SIPUMEX data indicates that there are a total of 576 bridges strategically positioned within the MHC network.

SIPUMEX employs a rating index (B_R) system to determine the condition of bridges and to carry out the necessary actions for their maintenance or reparation. This scale ranges from 0 for bridges that are in excellent condition to 5 for bridges with significant harm that requires immediate attention. The bridge scale, description and corresponding time intervals between two consecutive interventions, G_{min} and G_{max}, are presented in Table 5.2. It is noted that the time intervals in the description are only established for rating indices $B_R = \{3, 4, 5\}$. However, to offer a comprehensive illustration in this study, uniform increases of 2 years for the remaining rating indices are assumed. For $B_R = 2$, the time interval ranges from $G_{min} = 5$ and $G_{max} = 7$ and for $B_R = 1$, the time interval ranges from $G_{min} = 7$ and $G_{max} = 9$.

Table 5.2: SIPUMEX rating scale.

B_R	Description	G_{min}	G_{max}
0	Recently built or repaired structures, no problems.	–	–
1	Bridges in good condition. No attention is required.	*7*	*9*
2	Structures with minor problems, indefinite time frame for attention.	*5*	*7*
3	Significant or medium damage, repair required within 3 to 5 years.	3	5
4	High to severe damage, repair required within 1 to 2 years.	1	2
5	Extreme damage or risk of total failure. Repair required immediately or within one year	0	1

5.3.2 Intervention cost estimation

To quantify the financial aspects of the intervention planning, construction costs are estimated. The estimation of intervention costs, related to bridge maintenance and reparation, is conducted following the methodology presented in Section 5.2.2.

To illustrate this process, a specific example is provided. The MHC number 3, known as *Querétaro-Ciudad Juárez* in which a total of twelve bridges are located, as shown in Figure 5.2. The general information related to these bridges is summarized in Table 5.3. This information is derived from the SIPUMEX database and provides a concise overview of the key characteristics of these bridges. The construction costs, C_0, are estimated using the parametric cost approach specified by the SCT, for the year 2023, as documented in [213]. The specific cost breakdown for each bridge type is presented in Tables D.1.1 to D.1.3. It is noted that these costs are direct costs associated with the construction of the bridges, which depend on geometric characteristics such as the number of lanes, maximum span length, and maximum bridge height.

A value of 18 years is selected to encapsulate the maximal temporal extent of the interventions at least twice, in accordance with Table 5.3. The time interval $\Delta\tau = 1$ year, thus $T = 18$. Nevertheless, the methodology allows for a wider (or narrower) range of years to be used for the purpose of different analyses.

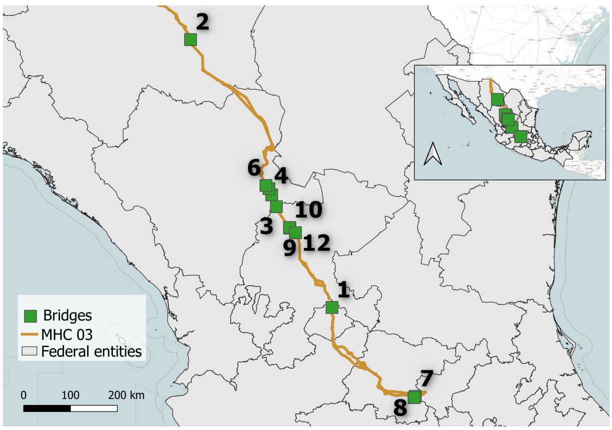

Figure 5.2: Bridges with a $B_R > 0$ located at MHC 3. Labels located next to each bridge represent its corresponding ID number.

Table 5.3: General information about bridges with a $B_R > 0$ located at the MHC 3. Bridge construction cost, C_0, in millions of Mexican pesos (MMP, 1 MP ≈ 0.05 EUR.)

Bridge (i)	Name	Lanes	Spans	Max span[m]	Total length[m]	AADT	B_R	C_0 [MMP]	β	G_{min} [Years]	G_{max} [Years]
1	San Pedro	4	1	9.8	9.8	6997	1	19.03	3.82	7	9
2	Maravillas	2	2	6	11.9	8009	2	3.28	3.30	5	7
3	San Antonio	2	1	18.7	18.7	5114	2	11.28	3.30	5	7
4	La Sed	2	1	10.5	10.5	4919	2	10.35	3.30	5	7
5	Sombreretillos	2	1	11.6	11.6	4378	2	10.35	3.30	5	7
6	Cerro Gordo	2	1	15.7	15.7	4748	1	11.28	3.82	7	9
7	El Sabino	2	2	7.3	14.6	9703	3	3.67	3.00	3	5
8	Apaseo el Alto II	2	2	6.4	12.7	12619	2	3.40	3.30	5	7
9	Las Nieves	2	2	6.3	11.7	5033	1	3.25	3.82	7	9
10	Los Gemelos I	2	1	6.1	6.1	5033	2	7.25	3.30	5	7
11	Los Gemelos II	2	1	6.1	6.1	5033	1	7.25	3.82	7	9
12	Nuevo Rio Grande	2	3	20.7	61.7	2850	2	11.54	3.30	5	7

To calculate the total intervention cost C_{BV}, Equations (5.3) and (5.5) are employed, utilizing the relevant data sourced from the SCT. The bridge repair costs C_R are determined using Equations (5.2) and (5.4). The grades for the computation of f_B adjusted to the size of the MHC network under study are shown in Table D.2.1. A direct association with the values of B_R shown Table 5.2 and the damage levels shown in Table 5.1 is made according to the corresponding descriptions. Hence the values of the reliability index β are directly inferred from the rating values. For example, a bridge with $B_R = 4$ corresponds to $\beta = 2.3$. It is noted that while the inferred β values serve the purpose of exemplification, they may not precisely correspond with reality. For the sake of simplicity, it is assumed that the maintenance costs, C_M, are equivalent to 15% of the repair costs, i.e., $C_M = 0.15C_R$. This is roughly equivalent to 3% of the bridge construction costs suggested by [200], particularly for bridges with a rating index of 2, a characteristic shared by the majority of bridges under study. It is noted that this assumption is made to illustrate and facilitate the use of the methodology presented herein. However, it is acknowledged that the assumption needs to be validated for all bridges, especially those with rating indices different from 2.

The user costs arising from the unavailability of bridges due to intervention actions are obtained using Equation (5.6). When bridge maintenance is executed, assuming that intervention works are conducted separately for each lane, a prolonged travel time (t_p) of approximately 1.5 minutes is considered. Furthermore, the unavailability period, T_U, due to maintenance is approximated at 2 months. The repair work duration spans 11 months, with a corresponding t_p of approximately 5 minutes, taking into account available alternate routes and considering that repair works are performed independently for each lane. This means that under neither of the two interventions under study will the bridge ever be fully closed. It is noted that, in practice, t_p could exceed the assumed values. This could depend on numerous factors such as the location and area of the bridges. However, for simplification purposes, the assumed unavailability periods and prolonged travel times are derived following the recommendations of [205] and [198].

For calculations involving the user costs, C_U and C_{ve} (see Equation (5.7)), an average hourly wage (W) of 36.62 MP (Mexican pesos) and an average of 1.8 passengers per vehicle (P_V) are considered, both obtained from data gathered by the National Institute of Statistics and Geography (INEGI, for its acronym in Spanish) [214] and the Mexican Institute of transport (IMT, for its acronym in Spanish) [215] correspondingly. Additionally, 20 weekdays (w_a) and 10 weekend days (w_b) are considered. To derive an estimate for weekend days, it is considered a cost equivalent to 50% ($\alpha = 0.5$) of the workday cost. The obtained intervention costs for the bridges located at MCH 3 are shown in Table 5.4. In Appendix D.2, a numeric example of the estimation of the intervention cost for one bridge is presented.

Table 5.4: Intervention costs in millions of Mexican pesos (MMP, 1 MP ≈ 0.05 EUR).

Bridge (i)	C_{BV} [MMP]	C_M [MMP]	$C_{U\|M}$ [MMP]	C_R [MMP]	$C_{U\|R}$ [MMP]
1	31.40	0.05	0.29	0.31	5.77
2	5.25	0.10	0.33	0.67	9.90
3	18.61	0.36	0.21	2.38	6.32
4	17.08	0.33	0.20	2.19	4.05
5	17.08	0.33	0.18	2.19	5.41
6	18.61	0.03	0.20	0.19	5.87
7	6.05	0.27	0.40	1.83	11.99
8	5.60	0.11	0.52	0.72	15.60
9	5.36	0.01	0.21	0.05	6.22
10	11.96	0.23	0.21	1.53	4.15
11	11.96	0.02	0.21	0.12	4.15
12	19.32	0.37	0.35	2.47	4.31

5

5.3.3 Bridge deterioration modeling

Bridge deterioration modelling plays a crucial role in formulating effective bridge maintenance programs. An accurate estimation of a bridge's rate of deterioration enables bridge owners to plan their budgets efficiently for necessary interventions. In this context, the use of a deterioration model based on the Simplified Kaplan-Meier probabilistic deterioration model specifically designed for prestressed concrete superstructures in the United States [216] is illustrated. This simplified deterioration model adopts the characteristics of a stationary Markov-chain model.

In the United States, bridge ratings range from 0 to 9, with 9 being in excellent condition. On the other hand, Mexican bridges follow a scale from 5 to 0, where 0 represents an excellent condition or recently built/repaired structures. To align these differing rating systems, a straightforward correspondence is established based on the interpretation of each rating. For instance, a US bridge rated at 7, categorized as being in Good Condition, corresponds to a Mexican bridge with a rating of 1. It is noted that this example might not represent the actual relationship between the bridge rating systems of the United States and Mexico. Bridge rating systems are considerably intricate and encompass various other influential factors. For comprehensive and bridge-specific models, sophisticated methodologies such as Time In Condition Rating or Markov Transition Probability should be employed [216].

The transition probability matrix used for making predictions about condition ratings based on the Simplified Kaplan-Meier probabilistic deterioration model simplifies to Equation (5.23):

$$P = \begin{bmatrix} 0.96 & 0.04 & 0 & 0 & 0 & 0 & 0 & 0 & 0 \\ 0 & 0.94 & 0.06 & 0 & 0 & 0 & 0 & 0 & 0 \\ 0 & 0 & 0.97 & 0.03 & 0 & 0 & 0 & 0 & 0 \\ 0 & 0 & 0 & 0.91 & 0.09 & 0 & 0 & 0 & 0 \\ 0 & 0 & 0 & 0 & 0.96 & 0.04 & 0 & 0 & 0 \\ 0 & 0 & 0 & 0 & 0 & 0.99 & 0.01 & 0 & 0 \\ 0 & 0 & 0 & 0 & 0 & 0 & 0.75 & 0.25 & 0 \\ 0 & 0 & 0 & 0 & 0 & 0 & 0 & 0.75 & 0.25 \\ 0 & 0 & 0 & 0 & 0 & 0 & 0 & 0 & 1 \end{bmatrix} \tag{5.23}$$

For illustrative purposes, the costs associated with the bridge *El Sabino* (bridge $i = 7$, according to Table 5.3) for deterioration for the first 11-year costs are shown in Table 5.5. It is noted that the parameters $G_{\min,k}$ and $G_{\max,k}$ maintain a consistent value over the entire duration of the analysis, regardless of the extent of degradation encountered by the bridge at each time step. This consistency arises from the underlying applied degradation model. Specifically, the bridge rating remains unchanged during intervals between two successive maintenance interventions that occur within intervals of less than 15 years, particularly in cases where the initial rating of the bridge is below 4. As can be seen in Table 5.5, the rating of bridge *El Sabino* (initial rating of 3) changes to 3.25 after 11 years. However, due to rounding, the rating value remains classified as 3. In the case of bridges with an initial rating of 4, progression to level 5 occurs within a mere 3-year time frame. As a result, repairing these bridges within the initial 2 years presumably would be a more cost-effective strategy than their continuous maintenance.

5

Table 5.5: Bridge *El Sabino* intervention costs associated with bridge deterioration rating using the Simplified Kaplan-Meier probabilistic deterioration model

Year	0	1	2	3	4	5	6	7	8	9	10
B_R	3.00	3.01	3.03	3.05	3.07	3.10	3.12	3.15	3.18	3.22	3.25
β	3.00	2.99	2.98	2.97	2.95	2.93	2.91	2.89	2.87	2.85	2.83
f_R	0.30	0.31	0.32	0.33	0.34	0.35	0.36	0.38	0.40	0.41	0.43
C_R[MMP]	1.83	1.87	1.92	1.98	2.05	2.12	2.21	2.30	2.40	2.51	2.62
C_M[MMP]	0.27	0.28	0.29	0.30	0.31	0.32	0.33	0.35	0.36	0.38	0.39

Notice that the costs shown in Table 5.5 must be affected according to a simple investment principle. A capital denoted as CAP, when invested over $T\Delta\tau$ years at an interest rate of ir, leads to an outcome denoted as $C = \mathrm{CAP}(1+ir)^{T\Delta\tau}$ [217]. Employing an interest rate of 4.5%, which corresponds to the average inflation rate of Mexico during the interval 2012-2022 [218]. The total cost of bridge maintenance interventions $C_M + C_{U|M}$ per bridge and the total cost of bridge repair interventions $C_R + C_{U|R}$, for the first 5 years, are shown in Table 5.6.

Once the direct costs given the deterioration model and the user costs are estimated for all the bridges under study, the following section presents the application of the B-3C concept optimization model.

5.3.4 Relationship matrices

In the MCH 3, there are three clusters of bridges closely located to each other, assuming that a bridge pertains to a cluster when the distance between other bridges is less than or equal to 10 km, as illustrated in Figure 5.2. These clusters are: 1) bridges $i = \{5, 6\}$, 2)

Table 5.6: Annual total costs of bridge maintenance, $C_M + C_{U|M}$, and repair, $C_R + C_{U|R}$, interventions. Costs in [MMP]

Bridge (i)	$C_M + C_{U\|M}$ [MMP]					$C_R + C_{U\|R}$				
	Year									
	0	1	2	3	4	0	1	2	3	4
1	0.34	0.35	0.38	0.40	0.42	6.08	6.38	6.70	7.03	7.39
2	0.43	0.45	0.48	0.51	0.53	10.57	11.08	11.60	12.15	12.73
3	0.57	0.61	0.65	0.70	0.74	8.70	9.19	9.71	10.25	10.82
4	0.53	0.57	0.61	0.65	0.69	6.24	6.61	7.00	7.41	7.84
5	0.51	0.55	0.58	0.62	0.67	7.60	8.03	8.48	8.96	9.46
6	0.22	0.24	0.25	0.26	0.28	6.06	6.34	6.65	6.97	7.30
7	0.67	0.71	0.75	0.80	0.84	13.82	14.48	15.19	15.94	16.75
8	0.63	0.66	0.69	0.73	0.77	16.31	17.08	17.88	18.71	19.59
9	0.22	0.23	0.24	0.25	0.26	6.28	6.56	6.86	7.18	7.51
10	0.44	0.47	0.50	0.53	0.56	5.68	6.00	6.33	6.68	7.05
11	0.23	0.24	0.25	0.26	0.28	4.27	4.47	4.68	4.91	5.14
12	0.72	0.77	0.82	0.87	0.93	6.78	7.19	7.61	8.06	8.54

bridges $i = \{7, 8\}$ and 3) bridges $i = \{7, 8, 9\}$. Any intervention on one bridge within a cluster will impact the performance of other bridges in the same cluster. Performing interventions either on bridges $i = \{1, 2, 3, 4, 12\}$ will not affect any of the other bridges.

For example, Table 5.7 presents the information necessary to compute the interaction matrix for cluster 3 (see Figure 5.3) assuming a $t_p = 5$ minutes for all bridges. The first two columns display the bridge indices, indicating the direction of travel flow from bridge i to j. The third column represents the route travel time between bridge i and bridge j, assuming free flow and a constant travel speed of 60 km/hr. The fourth column denotes the prolonged travel time caused by the intervention. Columns five to seven display the route travel time between bridge i and bridge j caused by intervention on bridge i. Columns eight to ten correspond to computed the elements of the interaction matrix, I, resulting from intervention on bridge i using Equation (5.9). Finally, column eleven shows the selected element for the interaction matrix, which corresponds to the maximum value obtained from interventions on individual bridges, i.e., the maximum value of columns eight to ten.

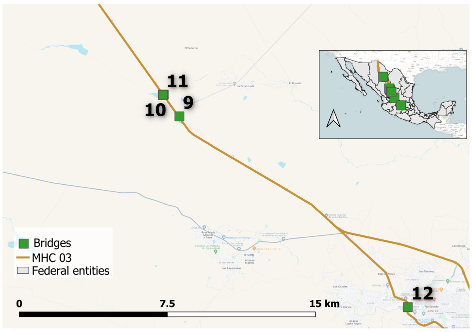

Figure 5.3: Bridges $i = \{9, 10, 11, 12\}$, according to the notation presented in Table 5.3 and shown in Figure 5.2.

It is noted that $I_{10,j}$ shows higher values when compared to $I_{9,j}$ and $I_{11,j}$. This suggests that intervention in bridge $i = 10$ has a more significant influence on other bridges, implying

Table 5.7: Travel times (in minutes), and partial effects caused by intervention in bridges $i = \{9, 10, 11\}$.

B_i	B_j	$tr_{i,j}$	$t_{p,i}$	$tr_{\text{int},9,j}$	$tr_{\text{int},10,j}$	$tr_{\text{int},11,j}$	$I_{9,j}$	$I_{10,j}$	$I_{11,j}$	$\max I_{i,j}$
9	10	1.44	5.00	6.44	1.44	1.44	0.78	0.00	0.00	0.78
9	11	1.45	5.00	6.45	6.45	1.45	0.78	0.78	0.00	0.78
10	11	0.04	5.00	0.04	5.04	0.04	0.00	0.99	0.00	0.99
10	9	1.44	5.00	1.44	6.44	1.44	0.00	0.78	0.00	0.78
11	9	1.45	5.00	1.45	6.45	6.45	0.00	0.78	0.78	0.78
11	10	0.04	5.00	0.04	0.04	5.04	0.00	0.00	0.99	0.99

a potentially more disruptive scenario compared to interventions on bridges $i = 9$ and $i = 11$. However, to capture the biggest influence, the maximum values of the computed interactions are selected. The result can be read as follows: executing an intervention in bridge $i = 9$ will affect 78% partially bridge $i = 10$ and $i = 11$. Performing and intervention in bridge $i = 10$ will affect 99% partially bridge $i = 11$[2].

Using the same procedure for the other clusters, results show that an intervention in bridge $i = 5$ will affect 34% partially bridge $i = 6$ and an intervention in bridge $i = 7$ will affect 56% partially bridge $i = 8$. Therefore, the interactions between the bridges in MHC 3 can be mathematically represented using Equation (5.24):

$$I = \begin{bmatrix} 1 & 0 & 0 & 0 & 0 & 0 & 0 & 0 & 0 & 0 & 0 & 0 \\ 0 & 1 & 0 & 0 & 0 & 0 & 0 & 0 & 0 & 0 & 0 & 0 \\ 0 & 0 & 1 & 0 & 0 & 0 & 0 & 0 & 0 & 0 & 0 & 0 \\ 0 & 0 & 0 & 1 & 0 & 0 & 0 & 0 & 0 & 0 & 0 & 0 \\ 0 & 0 & 0 & 0 & 1 & 0.34 & 0 & 0 & 0 & 0 & 0 & 0 \\ 0 & 0 & 0 & 0 & 0.34 & 1 & 0 & 0 & 0 & 0 & 0 & 0 \\ 0 & 0 & 0 & 0 & 0 & 0 & 1 & 0.56 & 0 & 0 & 0 & 0 \\ 0 & 0 & 0 & 0 & 0 & 0 & 0.56 & 1 & 0 & 0 & 0 & 0 \\ 0 & 0 & 0 & 0 & 0 & 0 & 0 & 0 & 1 & 0.78 & 0.78 & 0 \\ 0 & 0 & 0 & 0 & 0 & 0 & 0 & 0 & 0.78 & 1 & 0.99 & 0 \\ 0 & 0 & 0 & 0 & 0 & 0 & 0 & 0 & 0.78 & 0.99 & 1 & 0 \\ 0 & 0 & 0 & 0 & 0 & 0 & 0 & 0 & 0 & 0 & 0 & 1 \end{bmatrix} \tag{5.24}$$

Each intervention is associated with a specific bridge. As a result, a total of $K = 24$ intervention types are established, since there are 12 bridges and 2 possible interventions (i.e., maintain or repair) for each bridge. This breaks down into 12 maintenance intervention types $k = \{1, .., 12\}$ and 12 repair intervention types $k = \{13, ..., 24\}$ according to the notation presented in Section 5.2.2. In Equation (5.25) the relation matrix between these intervention types and the bridges is shown:

$$R = [I_{12}|I_{12}] \tag{5.25}$$

where I_{12} represents the identity matrix of size 12×12

5.3.5 MHC 3 results

The optimal intervention program is obtained through the optimization problem Equation (5.11) to Equation (5.22). In the given example, the most critical state is defined as those exhibiting substantial damage, necessitating interventions within a timeframe of 3 to 5 years for bridge $i = 7$ (see Table 5.3). Consequently, no immediate bridge repairs

[2]It is noted that bridges $i = 10$ and $i = 11$ are in close proximity. By reviewing the bridge database and satellite images, these bridges span two adjacent branches of a river.

are necessary. However, to delve into the application of the B-3C method, two scenarios are presented, (1) a case where no repair is needed and (2) a case where bridge $i = \{7, 8, 9\}$ must be repaired. For Scenario (1) an annual budget constraint of 0.61 MMP ($E_t = 0.61$ for $t = \{1, ..., T\}$) it is assumed, roughly equivalent to 0.6% of the MHC 3 bridge network total value. Additionally, an interest rate of 4.5% is applied. On the other hand, for Scenario (2), where repairs are indeed necessary, and prompt action is preferred within the initial two years due to cost escalation, an extra annual budget of 1.2 MMP. i.e., $E_t = 1.2$ for $t = \{1, 2\}$ and $E_t = 0.61$ for $t = \{3, ..., T\}$ is allocated. This budget (1.2 MMP) constitutes approximately 1.2% of the MHC 3 bridges value, specifically dedicated to facilitating the required repairs.

Given the escalating costs resulting from the bridge degradation, an initial inference might be that initiating interventions during the initial years of analysis would lead to cost benefits. However, adopting this approach would require a more frequent intervention schedule over the study period. The advantage of the methodology presented herein is the ability to determine the optimal sequence that minimizes the total number of interventions while ensuring early implementation to reduce overall expenses.

5

The number of decision variables of the demonstrative example is $T \times K = 18 \times 24 = 432$ ($K = 16$ is the number of intervention types). The optimization problem was solved using the Python `scipy` [219] Mixed-Integer Linear Programming algorithm `scipy.optimize.milp`. Tables 5.8 and 5.9 show the optimal intervention program of the intervention types for a period of 18-time steps for Scenario (1) described in Section 5.3.4.

In the figure depicted in Table 5.8, every row on the graph represents the intervention program of one intervention type, where blue squares represent maintenance intervention and red triangles represent repair intervention (see Scenario (2) Table D.3.1). As can be seen, the optimization algorithm assigns the year of intervention, according to the decision matrix $\mathbf{D}$, in order to minimize the total cost at the end of the study period given the minimum and maximum time between interventions and the annual budget constraints. The table in Table 5.8 shows, in net present value, both the annual budget constraint and the direct cost. Additionally, the ratio between direct cost and the annual budget is presented, which shows that the total direct cost is always below the annual budget available.

Table 5.9 shows an overview of the optimal intervention program. The first column identifies the bridges in the provided example. The second column indicates the recommended year for conducting repair interventions. Columns 3, 4, and 5 display the years assigned for three maintenance interventions. The remaining columns, 6 to 10, present the corresponding total costs for the interventions. Similarly, the results of Scenario (2) are depicted in Table D.3.2. The total cost for Scenario (1) corresponds to $C_{S_1} = 22.82$ MMP while for Scenario (2), the total cost is $C_{S_2} = 76.65$ MMP. C_{S_1} amounts to approximately 30% of the total cost C_{S_2}. However, when considering only the total direct cost for both scenarios, $C_{D_{S_1}}$ and $C_{D_{S_2}}$ respectively, the direct cost in Scenario (1), $C_{D_{S_1}} = 11.42$ MMP, represents roughly 2% more of the total direct cost seen in Scenario (2) ($C_{D_{S_2}} = 11.15$ MMP). This comparison suggests that when looking solely at the direct cost, Scenario (1) could be a more effective strategy due to its higher investment compared to Scenario (2). However, the lower direct cost of Scenario (2) is attributed to the state of bridges $i = 8$ and $i = 9$ with $B_R = 2$ and $B_R = 1$ respectively, leading to cheaper intervention costs. In real-life bridge scenarios, these bridges would not need repair, as shown in Table 1. In a practical scenario where bridges requiring repair have $B_R \geq 3$, Scenario (2) may be a better strategy.

By allocating an additional budget for repair, some bridges will be completely repaired, resulting in a healthier infrastructure network. It is crucial to highlight the importance of considering the interconnected effects of interventions on individual bridges within the network system. If these effects are not taken into account, i.e., $I = [I_{12}]$ the total cost could be significantly underestimated. For example, without considering the spatial proximity of the bridges for Scenario (1), the total cost corresponds to $C_{S_1|I=[I_{12}]} = 19.12$ MMP. However, this estimation would be erroneous, representing a deviation of 3.6 MMP from the actual value. This discrepancy translates to approximately 3.6% of the total value of the bridge network.

Table 5.8: Optimal intervention program Scenario (1). Annual cost expressed in net present value (NPV). E_t: annual budget constrain, C_D: total direct cost ($C_M + C_R$).

Intervention program

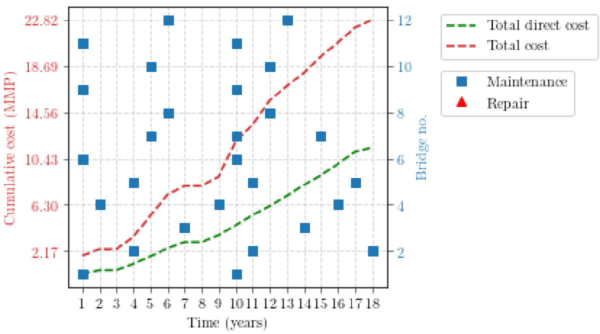

Annual cost (NPV)

Year	E_t [MMP]	C_D [MPP]	$\frac{C_D}{E_t}$
1	0.61	0.10	16%
2	0.61	0.33	54%
4	0.61	0.46	75%
5	0.61	0.55	89%
6	0.61	0.55	89%
7	0.61	0.42	68%
9	0.61	0.41	67%
10	0.61	0.56	92%
11	0.61	0.57	94%
12	0.61	0.47	76%
13	0.61	0.52	86%
14	0.61	0.52	85%
15	0.61	0.44	73%
16	0.61	0.50	82%
17	0.61	0.52	85%
18	0.61	0.16	27%

Table 5.9: Overview of Scenario (1) results. Total cumulative cost, $C = 22.82$ MMP, total direct cost, $C_D = C_M + C_R = 11.38$ MMP. int_n: intervention number in year $t\Delta\tau$.

Bridge (i)	Repair int_1	Maintenance int_1	int_2	int_3	C_R	C_M	$C_{M\|U}$	$C_{R\|U}$	C
1	–	1	10	–	0.0	0.19	0.58	0.0	0.77
2	–	4	11	18	0.0	0.71	0.99	0.0	1.70
3	–	7	14	–	0.0	1.54	0.42	0.0	1.96
4	–	2	9	16	0.0	1.99	0.61	0.0	2.60
5	–	4	11	17	0.0	2.22	0.73	0.0	2.95
6	–	1	10	–	0.0	0.11	0.53	0.0	0.64
7	–	5	10	15	0.0	1.78	1.88	0.0	3.66
8	–	6	12	–	0.0	0.41	1.62	0.0	2.04
9	–	1	10	–	0.0	0.03	1.06	0.0	1.09
10	–	5	12	–	0.0	0.85	1.15	0.0	2.00
11	–	1	10	–	0.0	0.07	1.15	0.0	1.22
12	–	6	13	–	0.0	1.48	0.70	0.0	2.19
Total					0.00	11.38	11.42	0.00	22.82

5

5.3.6 Agency intervention program comparison

To evaluate the cost-effectiveness of the solutions, a comparison is made between the optimal intervention scheduling and the existing SIPUMEX intervention program adopted by the SCT, which operates in two stages. (I) Preliminary prioritization, this phase relies on the automated ranking system based on key factors such as bridge rating, average annual daily truck traffic (*AADTT*), and average annual daily traffic (*AADT*). (II) Final prioritization, a manual ranking process prioritizes bridges initially identified as high-ranking (urgent interventions) in the preliminary phase, while the rest are assessed by performing an individual review of the bridges and looking for the most damaged according to the condition of the individual components and photographic reports until the estimated budget has been reached [220, 221]. Usually, it is assumed that the minimum number of interventions implies the minimum cost [222]. This implies that the time within two consecutive interventions is $G_{min} = G_{max}$.

In Table 5.10, the comparison of intervention programs for Scenario (1) is shown. The table presents data regarding the bridges, including their ranking based on the SIPUMEX preliminary prioritization, the corresponding maintenance years, the total cost of these interventions (C^*), the total cost using the B-3C approach (C), and the percentage of savings obtained. The B-3C program achieves savings for most bridges. However, when considering the total cost, the results reveal that the optimal plan leads to a 14% reduction in costs compared to the SIPUMEX approach. Notice that, using the SIPUMEX approach for this particular example, there are $3^{12} = 531\,441$ (3 time-steps between $G_{min,k}$, $G_{max,k}$ and 12 bridges) possible combinations of time between intervals. The minimum total cost is obtained with $G_{max} = \{5,7,7,7,7,7,7,7,9,9,9,9\}$ resulting in a total $C^* = 26.54$ MMP. Additionally, taking into account the budget constraint of Scenario (1), it is notable that the allocated budget will be fully utilized by year 11, i.e, SIPUMEX costs are over the budget. Consequently, there will be no remaining budget for years 15 and 16, resulting in 7 bridges lacking maintenance intervention. The primary drawback of the SIPUMEX approach becomes evident in the large number of combinations that need evaluation to obtain the minimum total cost. For example, if applied to the entire network under study, it would necessitate assessing 3^{555} possible combinations, which is impractical.

Table 5.10: Comparison of the total cost between the bridge agency (C^*) and the B-3C (C) intervention programs for $T = 18$ years. int^*_n: intervention number in year $t\Delta\tau$ according agency approach.

Bridge(i)	B_R	AADTT	AADT	G_{max} [Years]	Maintence int^*_1	int^*_2	int^*_3	C^* [MMP]	C [MMP]	Saving [%]
7	3	2367	9703	5	6	11	16	3.83	3.66	4
10	2	3133	5033	7	8	15	–	1.73	2.00	-16
8	2	2778	12619	7	8	15	–	2.17	2.04	6
5	2	2211	4378	7	8	15	–	2.1	2.95	-40
3	2	2163	5114	7	8	15	–	3.08	1.96	36
4	2	2128	4919	7	8	15	–	2.97	2.60	12
12	2	1956	2850	7	8	15	–	3.71	2.19	41
2	2	893	8009	7	8	15	–	3.13	1.70	46
9	1	3133	5033	9	10	–	–	1.06	1.09	-3
11	1	3133	5033	9	10	–	–	1.19	1.22	-3
1	1	2348	6997	9	10	–	–	1.19	0.77	35
6	1	2211	4748	9	10	–	–	0.38	0.64	-68
							Total	26.54	22.82	14

5.3.7 Additional travel time sensibility analysis.

The additional travel time, t_p, depends on the type of intervention and the size of the bridge, which varies on every bridge in the network. Unfortunately, detailed data on the prolonged time required for each bridge is not available. As such, the precise quantification of time per bridge falls beyond the scope of this investigation.

It is expected that if there is a greater travel time, the total intervention cost will increase. On the other hand, reducing the travel time will decrease the total cost. Which is reflected directly in the interaction matrix, I (see Equation (5.9)). However, this also affects the scheduling using the current bridge agency approach. For comparison purposes, Scenario (1) is selected to model three cases of delay caused by maintenance: a 2-minute delay, a 30-minute delay, and a linear function that depends on the bridge area (B_A), i.e., $t_p = 0.01B_A + 1.45$. The linear relationship is established such that the minimum prolonged time (the prolonged time for the smallest bridge) is 2 minutes, and the maximum prolonged time is 62 minutes.

It is noted that these cases are for exemplification purposes only and do not represent the reality of individual bridges or any bridge network. The results are presented in Table 5.11. As observed, the table illustrates the sensitivity of total costs to the choice of prolonged travel time. Additionally, the table shows the savings percentage associated with the comparison between the two approaches. These percentages indicate the potential cost savings achieved by opting for the B-3C program over the agency program. For instance, at a prolonged time of 2 minutes, B-3C achieves approximately 11.4% savings in terms of total intervention costs. Overall, the B-3C methodology consistently reduces the total cost compared to the agency, under identical assumptions.

5

Table 5.11: Comparison of the total costs for Scenario (1) between the agency approach (C^*) and B-3C (C).Intervention programs for $T = 18$ years assuming different prolonged times.

t_p [min.]	C^* [MMP]	C [MMP]	Saving [%]
2	28.51	25.26	11.40
30	297.92	265.51	10.88
Linear	45.99	37.32	18.85

5.4 Application to the entire bridge portfolio

After explaining the proposed methodology and presenting results for the bridges at MHC 3, the optimal intervention plans for the entire bridge portfolio. For this investigation, bridges with a rating greater than 0 are used as a case study, i.e., 555 bridges in total. The geographical distribution of these bridges can be visualized in Figure 5.4.

According to the information in Table 5.2, bridges with a rating of 5 are marked for repair. It is noted that, as reported in the SIPUMEX database, no bridges fall into this category. Consequently, there is no immediate need for bridge repairs based on the available data. Nonetheless, for cost comparison, similar to the case illustrated in Section 5.3.4, two scenarios are presented. The first one, Scenario (3), assumes that no repairs are necessary. The second, Scenario (4), assumes a case where bridges with a rating above 3 require repair (17 bridges). Furthermore, since one of the advantages of the proposed methodology is that

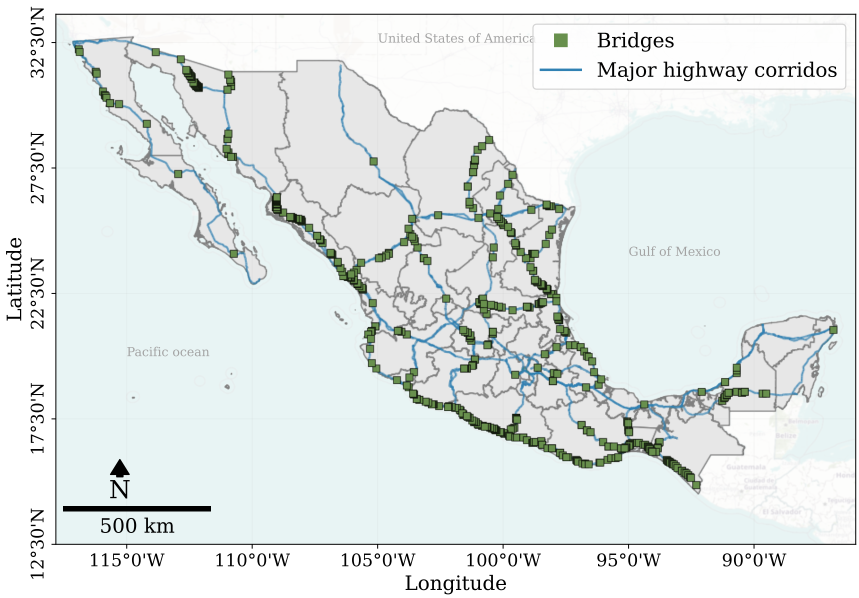

Figure 5.4: Location of the bridges under study.

central interventions can be chosen based on any bridge performance indicator, a Scenario (5) is also considered. For this scenario, the load effect performance indicator, which refers to the ratio between the extreme traffic load effect selected and the characteristic load effect induced by the design live load model [223], is used. Particularly the bending moment with a 50-year return period performance indicator M_{50r}. Scenario (5) assumes that bridges with $B_R > 3$ or $M_{50r} > 1.56$ require repair intervention (38 bridges). For complete details regarding M_{50r} bridge performance indicator, the reader is referred to [223].

Similar to the approach detailed in Section 5.3.2, the Simplified Kaplan-Meier probabilistic deterioration model is used, the percentage of interaction, the analysis period, and the interest rate. Intervention costs were estimated as outlined in Section 5.2.2. In terms of budget limitations, for Scenario (3) an annual budget of 1.35% of the total bridge network value (98.44 MMP) is assumed. Regarding Scenario (4) and (5) approximately 1.5% of the total bridge network value (around 109.3 MMP) was allocated for the first two years to cover repairs for the selected bridges. For subsequent years, the budget constraint was set to about 1% of the total bridge network value (69.3 MMP). Notice that the budget limitations presented represent the minimum required funds to apply interventions to all the bridges under study.

The optimization problem involved a total of 19 980 variables, including 1110 intervention types. The optimization procedure was executed using the Python algorithm `scipy.optimize.milp` on a laptop running Windows 10, equipped with an Intel Core i7−8665U CPU @ 1.90GHz, and 32 GB of RAM. The entire simulation process took approximately 28 minutes. The budget constraints, total direct costs and total costs of the optimal intervention plan for the 555 studied are presented in Table 5.12. A graphical representation of the optimal intervention plan for Scenario (4) is shown in Figure 5.5 while the corresponding plan for Scenarios (3) and (5) are shown in Figures D.3.1 and D.3.2. The estimated intervention costs and the optimal program overview can be found in the supplementary material.

Table 5.12: Overview of optimal intervention results for Scenarios (3), (4) and (5).

Scenario	E_M [MMP]	E_R [MMP]	C_D [MMP]	C [MMP]
(3)	98.44	–	2060.49	2829.02
(4)	69.30	109.3	1523.69	2360.10
(5)	69.30	109.3	1543.42	2560.29

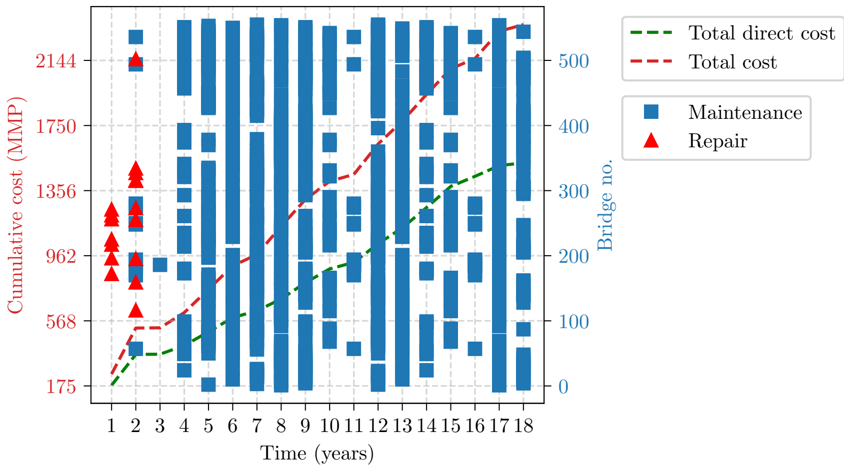

Figure 5.5: Optimal intervention program for the 555 bridges under Scenario (4).

The analysis reveals three distinct cost scenarios for managing bridge infrastructure. First, the total cost for performing maintenance exclusively (C_{S_3}), amounts to approximately 2828.98 MMP. Second, the alternative strategy involves repairing bridges with a condition index $B_R > 3$ and maintaining the others (C_{S_4}). This approach leads to a cost of approximately 2359.95 MMP. Finally, the total cost obtained for Scenario (5) C_{S_5} amounts to approximately 2560.29 MMP. Opting for the C_{S_4} approach results in a cost reduction of 16.5% compared to the C_{S_3} strategy.

The cost ratio between the Scenarios (3) and (4) approaches shows the economic advantage of the C_{S_4} strategy. Specifically, C_{S_4} correspond to 83.5% of the cost of C_{S_3}. This indicates that the C_{S_4} approach is more cost-effective, saving nearly 17% of the expenses associated with maintenance. Additionally, the analysis considers the direct costs associated with both strategies. For the C_{S_3} approach, the direct cost ($C_{D_{S_3}}$), amounts to 2060.49 MMP. In contrast, the C_{S_4} approach provides lower direct costs, with $C_{D_{S_4}}$ of 1523.69 MMP. This difference results in a 26% reduction in direct costs when opting for the C_{S_4} approach. The direct costs of scenarios (4) and (5) are virtually identical, the cost ratio C_{S_4}/C_{S_5} corresponds to 92.1%. The marginal difference suggests that opting for strategy (5) might be a better choice, as it benefits more bridges while guaranteeing the adaptability of the bridge network to the actual traffic load demands.

Furthermore, when comparing the total cost of Scenario (3) with the total cost obtained with the agency approach ($C^* = 3075.9$ MMP, assuming the time within two consecutive interventions $G_{min} = G_{max}$) described in Section 5.3.6, an 8% reduction in total costs is observed when applying the B-3C approach. It is noted that when the interaction effects within the bridges are not taken into account, i.e., $I = [I_{555}]$ the total costs for Scenario (3) corresponds to $C_{S_3|I=[I_{555}]} = 2621.93$ MMP, representing a deviation of 266.6 MMP from the actual value (2.8% of the bridge network total value). When compared with the optimal result of Scenario (4) with the agency approach a reduction of around 23% was found. It is pointed out that given the budget constraints, opting for the agency approach will be enough to fund interventions up to year 15.

5.5 Conclusions

5

This chapter presents a novel methodology for optimizing bridge intervention planning, named B-3C approach, based on the multi-system optimization technique known as the integrative 3C concept. The proposed methodology takes into consideration the interactions between various assets within a bridge network, including different types of interventions. To model these interactions, the employed approach utilizes an interaction matrix capable of representing diverse interdependencies caused by the spatial proximity of the bridges. Additionally, a relation matrix is established to specify which intervention type affects each asset. In the specific context under study, the focus is on two intervention types: maintenance and repair. Furthermore, the methodology enables the distinction between central and non-central intervention types by considering the time intervals between successive interventions. This allows the incorporation of various bridge performance metrics into the analysis, facilitating the prioritization of central interventions. The intervention scheduling approach is formalized by developing an optimization mathematical model that incorporates pre-established constraints.

The main goal of the optimization process in this study is to minimize the total cost associated with implementing interventions. This objective is achieved through the utilization of a global intervention cost function that accounts for the direct costs of the interventions, the user costs resulting from the interventions, and the bridge deterioration model. It is acknowledged that bridge managers often encounter additional optimization goals, or agencies may have varying performance criteria for different bridges or groups of bridges. However, in most cases, during a given planning exercise, minimizing costs would support the manager in economically prioritizing bridges to address specific optimization goals.

To demonstrate the practicality of the presented methodology, a numerical example involving a network of 555 bridges and four scenarios is provided. This methodology offers a clear benefit by helping to determine the most efficient sequence for interventions that minimize the overall number of required interventions while ensuring early implementation to lower costs. The results of the numerical example emphasize the clear cost-saving advantages and the importance of including the interaction matrix. Specifically, by combining bridge repairs for those with a condition rating index exceeding 3 and maintenance for the rest, a reduction of 23% in the total cost is achieved when compared to the bridge management agency approach based on exclusive maintenance. Notably, when the interaction matrix is not considered, deviations in total costs of up to 3.6% of the total bridge network value have been observed. Furthermore, a step-by-step description of how to incorporate the bridge state into the cost estimation is offered. This estimation, which is a function of the bridge reliability index, is dynamically considered in the optimization process.

It is noted that the principal sources of uncertainty in this study are the deterioration model, the average annual inflation rate, and the extent of the impact induced by interventions on other bridges, as indicated by the interaction matrix. The interaction matrix analysis focuses solely on bridges i to j (or vice-versa). In cases where additional interventions on other bridges are simultaneous with bridges i and j, the interaction matrix cannot account for this scenario. This limitation arises from the nature of our simplified network analysis to estimate travel time calculations, which do not allow for the straightforward addition of various elements in the interaction matrix. However, the variables have been quantified in a simplified manner solely for illustrative purposes. Properly quantifying these variables for each bridge within the network will lead to a more precise estimation of the optimal intervention plan. The limitations of this study underscore the necessity for future studies to (1) explore more advanced methodologies for computing the interaction matrix and (2) investigate the effects of different intervention activities, such as rehabilitation and replacement, and their integration into the framework. This deeper exploration will contribute to refining our approach and enhancing our understanding of how various repair strategies impact optimization outcomes.

While the optimal intervention program derived from the analysis may initially appear random, these findings result from a rigorous optimization process. They exhibit better performance compared to what could be achieved through human intuition, especially when dealing with extended analysis periods and complex bridge networks with numerous assets. Hence, the methodology presented herein highlights its practical value as a bridge management optimization tool. It can help transportation agencies to implement and explore various scenarios by adjusting the time between consecutive interventions and budget constraints. This methodology helps by facilitating the assessment and comparison of associated costs to support a more comprehensive analysis and informed decision-making.

6

Conclusions

This thesis has presented developments on one topic with different components to enhance the reliability estimates of bridges at a network level to assist the development and implementation of optimal bridge intervention strategies. These components include the generation of synthetic data for heavy vehicles, identification of hazardous road locations, estimation of bridge criticality, and scheduling of optimal interventions. While each of the chapters in this thesis contains a discussion of specific results and conclusions, Section 6.1 summarizes the main findings for the four research topics, and Section 6.2 summarizes the main recommendations for both case study, as well as further research. Section 6.3 provides some closing remarks.

6.1 Main findings

6.1.1 Synthetic data of heavy vehicles

In Chapter 2, an enhanced methodology for computing synthetic WIM observations of heavy vehicles is introduced, utilizing GCBNs. Resulting in a model that outputs comprehensive data, including vehicle type, total vehicle weight, individual axle loads, total vehicle length, and inter-axle distances. Eight high-dimensional GCBNs were quantified, with six of them based on WIM data from the Netherlands highway network. The remaining GCBNs were quantified using WIM data from a city route in Rotterdam and Araranguá (Brazil). The GCBN models accurately replicate the dependence structure of empirical data, with minor differences observed between simulated and observed axle loads and inter-axle distances.

To enhance accessibility, a GUI was developed for the six Dutch WIM highways under study. The model's applicability in the absence of WIM data was demonstrated by using the GUI with data gathered with less-sophisticated traffic counters from Toluca (Mexico). The presented framework for synthetic WIM observations can be applied using data from any WIM location, incorporating site-specific records and vehicle types. The following key findings are presented:

- Simulating the different vehicle types presented in a WIM database, using GCBNs, can be achieved either by clustering vehicles based on the number of axles, body configuration, or vehicle code classification.

- GM distributions can effectively model axle loads and GVWs of heavy vehicles due to the inherent multimodal nature of the data. This is particularly evident in the distinct modes observed, such as empty trucks and loaded trucks, when analyzing GVWs for example.
- Using empirical distributions for modelling inter-axle distances exhibits better performance when compared with continuous distributions. This is due to the finite number of vehicle distances associated with distinct vehicle types.
- Filtering criteria are essential to exclude irrelevant or erroneous data, reducing the risk of misleading information. This process ensures that quality data are retained for analysis, enhancing the consistency and accuracy of the results.
- Heavier and longer vehicles circulate on the Dutch motorways compared to those circulating on city routes. This trend is primarily due to the capacity of a motorway to accommodate larger vehicles and longer distances, while city routes often have restrictions on vehicle size and weight.
- The primary goal of the model is to approximate the general traffic configuration, rather than aiming for exact replication of every individual observation in the database, particularly for future investigations into bridge reliability assessment.

6.1.2 Road hazardous locations identification

Chapter 3 introduces a methodology to identify potentially hazardous locations within a road network by computing and mapping EGVWs when axle load information is limited. The study focuses on the 15 major highway corridors network of Mexico, utilizing data from less-sophisticated traffic counters. The extreme traffic events are computed using extreme value theory and a Gaussian copula-based Bayesian Network (GCBN) approach. The GCBN model, named GCBN_{EECAN}, is developed to generate synthetic axle loads for Mexican heavy vehicles, utilizing axle load measurements from 223 origin-destination surveys conducted between 2002 and 2017. Over 180 million synthetic heavy vehicles are computed using 1777 site-specific GCBNs corresponding to the studied counting stations. The analysis includes estimating characteristic values of GVW with a 50-year return period and a 1000-year return period, revealing hazardous locations on major highway corridors.

Furthermore, a user interface is provided to facilitate the generation of synthetic axle load observations of Mexican heavy vehicles. The importance of using WIM systems for additional traffic data to enhance accuracy and reliability is acknowledged. The following key findings are presented:

- By analyzing data from 1,777 vehicle counting stations, it has been further validated that the methodology developed in Chapter 2 can effectively estimate individual axle loads using heavy vehicle configurations, i.e., vehicle type, number of axles, and the corresponding proportions of the traffic flow.
- Extrapolations using the generalized extreme value distribution resulted in unrealistically large gross vehicle weights at several stations. This outcome highlighted the

significant impact of the chosen distribution type on extrapolation results. To address this, the fitting procedure was improved by truncating the likelihood function. By setting a gross vehicle weight (GVW) threshold, it was ensured that for values below this threshold, only the probability of being smaller than the threshold was considered, and for values at or above the threshold, only the probability density was included. This approach provided a more accurate representation of the data.

- The methodology for estimating and mapping extreme GVWs effectively detects trends in extreme GVWs at the counting points analyzed in this study. This is evidenced by the similarities between the heat map showing the concentration of the statistically heaviest vehicle type and the estimated heaviest GVWs with a 50-year return period.

- Regarding the statistical analysis of the databases used in this study, it was found that the most common heavy vehicle types, accounting for 95% of surveyed heavy vehicles, are C2, C3, T3S2, T3S3, and T3S2R4. Among these, the nine-axle T3S2R4 is the heaviest vehicle type in the database, with a maximum recorded gross vehicle weight of 975.76 kN, reported in 2004. Additionally, the maximum gross vehicle weight reported each year is consistently under 980 kN, suggesting that this may be the maximum capacity of the scales used at the survey stations.

- Around 80% of the study stations have gross vehicle weights with a 50-year return period (GVW_{50}) exceeding 980 kN (100 tons). This is consistent with data from the EECAN database, which shows that the median value of the maximum GVW observed across all survey stations is 964 kN. Furthermore, trucks with GVWs over 1000 kN have been recorded in central Mexico, specifically on the Irapuato – La Piedad highway.

- Hazardous locations with $GVW_{50} > 1190$ kN (above the 75th percentile of the estimated GVW_{50} values) are concentrated along specific major highway corridors. These corridors cross several federal entities, including Colima, Tabasco, México, Puebla, Nuevo León, Tamaulipas, Querétaro, Guanajuato, Aguascalientes, Jalisco, and Zacatecas. This concentration, speculatively, can be attributed to several factors: (i) Colima hosts the largest seaport in the country. (ii) Tabasco hosts one of most of Mexico's important oil, industrial and commercial seaports. (iii) México and Puebla are leading regions in the automotive industry. The most important industrial corridos (iv) The Northern Economic Corridor runs through Nuevo León and Tamaulipas and (v) The Bajío Industrial Corridor along Querétaro, Guanajuato, Aguascalientes, Jalisco, and Zacatecas.

6.1.3 Bridge criticality estimation

Chapter 4 presents a four-step methodology for estimating bridge criticality as a load effect (extreme bending moment and extreme shear force) performance indicator in a national bridge network, particularly under conditions of limited information. The approach allows for visualizing and evaluating the criticality of individual bridges within the network by assessing the relationship between extreme traffic load effects and those generated by the design live load model. The method is characterized by its low information intensity per bridge including the number of spans, length, lanes, width, and design live load to name a few. Traffic information requirements include Annual Average Daily Traffic and the proportion per vehicle type.

By using GCBNs to generate site-specific synthetic observations of heavy vehicles, the traffic flow is simulated by estimating inter-vehicle gaps using auto-correlated couplas. Long-run traffic load simulations provide insights into bridge load effects, and extreme load effects are estimated using the block maxima extreme value analysis approach. The four-step methodology is applied to a case study involving 576 bridges on major toll-free highways in Mexico, the outputs of the methodology are comprehensive national highway network maps, identifying spatial patterns and relationships of extreme load effects and bridge criticality. The following key findings are presented:

- Low correlations between inter-vehicle gaps (the space between two vehicles travelling in the same lane on a highway) are consistently noted across the majority of hours throughout the day. This pattern implies relatively independent behaviour during different hours, except for instances during both peak hours and low-traffic hours.
- Inter-vehicle gaps are site-sensitive and can vary significantly based on the specific characteristics and conditions of each region's transportation network. Hence the correlation behavior of inter-vehicle gaps is strongly influenced by the database.
- The maximum load effect is caused by individual heavy vehicles in around 92% of the bridges under study. This phenomenon is attributed to the prevalent short span lengths characterizing the majority of bridges within the network.
- Regarding the two-lane bridges included in the bridge network under study (445 in total), the application of Turkstra's Rule simplified model reveals that the 50-year loading event consists of the 50-year truck in the slow lane, combined with the one-day return period truck for 280 bridges and the one-week return period truck for the remaining 165 bridges.
- Turkstra's Rule simplified model provides accurate estimations of the extreme load effects in 362 out of the 445 two-lane bridges with discrepancies ranging from -0.3% to 3.9%. Nevertheless, a trial-and-error approach is needed to derive the value of the axle placing distance alpha.
- The bridge criticality performance indicator for bending moment and shear force with a 50-year return period indicates that, in most cases, the obtained values are significantly higher when compared to those generated by the AASHTO standard HS truck live loads. Specifically, they can be up to 1.71 times larger for bending moments and up to 1.67 times larger for shear forces. This may raise concerns about accelerated structural deterioration, increased maintenance costs, and a higher frequency of inspections.
- The highest bridge criticality values (ratios above 1.42) are primarily concentrated on the highway that connects the cities of Caborca and Sonoyta in northern Mexico. This could be attributed to the design live load model employed for these bridges.

Given that these are short-span bridges, the design live load assumes a truckload of 320 kN (HS15). However, according to the findings outlined in Chapter 3, a GVW with a 50-year return period ranging between 1022 and 1131 kN is expected for these particular locations.

6.1.4 Optimal intervention scheduling

Chapter 5 introduces the B-3C approach, a novel methodology for optimizing bridge intervention planning based on the integrative 3C concept of multi-system optimization. The approach considers interactions among diverse bridges in a bridge network, incorporating intervention types, and a deterioration model with a focus on maintenance and repair interventions. The methodology formulates an optimization mathematical model to minimize the total cost associated with interventions. It employs an interaction matrix to represent interdependencies and a relation matrix to specify intervention additional costs. Additionally, incorporates direct and user costs, along with a bridge deterioration model, subject to predetermined constraints.

The optimization process aims to efficiently sequence interventions, minimizing the overall number of interventions while ensuring cost reduction. The effectiveness of the B-3C approach is illustrated through a numerical example featuring a portfolio of 555 bridges within the Mexican bridge management system, SIPUMEX. Five distinct scenarios, including a comparative analysis with the SIPUMEX scheduling approach, further demonstrate the efficacy of the methodology. The following key findings are presented:

- Regarding the Simplified Kaplan-Meier probabilistic deterioration-based model, it is observed that for bridges rated on a scale from zero to five (where zero indicates a new bridge and five indicates an immediate bridge intervention), such as the SIPUMEX bridge rating, the bridge rating remains marginally unchanged during intervals between two successive maintenance interventions that occur within intervals of less than 15 years. This trend is particularly notable when the initial rating of the bridge is below four.

- Furthermore, in the case of bridges with an initial SIPUMEX bridge rating of four, deterioration to level five occurs within a 3-year time frame. As a result, repairing these bridges within the initial two years suggests a more cost-effective strategy than their continuous maintenance.

- Combining bridge repairs for those with a condition rating index exceeding three and maintenance for others results in a substantial 23% reduction in total costs compared to an exclusive SIPUMEX maintenance approach.

- It is noted the importance of considering the interconnected effects (additional indirect costs) of interventions on individual bridges within the network system. The total cost could be underestimated if the interconnected effects are not taken into account. For example, for the case study, a discrepancy of approximately 3.6% of the total value of the bridge network was found.

- Incorporating bridge performance indicators, such as condition state and the criticality of traffic load effects, can help differentiate between central and non-central intervention priorities. Additionally, considering deterioration models and the interdependencies among bridges in the portfolio, which arise due to the spatial proximity of objects within the network, when developing optimal budget allocation algorithms, can improve the overall performance of bridge systems.

6.2 Recommendations

6.2.1 Recommendation for the case study

In Chapters 3 and 4 we delivered the first comprehensive spatial analysis and the largest dataset of extreme gross vehicle weights, extreme traffic load effects (bending moments and shear forces) in bridges, and bridge performance indicators due to traffic loads (bridge criticality) for the fifteen major highway corridors of Mexico. This work not only shows the applicability of the proposed methodologies but also underscores the practical utility of the generated maps in identifying potential hazardous locations. The findings lead to the following recommendations:

- It is suggested that future Statistic Field Study of Domestic Road Transportation, EECAN, study focus on the corridors a) *México —Nuevo Laredo, Piedras Negras* and b) *México —Puebla, Progreso* since they present the heaviest vehicle events compared to other corridors.

- It is suggested that Weight-In-Motion (WIM) system stations be installed on major highway corridors: a) *México—Nuevo Laredo, Piedras Negras*, b) *Querétaro—Ciudad Juárez*, c) *Acapulco—Veracruz*, d) *Manzanillo—Tampico, Lázaro Cárdenas*, and e) *México—Puebla—Progreso.* Particularly, in the highway segments that cross the federal entities: *Aguascalientes*, *Colima*, *Guanajuato*, *Jalisco*, *México*, *Nuevo León*, *Puebla*, *Querétaro*, *Tabasco*, *Tamaulipas*, and *Zacatecas.* This is because, in those locations, gross vehicle weights exceeding 1190 kN ($GVW_{50} > 1190$) with a return period of 50 years were found.

- It is recommended that future SIMPUMEX inspections gather more detailed information on bridges with a load-effect performance indicator for bending moment above 1, considering a 50-year return period ($M_{50,r} > 1$). This recommendation is particularly pertinent for reinforced concrete bridges, as prestressed concrete bridges typically have a large capacity to sustain traffic loads. Special attention should be given to highway corridors where the highest percentage of bridges with $M_{50,r} > 1$ is found, corresponding to major highway corridors: a) *Peninsula de Yucatán* (89%), b) *Circuito Transístmico* (76%), and c) *México-Nogales, Tijuana* (71%).

- It is recommended that future SIMPUMEX inspections gather more detailed information on bridges with a load-effect performance indicator for share force above 1, considering a 50-year return period ($V_{50,r} > 1$). Particularly, in highway corridors where the highest percentage of their bridges with $V_{50,r} > 1$ is presented, corresponding to major highway corridors: a) *México-Nogales, Tijuana* (60%), b) *Acapulco -Veracruz* (58%), and c) *Circuito Transístmico* (60%).

- Future SIMPUMEX studies should prioritize inspections on two out of the fifteen major highway corridors: a) *Peninsula de Yucatán* and b) *México-Nogales, Tijuana.*

This is because, in a), the estimated characteristic load effect in 16 out of its 18 bridges exceeds the design values specified by the corresponding live load model reported in the SIPUMEX database. Similar behaviour is observed in b) with 103 of its 145 exceeding the design values. Additionally b) is the major highway corridor with the most bridges in the Mexican Federal highway network.

- It is recommended to consider the additional costs resulting from spatially proximate interventions on individual bridges within the network when allocating the budget for bridge maintenance and repair activities. Failing to account for these costs may result in underestimating the total costs involved.
- Regarding optimal budget allocation for bridge maintenance and repair activities, it is suggested to consider repairing bridges with SIPUMEX bridge rating above 3 ($B_R > 3$) or $M_{50,r} > 1.56$ and provide matinees to the rest of the bridges. This strategy benefits more bridges while guaranteeing the adaptability of the bridge network to the actual traffic load demands.
- It is recommended that the Mexican authorities provide more freely available comprehensive bridge data, such as materials and longitudinal and transversal layouts. This data would not only enrich academic understanding but also serve the public interest by promoting transparency and awareness of infrastructure quality and safety.

6.2.2 Recommendation for future research

Based on the conclusions and findings discussed in the previous chapters, a set of recommendations arises to enhance the approaches employed in this thesis.

- Dependence between axle loads in longer vehicles: Further investigation into the dependence between axle loads in longer vehicles could enhance the model for generating synthetic heavy vehicles. This exploration may offer formal evidence supporting the idea that longer vehicles have the capacity to carry heavier loads on the last axle, explaining the high correlations associated with this specific axle.
- Validation of load effects: Further validation is essential to confirm load effects using real bridge-specific influence lines. Theoretical influence lines may deviate from real ones due to uncertainties related to bridge conditions, including support conditions and changes in bridge stiffness.
- Alternative methods for estimating extreme load effects (ELEs): Moreover, future investigations can explore alternative methods for estimating ELEs. In particular, the Peaks-Over-Threshold method appears to be a logical initial approach. Additionally, the Bayesian Inference statistical method can be employed to investigate the influence of statistical uncertainty in parameters of the distribution models, due to the limited amount of data, used to compute characteristic values.
- Applicability of Methodologies: Future research can assess the applicability of the methodologies presented in various networks to measure their effectiveness as a general approach. Regions where robust BMSs and WIM data are available (United

States and Europe for example) present opportunities for applying the methodology to their respective networks. For instance, quantifying a Bayesian Network model with WIM datasets and evaluating its performance relative to the Mexican quantification, as well as combining these datasets, could provide valuable insights. This approach allows for creating multiple scenarios with varying traffic volumes and different vehicle configurations crossing specific bridges.

- Methodology Extensions: The methodologies presented in Chapters 3 and 4 are currently limited to the investigation of extreme loads, bending moments, and shear forces. However, potential extensions of this methodology to assist in the investigation of fatigue or other failure mechanisms in bridges are viable.

- Principal Sources of Uncertainty: It is important to note that the principal sources of uncertainty in the methodology presented in Chapter 5 are: the deterioration model, the extent of the impact induced by interventions on other bridges (indicated by the interaction matrix), and the average annual inflation rate. Properly quantifying these variables for each bridge within the network will lead to a more precise estimation of the optimal intervention plan.

6.3 Closing remarks

This thesis focuses on enhancing the reliability estimates of bridges at a network level for the development and implementation of intervention strategies. The central theme involves four research topics. Within each of these topics, the approaches employed have proven effective in modeling the dependence between traffic load variables. This enhances the accuracy of reliability estimates, thereby helping decision-making in bridge management strategies.

While basic road infrastructure management tools, such as a single-module Bridge Management System, fulfill their purpose in overseeing locations or bridges at a fundamental level, there is room for improvement, particularly in addressing risks that cannot be detected by visual inspections. A viable solution involves implementing tools that facilitate the acquisition, processing, and comprehensive analysis of information using risk-based and probabilistic reliability methodologies. This approach enables the formulation of strategic action plans aimed at preserving structural integrity and ensuring user safety.

The insights presented in this thesis advocate for integrating these subjects into our reliability estimates and bridge management decisions due to their alignment with the existing knowledge base. Acknowledging the limitations and uncertainties of the approaches used, the primary objective was to develop a general and straightforward framework to assist local authorities in regions where WIM systems are not the primary source of traffic data providing them with the tools necessary to make more informed bridge management decisions.

Appendices

A

A Modelling Weigh-in-Motion System Data

A.1 Traffic data

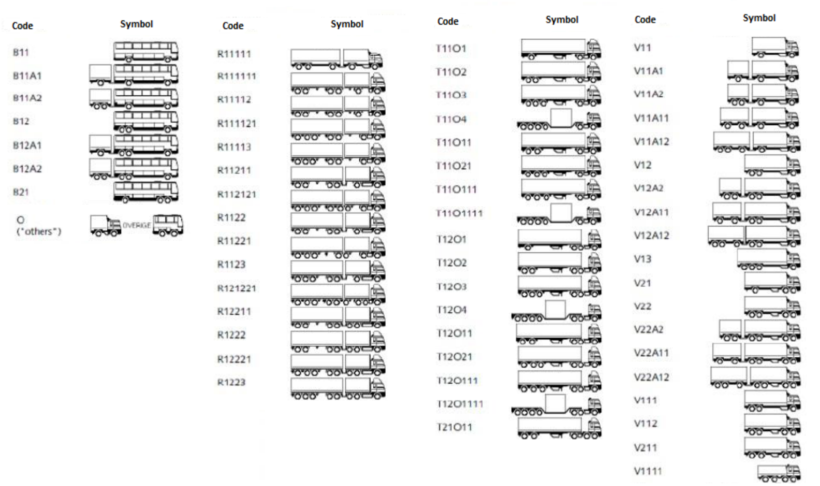

Figure A.1.1: Most observed vehicle codes in the Dutch WIM measurements (April 2013).

A

Table A.1.1: Filtered criteria described in [27] and [67].

	Filter
1	Wheelbase length less than 1 m.
2	Wheelbase less than 30 m and first or last spacing above 10 m.
3	Wheelbase larger than 40 m.
4	Trucks with axle load bellow or equal to 0 tons.
5	Any axle weight larger than 40 tons.
6	Any axle weight larger than 15 tons and above 85% of gross vehicle weight.
7	Trucks with gross weight below or equal to 0 tons.
8	Sum of axle loads not within 50 kg of gross vehicle weight.
9	Truck with closely spaced, i.e. less or equal to 2 m first two axles, one of which is larger than 10 tons and over 2.5 times heavier than other axles.
10	First spacing larger than 15 m.
11	Any spacing less than 0,4 m.
12	Miss match between the number of axle spacings and the number of axle loads.
13	Sum of axle spacings not within 50 mm of wheelbase.
14	Number of axles below or equal to 1.
15	First axle spacing in the interval of 10 m – 15 m.
16	Each spacing in the range of 0,4 m – 0,7 m.
17	Each spacing in the range of 0,7 m – 1,0 m.
18	Each axle load in the interval of 25 tons – 40 tons.
19	Each axle load below 0,5 tons.
20	Vehicles with the same WIM identification number (ID).
21	Vehicles with a gross vehicle weight below 3,56 tons.
22	Vehicles with a gross vehicle weight above 112 tons.
23	Vehicles with a speed greater than 120 km/h.
24	The vehicles with gross vehicle weight larger than 71.3 tons and or length bumper-to–bumper above 25,5 m and axle spacing above 12,5 m (data related to a combination of two vehicles).
25	Vehicles with inter-axle distances less than 75 cm.
26	Duplicate records.

A

Table A.1.2: Created vehicle types from all observed Dutch WIM codes (April 2013).

Item	Class	Code											
1	B2	B11	B2										
2	B3	B111	B12	B3									
3	O3	O3											
4	O4	O4											
5	O5	O5											
6	O6	O6											
7	O8	O8											
8	O9	O9											
9	O10	O=											
10	O11	O>											
11	R5	R11111	R1112	R1211	R122								
12	R6	R111111	R11112	R11121	R1113	R11211	R1122	R12111					
		R1212	R123	R1311	R132								
13	R7	R1111111	R111112	R111121	R11113	R111211	R11122	R112111					
		R124	R13111	R133	R2221	R223	R11311	R1123					
		R1132	R115	R121111	R12112	R1213	R12211	R1222					
		R11212	R11221										
14	R8	R11111111	R1111112	R1111121	R111113	R111122	R1112111	R111212	R111221	R11123	R1121111	R112112	R112121
		R11213	R112211	R11222	R1124	R113111	R11312	R11321	R1133	R1211111	R121112	R121121	R12113
		R121211	R12122	R1214	R122111	R12212	R12221	R1223	R12311	R1232	R125	R131111	R1313
		R13211	R1322	R134	R2123	R2213	R2222	R224					
15	R9	R1112121	R1112211	R11124	R1121121	R112113	R1122111	R112221	R11223	R1125	R1134	R12111111	R1211112
		R1211121	R121113	R1212111	R121212	R121221	R12123	R1221111	R122112	R122121	R12213	R1224	R123111
		R12321	R1233	R126	R1314	R132111	R13221	R1323	R1332	R1341	R135	R1413	R144
		R2214	R2223	R225	R234	R3312	R54						
16	T3	T11O1											
17	T4	T111O1	T11O11	T11O2	T12O1	T21O1	T2O2						
18	T5	T111O11	T111O2	T11O111	T11O12	T11O21	T11O3						
		T12O11	T12O2	T21O11	T21O2	T2O21	T2O3	T3O2					
19	T6	T111O111	T111O12	T111O21	T111O3	T11O1111	T11O112	T11O121	T11O13	T11O211	T11O22	T11O31	T11O4
		T12O111	T12O12	T12O21	T12O3	T21O111	T21O12	T21O21	T21O3	T2O22	T2O4	T3O3	
20	T7	T111O112	T111O121	T111O13	T111O22	T111O31	T111O4	T12O1111	T12O112	T12O121	T12O13	T12O211	T12O22
		T12O31	T12O4	T21O211	T21O22	T21O4	T3O4						
21	V2	V11											
22	V3	V111	V11A1	V12	V21	V3							
23	V4	V1111	V112	V11A11	V11A2	V121	V13	V211	V22	V4			
24	V5	V111A11	V111A2	V11A111	V11A12	V12A11	V12A2	V21A11	V21A2				
25	V6	V1111A11	V1111A2	V111A111	V111A12	V112A11	V112A2	V121A11	V12A111	V12A12	V12A21	V12A3	V13A11
		V13A2	V211A11	V211A2	V21A12	V22A11	V22A2						
26	V7	V1111A111	V1111A12	V1111A3	V112A111	V112A12	V112A21	V112A3	V121A111	V121A12	V121A3	V13A111	V13A12
		V13A21	V13A3	V211A12	V211A3	V22A111	V22A12	V22A21	V22A3	V4A12			

A.2 GCBN MODEL

table A.2.1 shows the unconditional rank correlations $r(X_{i,j}, X_{i,j-1})$, for all i and $j > 1$ (according to the notation in section 2.3.3), between individual axle loads per vehicle type for the GCBN A15-L model. The first two columns indicate the vehicle type i and the name, the third column, the corresponding number of axles (n_i). Every entry in the next 10 columns indicates the rank correlations between the first and second axle ($X_{i,1}, X_{i,2}$), second and third ($X_{i,2}, X_{i,3}$), and so on until the 10th and 11th axle ($X_{i,10}, X_{i,11}$) per vehicle type. The last column indicates the rank correlations between the last vehicle axle and the total vehicle length ($X_{i,n_i}, X_{i,n_{i+1}}$). As the number of axles increases, the correlations are stronger in the axles close to the end of the vehicle. In contrast, the correlation between X_{i,n_i} and $X_{i,n_{i+1}}$ and, as is expected, is low.

Table A.2.1: Rank correlation per vehicle type between axles A15-L location.

Vehicle (i)	Type	No Axles (n_i)	$X_{i,1}, X_{i,2}$	$X_{i,2}, X_{i,3}$	$X_{i,3}, X_{i,4}$	$X_{i,4}, X_{i,5}$	$X_{i,5}, X_{i,6}$	$X_{i,6}, X_{i,7}$	$X_{i,7}, X_{i,8}$	$X_{i,8}, X_{i,9}$	$X_{i,9}, X_{i,10}$	$X_{i,10}, X_{i,11}$	$X_{i,n_i}, X_{i,n_{i+1}}$
1	B2	2	0.87										0.2
2	B3	3	0.81	0.85									0.31
3	O3	3	0.62	-0.1									0.09
4	O4	4	0.61	0.03	0.73								0.26
5	O5	5	0.64	0.06	0.66	0.73							0.04
6	O6	6	0.32	0.08	0.95	0.63	0.99						-0.28
7	O8	8	0.75	0.81	0.79	0.65	0.95	0.93	0.97				-0.19
8	O9	9	0.75	0.61	0.85	0.49	0.83	0.99	0.99	0.98			0.27
9	O10	10	0.73	0.4	0.49	0.71	0.71	0.98	0.99	0.99	0.98		-0.79
10	R5	5	0.7	0.22	0.6	0.92							-0.04
11	R6	6	0.01	0.16	0.94	0.47	0.96						0.43
12	R7	7	0.42	0.12	0.89	0.84	0.89	0.99					0.08
13	R8	8	0.48	0.41	0.66	0.76	0.8	0.87	0.94				-0.06
14	R9	9	0.48	0.66	0.62	0.37	0.98	0.85	0.99	0.99			-0.16
15	T3	3	0.45	0.54									0.36
16	T4	4	0.58	0.74	0.96								0.4
17	T5	5	0.77	0.82	0.99	0.98							0.05
18	T6	6	0.44	0.28	0.65	0.99	0.99						-0.2
19	T7	7	0.51	0.51	0.63	0.95	0.96	0.93					-0.21
20	V2	2	0.81										0.54
21	V3	3	0.59	0.6									-0.21
22	V4	4	0.42	0.42	0.9								-0.1
23	V5	5	0.56	0.59	0.59	0.93							0.12
24	V6	6	0.57	0.45	0.55	0.72	0.95						-0.05
25	V7	7	0.49	0.36	0.7	0.46	0.83	0.99					-0.15

Similarly, table A.2.2 shows the rank correlations between individual inter-axle distances per vehicle type. The first two columns indicate the vehicle type (i) and the corresponding name, the third column, the number of axles per vehicle type (n_i). The fourth column indicates the rank correlation between the total vehicle length and the first axle distance ($X_{i,n_{i+1}}, X_{i,n_{i+1+1}}$). The next 10 columns indicate the rank correlations between the first and second axle distance ($X_{i,n_{i+1+1}}, X_{i,n_{i+1+2}}$), second and third ($X_{i,n_{i+1+2}}, X_{i,n_{i+1+3}}$), and so on until the 10th and 11th axle ($X_{i,n_{i+1+10}}, X_{i,n_{i+1+11}}$) per vehicle type. Notice that the correlations almost zero is observed in some cases. The corresponding rank correlations matrices between the random variables, as colour maps, for the six WIM locations can be found in figures A.2.1 to A.2.3. After the detailing of three categories of the framework, in the successive section the results and validation of the GCBN will be discussed.

figures A.2.1 to A.2.3 shows the corresponding rank correlations matrices between the random variables, as colour maps, for the six studied dutch WIM locations described in section 2.3.1.

Table A.2.2: Rank correlation per vehicle type between inter axle distances for A15-L location.

Vehicle (i)	Type	No Axles (n_i)	$X_{i,n_{i+1}}, X_{i,n_{i+1+1}}$	$X_{i,n_{i+1+1}}, X_{i,n_{i+1+2}}$	$X_{i,n_{i+1+2}}, X_{i,n_{i+1+3}}$	$X_{i,n_{i+1+3}}, X_{i,n_{i+1+4}}$	$X_{i,n_{i+1+4}}, X_{i,n_{i+1+5}}$	$X_{i,n_{i+1+5}}, X_{i,n_{i+1+6}}$	$X_{i,n_{i+1+6}}, X_{i,n_{i+1+7}}$	$X_{i,n_{i+1+7}}, X_{i,n_{i+1+8}}$	$X_{i,n_{i+1+8}}, X_{i,n_{i+1+9}}$	$X_{i,n_{i+1+9}}, X_{i,n_{i+1+10}}$
1	B2	2	0.63	0.11								
2	B3	3	0.28	-0.03	0.03							
3	O3	3	0.04	0.11	-0.33							
4	O4	4	0.06	0.15	0.37	0.13						
5	O5	5	0.16	0.34	0.54	-0.39	-0.22					
6	O6	6	0.48	0.18	-0.09	-0.28	-0.42	0.01				
7	O8	8	0.09	0.14	-0.84	-0.49	-0.82	-0.39	-0.52	-0.23		
8	O9	9	0.44	0.27	-0.77	-0.79	-0.82	-0.39	-0.28	-0.05	0.73	
9	O10	10	0.6	0.77	0.18	0.32	-0.64	-0.58	-0.22	0.46	0.35	0.01
10	R5	5	0.15	-0.07	0.51	0.19	0.05					
11	R6	6	-0.1	-0.23	-0.27	-0.31	-0.07	0.07				
12	R7	7	0.16	0.03	-0.11	-0.68	-0.09	-0.75	0.33			
13	R8	8	0.15	0	0.07	-0.54	-0.19	-0.71	-0.68	0.25		
14	R9	9	0.23	0.18	-0.35	-0.49	-0.64	-0.49	-0.55	-0.41	0.32	
15	T3	3	0.22	-0.16	-0.06							
16	T4	4	0.27	-0.13	0.02	-0.25						
17	T5	5	0.28	-0.21	-0.07	-0.18	0.25					
18	T6	6	0.21	0.15	0.15	-0.22	-0.27	0.59				
19	T7	7	-0.08	-0.16	0.41	-0.16	-0.26	-0.27	-0.06			
20	V2	2	0.52	0.31								
21	V3	3	0.18	0.07	-0.21							
22	V4	4	0.28	0.17	0.75	-0.1						
23	V5	5	0.41	0.15	-0.25	-0.39	-0.38					
24	V6	6	0.29	0.03	-0.48	-0.41	-0.22	-0.15				
25	V7	7	0.08	0.07	-0.71	-0.04	-0.06	-0.41	-0.19			

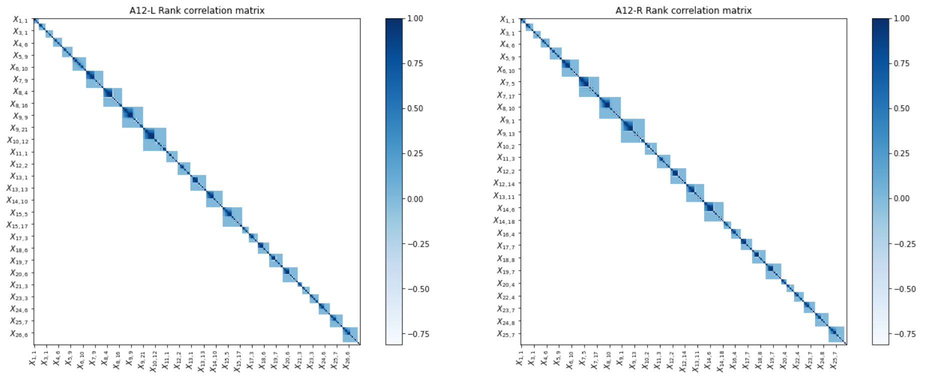

(a) (b)

Figure A.2.1: Bayesian Network rank correlation matrix corresponding to the Dutch A12 highway. a) left lane and b) right lane.

A

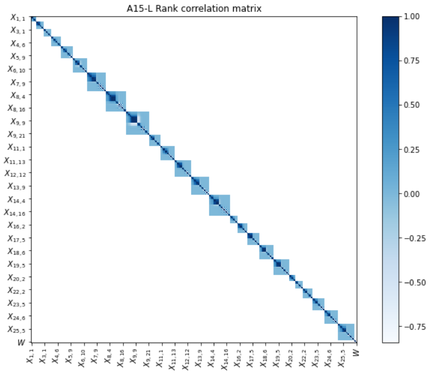

(a)

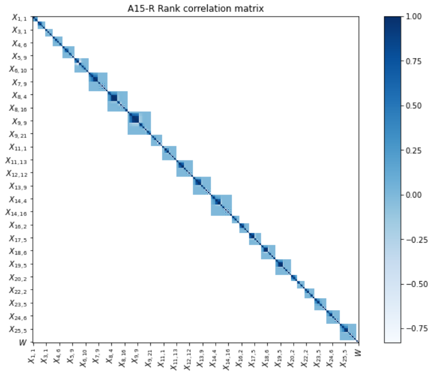

(b)

Figure A.2.2: Bayesian Network rank correlation matrix corresponding to the Dutch A15 highway. a) left lane and b) right lane.

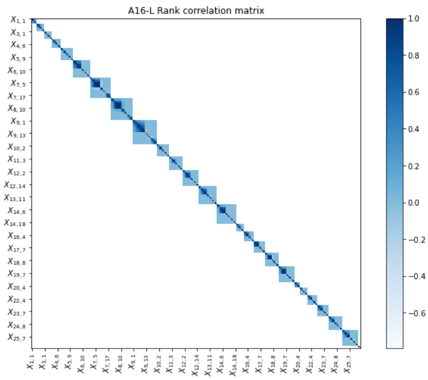

(a)

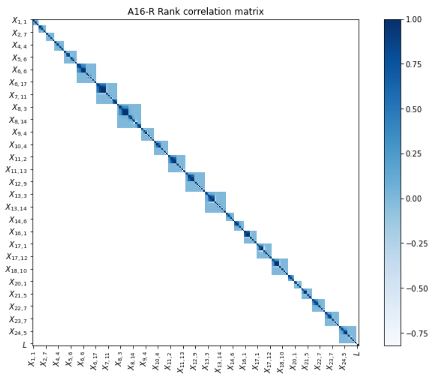

(b)

Figure A.2.3: Bayesian Network rank correlation matrix corresponding to the Dutch A16 highway. a) left lane and b) right lane.

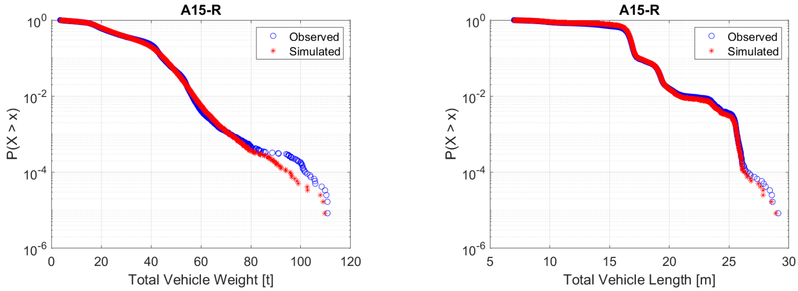

(a) (b)

Figure A.2.4: Comparison between variables of interest generated by the BN model and the WIM data in highway A15: (a) Total vehicle weight [kg] comparison right lane; (b) Total vehicle length [cm] comparison right lane.

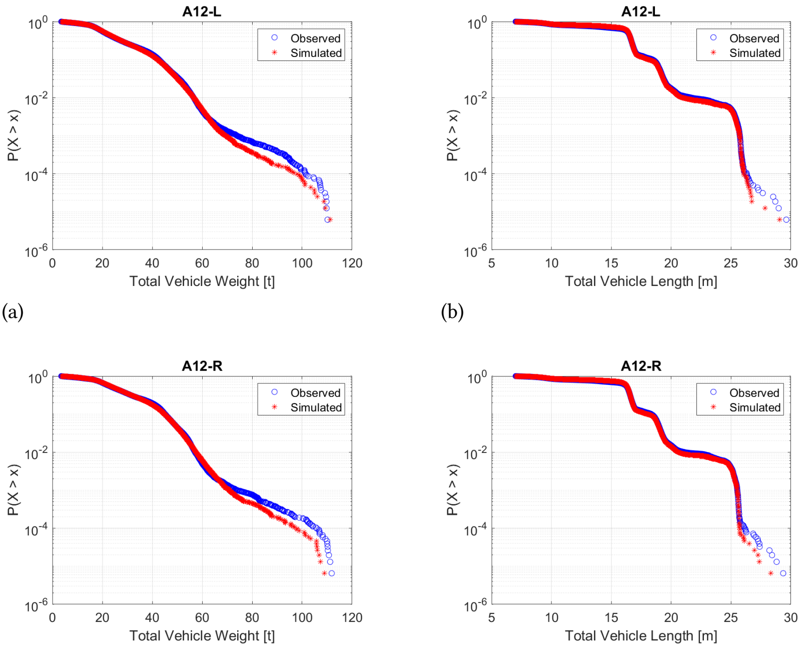

(a) (b) (c) (d)

Figure A.2.5: Comparison between variables of interest generated by the BN model and the WIM data in both driving directions of highway A12: (a) Total vehicle weight [t] comparison left lane; (b) Total vehicle length [m] comparison left lane; (c) Total vehicle weight [t] comparison right lane; (d) Total vehicle length [m] comparison right lane.

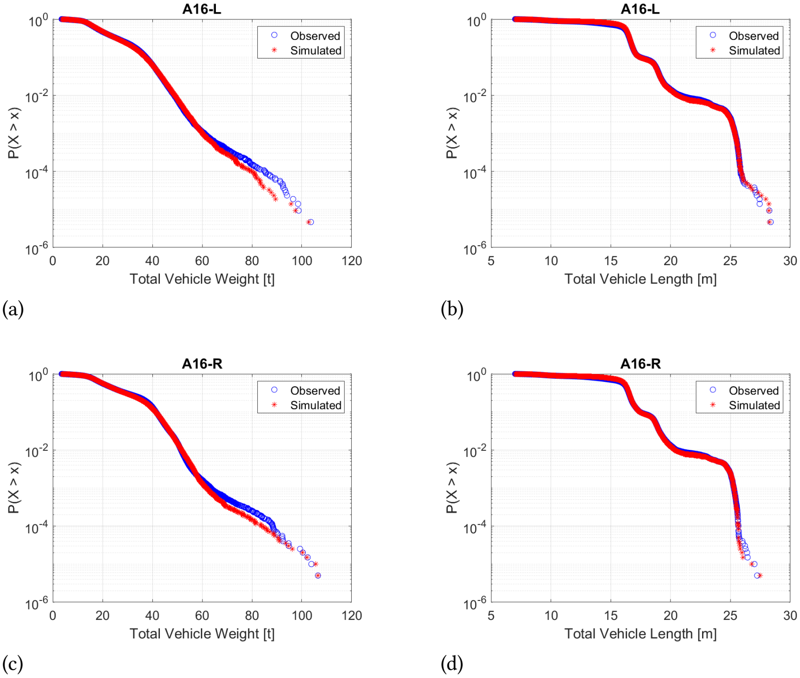

Figure A.2.6: Comparison between variables of interest generated by the BN model and the WIM data in both driving directions of highway A16: (a) Total vehicle weight [t] comparison left lane; (b) Total vehicle length [m] comparison left lane; (c) Total vehicle weight [t] comparison right lane; (d) Total vehicle length [t] comparison right lane.

A

Split data analysis

To further investigate model validity, we split the data set into an 80:20 ratio (80% of the data set goes into the training set and 20% of the data set goes into the testing set). figure A.2.7 shows a comparison between synthetic data generated by the model quantified with the training data set and the observations of the test data set. The observations correspond to the A16-R highway. Additionally, figure A.2.8 shows the same comparison for the two-axle vehicle B2 of total vehicle weight, total vehicle length, axle loads and inter-axle distances. As can be seen in figures A.2.7 and A.2.8 the model is able to represent the data points in the training data set to a good degree. Same type of analysis was performed with data corresponding to other highways and vehicle types in our database. The patterns are similar to those briefly presented here. The model captures the main complexities of the data set.

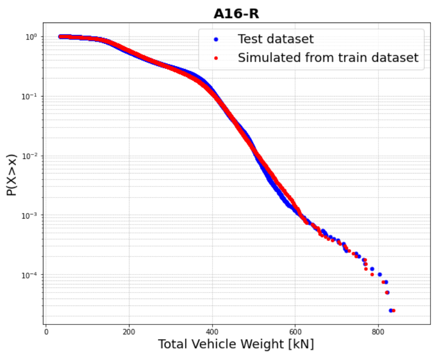

(a)

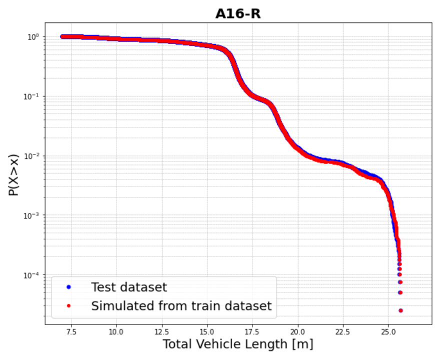

(b)

Figure A.2.7: Comparison between data generated by the trained model and test data set for a)total vehicle weight and b)total vehicle length (all vehicle types)

A

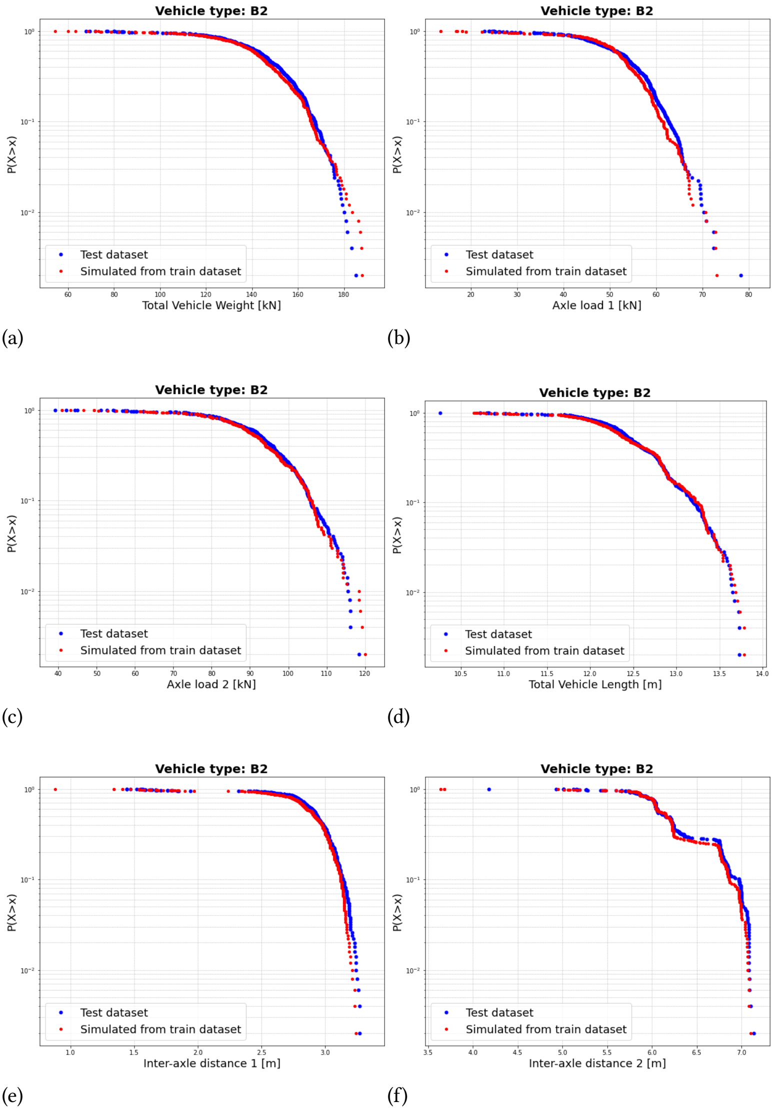

Figure A.2.8: Comparison between data generated by the trained model and test data set: a)total vehicle weight, b) and c) axle loads, d) total vehicle length and e) and f) inter-axle distances of the vehicle type B2.

A.3 GUI quick user guide

The Graphical User Interface GCBN WIM computes synthetic WIM data. The observations correspond to April 2013 for three Dutch locations in both the right (R) and the left (L) driving directions. The measurements were taken on highways A12 (km 42) Woerden, A15 (km 92) Gorinchem, and A16 (km 41) Gravendeel. Additionally, a hypothetical highway was created which is a combination of all six available WIM locations in the model. Thus, each simulated vehicle randomly chooses one of the locations to compute the synthetic data. The 26 codes (vehicle types) used in the GUI WIM consist of a letter and a number that define the number of axles. The letter represents the vehicle configurations: Buses (B), Tractor - Semitrailer - Trailer (R), Tractor - Semitrailer (T), Single-unit multi-axle vehicle and/or Single unit multi-axle vehicle - Semitrailer (V) and Others vehicles (O). For example, a seven-axle vehicle with the configuration Tractor - Semitrailer is coded as T7. The vehicle types and the silhouette are presented infigure A.3.1.

Vehicle	Type	Silhouette
1	B2	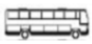
2	B3	
3	O0	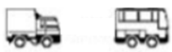
4	O3	
5	O4	
6	O5	
7	O6	
8	O7	
9	O8	
10	O9	
11	R5	
12	R6	
13	R7	
14	R8	
15	R9	

Vehicle	Type	Silhouette
16	T3	
17	T4	
18	T5	
19	T6	
20	T7	
21	V2	
22	V3	
23	V4	
24	V5	
25	V6	
26	V7	

Figure A.3.1: Available vehicle types.

To compute the desired amount of WIM observations, in the main window of the GUI (see figure A.3.2), the user can choose between the 26 vehicle types and the seven locations (A12-L, A12-R, A15-L, A15-R, A16-L, A16-R, and Hypothetical). The option for choosing the desired units is also available. Additionally, there are three main checkboxes: (i) vehicle type subset, (ii) correlation matrix plot, and (iii) Bayesian network plot. Which actions are described next:

(i) If the “Vehicle Type Subset" check box is selected. The user needs to select at least 4 of the available 26 vehicle types and provide their corresponding proportions. Otherwise, 26 vehicle types will be used to generate synthetic observations.

(ii) If the “Correlation Matrix Plot" check box is selected. The rank correlation matrix plot will be shown as a colour map (figure A.3.3a)

(iii) If the “Bayesian Network Plot" check box is selected. The Non-Parametric Bayesian Network (GCBN) direct acyclic graph will be shown (figure A.3.3b).

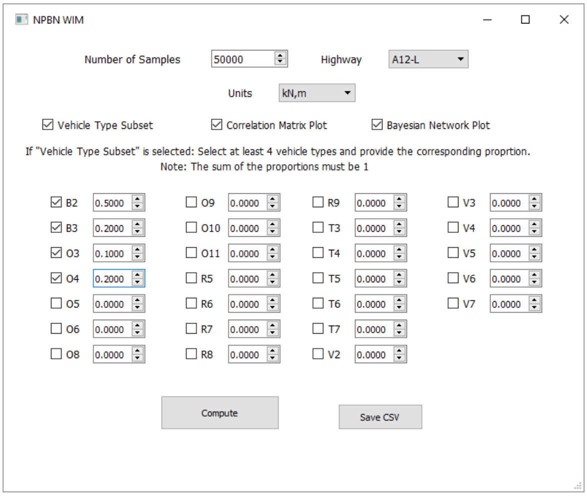

Figure A.3.2: GUI main window.

If the user chooses a Hypothetical highway no rank correlation matrix plot nor GCBN direct acyclic graph will be shown. Once all the values are set, by pressing the button “Compute” the synthetic WIM observations will be generated. Plots of histograms and exceedance probability plots of total weight (W) and total vehicle length (L) will be generated automatically (see figure A.3.4). Finally, the computed data can be stored in a comma-separated values (CSV) file by pressing the button “Save CSV”.

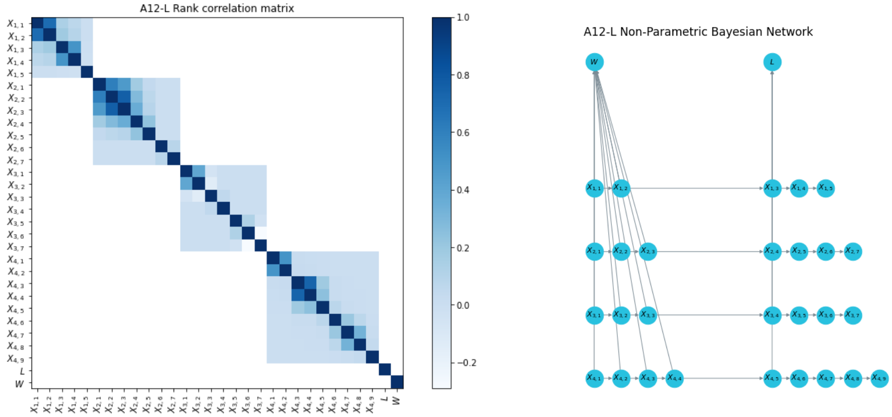

(a) (b)

Figure A.3.3: a) Rank correlation matrix colour map and b) GCBN direct acyclic graph.

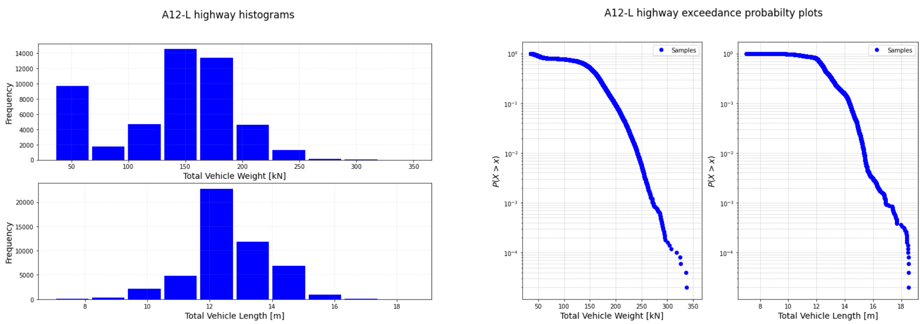

(a) (b)

Figure A.3.4: a) Computed W and L histograms b) Computed W and L exceedance probability plots.

B

Mapping hazardous locations due to extreme gross vehicle weights.

B.1 Axle load distributions

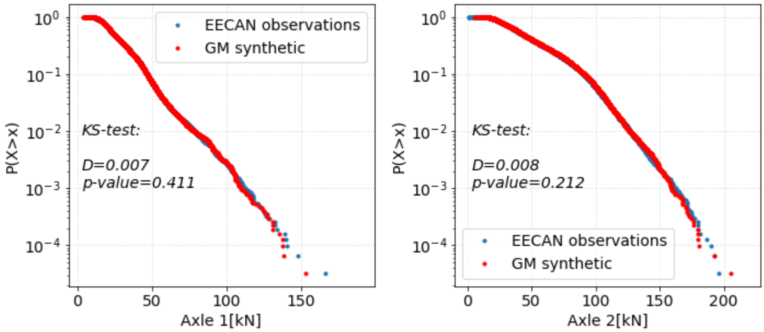

Figure B.1.1: Agreement between simulated and observed axle loads for vehicle type C2. The results from the two-sample Kolmogorov-Smirnov (KS) test indicate that it is likely that the two samples were drawn from the same distribution (D test statistic is close to 0). Moreover, since the p-value is greater than 0.05, there is sufficient evidence to conclude that the two datasets come from the same distribution.

Table B.1.1: Gaussian mixture components representing the axles of vehicle type C3

Axle 1 ($X_{2,1}$)				Axle 2 ($X_{2,2}$)				Axle 3 ($X_{2,3}$)			
g	π_g	μ_g [kN]	σ_g [kN]	g	π_g	μ_g [kN]	σ_g [kN]	g	π_g	μ_g [kN]	σ_g [kN]
1	0.26	29.07	4.25	1	0.23	53.13	8.68	1	0.2	50.73	8.84
2	0.22	44.09	5.60	2	0.16	90.66	15.36	2	0.15	89.28	13.78
3	0.03	74.24	25.71	3	0.32	35.98	6.89	3	0.34	34.77	6.61
4	0.13	18.92	4.26	4	0.17	73.85	10.98	4	0.17	72.35	10.30
5	0.08	53.1	7.98	5	0.06	85.45	29.88	5	0.1	20.15	5.15
6	0.28	37.23	4.58	6	0.07	19.48	4.00	6	0.05	96.98	22.68

Table B.1.2: Gaussian mixture components representing the axles of vehicle type T3S2

Axle 1 ($X_{3,1}$)				Axle 2 ($X_{3,2}$)			
g	π_g	μ_g [kN]	σ_g [kN]	g	π_g	μ_g [kN]	σ_g [kN]
1	0.14	30.15	7.97	1	0.24	44.91	7.02
2	0.34	41.76	4.50	2	0.21	73.99	8.50
3	0.03	55.98	10.27	3	0.16	88.02	11.86
4	0.3	34.95	5.29	4	0.13	34.26	8.45
5	0.16	48.07	5.44	5	0.2	58.76	7.09
6	0.03	75.6	23.81	6	0.05	93.94	23.34

Axle 3 ($X_{3,3}$)				Axle 4 ($X_{3,4}$)				Axle 5 ($X_{3,5}$)			
g	π_g	μ_g [kN]	σ_g [kN]	g	π_g	μ_g [kN]	σ_g [kN]	g	π_g	μ_g [kN]	σ_g [kN]
1	0.23	43.06	7.29	1	0.23	38.18	6.65	1	0.19	53.04	7.5
2	0.22	73.39	8.92	2	0.19	68.63	9.08	2	0.18	83.79	13.05
3	0.17	86.65	12.64	3	0.17	84.18	12.61	3	0.2	68.81	9.25
4	0.14	33.24	8.30	4	0.2	53.38	7.56	4	0.06	86.96	25.67
5	0.21	57.26	7.30	5	0.15	28.07	7.33	5	0.14	28.13	7.05
6	0.05	90.06	25.59	6	0.06	88.59	23.79	6	0.22	38.18	6.57

Table B.1.3: Gaussian mixture components representing the axles of vehicle type T3S3

Axle 1 ($X_{4,1}$)				Axle 2 ($X_{4,2}$)				Axle 3 ($X_{4,3}$)			
g	π_g	μ_g [kN]	σ_g [kN]	g	π_g	μ_g [kN]	σ_g [kN]	g	π_g	μ_g [kN]	σ_g [kN]
1	0.32	45.12	7.78	1	0.08	105.73	20.99	1	0.2	83.34	10.66
2	0.15	24.56	5.35	2	0.25	48.12	7.53	2	0.21	47.88	8.60
3	0.52	39.41	5.76	3	0.21	96.78	12.63	3	0.21	95.17	14.33
4	0.02	63.54	21.11	4	0.14	31.62	7.90	4	0.12	63.96	10.37
-	-	-	-	5	0.14	66.85	8.74	5	0.09	99.49	22.58
-	-	-	-	6	0.19	86.06	9.70	6	0.17	33.56	8.28

Axle 4 ($X_{4,4}$)				Axle 5 ($X_{4,5}$)				Axle 6 ($X_{4,6}$)			
g	π_g	μ_g [kN]	σ_g [kN]	g	π_g	μ_g [kN]	σ_g [kN]	g	π_g	μ_g [kN]	σ_g [kN]
1	0.21	41.88	9.92	1	0.2	26.38	6.53	1	0.19	40.7	9.57
2	0.12	86.78	21.10	2	0.19	71.44	10.59	2	0.24	76.29	9.72
3	0.27	80.15	12.58	3	0.09	89.81	19.52	3	0.04	85.43	28.74
4	0.18	65.32	11.33	4	0.13	55.51	9.81	4	0.22	27.53	7.46
5	0.22	27	7.75	5	0.21	83.43	11.50	5	0.14	58.66	9.63
-	-	-	-	6	0.18	38.4	8.51	6	0.17	89.03	14.89

B

Table B.1.4: Gaussian mixture components representing the axles of vehicle type T3S2R4

Axle 1 ($X_{5,1}$)				Axle 2 ($X_{5,2}$)				Axle 3 ($X_{5,3}$)			
g	π_g	μ_g [kN]	σ_g [kN]	g	π_g	μ_g [kN]	σ_g [kN]	g	π_g	μ_g [kN]	σ_g [kN]
1	0.4	38.02	4.59	1	0.2	74.38	12.72	1	0.2	81.85	13.71
2	0.1	16.37	2.56	2	0.25	39.78	7.03	2	0.1	21.52	3.78
3	0.28	45.85	7.58	3	0.19	89.59	14.73	3	0.13	90.99	16.70
4	0.21	30.76	5.03	4	0.22	57.16	9.15	4	0.19	51.84	8.09
5	0	62.11	24.00	5	0.03	99.79	28.09	5	0.22	37.93	6.53
-	-	-	-	6	0.1	21.72	3.69	6	0.16	67.07	9.54

Axle 4 ($X_{4,4}$)				Axle 5 ($X_{4,5}$)				Axle 6 ($X_{5,6}$)			
g	π_g	μ_g [kN]	σ_g [kN]	g	π_g	μ_g [kN]	σ_g [kN]	g	π_g	μ_g [kN]	σ_g [kN]
1	0.24	33.87	7.93	1	0.22	51.19	9.49	1	0.06	90.35	28.24
2	0.08	82.52	22.18	2	0.22	84.81	13.82	2	0.3	48.27	10.56
3	0.19	51.16	9.87	3	0.25	33.26	7.22	3	0.33	73.99	14.28
4	0.2	83.85	14.37	4	0.11	20.28	4.53	4	0.32	29.28	8.14
5	0.16	64.9	11.00	5	0.17	66.87	10.88	-	-	-	-
6	0.13	21.48	5.56	6	0.03	85.2	26.05	-	-	-	-

Axle 7 ($X_{5,7}$)				Axle 8 ($X_{5,8}$)				Axle 9 ($X_{5,9}$)			
g	π_g	μ_g [kN]	σ_g [kN]	g	π_g	μ_g [kN]	σ_g [kN]	g	π_g	μ_g [kN]	σ_g [kN]
1	0.19	59.04	10.20	1	0.11	16.46	4.82	1	0.26	30.87	6.24
2	0.26	32.19	6.45	2	0.18	79.69	14.29	2	0.14	83.11	18.19
3	0.08	74.13	21.19	3	0.25	30.88	5.91	3	0.23	71.99	14.47
4	0.19	74.71	13.88	4	0.17	60.41	10.13	4	0.09	15.79	4.35
5	0.12	19.12	5.83	5	0.09	87.04	18.43	5	0.27	48.69	8.86
6	0.16	45.98	7.71	6	0.19	46.65	7.82	-	-	-	-

B

B.2 Vehicular survey and counting stations

(a)

(b)

Figure B.2.1: Vehicular survey and counting stations. a) Installed EECAN survey stations from 2002 to 2017 (233 survey stations) and b) Installed *Datos viales* counting stations in 2018 (1777 counting stations). Notice that not all the survey stations are located on the MHC.

B.3 Sensitivity analysis on SEA

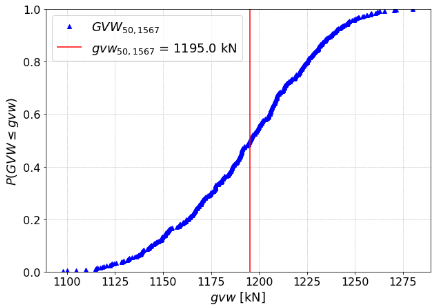

(a)

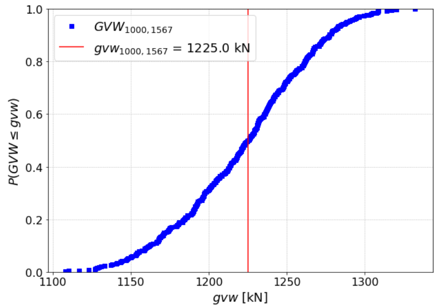

(b)

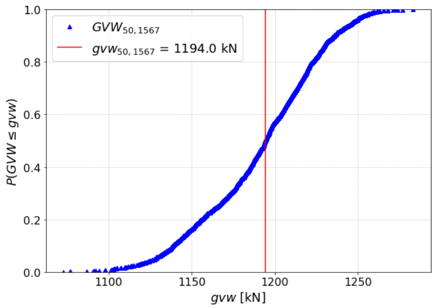

(c)

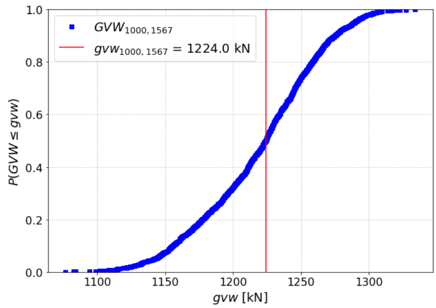

(d)

Figure B.3.1: Sensitivity analysis on SEA in terms of the number of extrapolations performed for CS *Veracruz* ($c = 1567$). (a) Distribution of $GVW_{50,1567}$ values computed 500 times, (b) Distribution of $GVW_{1000,1567}$ values computed 500 times, (c) Distribution of $GVW_{50,1567}$ values computed 1500 times, (d) Distribution of $GVW_{1000,1567}$ values computed 1500 times. The red line represents the 50th percentile (reported value).

B

B.4 Extreme Gross Vehicle Weights

Table B.4.1: Percentiles of the gross vehicle weight with 50-years return period distribution (GVW_{50}) per major highway corridor

Major highway corridor	gvw_{50}				
	P5	P25	P50	P75	P95
06. Transpeninsular Baja California	621.5	850.9	944.6	1006.4	1064.5
15. Del Pacifico	676.6	803.5	923.6	993.0	1122.7
04. México – Tuxpan	802.5	984.0	1049.1	1110.4	1132.9
01. México – Nogales, Tijuana	773.9	1034.8	1130.5	1167.8	1192.5
14. Peninsular de Yucatán	902.3	976.2	1101.1	1148.8	1196.4
05. Mazatlán – Matamoros	762.3	1019.0	1068.5	1145.9	1201.7
03. Querétaro – Ciudad Juárez	926.0	1101.1	1146.3	1183.6	1222.3
10. Altiplano	1041.7	1111.5	1141.1	1177.7	1227.0
08. Veracruz – Monterrey, Matamoros	986.7	1110.7	1156.2	1189.1	1227.6
13. Circuito Transístmico	857.2	1077.2	1140.6	1173.4	1228.9
09. Manzanillo – Tampico, Lázaro Cárdenas	797.5	1029.0	1128.3	1192.4	1236.1
12. Puebla – Oaxaca – Ciudad Hidalgo	806.0	1020.4	1103.8	1142.0	1244.5
07. Acapulco – Veracruz	870.8	1015.0	1102.1	1160.7	1249.4
11. México – Puebla – Progreso	955.6	1073.3	1160.3	1231.0	1263.4
02. México – Nuevo Laredo, Piedras Negras	980.7	1114.3	1167.8	1218.2	1266.9

Table B.4.2: Percentiles of the gross vehicle weight with 1000-years return period distribution (GVW_{1000}) per major highway corridor

Major highway corridor	gvw_{1000}				
	P5	P25	P50	P75	P95
06. Transpeninsular Baja California	648.1	877.8	971.3	1026.6	1086.8
15. Del Pacifico	690.9	822.0	949.7	1017.7	1155.4
04. México – Tuxpan	818.7	1004.3	1075.5	1132.6	1161.3
01. México – Nogales, Tijuana	792.0	1058.6	1150.4	1190.2	1215.7
14. Peninsular de Yucatán	919.7	998.8	1121.2	1174.2	1224.1
05. Mazatlán – Matamoros	782.7	1041.0	1093.3	1169.5	1224.9
03. Querétaro – Ciudad Juárez	951.5	1122.6	1169.7	1204.8	1248.8
08. Veracruz – Monterrey, Matamoros	1007.7	1137.0	1177.7	1212.0	1253.8
10. Altiplano	1061.4	1130.1	1166.0	1203.7	1254.1
13. Circuito Transístmico	883.3	1094.0	1161.4	1201.8	1258.1
09. Manzanillo – Tampico, Lázaro Cárdenas	815.8	1049.5	1147.5	1215.5	1268.0
12. Puebla – Oaxaca – Ciudad Hidalgo	832.5	1041.2	1127.0	1167.0	1271.2
07. Acapulco – Veracruz	891.7	1038.4	1125.1	1182.9	1274.9
11. México – Puebla – Progreso	974.4	1094.3	1182.5	1255.0	1290.4
02. México – Nuevo Laredo, Piedras Negras	1001.0	1135.1	1194.1	1242.2	1293.4

B

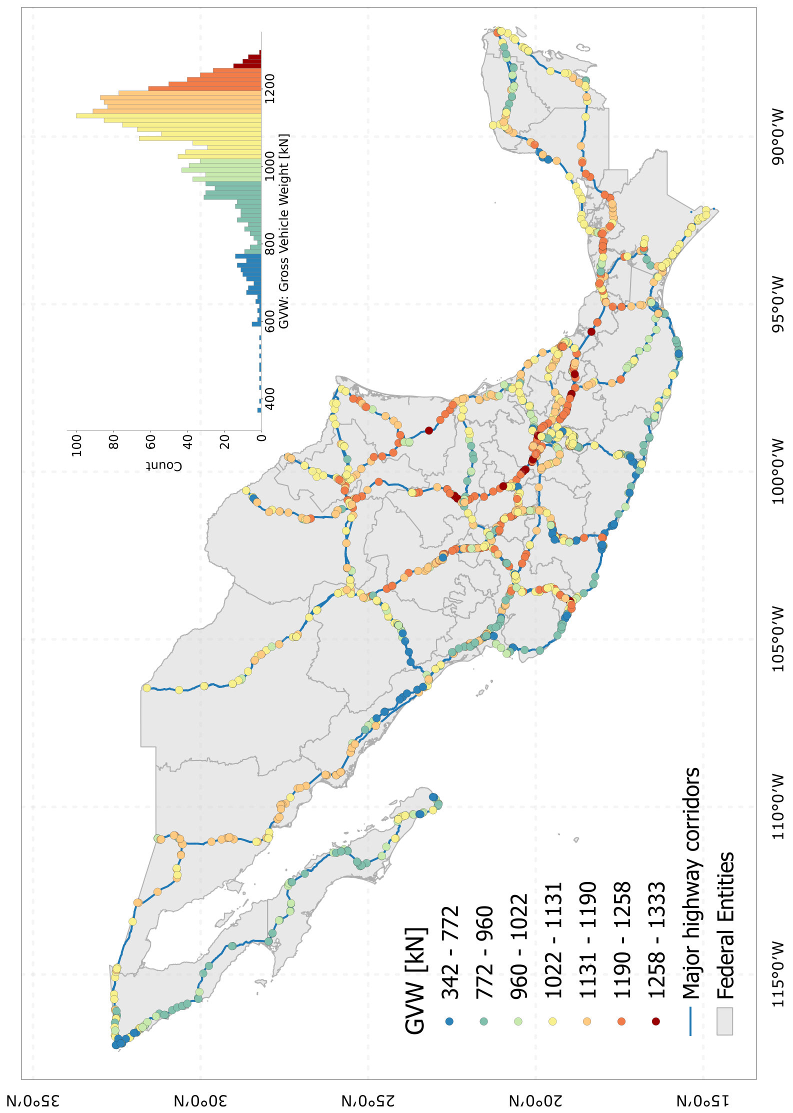

Figure B.4.1: Gross vehicle weight [kN] with 50-year return period.

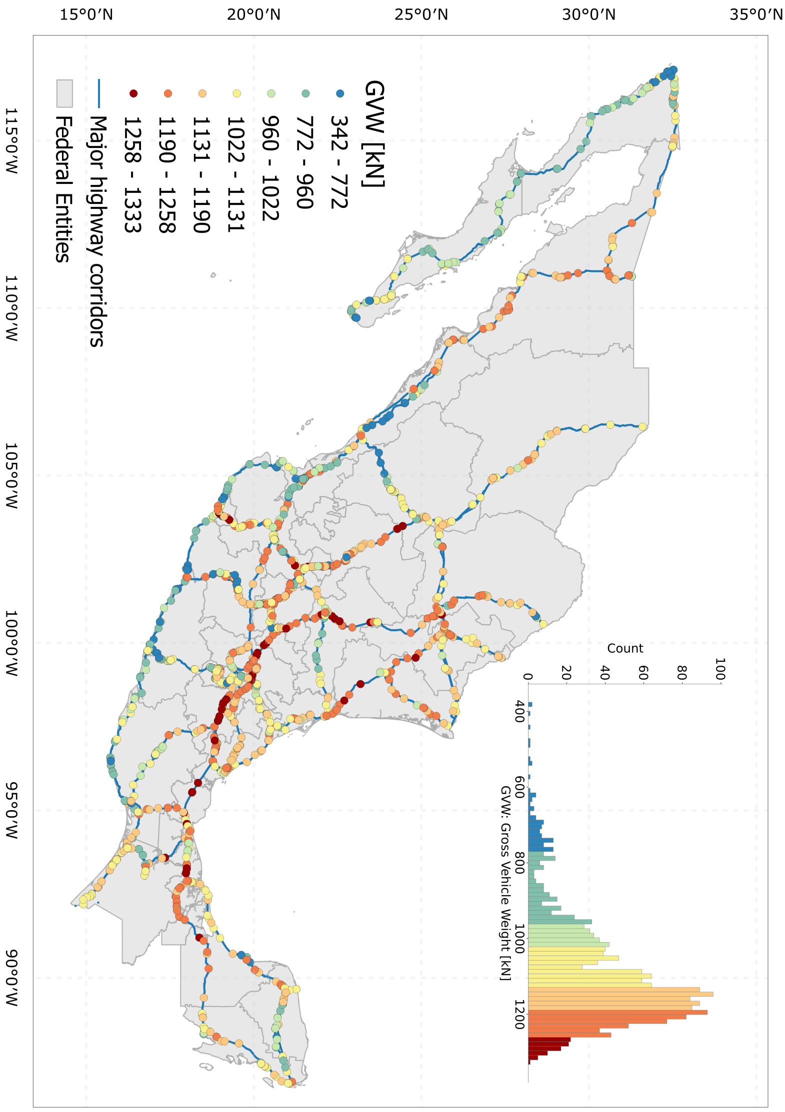

Figure B.4.2: Gross vehicle weight [kN] with 1000-year return period.

C

Estimating bridge criticality due to extreme traffic loads.

C.1 Inter-axle distances

Table C.1.1: Inter-axle distances (D) general statistics, mean and coefficient of variation (cv) comparison. Reported (Rep.) in [146] and simulated (Sim.)

Type	Statistic	D_{1-2}		D_{2-3}		D_{3-4}		D_{4-5}		D_{5-6}		D_{6-7}		D_{7-8}		D_{8-9}	
		Rep.	Sim.	*Rep.*	Sim.	*Rep.*	Sim.	*Rep.*	Sim.	*Rep.*	Sim.	*Rep.*	Sim.	*Rep.*	Sim.	*Rep.*	Sim.
C2	mean	*528.12*	529.54	–	–	–	–	–	–	–	–	–	–	–	–	–	–
	cv	*0.71*	0.19	–	–	–	–	–	–	–	–	–	–	–	–	–	–
C3	mean	*502.42*	502.56	*127.22*	128.98	–	–	–	–	–	–	–	–	–	–	–	–
	cv	*0.10*	0.11	*0.06*	0.07	–	–	–	–	–	–	–	–	–	–	–	–
T3S2	mean	*452.39*	452.80	*135.99*	134.72	*818.04*	837.25	*115.11*	129.19	–	–	–	–	–	–	–	–
	cv	*0.12*	0.14	*0.07*	0.10	*0.17*	0.11	*0.09*	0.07	–	–	–	–	–	–	–	–
T3S3	mean	*545.81*	455.43	*136.74*	135.31	*657.99*	661.64	*119.01*	128.73	*117.43*	128.84	–	–	–	–	–	–
	cv	*0.09*	0.14	*0.70*	0.04	*0.16*	0.11	*0.08*	0.07	*0.08*	0.08	–	–	–	–	–	–
T3S2R4	mean	*481.79*	455.12	*141.95*	137.82	*672.76*	653.05	*122.27*	128.87	*238.21*	197.12	*118.88*	129.07	*591.94*	577.82	*110.78*	129.05
	cv	*0.10*	0.21	*0.07*	0.12	*0.28*	0.08	*0.16*	0.08	*0.08*	0.07	*0.20*	0.07	*0.20*	0.15	*0.10*	0.07

C.2 Auto-correlated time series

[1]Notice that low correlations are observed in the majority of the hours throughout the day. This observation suggests relatively independent behaviour during different hours of the day. This could indicate that the occurrence of events or patterns on this particular weekday is not strongly influenced by the time of day. However, since the empirical data observations are limited in quantity, the fitted copula models are used to generate additional synthetic observations.

Table C.2.1: Fitted copulas of the auto-correlated time series for weekday number 16.[1]

Hour	Copula	Name	θ	ρ	Number of Observations
0	$C_{\theta_Y}^{16,0}\{F(y_t),F(y_{t-1})\}$	Clayton	0.08	0.06	91
1	$C_{\theta_Y}^{16,1}\{F(y_t),F(y_{t-1})\}$	Frank	-1.01	-0.17	82
2	$C_{\theta_Y}^{16,2}\{F(y_t),F(y_{t-1})\}$	Joe	1.07	0.06	129
3	$C_{\theta_Y}^{16,3}\{F(y_t),F(y_{t-1})\}$	Joe 270° rotated	1.05	-0.05	275
4	$C_{\theta_Y}^{16,4}\{F(y_t),F(y_{t-1})\}$	Frank	-0.41	-0.08	622
5	$C_{\theta_Y}^{16,5}\{F(y_t),F(y_{t-1})\}$	Frank	-0.66	-0.11	559
6	$C_{\theta_Y}^{16,6}\{F(y_t),F(y_{t-1})\}$	Frank	-0.72	-0.13	387
7	$C_{\theta_Y}^{16,7}\{F(y_t),F(y_{t-1})\}$	Frank	0.18	0.03	439
8	$C_{\theta_Y}^{16,8}\{F(y_t),F(y_{t-1})\}$	Frank	-0.29	-0.05	482
9	$C_{\theta_Y}^{16,9}\{F(y_t),F(y_{t-1})\}$	Clayton 270° rotated	0.03	-0.02	505
10	$C_{\theta_Y}^{16,10}\{F(y_t),F(y_{t-1})\}$	Frank	-0.17	-0.03	443
11	$C_{\theta_Y}^{16,11}\{F(y_t),F(y_{t-1})\}$	Clayton 180° rotated	0.07	0.05	449
12	$C_{\theta_Y}^{16,12}\{F(y_t),F(y_{t-1})\}$	Frank	-0.41	-0.08	492
13	$C_{\theta_Y}^{16,13}\{F(y_t),F(y_{t-1})\}$	Gumbel 90° rotated	1.06	-0.09	400
14	$C_{\theta_Y}^{16,14}\{F(y_t),F(y_{t-1})\}$	Frank	-0.24	-0.05	387
15	$C_{\theta_Y}^{16,15}\{F(y_t),F(y_{t-1})\}$	Gaussian	-0.11	-0.11	334
16	$C_{\theta_Y}^{16,16}\{F(y_t),F(y_{t-1})\}$	Frank	0.33	0.06	308
17	$C_{\theta_Y}^{16,17}\{F(y_t),F(y_{t-1})\}$	Clayton 270° rotated	0.22	-0.16	190
18	$C_{\theta_Y}^{16,18}\{F(y_t),F(y_{t-1})\}$	Clayton 180° rotated	0.12	0.09	151
19	$C_{\theta_Y}^{16,19}\{F(y_t),F(y_{t-1})\}$	Clayton 270° rotated	0.03	-0.03	100
20	$C_{\theta_Y}^{16,20}\{F(y_t),F(y_{t-1})\}$	Clayton	0.04	0.03	93
21	$C_{\theta_Y}^{16,21}\{F(y_t),F(y_{t-1})\}$	Joe	1.10	0.09	83
22	$C_{\theta_Y}^{16,22}\{F(y_t),F(y_{t-1})\}$	Clayton 90° rotated	0.36	-0.23	79
23	$C_{\theta_Y}^{16,23}\{F(y_t),F(y_{t-1})\}$	Clayton 90° rotated	0.28	-0.19	79

C.3 SYNTHETIC TRAFFIC

Table C.3.1: Example of a random realisation (output) of the synthetic traffic for the bridge *El Rosario I*. The first column in the table represents the ID of the synthetic observation, the second the vehicle type, the third the gross vehicle weight in kN and columns 4 to 12 the individual axle load (A) in kN.

ID	Type	GVW	A1	A2	A3	A4	A5	A6	A7	A8	A9
0	T3S2	157.20	30.01	34.33	34.57	30.69	27.61	–	–	–	–
1	T3S2	315.58	34.81	73.55	69.13	71.22	66.87	–	–	–	–
…	⋮	⋮	⋮	⋮	⋮	⋮	⋮	⋮	⋮	⋮	⋮
208	C3	137.40	34.87	39.18	63.35	–	–	–	–	–	–
209	T3S2	231.84	47.70	47.29	34.74	52.82	49.30	–	–	–	–

table C.3.1 Continued. The first column of this table corresponds to the 13th column of table C.3.1 representing the total length of the HV in meters, columns 14 to 22 represent individual inter-axle distances (D in m) and the last column the inter-vehicle gap (IVG in m.)

Length	D1	D2	D3	D4	D5	D6	D7	D8	D9	IVG
16.76	1.78	3.81	5.62	1.31	1.31	–	–	–	–	–
15.95	1.91	3.71	4.77	1.79	1.79	–	–	–	–	606.07
⋮	⋮	…	⋮	⋮	⋮	⋮	⋮	⋮	⋮	⋮
8.37	0.84	4.33	1.02	–	–	–	–	–	–	542.97
16.55	1.76	3.73	5.56	1.32	1.32	–	–	–	–	464.49

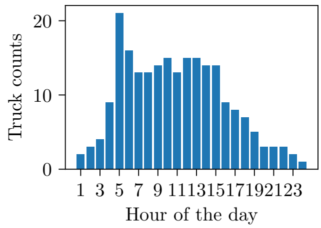

Figure C.3.1: One random simulation of 24 hours of traffic flow of bridge *El Rosario I* Lane 1.

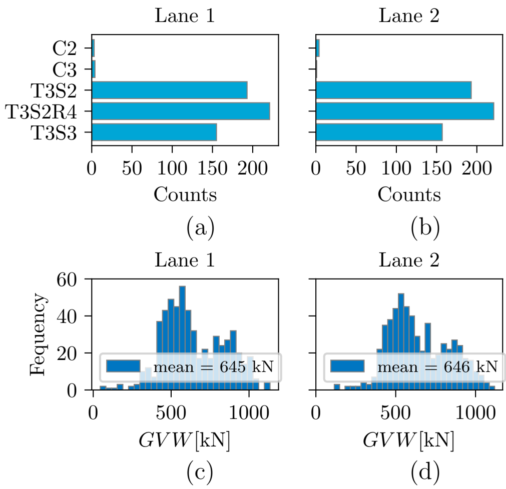

Figure C.3.2: Lanes 1 and 2 distributions of vehicle types that caused the maximum 200-day absolute bending moment for the studied bridges. (a)-(b) Bar plot of individual vehicle type counts. (c)-(d) Gross vehicle weight histogram.

C

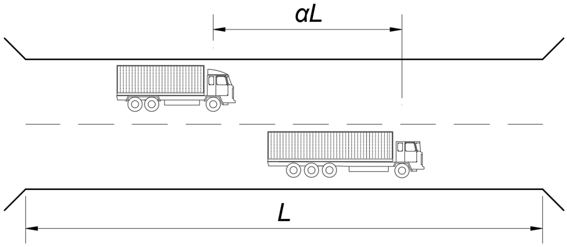

(a)

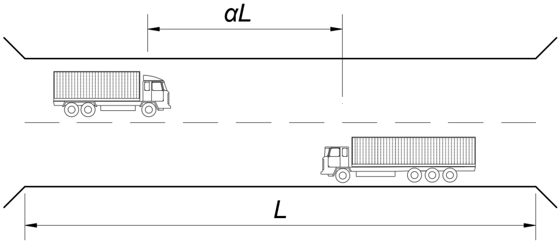

(b)

Figure C.3.3: Traffic scenario that causes the extreme loading event for two-lane simple supported birdges. a) same direction lanes, b) opposite direction lanes

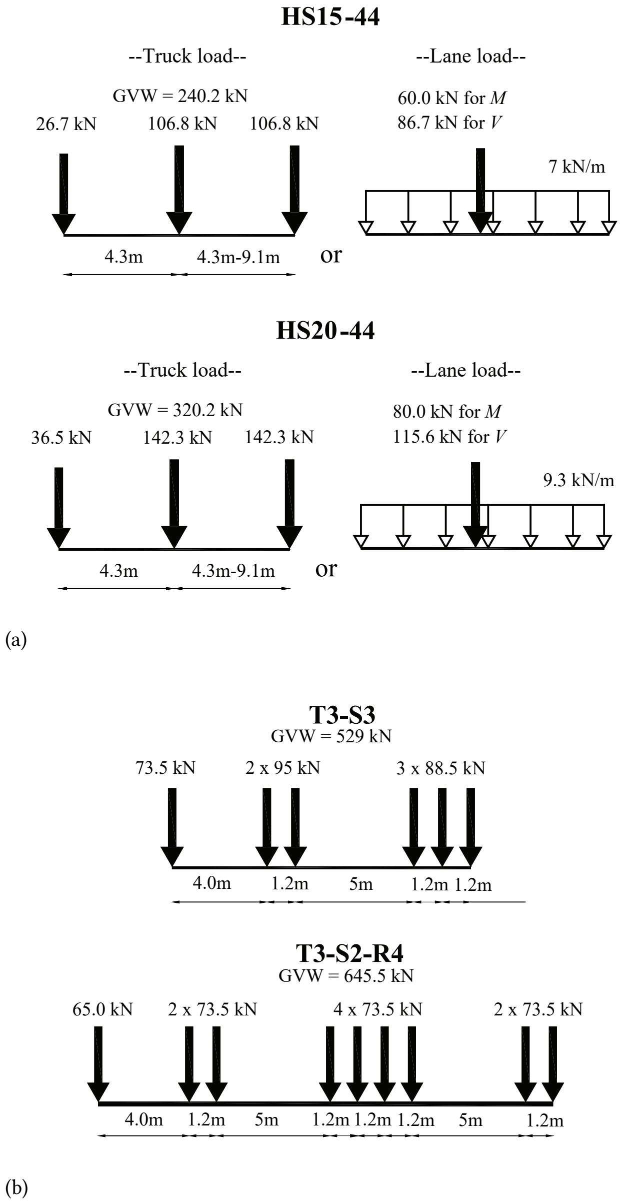

Figure C.3.4: Traffic Live load models reported in SIPUMEX database (a) AASHTO Standard HS Trucks and lane loadings, (b) Maximum allowable axle loads for the trucks types T3-S3 and T3-S2-R4

C.4 Extreme load effects and bridge criticality

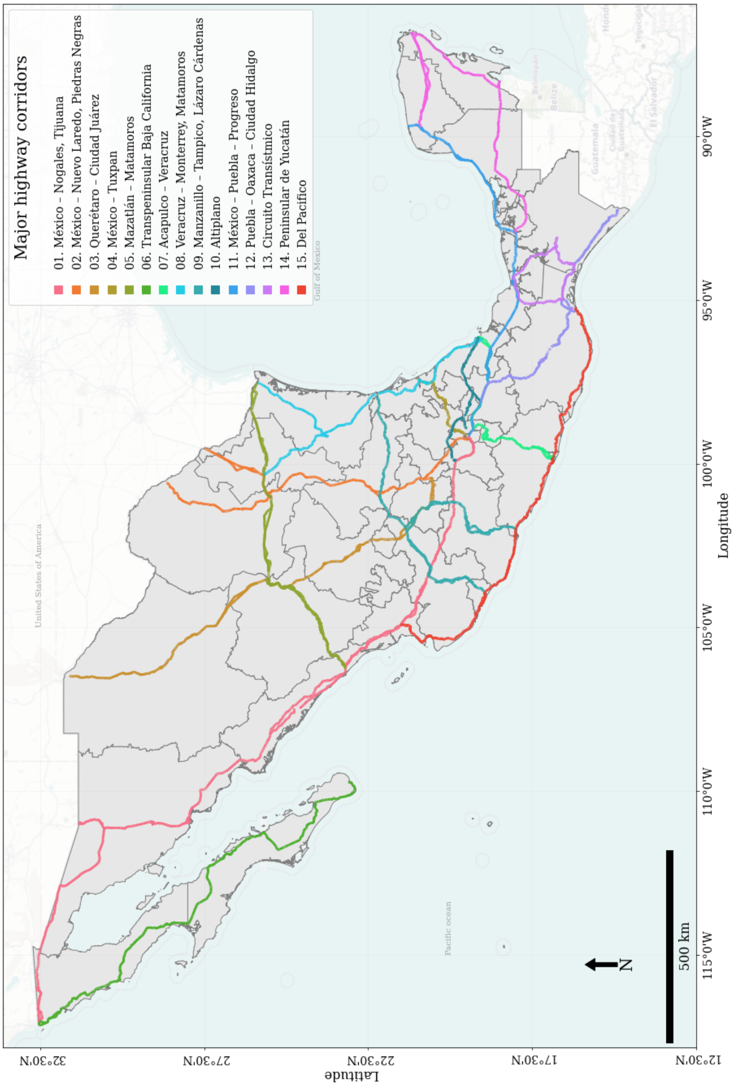

Figure C.4.1: Major highway corridors of Mexico.

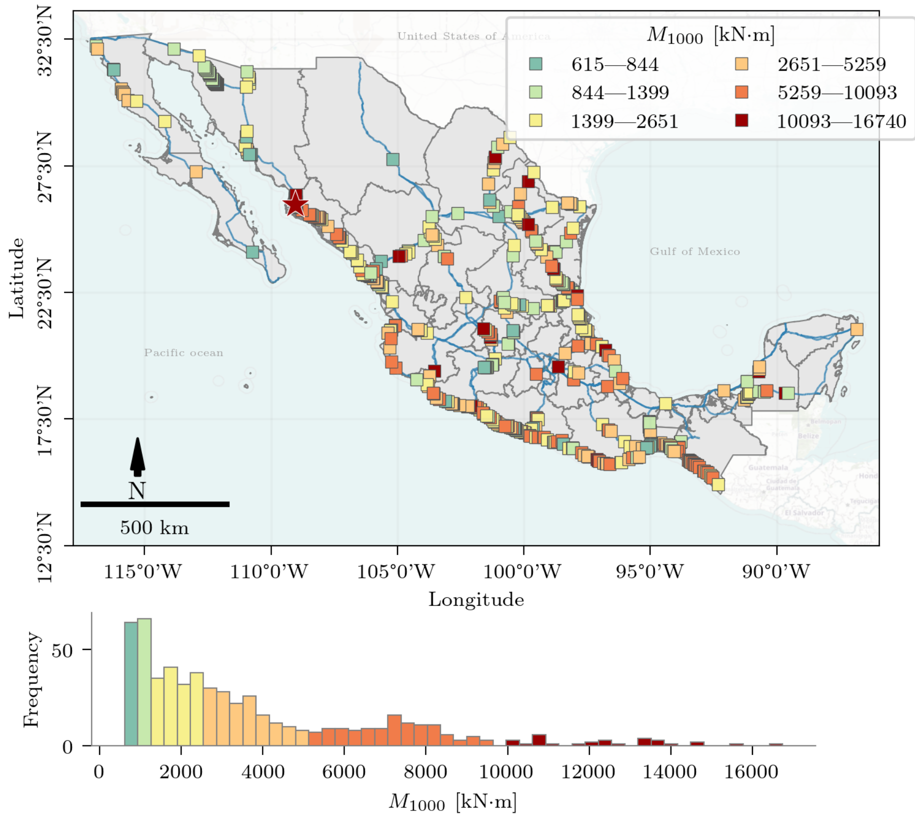

Figure C.4.2: Extreme bending moments with a 1000-year return period (M_{1000}). The star marker represents the bridge with the highest M_{1000} corresponding to *Rio Fuerte* bridge with M_{1000} = 16739.7 kNm.

C

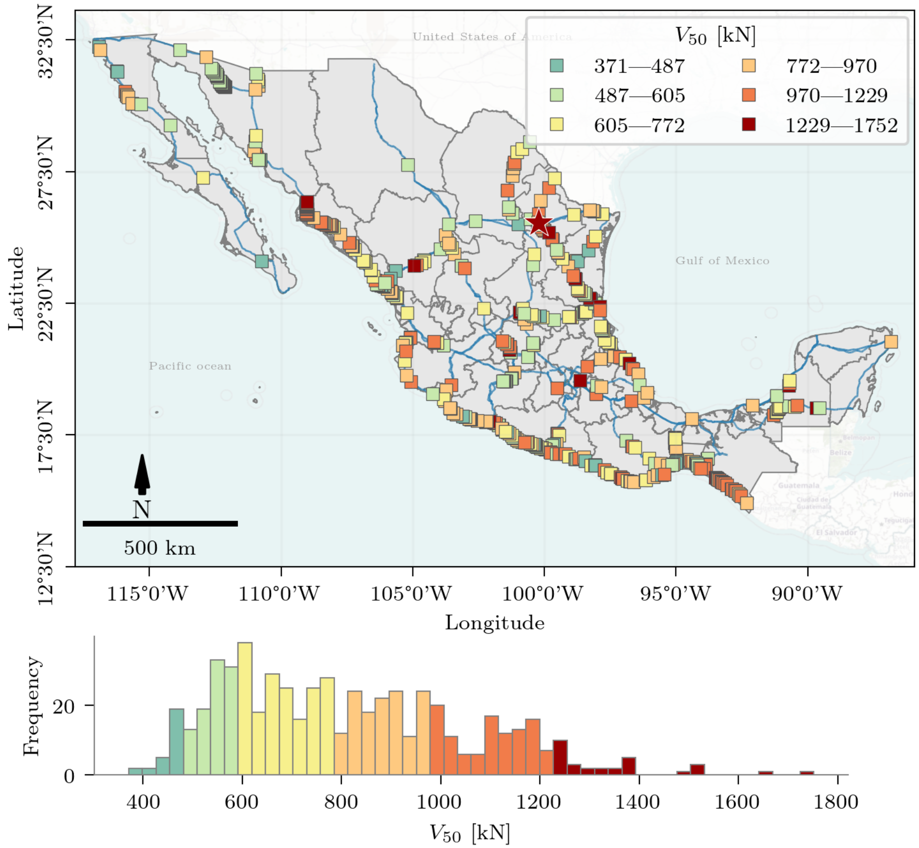

Figure C.4.3: Extreme shear forces with a 50-year return period (V_{50}).The star marker represents the bridge with the highest V_{50} corresponding to *El Uro* bridge with $V_{50} = 1752.2$ kN.

C

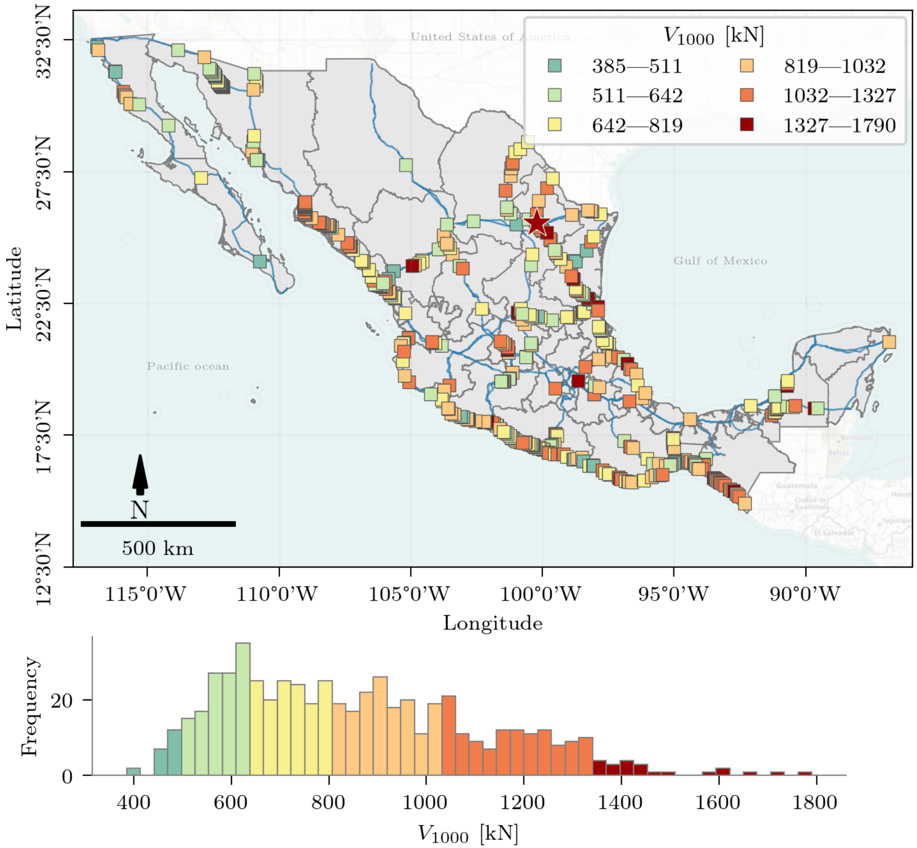

Figure C.4.4: Extreme shear forces with a 1000-year return period (V_{1000}).The star marker represents the bridge with the highest V_{1000} corresponding to *El Uro* bridge with V_{1000} = 1790.4 kNm.

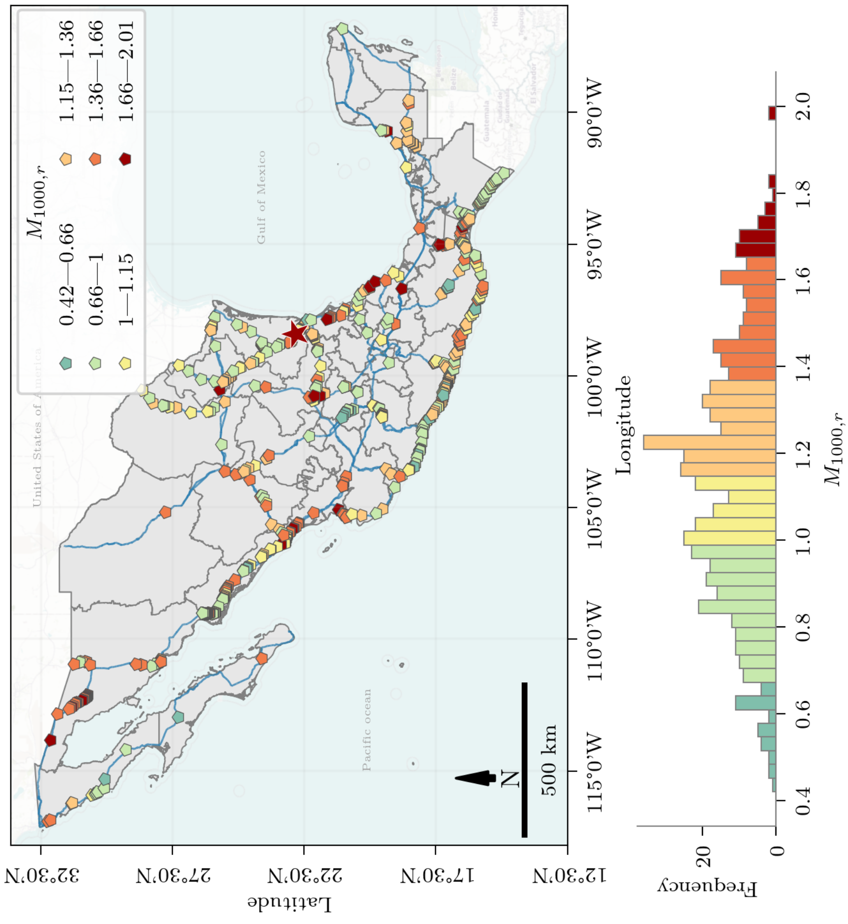

Figure C.4.5: Extreme bending moment with 1000-year return period ratios ($M_{1000,r}$). Each pentagon shape marker represents a computed ratio per bridge. The star marker represents the bridge with the highest $M_{1000,r}$ corresponding to *El Cojo* bridge with $M_{1000,r} = 2$.

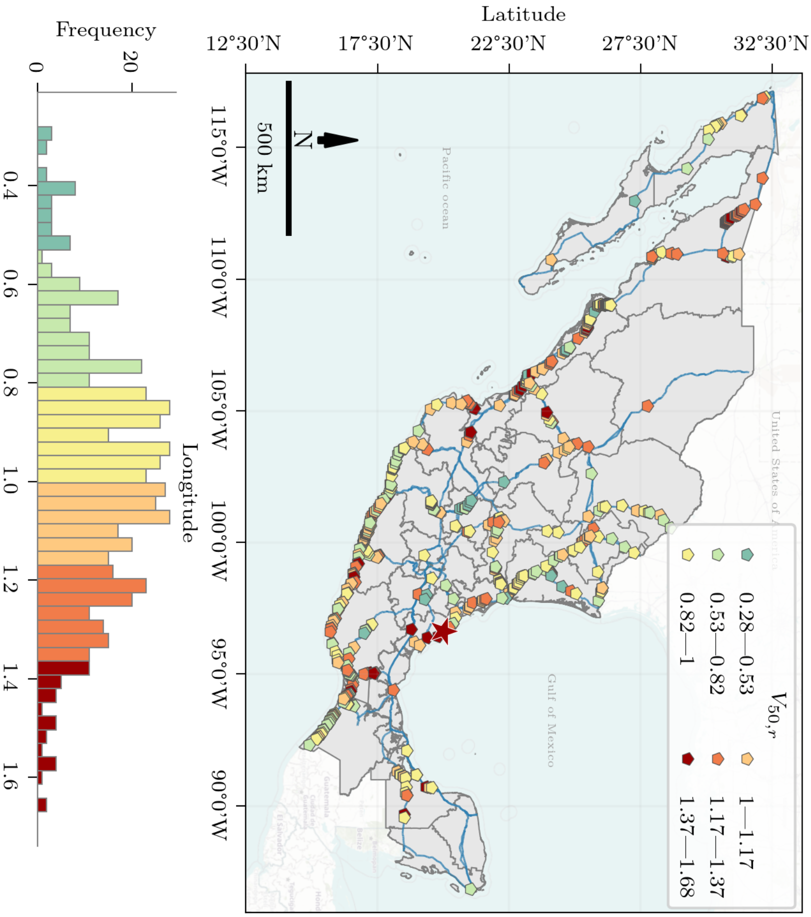

Figure C.4.6: Extreme shear force with 50-year return period ratios ($V_{50,r}$). Each pentagon shape marker represents a computed ratio per bridge. The star marker represents the bridge with the highest $V_{50,r}$ corresponding to *Miraflores* bridge $V_{50,r} = 1.67$.

C

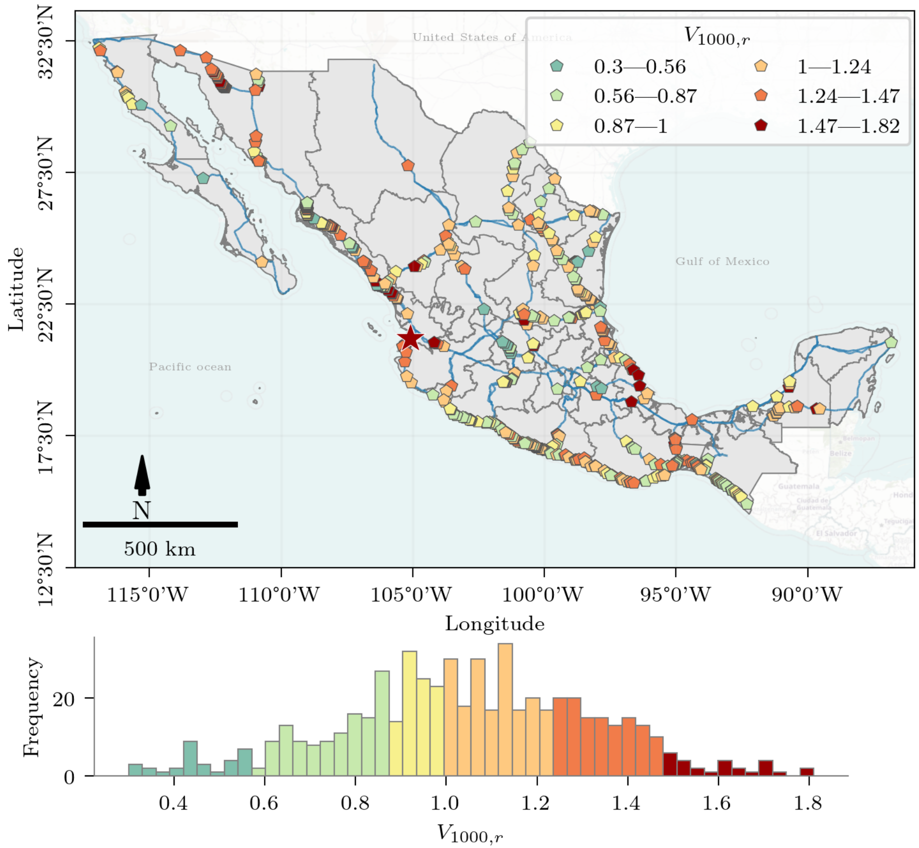

Figure C.4.7: Extreme shear force with 1000-year return period ratios ($V_{1000,r}$). Each pentagon shape marker represents a computed ratio per bridge. The star marker represents the bridge with the highest $V_{1000,r}$ corresponding to *Las Piedras* bridge with $V_{50,r} = 1.81$.

D

Optimization approach for managing bridge interventions.

D.1 Parametric construction costs

Table D.1.1: *Parametric construction costs* in Mexican Pesos (MP). Concrete beam bridges without intermediate structure. Includes: cuts, fills, abutments, accesses, superstructure with pre-stressed concrete beams, asphalt layer, joints, parapets and signage. For concrete slab bridges, 70% of the costs are assumed.

No. of lanes	Max span	Unit	Direct cost [MP]
2	15	Bridge	10 353 778
2	25	Bridge	11 280 353
2	30	Bridge	14 559 583
2	40	Bridge	14 127 962
4	15	Bridge	19 032 768
4	25	Bridge	20 106 031
4	30	Bridge	26 460 126
4	40	Bridge	34 544 300
6	15	Bridge	34 258 983
6	25	Bridge	36 190 855
6	30	Bridge	47 628 227
6	40	Bridge	47 628 227

Table D.1.2: *Parametric construction costs* in Mexican Pesos (MP). Overhead vehicular passes (PSV). Includes: cuts, fills, accesses, superstructure with pre-stressed concrete beams, asphalt layer, joints, parapets and signage. For concrete slab bridges, 70% of the costs are assumed.

No. of lanes	Max span [m]	No. lanes to cross	Unit	Direct cost [MP]
2	7	2	Pass	8 898 536
4	7	2	Pass	16 554 835
6	7	2	Pass	26 668 348
2	14	4	Pass	16 102 709
4	14	4	Pass	30 247 888
6	14	4	Pass	44 392 957
2	21	6	Pass	41 786 188
4	21	6	Pass	74 534 110
6	21	6	Pass	107 281 987

Table D.1.3: *Parametric construction costs* in Mexican Pesos (MP). Concrete beam bridges with intermediate structure (multi-span bridge). (i) Bridge abutment access. Includes: excavations, backfill, superstructure, asphalt layer, joints, parapets and signage. (ii) Bridge. Includes: cuts, fills, abutments, accesses, foundations, superstructure with pre-stressed concrete beams, asphalt layer, joints, parapets and signage. For concrete slab bridges, 70% of the costs are assumed.

No. of lanes	Max height	Unit	Direct cost [MP]
2	–	Set	1 563 989
4	–	Set	2 172 942
6	–	Set	3 191 973
2	5.5	m	144 205
2	15	m	161 613
2	20	m	243 584
2	30	m	153 424
4	5.5	m	196 204
4	15	m	244 212
4	20	m	254 072
4	30	m	281 301
6	5.5	m	261 561
6	15	m	263 614
6	20	m	253 445
6	30	m	296 772

D.2 INTERVENTION COST ESTIMATION

To illustrate this process, a specific example is provided for the bridge *El Sabino*. According to Table 5.3, this bridge has an $B_R = 3$. Hence the corresponding value of the reliability index is $\beta = 3$ according Table 5.1. The grades to compute the bridge importance factor f_B are shown in Table D.2.1. The corresponding grades are: $S_{RC} = 5$, $S_{AADT} = 2$,$S_{DD} = 5$, $S_{LS} = 1$ and $S_{TL} = 1$. For the sake of simplicity, the assumption is adopted that the maintenance costs, C_M, are equivalent to 15% of the repair costs, i.e., $C_M = 0.15C_R$.

Table D.2.1: Grades for assessment of bridge importance factor f_B in the network level according to five criteria [207]. Adjusted to the size of the MHC network under study.

Road Category	S_{RC}	Annual Average Daily Traffic [N Vehicles]	S_{AADT}	Detour Distance [km]	S_{DD}	Longest Span [m]	S_{LS}	Total Length [m]	S_{TL}
unknown road	1	<70	1	adjacent lane	1	<6	1	<6	1
local road	2	70–1944	2	<5	2	6–19	2	6–170	2
inter–state road	3	1944–3819	3	5–20	3	19–32	3	170–334	3
state road	4	38919–5693	4	20–60	4	32–45	4	334–499	4
highway	5	>5693	5	>60	5	>45	5	>499	5

$$
\begin{aligned}
f_B &= 1 + \frac{1}{5}\left[0.25(5+2+5) + 0.125(1+1)\right] = 1.65 \\
f_R &= 0.3613(3)^2 - 2.8572(3) + 5.622 = 0.302 \\
C_{BV} &= 1.65(3.67) = 6.05 \text{ MMP} \\
C_R &= 0.302(6.05) = 1.83 \text{ MMP} \\
C_M &= 0.15(1.83) = 0.27 \text{ MMP}
\end{aligned}
$$

Regarding the user costs arising from the unavailability of bridges due to intervention actions, Equation (5.6) for its computation is employed. Consequently, $C_{V|U}$ and the total cost per vehicle per month, for each minute of prolonged travel time, is computed as follows:

$$
C_{ve} = \left[\frac{W\,P_{ve}}{60} 20 + 0.5 \frac{W\,P_{ve}}{60} 10\right] t_p \tag{D.2.1}
$$

The user costs arising from the unavailability of the bridge *El Sabino* due to maintenance ($C_{U|M}$) and due to repair ($C_{U|R}$) interventions are:

$$
\begin{aligned}
C_{ve|M} &= \left[\frac{36.62(1.8)}{60} 20 + 0.5 \frac{36.62(1.8)}{60} 10\right] 1.5 = 41.20 \ \tfrac{\text{MP}\cdot\text{day}}{\text{vehicles}\cdot\text{month}} \\
C_{ve|R} &= \left[\frac{36.62(1.8)}{60} 20 + 0.5 \frac{36.62(1.8)}{60} 10\right] 5 = 137.33 \ \tfrac{\text{MP}\cdot\text{day}}{\text{vehicles}\cdot\text{month}} \\
C_{U|M} &= \frac{9703(41.20)1}{1\,000\,000} = 0.40 \text{ MMP} \\
C_{U|R} &= \frac{9703(137.33)9}{1\,000\,000} = 11.99 \text{ MMP}
\end{aligned}
$$

D.3 Optimal intervention program for specific scenarios

Table D.3.1: Optimal intervention program Scenario (2). Annual cost expressed in net present value (NPV). E_t: annual budget constrain, C_D: total direct cost ($C_M + C_R$).

Intervention program

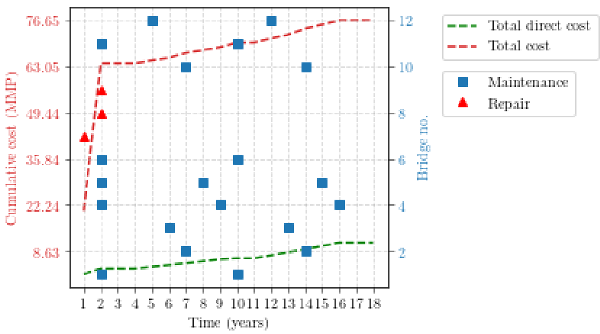

Annual cost (NPV)

Year	E_t [MMP]	C_D [MPP]	$\frac{C_D}{E_t}$
1	1.81	1.75	97%
2	1.81	1.52	84%
5	0.61	0.41	67%
6	0.61	0.41	67%
7	0.61	0.39	64%
8	0.61	0.40	66%
9	0.61	0.41	67%
10	0.61	0.18	30%
12	0.61	0.51	84%
13	0.61	0.51	83%
14	0.61	0.48	79%
15	0.61	0.49	80%
16	0.61	0.50	83%

Table D.3.2: Overview of Scenario (2) results. Total cumulative cost, $C = 76.6$ MMP, total direct cost, $C_D = C_M + C_R = 11.2$ MMP. int_n: intervention number in year $t\Delta\tau$.

Bridge (i)	Repair int_1	Maintenance int_1	int_2	int_3	C_R	C_M	$C_{M\|U}$	$C_{R\|U}$	C
1	–	2	10	–	0.0	0.2	0.6	0.0	0.8
2	–	7	14	–	0.0	0.4	0.7	0.0	1.1
3	–	6	13	–	0.0	1.4	0.4	0.0	1.9
4	–	2	9	16	0.0	2.0	0.6	0.0	2.6
5	–	2	8	15	0.0	1.9	0.7	0.0	2.6
6	–	2	10		0.0	0.1	0.5	0.0	0.6
7	1	–	–	–	1.8	0.0	0.0	18.7	20.6
8	2	–	–	–	0.8	0.0	0.0	24.4	25.1
9	2	–	–	–	0.1	0.0	0.0	15.9	15.9
10	–	7	14	–	0.0	1.0	1.2	0.0	2.1
11	–	2	10	–	0.0	0.1	1.2	0.0	1.2
12	–	5	12	–	0.0	1.4	0.7	0.0	2.1
Total					2.7	8.5	6.5	59.0	76.6

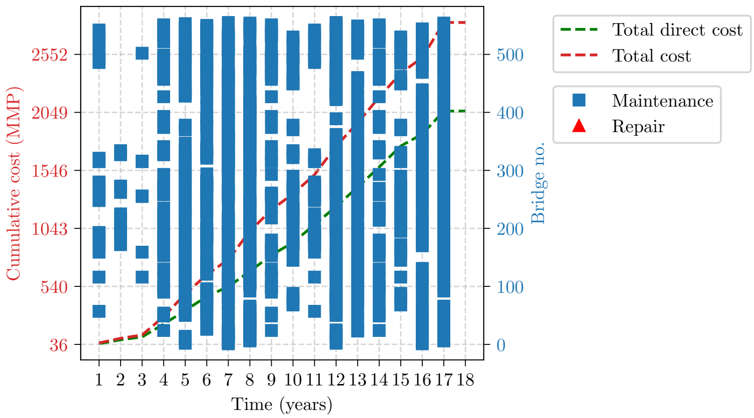

Figure D.3.1: Optimal intervention program for the 555 bridges under Scenario (3).

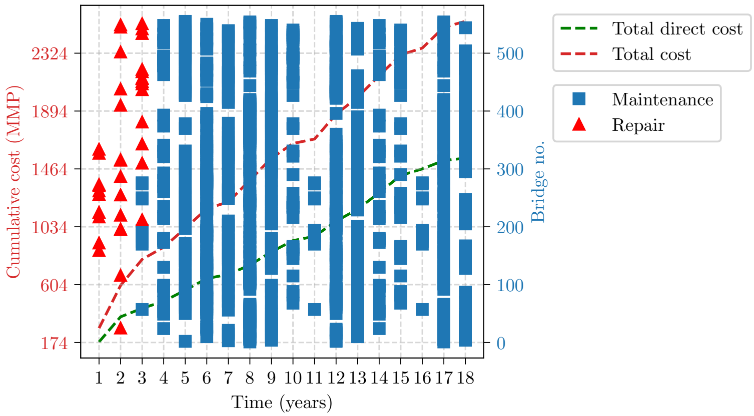

Figure D.3.2: Optimal intervention program for the 555 bridges under Scenario (5).

Bibliography

References

[1] Mezgeen Rasol, Jorge C. Pais, Vega Pérez-Gracia, Mercedes Solla, Francisco M. Fernandes, Simona Fontul, David Ayala-Cabrera, Franziska Schmidt, and Hossein Assadollahi. Gpr monitoring for road transport infrastructure: A systematic review and machine learning insights. *Construction and Building Materials*, 324:126686, 2022.

[2] Anup Kumar Pandey, Rahat Iqbal, Tomasz Maniak, Charalampos Karyotis, Stephen Akuma, and Vasile Palade. Convolution neural networks for pothole detection of critical road infrastructure. *Computers and Electrical Engineering*, 99:107725, 2022.

[3] Maria Nogal, Alan O'Connor, Brian Caulfield, and Beatriz Martinez-Pastor. Resilience of traffic networks: From perturbation to recovery via a dynamic restricted equilibrium model. *Reliability Engineering & System Safety*, 156:84–96, 2016.

[4] Daniel N. Farhey. Structural performances of bridge types in the u.s. national bridge inventory. *Infrastructures*, 3(1), 2018.

[5] C. B. L. Olivera, M. Greco, and T. N. Bittencourt. Analysis of the brazilian federal bridge inventory. *Revista IBRACON de Estruturas e Materiais*, 12(1):1–3, feb 2019.

[6] COST 345 (Programme). Cost 345 : procedures required for assessing highway structures : working group 1 report on the current stock of highway structures in European countries the cost of their replacement and the annual costs of maintaining repairing and renewing them. Technical report, European Commission - Directorate General Research., 2003.

[7] Lu Deng and Wangchen Yan. Vehicle weight limits and overload permit checking considering the cumulative fatigue damage of bridges. *Journal of Bridge Engineering*, 23(7):04018045, 2018.

[8] Mariana Bosso, Kamilla L. Vasconcelos, Linda Lee Ho, and Liedi L.B. Bernucci. Use of regression trees to predict overweight trucks from historical weigh-in-motion data. *Journal of Traffic and Transportation Engineering (English Edition)*, 7(6):843–859, 2020.

[9] Fatima Ahmed Alkhoori and Praveen Kumar Maghelal. Regulating the overloading of heavy commercial vehicles: Assessment of land transport operators in abu dhabi. *Transportation Research Part A: Policy and Practice*, 154:287–299, 2021.

[10] Dawid Rys and Piotr Jaskula. Effect of overloaded vehicles on whole life cycle cost of flexible pavements. In Kun Zhang, Rongqiao Xu, and Shih-Huang Chen, editors, *Testing and Characterization of Asphalt Materials and Pavement Structures*, pages 104–117, Cham, 2019. Springer International Publishing.

[11] George Yannis and Antonis Chaziris. Transport System and Infrastructure. *Transportation Research Procedia*, 60:6–11, 2022.

[12] Eugene J OBrien, Albert Daly, Alan J O'Connor, Fergal Cahill, and John E Arrigan. Increasing Truck Weight Limits: Implications for Bridges. *Procedia - Social and Behavioral Sciences*, 48:2071–2080, 2012.

[13] Mustapha Mohammed Alhaji, Musa Alhassan, Taiye Waheed Adejumo, and Hamidu Abdulkadir. Road pavement collapse from overloaded trucks due to traffic diversion: A case study of minna-kateregi-bida road, nigeria. *Engineering Failure Analysis*, 131:105829, 2022.

[14] Eugene J. OBrien and Bernard Enright. Using weigh-in-motion data to determine aggressiveness of traffic for bridge loading. *Journal of Bridge Engineering*, 18(3):232–239, 2013.

[15] Cathal Leahy, Eugene J O'Brien, Bernard Enright, and Richard Power. Estimating characteristic bridge traffic load effects using bayesian statistics. 2015.

[16] Bernard Enright, Eugene J. OBrien, and Cathal Leahy. Identifying and modelling permit trucks for bridge loading. *Proceedings of the Institution of Civil Engineers - Bridge Engineering*, 169(4):235–244, 2016.

[17] Evelyn Mühlhofer, Elco E. Koks, Chahan M. Kropf, Giovanni Sansavini, and David N. Bresch. A generalized natural hazard risk modelling framework for infrastructure failure cascades. *Reliability Engineering & System Safety*, 234:109194, 2023.

[18] Francesco Cavalieri, Paolo Franchin, and Sonia Giovinazzi. Multi-hazard assessment of increased flooding hazard due to earthquake-induced damage to the natural drainage system. *Reliability Engineering & System Safety*, 237:109348, 2023.

[19] Lindung Zalbuin Mase. Local seismic hazard map based on the response spectra of stiff and very dense soils in bengkulu city, indonesia. *Geodesy and Geodynamics*, 13(6):573–584, 2022.

[20] Seung-Kwon Seo, Young-Gak Yoon, Ju sung Lee, Jonggeol Na, and Chul-Jin Lee. Deep neural network-based optimization framework for safety evacuation route during toxic gas leak incidents. *Reliability Engineering & System Safety*, 218:108102, 2022.

[21] Rodrigo Silva-Lopez, Gitanjali Bhattacharjee, Alan Poulos, and Jack W. Baker. Commuter welfare-based probabilistic seismic risk assessment of regional road networks. *Reliability Engineering & System Safety*, 227:108730, 2022.

[22] Raif C.B. Bucar and Yeganeh M. Hayeri. Quantitative flood risk evaluation to improve drivers' route choice decisions during disruptive precipitation. *Reliability Engineering & System Safety*, 219:108202, 2022.

[23] Qiang Liu, Aiping Tang, Delong Huang, Ziyuan Huang, Bin Zhang, and Xiuchen Xu. Total probabilistic measure for the potential risk of regional roads exposed to landslides. *Reliability Engineering & System Safety*, 228:108822, 2022.

[24] Graziano Fiorillo and Hani Nassif. Development of a risk assessment module for bridge management systems in new jersey. *Transportation Research Record*, 2674(9):324–337, 2020.

[25] Yongze Song, Xiangyu Wang, Graeme Wright, Dominique Thatcher, Peng Wu, and Pascal Felix. Traffic volume prediction with segment-based regression kriging and its implementation in assessing the impact of heavy vehicles. *IEEE Transactions on Intelligent Transportation Systems*, 20(1):232–243, 2019.

[26] Yingfeng Li, Jerry T Le, Danny R Middleton, and Cesar A Quiroga. Mapping Oversized and Overweight Truck Routes with Procedure Based on Geographic Information Systems. *Transportation Research Record*, 2291(1):8–16, 2012.

[27] Aleš Žnidarič Kreslin, Maja, Cathal Leahy, Eugene OBrien, Franziska Schmidt, and Claus Pedersen. Guidelines on collecting WIM data and forecasting of traffic load effects on bridges. Technical report, Conference of European Directors of Road, 2016.

[28] Ajith Kumar Parlikad Manu Sasidharan and Jennifer Schooling. Risk-informed asset management to tackle scouring on bridges across transport networks. *Structure and Infrastructure Engineering*, 18(9):1300–1316, 2022.

[29] César Crespo-Minguillón and Juan R Casas. A comprehensive traffic load model for bridge safety checking. *Structural Safety*, 19(4):339–359, 1997.

[30] Federal Highway Administration's Intelligent Transportation Systems Program Office. A Summary of Vehicle Detection and Surveillance Technologies used in Intelligent Trasportation Systems. Technical report, 2007.

[31] Srinivas S., Menon Devdas, and Meher Prasad A. Multivariate Simulation and Multimodal Dependence Modeling of Vehicle Axle Weights with Copulas. *Journal of Transportation Engineering*, 132(12):945–955, dec 2006.

[32] Jihwan Kim and Junho Song. A Comprehensive Probabilistic Model of Traffic Loads based on Weigh-in-Motion Data for Applications to Bridge Structures. *KSCE Journal of Civil Engineering*, 23(8):3628–3643, 2019.

[33] Zhenming Xie and Rajesh Rajamani. Vehicle counting and maneuver classification with support vector machines using low-density flash lidar. *IEEE Transactions on Vehicular Technology*, 71(1):86–97, 2022.

[34] Aderonke A Oni and Nicholas Kajoh. Video-based vehicle counting system for urban roads in nigeria using yolo and dcf-csr algorithms. *International Journal of Engineering Research and Technology*, 12(12):2550–2558, 2019.

[35] P Beyer. Non-intrusive detection, the way forward. Southern African Transport Conference, 2015.

[36] KO Kusimo and FO Okafor. Comparative analysis of mechanical and manual modes of traffic survey for traffic load determination. *Nigerian Journal of Technology*, 35(2):226–233, 2016.

[37] Ørjan Tveit and Wen Xu. Cooperative Self-declaring of Weight for Trucks. *Transportation Research Procedia*, 14:1500–1505, 2016.

[38] Matthew Sjaarda, Thierry Meystre, Alain Nussbaumer, and Manfred A. Hirt. A systematic approach to estimating traffic load effects on bridges using weigh-in-motion data. *Stahlbau*, 89(7):585–598, 2020.

[39] Johan Maljaars. Evaluation of traffic load models for fatigue verification of european road bridges. *Engineering Structures*, 225:111326, 2020.

[40] Alberto Martini, Eleonora M. Tronci, Maria Q. Feng, and Ryan Y. Leung. A computer vision-based method for bridge model updating using displacement influence lines. *Engineering Structures*, 259:114129, 2022.

[41] Çağrı Demir and Murat Dicleli. Live load effects in hammer-head piers of continuous highway bridges and design equations based on numerical simulations verified by field tests. *Engineering Structures*, 279:115614, 2023.

[42] Ye Xia, Xiaoming Lei, Peng Wang, and Limin Sun. A data-driven approach for regional bridge condition assessment using inspection reports. *Structural Control and Health Monitoring*, 29(4):e2915, 2022.

[43] David de León Escobedo and Andrés Torres Acosta. Bridge preventive maintenance based on life-cycle assessment. *Revista Técnica de la Facultad de Ingeniería Universidad del Zulia*, 33:3 – 10, 04 2010.

[44] Abdollah Shafieezadeh Ehsan Fereshtehnejad and Jieun Hur. Optimal budget allocation for bridge portfolios with element-level inspection data: a constrained integer linear programming formulation. *Structure and Infrastructure Engineering*, 18(6):864–878, 2022.

[45] Eslam Mohammed Abdelkader, Osama Moselhi, Mohamed Marzouk, and Tarek Zayed. An exponential chaotic differential evolution algorithm for optimizing bridge maintenance plans. *Automation in Construction*, 134:104107, 2022.

[46] Vandana Patidar, Samuel Labi, Kumares C Sinha, and Paul Thompson. Nchrp report 590: Multi-objective optimization for bridge management systems. *Transportation Research Board of the National Academies, Washington, DC*, 2007.

[47] Paul Koot, Miguel Angel Mendoza-Lugo, Dominik Paprotny, Oswaldo Morales-Nápoles, Elisa Ragno, and Daniël T.H. Worm. Pybanshee version (1.0): A python implementation of the matlab toolbox banshee for non-parametric bayesian networks with updated features. *SoftwareX*, 21:101279, 2023.

[48] Miguel Angel Mendoza-Lugo and Oswaldo Morales-Nápoles. Version 1.3-banshee—a matlab toolbox for non-parametric bayesian networks. *SoftwareX*, 23:101479, 2023.

[49] Judea Pearl. Chapter 2 - Bayesian Inference. pages 29–75. Morgan Kaufmann, San Francisco (CA), 1988.

[50] Martin Neil, Norman Fenton, and Lars Nielson. Building large-scale Bayesian networks. *The Knowledge Engineering Review*, 15(3):257–284, sep 2000.

[51] Oswaldo Morales-Nápoles and Raphaël D.J.M. Steenbergen. Large-scale hybrid bayesian network for traffic load modeling from weigh-in-motion system data. *Journal of Bridge Engineering*, 20(1):4014059, jan 2015.

[52] Bruce G. Marcot. Common quandaries and their practical solutions in Bayesian network modeling. *Ecological Modelling*, 358:1–9, aug 2017.

[53] Bruce G. Marcot and Trent D. Penman. Advances in Bayesian network modelling: Integration of modelling technologies. *Environmental Modelling & Software*, 111:386–393, jan 2019.

[54] P. Weber, G. Medina-Oliva, C. Simon, and B. Iung. Overview on Bayesian networks applications for dependability, risk analysis and maintenance areas. *Engineering Applications of Artificial Intelligence*, 25(4):671–682, jun 2012.

[55] A. Hanea, O. Morales Napoles, and D. Ababei. Non-parametric bayesian networks: Improving theory and reviewing applications. *Reliability Engineering & System Safety*, 144:265–284, 2015. cited By 43.

[56] D Kurowicka and R M Cooke. Distribution-Free Continuous Bayesian Belief Nets. In *Modern Statistical and Mathematical Methods in Reliability*, volume Volume 10 of *Series on Quality, Reliability and Engineering Statistics*, pages 309–322. World Scientific, oct 2005.

[57] Harry Joe. *Multivariate models and multivariate dependence concepts.* CRC Press, 1997.

[58] Christian Genest and Jock MacKay. The Joy of Copulas: Bivariate Distributions with Uniform Marginals. *The American Statistician*, 40(4):280–283, apr 1986.

[59] Oswaldo Morales-Nápoles and Raphaël D.J.M. Steenbergen. Analysis of axle and vehicle load properties through bayesian networks based on weigh-in-motion data. *Reliability Engineering & System Safety*, 125:153 – 164, 2014.

[60] A M Hanea, D Kurowicka, and R M Cooke. Hybrid Method for Quantifying and Analyzing Bayesian Belief Nets. *Quality and Reliability Engineering International*, 22(6):709–729, oct 2006.

[61] K Pearson. *On Further Methods of Determining Correlation.* Number v. 16 in Department of applied mathematics. University college, University of London. Drapers'company research memoirs. Dulau and Company, 1907.

[62] G Udny Yule and M G Kendall. An Introduction to the Theory of Statistics. *Journal of Symbolic Logic*, 16(1):51, 1951.

[63] A.C.W.M. Vrouwenvelder and P H Waarts. Traffic Loads on Bridges. *Structural Engineering International*, 3(3):169–177, aug 1993.

[64] R. Gillmann. Calibration and adjustment of Weigh-In-Motion data. *Transportation Research Record*, 1992.

[65] Kentucky Trasportation Center. Wim Data Collection and Analysis. Technical report, University of Kentucky, Kentucky, 2013.

[66] Rich Quinley. WIM Data Analyst's Manual. Technical report, FHWA Office of Pavement Technology, 2010.

[67] D.L. Allaix And and O. Morales Napoles A.H.J.M. Vervuurt. Traffic load model for short span bridges. Technical report, Nederlandse Organisatie voor Toegepast Natuurwetenschappelijk Onderzoek, Delft, 2015.

[68] Paul David McNicholas and Thomas Brendan Murphy. Parsimonious Gaussian mixture models. *Statistics and Computing*, 18(3):285–296, 2008.

[69] Bernard Enright and Eugene J. O'Brien. Monte carlo simulation of extreme traffic loading on short and medium span bridges. *Structure and Infrastructure Engineering*, 9(12):1267–1282, 2013.

[70] Jihwan Kim and Junho Song. Bayesian updating methodology for probabilistic model of bridge traffic loads using in-service data of traffic environment. *Structure and Infrastructure Engineering*, 0(0):1–16, 2021.

[71] D. McLachlan, G. J. and Peel. *Finite mixture models.* Wiley Series in Probability and Statistics, New York, 2000.

[72] H. Akaike. A new look at the statistical model identification. *IEEE Transactions on Automatic Control*, 19(6):716–723, 1974.

[73] Dominik Paprotny, Oswaldo Morales-Nápoles, Daniël T H Worm, and Elisa Ragno. BANSHEE–A MATLAB toolbox for Non-Parametric Bayesian Networks. *SoftwareX*, 12:100588, 2020.

[74] Richard H McCuen, Zachary Knight, and A Gillian Cutter. Evaluation of the nash–sutcliffe efficiency index. *Journal of hydrologic engineering*, 11(6):597–602, 2006.

[75] Cort J Willmott and Kenji Matsuura. Advantages of the mean absolute error (mae) over the root mean square error (rmse) in assessing average model performance. *Climate research*, 30(1):79–82, 2005.

[76] Grant Rutherford and Dean K. McNeill. Statistical vehicle classification methods derived from girder strains in bridges. *Canadian Journal of Civil Engineering*, 38(2):200–209, 2011.

[77] Baby Shalini Ravilla, Wolfgang Bein, and Yazmin Elizabet Martinez. Analysis of traffic based on signals using different feature inputs. In Shahram Latifi, editor, *ITNG 2021 18th International Conference on Information Technology-New Generations*, pages 239–243, Cham, 2021. Springer International Publishing.

[78] Nimra Shahid, Munam Ali Shah, Abid Khan, Carsten Maple, and Gwanggil Jeon. Towards greener smart cities and road traffic forecasting using air pollution data. *Sustainable Cities and Society*, 72:103062, 2021.

[79] Departamento Nacional De Infra-Estrutura De Transportes. Quadro De Fabricantes De Veículos, 2012.

[80] SCT. NOM-012-SCT-2-2017, Sobre el peso y dimensiones máximas con los que pueden circular los vehículos de autotransporte que transitan en las vías generales de comunicación de jurisdicción federal, 2017.

[81] Miguel Angel Mendoza-Lugo, Oswaldo Morales-Nápoles, and David Joaquín Delgado-Hernández. A Non-parametric Bayesian Network for multivariate probabilistic modelling of Weigh-in-Motion System Data. *Transportation Research Interdisciplinary Perspectives TA - TT -*, 13, 2022.

[82] Dirección General de Servicios Técnicos. Programa de Auscultación de la Red Carretera Federal. Technical report, Secretaria de Comunicaciones y Transportes, 2018.

[83] José Luis Hernández Gutiérrez, Veronica Soria Anguiano, and Marco Luis Dorado Pineda. Estudio estadístico de campo del autotransporte nacional: análisis estadístico de la información recopilada en las estaciones instaladas en 2017. Technical Report 75, IMT, 2018.

[84] Instituto Mexicano del Transporte. Consulta de la base de datos del eecan. https://www.imt.mx/micrositios/seguridad-y-operacion-del-transporte/estadisticas/consulta-del-eecan.html, 2022. Last accessed: 26-07-2022.

[85] Bernard Enright and Eugene J OBrien. Cleaning weigh-in-motion data: Techniques and recommendations. *University College Dublin & Dublin Institute of Technology*, 2011.

[86] Dirección General de Servicios Técnicos. Datos viales 2019. https://www.sct.gob.mx/carreteras/direccion-general-de-servicios-tecnicos/datos-viales/2019/, 2019. Last accessed: 17-05-2021.

[87] M.A. Mendoza Lugo and O. Morales Napoles. Vehicular loads hazard mapping through a bayesian network in the state of mexico. In Bruno Castanier, Marko Cepin, David Bigaud, and Christophe Berenguer, editors, *Proceedings of the 31st*

European Safety and Reliability Conference, pages 2510–2517. Research Publishing Services, 2021. Accepted Author Manuscript; 31st European Safety and Reliability Conference, ESREL 2021 ; Conference date: 19-09-2021 Through 23-09-2021.

[88] José Luis Hernández Gutiérrez, Veronica Soria Anguiano, and Marco Luis Dorado Pineda. Estudio estadístico de campo del autotransporte nacional: análisis estadístico de la información recopilada en las estaciones instaladas en 2017. Technical Report 71, IMT, 2017.

[89] Helmut Finner and Veronika Gontscharuk. Two-sample kolmogorov–smirnov-type tests revisited: old and new tests in terms of local levels. *The annals of statistics*, 46(6A):3014–3037, 2018.

[90] Arnaud de Myttenaere, Boris Golden, Bénédicte Le Grand, and Fabrice Rossi. Mean absolute percentage error for regression models. *Neurocomputing*, 192:38–48, 2016. Advances in artificial neural networks, machine learning and computational intelligence.

[91] Oswaldo Morales-Nápoles and Raphaël D.J.M. Steenbergen. Analysis of axle and vehicle load properties through Bayesian Networks based on Weigh-in-Motion data. *Reliability Engineering & System Safety*, 125:153–164, may 2014.

[92] Octavio A Rascón Chávez Rascó-Chávez. Formulación de la norma SCT de cargas vehiculares para diseño estructural de puentes carreteros. Technical report, Instituto Mexicano del Transporte, Queretaro, 2004.

[93] Standardization European Committee. Eurocode 1: Actions on structures - Part 2: Traffic loads on bridges, 2010.

[94] Shaochen Wang, Wende Tian, Chuankun Li, Zhe Cui, and Bin Liu. Mechanism-based deep learning for tray efficiency soft-sensing in distillation process. *Reliability Engineering & System Safety*, 231:109012, 2023.

[95] Shengli Liu and Yongtu Liang. Statistics of catastrophic hazardous liquid pipeline accidents. *Reliability Engineering & System Safety*, 208:107389, 2021.

[96] Xiaonong Hu, Genshen Fang, Jiayu Yang, Lin Zhao, and Yaojun Ge. Simplified models for uncertainty quantification of extreme events using monte carlo technique. *Reliability Engineering & System Safety*, 230:108935, 2023.

[97] Baorui Dai, Ye Xia, and Qi Li. An extreme value prediction method based on clustering algorithm. *Reliability Engineering & System Safety*, 222:108442, 2022.

[98] Baorui Dai, Dingjun Wu, and Qi Li. Investigation of multiple-presence factor for traffic loads on road-rail bridges based on a novel extreme value analysis approach. *Structural Safety*, 96:102199, 2022.

[99] Xiao-Yi Zhou, Franziska Schmidt, François Toutlemonde, and Bernard Jacob. A mixture peaks over threshold approach for predicting extreme bridge traffic load effects. *Probabilistic Engineering Mechanics*, 43:121–131, 2016.

[100] Emil Julius Gumbel. Les valeurs extrêmes des distributions statistiques. In *Annales de l'institut Henri Poincaré*, volume 5, pages 115–158, 1935.

[101] Curtis L. Smith. Representing external hazard initiating events using a bayesian approach and a generalized extreme value model. *Reliability Engineering & System Safety*, 193:106650, 2020.

[102] Darlene R. Goldstein. Partition resampling and extrapolation averaging: approximation methods for quantifying gene expression in large numbers of short oligonucleotide arrays. *Bioinformatics*, 22(19):2364–2372, 07 2006.

[103] Minjung Kwak. Genome-wide association study using truncated likelihood with incomplete information for stratum specific missingness. *Journal of the Korean Statistical Society*, 50(1):117–133, 2021.

[104] R.D.J.M. Steenbergen, O. Morales Napoles, and A.C.W.M. Vrouwenvelder. Algemene veiligheidsbeschouwing en modellering van wegverkeerbelasting voor brugconstructies. update van tno rapport 98-con-r1813. Technical report, TNO, 2012.

[105] A David García-Soto, Alejandro Hernández-Martínez, JG Valdez-Vazquez, and R Alejandra Vizguerra-Alvarez. Extreme live load effects on short and medium span continuous bridges from mexican wim data. In *Proceedings of the 10th International Conference on Short and Medium Span Bridges, 31st July–3 August*, 2018.

[106] A.D. García-Soto, A. Hernández-Martínez, and J.G. Valdés-Vázquez. Probabilistic assessment of a design truck model and live load factor from weigh-in-motion data for mexican highway bridge design. *Canadian Journal of Civil Engineering*, 42(11):970–974, 2015.

[107] Maria Pregnolato. Bridge safety is not for granted – a novel approach to bridge management. *Engineering Structures*, 196:109193, 2019.

[108] Ana Mandić Ivanković, Dominik Skokandić, Aleš Žnidarič, and Maja Kreslin. Bridge performance indicators based on traffic load monitoring. *Structure and Infrastructure Engineering*, 15(7):899–911, 2019.

[109] Matheus Silva Gonçalves, Rafael Holdorf Lopez, Elder Oroski, and Amir Mattar Valente. A bayesian algorithm with second order autoregressive errors for b-wim weight estimation. *Engineering Structures*, 250:113353, 2022.

[110] Zachary Hamida and James-A. Goulet. Network-scale deterioration modelling of bridges based on visual inspections and structural attributes. *Structural Safety*, 88:102024, 2021.

[111] Xiaoming Lei, Ye Xia, You Dong, and Limin Sun. Multi-level time-variant vulnerability assessment of deteriorating bridge networks with structural condition records. *Engineering Structures*, 266:114581, 2022.

[112] Xiaoming Lei, Ye Xia, Lu Deng, and Limin Sun. A deep reinforcement learning framework for life-cycle maintenance planning of regional deteriorating bridges using inspection data. *Structural and Multidisciplinary Optimization*, 65(5):149, 2022.

[113] Xiaoming Lei, You Dong, and Dan M Frangopol. Sustainable life-cycle maintenance policymaking for network-level deteriorating bridges with a convolutional autoencoder–structured reinforcement learning agent. *Journal of Bridge Engineering*, 28(9):04023063, 2023.

[114] Xiaoming Lei and You Dong. Deep reinforcement learning for optimal life-cycle management of deteriorating regional bridges using double-deep q-networks. *Smart Structures and Systems*, 30(6):571–582, 2022.

[115] Jiyu Xin, Dan M. Frangopol, Mitsuyoshi Akiyama, and Xu Han. Probabilistic life-cycle connectivity assessment of transportation networks using deep learning. *Journal of Bridge Engineering*, 28(9):04023066, 2023.

[116] Naiwei Lu, Yafei Ma, and Yang Liu. Evaluating probabilistic traffic load effects on large bridges using long-term traffic monitoring data. *Sensors*, 19(22), 2019.

[117] Yang Yu, C.S. Cai, Wei He, and Hui Peng. Prediction of bridge maximum load effects under growing traffic using non-stationary bayesian method. *Engineering Structures*, 185:171–183, 2019.

[118] B Jacob. Methods for the prediction of extreme vehicular loads and load effects on bridges. *Report of subgroup*, 8, 1991.

[119] Yang Liu, Qinyong Wang, and Naiwei Lu. Probabilistic evaluation of maximum dynamic traffic load effects on cable-supported bridges under actual heavy traffic loads. *Proceedings of the Institution of Mechanical Engineers, Part O: Journal of Risk and Reliability*, 235(1):108–119, 2021.

[120] Hassan Sarmadi and Ka-Veng Yuen. Early damage detection by an innovative unsupervised learning method based on kernel null space and peak-over-threshold. *Computer-Aided Civil and Infrastructure Engineering*, 36(9):1150–1167, 2021.

[121] E.J. OBrien, F. Schmidt, D. Hajializadeh, X.-Y. Zhou, B. Enright, C.C. Caprani, S. Wilson, and E. Sheils. A review of probabilistic methods of assessment of load effects in bridges. *Structural Safety*, 53:44–56, 2015.

[122] A. Naess and Johannes Ø. Røyset. Extensions of turkstra's rule and their application to combination of dependent load effects. *Structural Safety*, 22(2):129–143, 2000.

[123] Miriam Soriano, Joan R. Casas, and Michel Ghosn. Simplified probabilistic model for maximum traffic load from weigh-in-motion data. *Structure and Infrastructure Engineering*, 13(4):454–467, 2017.

[124] Eugene J. OBrien and Bernard Enright. Modeling same-direction two-lane traffic for bridge loading. *Structural Safety*, 33(4):296–304, 2011.

[125] Eugene OBrien, Bernard Enright, and Tony Dempsey. The influence of correlation on the extreme traffic loading of bridges. In *Fifth International Conference on Bridge Maintenance, Safety and Management*, pages 3827–3835, 07 2010.

[126] Zhibin Jin, Weizhan Liu, and Shiling Pei. Probabilistic evaluation of railway vehicle's safety on bridges under random earthquake and track irregularity excitations. *Engineering Structures*, 266:114527, 2022.

[127] Erica Arango, Monica Santamaria, Maria Nogal, Hélder S Sousa, and José C Matos. Flood risk assessment for road infrastructures using bayesian networks: case study of santarem-portugal. In *International Probabilistic Workshop 2022*, page 33–46. České vysoké učení technické v Praze, 2022.

[128] H.P. Hong, Q. Huang, W.J. Jiang, Q. Tang, and P. Jarrett. Tornado wind hazard mapping and equivalent tornado design wind profile for canada. *Structural Safety*, 91:102078, 2021.

[129] M. Cignetti, D. Godone, D. Bertolo, M. Paganone, P. Thuegaz, and D. Giordan. Rockfall susceptibility along the regional road network of aosta valley region (northwestern italy). *Journal of Maps*, 17(3):54–64, 2021.

[130] Xiaolong Ma, Wei Zhang, Xuan Li, and Zhixia Ding. Evaluating tsunami damage of wood residential buildings in a coastal community considering waterborne debris from buildings. *Engineering Structures*, 244:112761, 2021.

[131] Miguel Angel Mendoza-Lugo and Oswaldo Morales-Nápoles. Mapping hazardous locations on a road network due to extreme gross vehicle weights. *Reliability Engineering & System Safety*, page 109698, 2023.

[132] Blent.ai. Pycopula. an easy-to-use python library that allows you to study random variables dependencies with copulas. https://github.com/blent-ai/pycopula, 2019. Last accessed: 14-09-2022.

[133] Craig. Pynite. simple finite element analysis in python. https://github.com/JWock82/PyNite, 2018. Last accessed: 14-09-2022.

[134] Martin Fleischmann Kelsey Jordahl, Joris Van den Bossche and Jacob Wasserman. geopandas: v0.8.1. https://doi.org/10.5, 2020.

[135] QGIS Development Team. *QGIS Geographic Information System*. QGIS Association, 2022.

[136] Dirección General de Conservación de Carreteras. Puentes de la red federal de carreteras. sistema de puentes de méxico (sipumex) [bridges of the federal highway network. bridge system of mexico], 2021.

[137] Secretaria de Comunicaciones y Transporte. N·PRY·CAR·6·01·001, Ejecución de Proyectos de Nuevos Puentes y Estructuras Similares, 2001.

[138] American Association of State Highway and Transportation Officials. *Standard specifications for highway bridges.* Aashto, 2002.

[139] A.D. García-Soto, A. Hernández-Martínez, and J.G. Valdés-Vázquez. Probabilistic assessment of a design truck model and live load factor from weigh-in-motion data for mexican highway bridge design. *Canadian Journal of Civil Engineering*, 42(11):970–974, 2015.

[140] José Luis Gutiérrez Hernández and Nadia Gómez González. Análisis estadístico para la generación de información proveniente de estaciones dinámicas de medición de pesos, dimensiones y velocidades vehiculares para 2019. Technical report, SCT, 2021.

[141] Dirección General de Servicios Técnicos. Datos viales 2021. https://www.sct.gob.mx/carreteras/direccion-general-de-servicios-tecnicos/datos-viales/2021/, 2021. Last accessed: 29-01-2023.

[142] Oswaldo Morales-Nápoles and Raphaël D.J.M. Steenbergen. Analysis of axle and vehicle load properties through bayesian networks based on weigh-in-motion data. *Reliability Engineering & System Safety*, 125:153–164, 2014. Special issue of selected articles from ESREL 2012.

[143] G.A. Torres-Alves, C.M.P. 't Hart, O. Morales-Nápoles, and S.N. Jonkman. Structural reliability analysis of a submerged floating tunnel under copula-based traffic load simulations. *Engineering Structures*, 269:114752, 2022.

[144] AHJM Vervuurt, JP Pruiksma, RDJM Steenbergen, WMG Courage, S Miraglia, and O Morales Napoles. *Statische belastingen Herijking verkeersbelastingen voor brugconstructies op basis van WIM analyses van april 2013*, volume Droge kunstwerken. InfraQuest, 2015. TNO-2014-R11653.

[145] Alex Kosgodagan-Dalla Torre, Thomas G. Yeung, Oswaldo Morales-Nápoles, Bruno Castanier, Johan Maljaars, and Wim Courage. A two-dimension dynamic bayesian network for large-scale degradation modeling with an application to a bridges network. *Computer-Aided Civil and Infrastructure Engineering*, 32(8):641–656, 2017.

[146] O.A. Rascon Chavez, M. Brausse Moreno, and G. Ventura Suarez. Análisis normativo y estadístico de cargas vivas en puentes en méxico. *Publicación técnica*, 32(97), 1997.

[147] SCT. NOM-012-SCT-2-2017, Sobre el peso y dimensiones máximas con los que pueden circular los vehículos de autotransporte que transitan en las vías generales de comunicación de jurisdicción federal, 2017.

[148] Federal Highway Administration. Bridge Formula Weights. https://ops.fhwa.dot.gov/freight/publications/brdg_frm_wghts/, 2023. Accessed: May 30, 2023.

[149] Dong Guo and Colin C. Caprani. Traffic load patterning on long span bridges: A rational approach. *Structural Safety*, 77:18–29, 2019.

[150] M. Treiber, A. Hennecke, and D. Helbing. Microscopic simulation of congested traffic. In Dirk Helbing, Hans J. Herrmann, Michael Schreckenberg, and Dietrich E. Wolf, editors, *Traffic and Granular Flow '99*, pages 365–376, Berlin, Heidelberg, 2000. Springer Berlin Heidelberg.

[151] Colm Carey, Colin C. Caprani, and Bernard Enright. A pseudo-microsimulation approach for modelling congested traffic loading on long-span bridges. *Structure and Infrastructure Engineering*, 14(2):163–176, 2018.

[152] Liangfu Ge, Danhui Dan, Zijia Liu, and Xin Ruan. Intelligent simulation method of bridge traffic flow load combining machine vision and weigh-in-motion monitoring. *IEEE Transactions on Intelligent Transportation Systems*, 23(9):15313–15328, 2022.

[153] Danhui Dan, Zhaoyuan Xu, Kailong Zhang, and Xingfei Yan. Monitoring index of transverse collaborative working performance of assembled beam bridges based on transverse modal shape. *International Journal of Structural Stability and Dynamics*, 19, 04 2019.

[154] Colin C. Caprani, Eugene J. OBrien, and Alessandro Lipari. Long-span bridge traffic loading based on multi-lane traffic micro-simulation. *Engineering Structures*, 115:207–219, 2016.

[155] David Y. Yang and Dan M. Frangopol. Life-cycle management of deteriorating bridge networks with network-level risk bounds and system reliability analysis. *Structural Safety*, 83:101911, 2020.

[156] M. Sklar. *Fonctions de Répartition À N Dimensions Et Leurs Marges.* Université Paris 8, 1959.

[157] Harry Joe. *Dependence modeling with copulas.* CRC press, 2014.

[158] Andrew A. Neath and Joseph E. Cavanaugh. The bayesian information criterion: background, derivation, and applications. *WIREs Computational Statistics*, 4(2):199–203, 2012.

[159] Eulalia Szmidt and Janusz Kacprzyk. The spearman rank correlation coefficient between intuitionistic fuzzy sets. In *2010 5th IEEE international conference intelligent systems*, pages 276–280. IEEE, 2010.

[160] Graziano Fiorillo and Michel Ghosn. Application of influence lines for the ultimate capacity of beams under moving loads. *Engineering Structures*, 103:125–133, 2015.

[161] Martin Fußeder, Roland Wüchner, and Kai-Uwe Bletzinger. Towards a computational engineering tool for structural sensitivity analysis based on the method of influence functions. *Engineering Structures*, 265:114402, 2022.

[162] Eugene J. OBrien, Daniel Cantero, Bernard Enright, and Arturo González. Characteristic dynamic increment for extreme traffic loading events on short and medium span highway bridges. *Engineering Structures*, 32(12):3827–3835, 2010.

[163] Simon Frederick Bailey. Basic principles and load models for the structural safety evaluation of existing road bridges. Technical report, EPFL, 1996.

[164] Alan O'connor and Eugene J O'Brien. Traffic load modelling and factors influencing the accuracy of predicted extremes. *Canadian Journal of Civil Engineering*, 32(1):270–278, 2005.

[165] Colin C Caprani. *Probalistic analysis of highway bridge traffic loading*. PhD thesis, Technological University Dublin, 2005.

[166] D. Martucci, M. Civera, and C. Surace. Bridge monitoring: Application of the extreme function theory for damage detection on the i-40 case study. *Engineering Structures*, 279:115573, 2023.

[167] Enrique Castillo, Alan J. O'Connor, María Nogal, and Aida Calviño. On the physical and probabilistic consistency of some engineering random models. *Structural Safety*, 51:1–12, 2014.

[168] Raphaël D.J.M. la Gasse, Liesette C and Swaalf, Lisa and Steenbergen. Bayesian Inference and Maximum Likelihood Estimation for fitting Distribution Functions of Road Traffic Load Effects. In *14th International Conference on Applications of Statistics and Probability in Civil Engineering, ICASP14*, Dublin, 2023.

[169] Colin C Caprani, A Belay, and AJ O'Connor. Site-specific probabilistic load modelling for bridge reliability analysis. In *Proceedings of the 3rd. International Conference on Current and Future Trends in Bridge Design, Construction and Maintenance*, pages 341–348, 2003.

[170] Alan J O'Connor. *Probabilistic traffic load modelling for highway bridges*. PhD thesis, Trinity College Dublin, 2001.

[171] Cathal Leahy, Eugene OBrien, and Alan O'Connor. The effect of traffic growth on characteristic bridge load effects. *Transportation Research Procedia*, 14:3990–3999, 2016. Transport Research Arena TRA2016.

[172] E.J. OBrien, A. Bordallo-Ruiz, and B. Enright. Lifetime maximum load effects on short-span bridges subject to growing traffic volumes. *Structural Safety*, 50:113–122, 2014.

[173] Zeng Meng, Jingyu Zhao, and Chen Jiang. An efficient semi-analytical extreme value method for time-variant reliability analysis. *Structural and Multidisciplinary Optimization*, 64(3):1469–1480, 2021.

[174] Secretaria de Comunicaciones y Trasnporte. N·PRY·CAR·6·01·003, Cargas y Acciones, 2001.

[175] Standardization European Committee. EN 1991-2:2003 Eurocode 1: Actions on structures - Part 2: Traffic loads on bridges, 2003.

[176] Diario Oficial de la Federación. ACUERDO SS/3/2022 por el que se determina el calendario oficial de suspensión de labores para el año 2022., 2022.

[177] Farancis M. Mutua. The use of the akaike information criterion in the identification of an optimum flood frequency model. *Hydrological Sciences Journal*, 39(3):235–244, 1994.

[178] Delft High Performance Computing Centre (DHPC). *DelftBlue Supercomputer (Phase 1)*, 2022. https://www.tudelft.nl/dhpc/ark:/44463/DelftBluePhase1.

[179] A. Getachew and E. J. Obrien. Simplified site-specific traffic load models for bridge assessment. *Structure and Infrastructure Engineering*, 3(4):303–311, 2007.

[180] O.A.R. Chávez and Instituto Mexicano del Transporte. *Análisis normativo y estadístico de cargas vivas en puentes en México*. Publicación técnica. Instituto Mexicano del Transporte, Secretaría de Comunicaciones y Transportes, 1997.

[181] O.A.R. Chávez and Instituto Mexicano del Transporte. *Modelo de cargas vivas vehiculares para diseño estructural de puentes en México*. Publicación técnica. Instituto Mexicano del Transporte, Secretaría de Comunicaciones y Transportes, 1999.

[182] Mohammad Hosein Nili, Hosein Taghaddos, and Banafsheh Zahraie. Integrating discrete event simulation and genetic algorithm optimization for bridge maintenance planning. *Automation in Construction*, 122:103513, 2021.

[183] Mayer M. Melhem and Colin C. Caprani. Promoting probability-based bridge assessment in engineering practice: an australian case study. *Structure and Infrastructure Engineering*, 18(10-11):1472–1486, 2022.

[184] Alice Alipour and Behrouz Shafei. Assessment of postearthquake losses in a network of aging bridges. *Journal of Infrastructure Systems*, 22(2):04015023, 2016.

[185] Ning Zhang and Alice Alipour. A two-level mixed-integer programming model for bridge replacement prioritization. *Computer-Aided Civil and Infrastructure Engineering*, 35(2):116–133, 2020.

[186] Xu Han and Dan M. Frangopol. Risk-based optimal life-cycle maintenance strategy for bridge networks considering stochastic user equilibrium. *ASCE-ASME Journal of Risk and Uncertainty in Engineering Systems, Part A: Civil Engineering*, 8(2):04022011, 2022.

[187] Stefan L. Leiva-Maldonado Yina F. M. Moscoso, Luis F. Rincón and Jose A. S. C. Campos e Matos. Bridge deterioration models for different superstructure types using markov chains and two-step cluster analysis. *Structure and Infrastructure Engineering*, 0(0):1–11, 2022.

[188] Ricardo Monteiro Andres Abarca and Gerard J. O'Reilly. Seismic risk prioritisation schemes for reinforced concrete bridge portfolios. *Structure and Infrastructure Engineering*, 0(0):1–21, 2023.

[189] Graziano Fiorillo and Michel Ghosn. Risk-based life-cycle analysis of highway bridge networks under budget constraints. *Structure and Infrastructure Engineering*, 18(10-11):1457–1471, 2022.

[190] TaeHoon Hong and Makarand Hastak. Evaluation and determination of optimal mr&r strategies in concrete bridge decks. *Automation in Construction*, 16(2):165–175, 2007.

[191] Edward A. Baron, Neryvaldo Galvao, Marija Docevska, Jose C. Matos, and Goran Markovski. Application of quality control plan to existing bridges. *Structure and Infrastructure Engineering*, 19(7):990–1006, 2023.

[192] Mohammed Alsharqawi, Saleh Abu Dabous, Tarek Zayed, and Sadeque Hamdan. Budget optimization of concrete bridge decks under performance-based contract settings. *Journal of Construction Engineering and Management*, 147(6):04021040, 2021.

[193] Xu Han and Dan M. Frangopol. Life-cycle connectivity-based maintenance strategy for bridge networks subjected to corrosion considering correlation of bridge resistances. *Structure and Infrastructure Engineering*, 18(12):1614–1637, 2022.

[194] Zhibo Zhang, Samuel Labi, Jon D Fricker, and Kumares C Sinha. Strategic scheduling of infrastructure repair and maintenance: Volume 2—developing condition-based triggers for bridge maintenance and rehabilitation treatments. 2017.

[195] Joan R Casas, Francisco A Alonso-Farrera, and Manuel Nazar. Optimal joint maintenance and repair policies for bridge components. implementation in the bridge management system of chiapas (mexico). Technical report, 2006.

[196] Paolo Bocchini and Dan M. Frangopol. A probabilistic computational framework for bridge network optimal maintenance scheduling. *Reliability Engineering & System Safety*, 96(2):332–349, 2011.

[197] Omar Kammouh, Maria Nogal, Ruud Binnekamp, and A.R.M. Rogier Wolfert. Multi-system intervention optimization for interdependent infrastructure. *Automation in Construction*, 127:103698, 2021.

[198] Dominik Skokandić and Ana Mandić Ivanković. Value of additional traffic data in the context of bridge service-life management. *Structure and Infrastructure Engineering*, 18(4):456–475, 2022.

[199] M.J. Ryall. *Bridge Management (2nd Edition)*. Taylor & Francis, 2010.

[200] International Transport Forum. Transport infrastructure investment and maintenance spending: Maintenance Spending, 2023.

[201] Hernández Quinto and Ignacio Enrique. Conservación de puentes. Technical report, UNAM, 2007. Bridge Maintenance.

[202] John Palmer and Graham Cogswell. *Management of the Bridge Stock of a UK County for the 1990s*, pages 39–50. Springer US, Boston, MA, 1990.

[203] John E Harding, Parke Gerard, and M Ryall. *Bridge Management: Inspection, maintenance, assessment and repair.* CRC Press, 1990.

[204] J. de Brito, F.A. Branco, P. Thoft-Christensen, and J.D. Sørensen. An expert system for concrete bridge management. *Engineering Structures*, 19(7):519–526, 1997.

[205] Community Research and Development Information Service. Seron project: Final report. Technical report, European Commission, 2012.

[206] A Mandić Ivanković, M Kušter Marić, D Skokandić, E Njirić, and J Šiljeg. Finding the link between visual inspection and key performance indicators for road bridges. In *Proceedings of the Report on IABSE symposium GuimãraesS*, 2019.

[207] Ana Mandić Ivanković, Dominik Skokandić, Marija Kušter Marić, and Mladen Srbic. Performance-based ranking of existing road bridges. *Applied Sciences*, 11:4398, 05 2021.

[208] Gitanjali Bhattacharjee and Jack W. Baker. Using global variance-based sensitivity analysis to prioritise bridge retrofits in a regional road network subject to seismic hazard. *Structure and Infrastructure Engineering*, 19(2):164–177, 2023.

[209] Ginger Daniels, David R Ellis, and Win R Stockton. *Techniques for manually estimating road user costs associated with construction projects*, volume 3. Texas Transportation Institute College Station, TX, 1999.

[210] Erica Arango, Maria Nogal, Ming Yang, Hélder S. Sousa, Mark G. Stewart, and José C. Matos. Dynamic thresholds for the resilience assessment of road traffic networks to wildfires. *Reliability Engineering & System Safety*, 238:109407, 2023.

[211] V. H. Lad, D. A. Patel, K. A. Chauhan, and K. A. Patel. Development of fuzzy system dynamics model to forecast bridge resilience. *Journal of Bridge Engineering*, 27(12):04022114, 2022.

[212] Secretaría de Comunicaciones y Transportes. Infraestructura estratégica y prospectiva 2030 del subsector carretero, 2017. Strategic and prospective infrastructure 2030 of the road sub-sector.

[213] Secretaría de Comunicaciones y Transportes. Tabulador de costos paramétricos para la construcción y modernización de la infraestructura carretera 2023. Technical report, 2022. Parametric cost tabulator for the construction and modernization of the road infrastructure 2023.

[214] Instituto Nacional de Estadística y Geografía. Encuesta Nacional de Ingresos y Gastos de los Hogares 2022. Technical report, INEGI, 2023. National Household Income and Expenditures Survey 2022.

[215] Instituto Mexicano del Transporte. Estudio estadístico de campo, del autotransporte nacional análisis estadístico de la información recopilada para automóviles, en las estaciones instaladas en 2017. Technical report, IMT, 2020. Statistical field study, national auto transport Statistical analysis of the information collected for automobiles, in the stations installed in 2017.

[216] Tara L Cavalline, Matthew J Whelan, Brett Q Tempest, Raka Goyal, and Joshua D Ramsey. Determination of bridge deterioration models and bridge user costs for the ncdot bridge management system. *No. FHWA/NC/2014-07*, 2015.

[217] MJ Ryall. Whole-life costing, maintenance strategies and asset management. *Bridge Management*, pages 355–378, 2010.

[218] Instituto Nacional de Estadística y Geografía. Calculadora de Inflación: Índice Nacional de Precios al Consumidor, 2023. Inflation Calculator: National Consumer Price Index.

[219] Pauli Virtanen, Ralf Gommers, Travis E. Oliphant, Matt Haberland, Tyler Reddy, David Cournapeau, Evgeni Burovski, Pearu Peterson, Warren Weckesser, Jonathan Bright, et al. Scipy: Open source scientific tools for python. *Nature Methods*, 17:261–272, 2020.

[220] Flavia Sánchez Jacobo. Sistemas de gestión de puentes carreteros. Technical report, Instituto Politácnico Nacional, 2017. Road bridge management systems.

[221] Road Directorate. Manual de usuario. jerarquización de trabajos de reparación de puentes. Technical report, Denmark: Ministry of Transport, 1994. User's Manual. Hierarchy of bridge repair works.

[222] Bryan T Adey, Marcel Burkhalter, and Claudio Martani. Defining road service to facilitate road infrastructure asset management. *Infrastructure Asset Management*, 7(4):240–255, 2020.

[223] Miguel Angel Mendoza-Lugo, Maria Nogal, and Oswaldo Morales-Nápoles. Estimating bridge criticality due to extreme traffic loads in highway networks. *Engineering Structures*, 300:117172, 2024.

Acknowledgments

This journey has been long and challenging, marked by numerous difficulties, obstacles, and moments of joy. In this section, I would like to express my gratitude to those who have had a significant influence on my experience throughout my PhD journey.

I want to extend my gratitude to my PhD supervisors, Oswaldo Morales and Maria Nogal, who have guided me throughout this journey. Their patience, friendliness, and extensive knowledge have not only shaped my academic path but have also enriched my personal growth.

¿Qué pasó, doc?! Oswaldo, I am especially thankful for your belief in my potential. Your consistent support, motivation, and the challenges you presented have pushed me to grow in every aspect of my life. I truly appreciate how you encouraged me to pursue ambitious goals, including the endeavor of running a marathon. Your belief in my abilities has inspired me to push my limits, and I have learned invaluable lessons from your mentorship. Thank you for being a friend and for always reminding me that I am capable of achieving great things. Maria, thank you for inspiring me to maintain a constant and productive pace in my work. Your sharp insights have always pushed me to elevate my work. I admire your commitment to excellence and your passion for science, which are evident in everything you do. Your dedication motivates me to strive for the same qualities in my own research. I hope to one day embody the same attributes making you such an outstanding mentor.

I would like to thank my master's thesis supervisor, David Delgado, for his influence on my decision to pursue a PhD. Thank you for your support and for continuing to collaborate with me academically, which I truly enjoy. It's also important for me to express my heartfelt gratitude to my colleagues Peng Xu and Gina, without whom the first year of this adventure would have been incredibly daunting. Their support and camaraderie made all the difference. I recall the simple things that kept me going during those challenging times. Thank you, Peng Xu, for the wonderful evenings spent watching movies that opened my eyes to a world of cinema beyond the mainstream. Gina, I am very grateful for the advice you have given me in every aspect, not just academically. Our sessions where we ask each other "dumb" questions have been incredibly helpful in understanding concepts that have improved my work.

One of the aspects I truly appreciate about the PhD program is the opportunity to collaborate with people from different universities. In this sense, I have gained wonderful friends and colleagues from various universities. Brais, I cherish all the adventures we shared, like getting lost on the train. Santiago, you're such a cool guy, and I appreciate your positive energy. Erica, you have become a true friend *wey*. I enjoy our coffee conversations and the insights we share. Thank you for being such a supportive friend.

To everyone in the PSOR group —Robert, Danny, Bart, Dirk, Ties, Jerom, Sargol, Patricia, Mario, Su, and Juan— thank you for all the enjoyable drinks and good times. A special thanks to Robert for being there when I needed support. I have learned so much from working with you, and I truly admire your passion for teaching and your positive attitude towards others.

I consider myself a very lucky person because I have the support of my family. My brother, my nieces, my mom, my dad, and my wife all play a significant role in my life. Their love and encouragement inspire me every day. *Papá y mamá, siendo sincero, no sé qué haría sin su apoyo y la esperanza de volver a abrazarlos. Ustedes son mi ejemplo a seguir, y les agradezco de corazón porque nunca me ha faltado nada. No hay palabras que puedan describir lo mucho que les agradezco y cuánto los amo. Mi amada Nancy, siempre has sido un gran soporte que me ha mantenido a flote durante todos estos años. Me siento increíblemente afortunado de tenerte a mi lado, porque eres una persona con un corazón inmenso, siempre dispuesta a ayudarme, motivarme y comprenderme en cada paso del camino. Mi corazón se llena de alegría al recordar cada una de las aventuras que hemos vivido juntos. Desde los momentos más simples hasta las experiencias más emocionantes, cada instante a tu lado ha sido un regalo. Estoy emocionado por todas las nuevas aventuras que aún nos esperan, y sé que, con cada una de ellas, mi amor por ti solo seguirá creciendo.*

As I reflect on this journey, I can't help but appreciate the silver linings and the warmth of the friendships that have become the soundtrack of my PhD. Each person I've encountered has contributed to my growth and resilience, reminding me of the power of connection and support.

Miguel Angel Mendoza Lugo
Delft, 2025

Epilogue

Turn up the volume

Ten songs that I enjoy deeply

Before leaving, I would like to emphasize that music is a creative and supportive force. Everything I have shared with you throughout these pages would not have been possible without music. While I have a deep, almost religious appreciation for reggae (preferably in the format of vinyl records), my musical tastes are quite diverse. There are times when I immerse myself in cumbias for an entire week, spend countless hours enjoying rancheras, or listen for days to the songs my parents played during our road trips. However, I must confess that I have a strong preference for more melodic tunes. Every time I listen to the songs I am about to share with you, they always make me want to turn up the volume to the maximum. It is difficult to create a list of favorite songs because it is a function of both your mood and your environment. Hence, every song listed here is presented without a specific order, and their percentage of enjoyment content (PEC) is often interchangeable.

1. **Hold Down - The Kingstonians.** This song conveys the initial phrase of the thesis: 'Small axe fall big tree,' which can be interpreted as a synonym for the idea that persistence and determination can overcome larger obstacles or challenges.

2. **Sitting Round the Bend - The Hamlins.** A massive hit. The first time I heard it was on a sound system in UK. I was tired, but as soon as the first notes of that organ played, boom! The energy shot up to the max.

3. **Bag-A-Boo - Clancy Eccles.** A song that arises from the rivalry between producers Clancy Eccles and Lee Perry is a true musical gem, especially due to the hypnotizing flute that is in sync with the reggae shuffle.

4. **Don't you rock my boat - Bob Marley and the Wailers.** Bob Marley is not just roots reggae. The rock steady version of Don't you rock my boat is everything you could ask for in a good rock steady: masterful melodies and deep soul.

5. **Big Big Boss - Jhonny Moore.** A really motivating song, where the trumpet of Johnny 'Dizzy' Moore, a founding member of the pioneering group The Skatalites, makes you feel like a king, no matter where you are.

6. **Reality - Joy Mack.** Lovers rock at its finest—truly a heart-wrenching song for those who no longer want to be in an unfair relationship and have come to appreciate themselves.

7. **Saturday Night is Here Again - Panchila La Touche.** This song breathes life into its listener; there is nothing more to say, just listen to it.

8. **Down Stairs Rock - Determinations.** Since I started my journey into Jamaican music, reggae made in Japan has always been one of my favorites. Determinations was an exciting, dynamic, and fantastic band from Osaka, and their massive ska song 'Down Stairs Rock' always makes me jump.

9. **Runnin' Away - Frisco feat. Chee.** Frisco, another Japanese reggae band for which I have great admiration, is my favorite band from the Far East, and I have all their albums. 'Running Away' is a piece that masterfully combines the rhythm of the classic 'Love Has Found Its Way' by Dennis Brown with the lyrics of 'Running Away' by Sly and the Family Stone.

10. **Contra El Dragón - Los Acosta.** Because not everything is reggae. A hero, a princess, a dragon, and cumbia—what more could you ask for to be happy (or not...) and motivated?

A few more that do not fit due to lack of space and time.

- Corazón Solitario - Alberto Pedraza
- Dile - ICC
- Compré una cantina - Cardenales de Nuevo León
- Al gato y al ratoń - Banda Machos
- Hello Dolly - Pat Satchmo
- I'm the Ruler - Anthony Rocky Ellis.

Curriculum Vitæ

Miguel Angel Mendoza Lugo

Education

08/2016 - 08/2018	MSc. Civil Engineering | Structural engineering Faculty of Engineering Autonomous University of the State of Mexico.
08/2006 - 08/2011	B.Sc. Civil Engineering Faculty of Engineering Autonomous University of the State of Mexico.

Work experience

02/2024 - today	Scientist Innovator Unity of Mobility & Built Environment | Reliable Structures Nederlandse Organisatie voor toegepast-natuurwetenschappelijk onderzoek (TNO) *Conducting advanced research to enhance the reliability and safety of civil structures and developing practical, innovative solutions to societal challenges.*
01/2020 - 12/2024	Ph.D. candidate Department of Hydraulic Engineering Delft University of Technology *Research topic: Probabilistic-based methods for extreme traffic loads mapping to assist bridge portfolio management*
03/2022 - 12/2023	Part-time educational staff member Department of Hydraulic Engineering Delft University of Technology *Development of the online courses: (i) Learn Python for Civil Engineering and Geosciences and (ii) Probability and statistics applications for Modelling, Uncertainty, Data for Engineers.*
02/2021 - 11/2023	Teaching assistant Department of Hydraulic Engineering Delft University of Technology *Courses: (i) Probabilistic Design and Risk Management and (ii) Probabilistic Design in Hydraulic Engineering.*

01/2018 - 12/2019	Lecturer College of Architects of the State of Mexico and Autonomous University of the State of Mexico *Courses: (i) Supervision, and control of construction execution and (ii) Prestressed concrete.*
02/2013 - 12/2019	Concrete laboratory section head Construction materials properties laboratory, Autonomous University of the State of Mexico. *As a certified Quality Control Specialist (ema) for concrete and soils, I review construction materials and quality control records, ensuring adherence to official standards in commercial, industrial, and infrastructure projects. My role involves quality assurance, technical report writing, and overseeing field and laboratory reviews.*
01/2011 - 12/2012	Construction superintendent assistant and land Surveyor WP Constructions and Pavements S.A. de C.V and PEPCO Engineering S.A de C.V. *Construction management and surveying activities to construct storm sewer network systems.*

List of Publications

Peer-reviewed journal papers

1. van der Heijden, T., **Mendoza-Lugo, M.A.**, Palensky, P., van de Giesen, N., & Abraham, E. (2025). Incorporating risk in operational water resources management: Probabilistic forecasting, scenario generation, and optimal control. Water Resources Research, 61, e2024WR037115. doi: https://doi.org/10.1029/2024WR037115

2. **Mendoza-Lugo, M.A.**, Nogal, M., Morales-Nápoles, O. (2024). Network-level optimization approach for bridge interventions scheduling. Structure and Infrastructure Engineering. doi: https://www.tandfonline.com/doi/full/10.1080/15732479.2024.2403568 (This thesis)

3. Ramousse, B., **Mendoza-Lugo, M.A.**, Rongen, G., Morales-Nápoles, O. (2024). Elicitation of Rank Correlations with Probabilities of Concordance: Method and Application to Building Management. Entropy. doi: https://doi.org/10.3390/e26050360

4. **Mendoza-Lugo, M. A.**, Nogal, M., Morales-Nápoles, O. (2024). Estimating bridge criticality due to extreme traffic loads in highway networks. Engineering Structures. doi: https://doi.org/10.1016/j.engstruct.2023.117172 (This thesis)

5. **Mendoza-Lugo, M. A.**, Morales-Nápoles, O. (2023). Mapping hazardous locations on a road network due to extreme gross vehicle weights. Reliability Engineering and System Safety. doi: https://doi.org/10.1016/j.ress.2023.109698 (This thesis)

6. **Mendoza-Lugo, M. A.**, Morales-Nápoles, O. (2023). Version 1.3-BANSHEE; A MATLAB toolbox for Non-Parametric Bayesian Networks. SoftwareX, 23. doi: https://doi.org/10.1016/j.softx.2023.101479

7. Koot, P., **Mendoza-Lugo, M.A.**, Paprotny, D., Morales-Nápoles, O., Worm, D.T.H., Ragno, E. (2023). PyBanshee version (1.0): A Python implementation of the MATLAB toolbox BANSHEE for Non-Parametric Bayesian Networks with updated features. SoftwareX. doi: https://doi.org/10.1016/j.softx.2022.101279

8. **Mendoza-Lugo, M. A.**, Morales-Nápoles, O., & Delgado-Hernández, D. J. (2022). A Non-parametric Bayesian Network for multivariate probabilistic modelling of Weigh-in-Motion System Data. Transportation Research Interdisciplinary Perspectives, 13, 100552. doi: https://doi.org/10.1016/j.trip.2022.100552 (This thesis)

9. **Mendoza-Lugo, M. A.**, Delgado-Hernández, D.J., Morales-Nápoles, O. (2019). Reliability analysis of reinforced concrete vehicle bridge columns using non-parametric Bayesian networks. Engineering Structures, 188, pp. 178-187. doi:https://doi.org/10.1016/j.engstruct.2019.03.011

CONFERENCE CONTRIBUTIONS

1. **Mendoza-Lugo, M. A.**, Torres-Alves, G. A., Morales-Nápoles, O. (2023). Reliability analysis of the ancient Nezahualcoyotl's dike. Investigating failure due to overflow using an improved hydrological model. Proceedings of the 33rd European Safety and Reliability Conference. doi: https://doi.org/10.3850/978-981-18-8071-1_P279-cd

2. Mares-Nasarre, P., García-Maribona, J., **Mendoza-Lugo, M.A.**, Morales-Nápoles, O. (2023). A copula-based Bayesian Network to model wave climate multivariate uncertainty in the Alboran Sea. Proceedings of the 33rd European Safety and Reliability Conference. doi: https://doi.org/10.3850/978-981-18-8071-1_P091-cd

3. **Mendoza-Lugo, M. A.**, Morales-Nápoles, O. (2021). Vehicular Loads Hazard Mapping Through a Bayesian Network in the State of Mexico. Proceedings of the 31st European Safety and Reliability Conference. doi:https://doi.org/10.3850/978-981-18-2016-8_289-cd